Harnessing Biotransport Phenomena to Simplify Workflow for Clinical Metabolomics using Microsamples

by

Ramisa Fariha

Sc.M. Biomedical Engineering, Brown University, 2020

B.S. Biomedical Engineering, The Pennsylvania State University, 2017

A dissertation submitted in partial fulfillment of the requirements for the degree of

Doctor of Philosophy in Biomedical Engineering at Brown University

PROVIDENCE, RHODE ISLAND

May 2024

This dissertation by Ramisa Fariha is accepted in its present form by the Biomedical Engineering program, a joint program in the Division of Biology and Medicine and the School of Engineering as satisfying the dissertation requirement for the degree of Doctor of Philosophy.

Date:_____ _____

Anubhav Tripathi, Ph.D., Advisor

Recommended to the Graduate Council

Date:_____ _____

Vikas Srivastava, Ph.D., Reader

Date:_____ _____

John Marshall, Ph.D., Reader

Date:_____ _____

Edith Mathiowitz, Ph.D., Reader

Date:_____ _____

Carolina Haass-Koffler, Ph.D., Reader

Date:_____ _____

Stefani Thomas, Ph.D., Reader

Date:_____ _____

Angus Kingon, Ph.D., Reader

Approved by the Graduate Council

Date:_____ _____

Thomas A. Lewis, Ph.D., Dean of the Graduate School

Curriculum Vitae

Education and Research

Doctor of Philosophy in Biomedical Engineering, Tripathi Lab **Brown University**
Cumulative GPA: 4.00/4.00 Providence, RI**,** May 2024

Dissertation: "Harnessing Biotransport Phenomena in the Workflow Simplification of Metabolite Microsampling for Clinical LC-MS/MS Applications"

- Led collaboration studies with Perkin Elmer Inc. that brought in $300,000 research grant to Brown University as the Senior scientist in the *Clinical Diagnostics and Automation Team*.
- Developed and validated LC-MS/MS methods for microsampling of small molecules, steroids, and drug metabolites.
- Designed novel assay protocols (second tier) for micro-sample preparation of multiple matrices (whole blood, dried blood spots, serum, saliva, cerumen, and cell culture media).
- Performed extensive instrument troubleshooting (QSight 220 with LX50 modules), as well as assay troubleshooting.
- Programmed and executed complete automation of assays on robotic liquid handler (JANUS G3) for clinical applications.
- Spearheaded meetings with stakeholders presenting both research findings and financial aspects of projects (cost-analysis, profit per unit, etc.).
- Conceptualized study proposals focused on science and business impact and propelled these studies from ideation to products for corporate clients (See *'Research Projects'* section for a detailed list of research experience).
- Designed and developed a novel device for biospecimen sample preparation (patented).
- Trained, mentored, and managed a team of 4 graduate and 6 undergraduate researchers through independent thesis projects.
- Wrote five scientific journal articles and presented at seven national and international conferences.

Master of Science in Biomedical Engineering, Lee Lab **Brown University**
Cumulative GPA: 4.00/4.00 Providence, RI, May 2020

Thesis: Assessing Chemosensitivity in Breast Cancer Spheroids using Optical Coherence Tomography.

- Led an interdepartmental collaboration with the *Morgan lab for Tissue Engineering* and independently investigated a true longitudinal anti-cancer drug study on MCF7 breast cancer spheroids.
- Imaged 3-D tissues using Optical Coherence Tomography (OCT), collected data, and performed data analysis using MATLAB, while concurrently performing method validation using a Live-Dead Assay.
- Provided preliminary data and writing support for a successful R01 grant application to the National Cancer Institute ($1.07 M).

Bachelor of Science in Biomedical Engineering **the Pennsylvania State University**
Cumulative GPA: 3.34/4.00 State College, PA, May 2017

Project: Chemically Defined LaSR Medium for Long-term Cultivation of Human Pluripotent Stem Cells and Embryonic Stem Cells.

- Selected as the first Undergraduate Research Assistant at the *Lian Lab for Human Stem Cell Engineering*.
- Examined an in-house-developed cost-efficient chemical media for long-term growth and proliferation of human embryonic stem cells (hESCs) and induced pluripotent stem cells (iPSCs) growth.
- Investigated the early embryogenesis of mesodermal layers in hESCs over a 24-hour study period.

Work Experience

ACell Inc. (Integra LifeSciences) Columbia, MD
Research and Development Intern May 2017-April 2018

- Worked directly with Dr. Luai Huleihel on the Urinary Bladder Matrix (UBM) characterization study for its application in patient pericardium tissue reinforcement.
- Independently designed and manufactured tissue-based product iterations for large-animal testing.

- Presented work in weekly meetings to the Chief Scientific Officers (CSOs), and in monthly meetings to key stakeholders and investors (See *'Research Projects'* section for a detailed list of research experience).

Skills

- LC-MS/MS Assay Development
- Automation (JANUS G3 Platform)
- Mammalian Cell Culture
- 3-D Tissue Culture
- Immunolabeling
- DNA Quantification (Picogreen dsDNA assay)
- Histology (H&E staining)
- RT-qPCR (Taqman Chemistry)
- RNA Isolation
- cDNA Synthesis
- RNA Quantification
- BCA Protein Assay
- COMSOL Multiphysics
- MATLAB
- JMP Pro
- BMDM Isolation
- Microfluidic Chip Fabrication
- Device Design
- Optical Coherence Tomography
- Project Management
- Technical Writing
- Mimics
- Public Speaking
- 3matic
- Canva
- Fluent in Bengali
- Fluent in Hindi
- Troubleshooting (LC-MS/MS)

Professional Certifications

- Using Hardware, Software, and Peopleware to Plan Your Scientific Journey. *SLAS (2024).*
- Peptides and Proteins. *American Society for Mass Spectrometry* (2023).
- Metabolomics 201: Measuring Metabolism from Dried Blood Spots to Microsampling and More. *MSACL (2023)*.
- Introduction to Mass Spectrometry and its Applications within Drug Discovery. *SLAS* (2023).
- Sheridan Teaching Seminar (Engineering). *The Harriet W. Sheridan Center for Teaching and Learning* (Fall 2022).
- Brown Executive Scholars Training Program (BEST). *Brown University Graduate School* (2021-2022).
- LC-MSMSM 101: Getting Started with Quantitative LC-MS/MS in the Diagnostic Laboratory. *MSACL* (2021).
- Creating a Science-Based Web Presence. *Initiative to Maximize Student Development* (2019-2020).

Publications

Peer-Reviewed Manuscripts

- **Fariha, R.**, Murphy, J., Walters, N., Rothkopf, E., Okoh, O. D., Lawandy, N.M., Tripathi, *A. Precision through Electric-Field Assisted Automatable High Throughput Sample Preparation of Dried Blood Spots for Neonatal Abstinence Syndrome Detection* (Manuscript preprint available).
- **Fariha, R.**, Rothkopf, E., Haass-Koffler, C., Tripathi, A. *Opioid Quantification via Microsampling Techniques to Assess Opioid Use in Human Laboratory Studies* (Manuscript under final review).
- **Fariha, R.**, Rothkopf, E., Murphy, J., Walters, N., Okoh, O. D., Lawandy, N.M., Tripathi, A. *Electric-field Assisted Sample Preparation of Whole Blood and Dried Blood Spots for Steroid Quantification using LC-MS/MS* (Manuscript under final review).
- **Fariha, R.**, Okoh, O. D., Hamze, J., Rothkopf, E., Tripathi, A. *Understanding in vitro to in vivo Extrapolation Tissue Models: A Case of Microtissues and Paclitaxel* (Manuscript under review).
- **Fariha, R.**, Collin, H., Jabrah, M., Spooner, A., Tripathi, A. *Understanding Sample Preparation Workflow: Semi-Automated Preparation of Serum Testosterone for Detection Using LC-MS/MS* (Manuscript preprint available).
- **Fariha, R.**, Deshpande, P.S., Rothkopf, E., Jabrah, M., Spooner, A., Okoh, O. D., Tripathi, A. *An in-depth Analysis on Four Classes of Antidepressants Quantification from Human Serum using LC-MS/MS* (Scientific Reports, 2023).
- **Fariha, R.**, Collin, H., Jabrah, M., Spooner, A., Deshpande, P.S., Tripathi, A. *Simultaneous detection of Salivary Cortisol and Cortisone using a High-throughput Sample Preparation Method for LC-MS/MS* (SLAS Technology, 2022).

Conference Presentations

- **Fariha, R.**, Walters, N., Okoh, O. D., Haque, M. F., Tripathi, A. *LC-MS/MS Quantification of PARP-inhibitor uptake for Validating an Ovarian tumor on a Chip* (Accepted for presentation at SLAS 2024).
- **Fariha, R.**, Walters, N., Okoh, O. D., Tripathi, A. *Neonatal Abstinence Syndrome Detection using from DBS using LC-MS/MS* (Accepted for presentation at SLAS 2024)
- **Fariha, R.**, Okoh, O. D., Tripathi, A. *Microfluidic chip-based Remote Sample Collection and Preparation of Amphetamine for LC-MS/MS Application* (Accepted for presentation at SLAS 2024).
- **Fariha, R.**, Rothkopf, E., Murphy, J., Okoh, O. D., Walters, N., Tripathi, A. *LC-MS/MS Application for Early Detection of PCOS Using Electro-DBS Samples* (Accepted for presentation at SLAS 2024).
- **Fariha, R.**, Okoh, O. D., Hamze, J., Rothkopf, E., Ahmed, Z., Tripathi, A. *LC-MS/MS Application for an IVIVE Model Validation of MCF7 Microtissues* (Presented at ASMS 2023).
- **Fariha, R.**, Okoh, O. D., Sponer, A., Rothkopf, E., Tripathi, A. *An Automated Workflow for the Quantification of 8-Different Antidepressants Using LC-MS/MS* (Presented at ASMS 2023).
- **Fariha, R.**, Ahmed, Z., Hamze, J., Okoh, O. D., Rothkopf, E., Tripathi, A. *Application of LC-MS/MS to Assess the Chemosensitivity of Breast Cancer Spheroids for an In Vitro to In Vivo Extrapolation Analysis* (Presented at MSACL 2023).
- **Fariha, R.**, Rothkopf, E., Spooner, A., Okoh, O. D., Tripathi, A. *An in-depth Analysis on Four Classes of Antidepressants Quantification from Human Serum using LC-MS/MS* (Presented at SLAS 2023).
- **Fariha, R.** *Small Volume Quantification of Four Classes of Antidepressants for Post-Partum Depression Monitoring.* (Abstract presented at ICASE, August 2022).
- **Fariha, R.**, Deshpande, P.S., Rothkopf, E., Jabrah, M., Spooner, A., Okoh, O. D., Tripathi. *Simultaneous detection of Salivary Cortisol and Cortisone using a High-throughput Sample Preparation for LC-MS/MS* (Presented at MSACL 2022).
- Hill, C., Maharaj, R., Spooner, A., **Fariha, R**. *SimplicityLabCR: An Integrated Liquid-Handling LC-MS/MS Platform for Therapeutic Drug Monitoring* (Presented at the 19th International Congress of Therapeutic Drug Monitoring and Clinical Toxicology, 2021).
- **Fariha, R.**, Ip, B., Morgan, J., Lee, J. *Assessing Chemosensitivity in 3D Breast Cancer Spheroids using Optical Coherence Tomography* (Accepted for Northeast Bioengineering Conference, 2020).
- **Fariha, R.**, Ip, B., Morgan, J., Lee, J. *Establishing Optical Coherence Tomography (OCT) as an Effective Method for Investigating Cellular Viability in 3D Breast Cancer Spheroids* (Presented at the Women in STEM Symposium (WiSTEM), 2019).
- Zakhem, E., Huleihel, L., Alasadi, H., **Fariha, R.**, LeBrun, A., Baker, H. B., Remlinger, N.T., Gilbert, T. W. *A Comparison of the Composition and In Vitro Macrophage Response between MicroMatrix® and AmnioFill®* (Presented at the Symposium of Advanced Wound Care, November 2018.)
- Huleihel, L., **Fariha, R.**, LeBrun, A., N.T., Gilbert, T. W. *The Effects of Processing on Urinary Bladder Matrix (UBM) Characteristics* (10th Symposium on Biologic Scaffolds for Regenerative Medicine, May 2018).
- Lin, L., **Fariha, R.**, Randolph, L., Lian, X. *Chemically Defined LaSR Medium Supports Long-term Cultivation of Human Pluripotent Stem Cells and Embryonic Stem Cells* (Penn State Research Symposium, March 2017).

Selected Honors and Awards

- Young Investigator Award (MSACL 2022, 2023)
- Brown Graduate Student Contribution to Community Life Award (2020)
- Brown Graduate Community Fellowship (2018-2020)
- Robert and Louise Dickinson Scholarship in Engineering (2015-2017)
- Outstanding Multicultural President of the Year (2015)
- Council of Fellows Leadership Scholarship (2015)
- Miss Blue and White (2015)
- Chancellor's Scholarship (2015)
- Penn State Outstanding First-Year Student of the Year (2013-2014)

Professional and Honor Societies

- Society of Women Engineers (SWE)
- Females in Mass Spectrometry (FeMS)
- American Association for Cancer Research (AACR)
- American Society for Mass Spectrometry (ASMS)
- Society for Laboratory Automation and Screening (SLAS)

- American Alumni Association (AAA)
- Lambda Sigma National Honor Society
- Alpha Epsilon Delta, National Honor Society
- Omicron Delta Kappa, National Leadership Honor Society

Selected Leadership and Outreach

- Early Career Committee, Society for Laboratory Automation and Screening (SLAS) 2023-Present
- Chair of International Advocacy, Brown Graduate Student Council 2023-2024
- President, South Asian Scholars in STEM (SASS) 2022-2024
- Mentor, Society of Women Engineers (SWE) 2017-2023
- Graduate Coordinator, Global Brown Center 2019-2020
- Student Assistant- International Orientation, Brown Graduate School 2019-2019
- Member, Brown International Student Advisory Board 2018-2020
- Community Fellow, Brown Graduate School 2018-2020

Teaching

Adjunct Professor Providence, RI
Brown School of Professional Studies September 2019- Present

- Led "Introduction to Engineering & Design" summer sessions each accommodating 24 students over 5 sessions, imparting a comprehensive understanding of the fundamentals of engineering and design processes.
- Independently devised the course module, crafted assignments, and guided students in modeling original pseudo-prototypes for class presentations.

Teaching Assistant Providence, RI
School of Engineering, Brown University September 2022- Present

- Oversaw the *"Biomedical Engineering Design and Innovation"* course as the Head TA, actively guiding and mentoring student project groups, totaling over 40 students.

Research Projects

Tripathi Lab, Brown University

- **Organoid on a Chip for Precision Medicine (in collaboration with Revvity Inc.)**
  - Developed an easy-to-fabricate organ-on-a-chip platform for epithelial ovarian cells, both cancerous and benign in co-culture, to study PARP-inhibitor uptake for model validation.
  - Adapted and validated a LC-MS/MS method and converted this method into the manufacturing of Research Use Only (RUO) kits to quantify the PARP-inhibitor presence in cellular microenvironment.
- **High-throughput Multi-Matrix Opiate and Opioid Quantification using Microsampling**
  - Established a clinical collaboration with the Haass-Koffler lab for Behavioral and Social Sciences at Brown University and formulated a serum-based LC-MS/MS kit to quantify the presence of opiates, opioids, and their impact on oxytocin-craving.
  - Created and validated a RUO blood-based LC-MS/MS kit for opiates and opioids quantification in dried blood spots (DBS).
  - Designed and customized highly scalable, automation and high-throughput ready device for electric-field application for rapid opiate and opioid extraction across patient DBS.
- **Methadone Quantification in Blood for Limited Access Facility Application**
  - Created a low-cost microfluidic sample preparation device for quantification of methadone in whole human blood in limited access facilities.
  - Designed, manufactured, and validated a blood-based LC-MS/MS kit to quantify analyte recovery as a measure of device accuracy.
- **Dried Blood Spot Sample Preparation Analysis of Steroids for PCOS Detection using LC-MS/MS**
  - Developed and validated a whole blood-based LC-MS/MS steroids assay.
  - Assessed the potential of DBS for PCOS detection using custom-created disposable vials to study steroids recovery using electric-field.

- **Alternative Matrix Study: Human Cerumen to Detect Cortisol for Stress Monitoring (in collaboration with PerkinElmer)**
  - Investigated the potential of cerumen (earwax) as a matrix for LC-MS/MS applications for long-term stress management.
  - Devised and streamlined a protocol for the use of artificial cerumen in RUO kit development.
- **Antidepressant Detection in Human Serum (in collaboration with PerkinElmer)**
  - Developed a novel small volume LC-MS/MS based assay for the detection of multiple antidepressants of therapeutic ranges in human serum.
- ***LC-MS/MS Application for in vitro to in vivo Extrapolation Analysis of 3D-Microtissues***
  - Conducted a dose and time-dependent study to understand the impact of extracellular absorbance of chemotherapeutics in 3-D Microtissue™ molds, and its subsequent impact on MCF7 breast cancer tissue viability.
- **Simultaneous Detection of Cortisol-Cortisone in Human Saliva (in collaboration with PerkinElmer)**
  - Streamlined and established an automated easy-to-use micro-level sample LC-MS/MS based assay for high-throughput screening for cortisol and cortisone in human saliva samples.
- **Low-level Testosterone Detection from Human Serum using LC-MS/MS (in collaboration with PerkinElmer)**
  - Adapted and streamlined a diagnostic assay prototype for LC-MS/MS based detection of low-level testosterone from human serum for high-throughput screening.
  - Prototyped and tested this assay in multiple clinical settings bringing this technology from bench to bedside.

ACell Inc. (Integra LifeSciences)

- **UBM Characterization Study**
  - Validated standard operating procedures (SOP) for porcine bladders decellularization and executed multivariable characterization (histology, DNA, RNA, and protein quantification) prior to animal testing.
  - Investigated the effect of UBM on macrophage activation *in vitro* via mice bone marrow derived macrophage isolation.
  - Synthesized cDNA for downstream qPCR assay and gene expression analysis to assess decellularization efficiency before large-scale manufacturing.
- **Competitor Product Study**
  - Identified key competitor products in the market and performed extensive literary analysis on them.
  - Assessed their usability and performed scientific validation on the products from a user standpoint.
  - Quantified the cellular components in collagen, porcine bladder, and human tissue-based competitor products, and their subsequent impact on *in vitro* cellular models.
  - Created SOP for future in-house testing of similar competitor products.
- **Degradation Study**
  - Investigated the rate of degradation of varying wound sheet products using enzymatic digestion model for stability analysis.
- **DNA Specification Test**
  - Performed test method validation and assay optimization for native DNA quantification for products prior to clinical trials.
- **Animal Study- Wound Study**
  - Examined different wound treatments (UBM and competitor products) in pig models via gene expression analysis.
- **Pericardial Patch Study**
  - Investigated Urinary Bladder Matrix (UBM) decellularization to create pericardial patch devices for large animal testing.

Selected Press, Media, and Speaking Engagement

- Invited Speaker, "Accessibility in the Lab: Embracing Identity and Authenticity with Ramisa Fariha", *New Matter* (Podcast), (2024).
- Invited Speaker, "DEI in the Lab." *Society of Laboratory Automation and Screening (SLAS)* Conference, Boston (2024).
- Interview "A Young Bangladeshi Woman led the Research that is Promising." *The Daily Prothom Alo* (newspaper), Bangladesh (2023).
- Featured "Brown researchers develop new, automated, powerful diagnostic tool for drug detection." *Eureka Alert, AAAS* (web) (2023), and *ScienMag* (web) (2023).
- Invited Speaker, "How Can We Use Our Positions of Privilege to Amplify the Voices of The Marginalized." *John Hopkins University* (2023).
- Invited Speaker, "STEM Careers for Girls: Daring to dream, Achieving Greatness." *Nerd Community, Bangladesh* (web) (2023).
- Invited Speaker. *Girls FIRST Walton Robotics Event*, USA (2022).
- Featured Engineer. *STEMHer Magazine*, 6th Issue, Amazon (2021).
- Invited Speaker. *Penn State Behrend Gender Conference*, USA (2021).
- Invited Speaker. *Girls FIRST Robotics Career Exploration Event*, USA (2020).
- Invited Speaker. *Cross Legged with Hira Mehta* (Podcast), Mumbai, India (2020).
- Interview "From Narayanganj to the Ivy League." *The Business Standard* (newspaper), Bangladesh (2020).
- Featured. *With a Science Degree* (web), USA (2020).
- Panelist, "Graduate and Professional School for International Students." Brown University Watson Institution for International and Public Affairs (2019).

Other Work

Brown Center for Biomedical Engineering — Providence, RI
Communications Intern — 2018- 2020

- Conducted interviews, attended seminars and developed news content for Brown Institution for Biology, Medicine, and Engineering (bylines available at https://www.brown.edu/academics/ibeam/home).

The Kaharba Productions — Dhaka, Bangladesh
Research Assistant and Junior Copywriter — 2012-2015

- Conducted pre-production research- including project analysis, feasibility, cost of production, etc. for documentary projects for clients such as UNICEF, US Embassy, SwissContact, and developed web content for the official website.

Admissions, Penn State, Erie — Erie, PA
Student Assistant — 2014-2015

- Maintained international student database, served as an office assistant, and worked at various events such as open houses, science fairs etc.

Acknowledgment

Even though I have been mentally curating my list of *thank you*s for a while now, in true Fari-fashion, this is the last thing I am putting together prior to submission. This is because I have been afraid to be vulnerable and letting go of the safety cocoon as a student. This is not the first time I am listing my gratitude to people around the world, but in all honesty, my doctoral dream would never have become a reality had it not been for my advisor Dr. Anubhav Tripathi. When every single door was closed for me during the COVID-19 pandemic, one email and a subsequent Zoom call with Dr. Tripathi changed my life. I have seen him vouch for me and be my biggest cheerleader in situations where I did not believe in myself as a scientist. In my short time with him, I have learned so much about managing up-and-down in STEM, how to thrive in a collaborative environment, and never saying 'no' to opportunities. While my Papa gave me wings in life to fly, Dr. Tripathi gave me the wings in science to fly. Just how Papa never stopped me from chasing my dreams, Dr. Tripathi never stopped me from being a crazy scientist. And for that, I am truly thankful. And not just him, I owe a big thank you to Lindsay, Cel, and Kiara for welcoming me to the lab with wide arms and being my confidants throughout the journey. And of course, nothing in my PhD would have ever seen the light of the day if it weren't for Collin Hill. Collin is one of the most gifted and kindest scientists you will ever meet, who knows more than most people and will still stay humble. Collin taught me the ABCs of mass spectrometry, and pretty much everything I needed to put this entire body of work together. Without his expertise and ears to listen to me crying about the QSight on a random Friday night, I don't think I would have survived this journey. Collin, my friend, you are a gem and a brilliant scientist that deserves a huge round of applause. And of course, I want thank

Jason Pfail, my QSight Engineer who have spent days fixing my instrument, and once I had evolved to be a handy man, he spent hours cheering me on through the phone (including the day of Thanksgiving) while I battled against that monster!

Science, of course, is never a one man show. A lot of the time, it takes the 'human side' of a scientist to understand another scientist and keep the gears turning. As a only STEM person in my family, my source of support, understanding and cheering through the *darkest days* (read: days where the data did not look as expected), I remember members of the scientific community who have helped me out. First and foremost, I want to thank Dr. Angus Kingon for being one of the truest yet kindest critics on planet Earth. While Angus was the last to join my thesis committee, he is always the first to ask how I am doing, and the first to offer help. Even during the world lockdown, Angus made sure to check in on me, and offered to help me in every possible way! Individuals like him have made Brown the institution that it is and will continue to bring us alumni back because we know that individuals like Angus exist who respect the human limitations of students. And this thank extends beyond him! A big thank you to Dr. John Marshall, Dr. Edith Mathiowitz, and Dr. Vikas Srivastava for all their love and support, always. Hearing a legend like Edith say, "You will be fine, my dear," is what kept me afloat amidst several meltdowns. I also want to thank Dr. Stefani Thomas- a fellow woman in STEM, and an inspiration. Stefani not only made it a duty to be a responsible external advisor to me, but truly paved the way for women of color to find their space in the world of mass spectrometry. She has helped me network with thought leaders in the field, and truly gave it her all to ensure that I learned and grew from my PhD experience. And finally, Dr. Carolina Haass-Koffler, my dearest

collaborator, educator, and unsung hero- thank you for having my back! Collaborating with you has been such a joyous experience, and I have learned more from you than I would have from taking a hundred courses! Your enthusiasm to mentor and help students perform their best has truly made a difference in my journey as a scientist. I am so thankful that you are a part of the scientific community, and I am looking forward to future collaborations with you! And of course, I want to thank Andrew Creamer- the best librarian in the universe- without whose constant support to my quixotic article requests at the oddest hours, this thesis would be truly incomplete.

In addition to all these wonderful individuals, I want to thank several other scientific mentors who have helped my PhD work possible: Dr. Donald Chace and Dr. Timothy Garrett- for educating me about microsampling, Grace Van Der Gugten- for listening to my rant on steroids and being the best scientific sounding board in the world, Dr. David Colquhoun- for being a true joy and helping me embrace my authentic self in STEM. Also special thanks to Dr. Marissa Jones and Dr. Emily Britton for being my career coaches and for truly showing me what 'giving back' means as a female in mass spec.

Now that I have thanked people who have coached and taught me, I want to thank people who have made the work for this thesis happen- my colleagues and co-inventors. Firstly, John Murphy a.k.a. Santa Claus- you are a beast! You have made all my visions into reality, and given me the speed I needed, and the encouragement I needed when the world came crushing down. Even when you did not need to, you spent countless hours hand-tightening those tiny screws because I wanted to 'automate' everything. Thank you for encouraging

me to dream and helping my dreams come to reality. To my students- my kids- my colleagues- Mohannad, Adam, Emma, David, Nondi, Farhan, Prutha, Ells, and Jad- you have all played instrumental roles in making all our 'innovations' happen. I have learned so much from each one of you, and you have all brought me so much joy during our time together. Kids, you are all incredibly talented, and know that I have always got your back. I hope you all come across someone in your life who will bring you the same pride, joy, and love, as you have brought me. And not just you all, I am thankful to your families, especially Emma and David's mothers, for being a mother figure to me during this journey, and for always showering me with so much love and blessings. Additionally, I want to thank the village of people who helped me keep my life together (within and outside the lab) at Brown with their consistent hard work (and I want to say 'love' for me, because let's face it, you all laughed at my jokes): Dr. Kofron, Dr. Gray, Dr. Ip (Blanche), Dr. Shukla, Dean Russell, John Lee, Carolyn, Lori, Jess, Melodie, Candace, Beth, Dary, Bob, Weibin, and the entire ecosystem of wonderful human beings who keep the School of Engineering system afloat. You all deserve so much love and appreciation!

In case you have ventured into my dissertation, and for some odd reason you are reading this, I do not want to bore you with more names since they will not mean anything to you anyway. However, my story will be incomplete if I do not thank those who mean more to me than life itself. I want to thank almighty Allah for giving me my family, without whom none of this would be possible. Maa, thank you for being my hero, my alarm clock, my rock; thank you for sacrificing your dreams so I could live mine. Papa, thank you for giving me everything you have- and more- and for raising me to be my authentic self. Bhaiya,

thank you for being you, and for everything you have ever done for me- including giving me Bhabi and Aarish. Maa, Papa, Bhaiya, Bhabi, and Aarish- we have done it! We are all doctors.

To Dadu and Baba- two of the most loving individuals who have been my biggest cheerleaders ever- I am sorry for not being there when you needed me. Sorry that I could not come to say bye to you. But I know that you are both so proud of me. Baba- thank you for teaching me what a screw and what a wrench is- you have made me an engineer. Dadu- thank you for teaching me everything- including how to spell my name. I really miss you both so much.

And of course, to my friends and other members of the family- thank you. I had every intention of not naming people, but of course, I have to thank Julian for actually sitting down on Zoom calls with me- helping me survive the stats-apocalypse, watching my cry and put this dissertation together, and being my human-version of lavender tea. Thanks, brother, for helping me make sense as I put words into paper with Papa at the hospital. This thesis would have never seen the light of the day if you had not been my personal human-GPT.

Speaking of which- shout out to the doctors at the Miriam Hospital for keeping my Papa alive and in one-piece as I toiled through my dissertation and defense.

Okay, so to summarize thank you to Allah, my family, my friends (you are ALL very important to me), my colleagues, my advisor, my thesis committee, my students, and members of the Brown Community. And yes, Albert (my therapist), and Tanya (my doctor)- thank you for keeping me alive. Oh, and Tony at Heng Thai for the food, and Red Bull. In all honesty, you all should officially rename yourselves to Dr. Heng Thai and Dr. Red Bull.

I love you all. Thank you for being a part of my story.

Abstract

Despite the existence of metabolomics as a field for nearly two decades, challenges of sample preparation limit the large-scale application and throughput of targeted metabolomics for tier-2 diagnostics. In-depth understanding of the sample microenvironment can enable workflow simplification of clinical samples, especially micro-scale samples, or microsamples, and help us develop technologies for immediate clinical translation. This includes addressing the issues of sample volumes, sample transport, and the cost associated with assay development. With our understanding of the current state of clinical metabolomics in the United States, and the challenges associated with microsample analyte recovery for liquid chromatography tandem mass spectrometry quantification, we have performed several analyses leveraging this technology to advance its capabilities for clinical diagnostics. Combining engineering principles with the knowledge of clinical chemistry, we present innovations that can alter the landscape of sample preparation methods and their subsequent automatability for patient sample testing.

Table of Contents

Chapter 1: Introduction

1.1. Motivation

Each year, a staggering 5.7 to 8.4 million deaths, constituting approximately 15% of fatalities in low- and middle-income countries, are attributed to inadequate healthcare quality [1]. Notably, global preventable newborn deaths number around one million, underscoring the critical role of high-quality patient care [1]. This issue is particularly pronounced in focus regions like Southeast Asia, where evidence-based interventions in healthcare quality are paramount [2]. The pervasive challenge of limited access to advanced medical technologies in these regions remains a significant impediment to transforming healthcare delivery. Even in high-income countries, the alarming statistic that 1 in 10 patients experiences harm during hospital care necessitates urgent attention [1]. Consequently, there is an imperative for the development of non-invasive, accurate diagnostic strategies applicable to a diverse range of diseases, including metabolic disorders, reproductive diseases, and substance abuse [3].

This underscores the acute necessity to enhance the front-end sample processing techniques for specimens collected both within the United States and globally, with the goal of facilitating more robust quantitative data generation. The focal point of this dissertation is the utilization of small volumes (microsamples) of various biofluids, such as blood, serum, plasma, saliva, cerumen, and dried blood spots, for clinical metabolomics applications. Metabolomics, elucidating the small molecules governing disease phenotypes, serves as the linchpin of this translational research, addressing current limitations across a spectrum of disorders. The innovative approach involves liquid chromatography tandem mass spectrometry (LC-MS/MS)-based analysis of metabolites, seamlessly interfacing with robotic liquid handling systems to achieve high-throughput outcomes.

1.2. Clinical Metabolomics for Screening and Diagnosis

Amidst the escalating global challenges posed by both infectious and noninfectious diseases, the prevailing paradigm in medical care predominantly emphasizes post-disease

intervention rather than proactive prevention [4]. The intricacies of human biology, characterized by inherent heterogeneity influenced by genetic, environmental, and lifestyle factors, underscore the critical need for individual "omics" analyses. These encompass genomics, transcriptomics, proteomics, metabolomics, and lipidomics, collectively recognized as paramount in unraveling the nuanced molecular complexity of diseases and monitoring their progression over time [5].

In the realm of cutting-edge advancements and innovations, the prospect of examining multi-omics data at the individual patient level has emerged, although its large-scale clinical implementation remains in the nascent stages [6]. Within the diverse landscape of "omics" studies, the exploration of the complete set of metabolites, known as the metabolome, from a specific sample stands out as a profound avenue. This approach provides a unique vantage point to comprehend the regulation of the genome, transcriptome, and proteome, thereby influencing the manifestation of disease phenotypes.

Strategic efforts have been dedicated to integrating metabolomics into traditional epidemiologic research and personalized medicine, aiming to broaden the horizons of data applicability for targeted clinical metabolomics diagnostics [7-9]. This concerted endeavor opens new frontiers in understanding and harnessing the potential of individualized molecular profiles, paving the way for transformative applications in the scientific and medical communities.

1.3.Sample Preparation: Current State, Challenges and Innovations

One advantage of clinical metabolomics is that any available biospecimen can be tested for its potential to serve as a diagnostic matrix. This can be sweat, tear, earwax, saliva, serum, whole blood, or ascites [10, 12]. Limitations, however, exist in that the bioavailability of different metabolites vary greatly in different source materials, and not all of them are extensively investigated to establish concentration ranges for targeted metabolomics analysis [11]. This becomes an even bigger challenge in the development of Tier-2 diagnostics, i.e., wherein

laboratories receive samples to generate confirmatory data of the finding from Tier-1 tests, often requiring complicated workflows and sensitive instruments [13]. While whole blood is the ideal diagnostic material, the trauma associated with sample collection, as well as elaborate and expensive workflows cumulatively demand for non-invasive sample collection methods and simpler workflows. This expands beyond whole blood to almost any biofluid that requires special donors and processing to be utilized as a base matrix [15 16]. As a result, not only it is crucial to development diagnostic assays and protocols that require a small patient volume for disease detection, but it is also important to develop sample preparation methodologies that can provide highly specific and accurate results from small standard reference materials as well (for example, Chapter 2 highlights the use of artificial saliva to create diagnostic prototype for Congenital Adrenal Hyperplasia detection). One way of achieving this would be to manipulate the microenvironment of the metabolites, i.e., their milieu in the sample source to enhance analyte extraction. This can be done through introducing engineering strategies to impact the viscosity, momentum, and microfluidic flow within a system, especially via the introduction of novel concepts, designs, and devices. Different chapters throughout this thesis describe how a sample microenvironment can be best triggered to work with microsamples, especially dried blood spots, of different biospecimens to detect different disorders in targeted metabolomics assays.

1.3.1. Unlocking the Potential: Microsampling with Dried Blood Spots (DBS)

Dried Blood Spots (DBS) represent minute samples of venous blood collected onto absorbent filter paper, a technique pioneered by Dr. Robert Gutherie and Dr. Ada Susi in 1961 for detecting phenylketonuria (PKU) in newborns. Over the years, DBS has evolved as a versatile tool, offering advantages such as minimal invasiveness, low blood volume requirements, and cost-effectiveness in collection, transport, and storage. Widely adopted for diverse applications, DBS

finds utility in detecting HIV, hepatitis B and C, metabolic disorders, toxicology, drug distribution, genetic studies, pollutant exposure tracking, clinical biomarker measurement, and drug adherence monitoring [17].

Despite technical advancements enhancing DBS processing and analysis, persistent drawbacks, such as hematocrit and chromatographic effects, restrict their applicability in certain fields. DBS, however, possesses the unique ability to serve as a good source of diagnostic matrix for use in low-resource settings or low-income communities [18-20]. Particularly in areas lacking infrastructure for large-scale sample storage, DBS emerge as an alternative with less stringent requirements for collection and analysis, allowing needle pricks at any location in the body and eliminating the need for controlled temperature storage.

Researchers leverage DBS to detect infectious diseases, including HIV-1, HCV, HSV DNA, and leishmaniasis, showcasing their efficacy in identifying infections even in asymptomatic patients. Large-scale testing facilitated by DBS enables early detection, treatment, and risk reduction, minimizing the development of infections. Immune biomarkers present in known diseases are employed to test newborns, offering insights into their likelihood of developing similar conditions [20-22]. With these advancements, DBS serves as a transformative tool for implementing widespread testing in low-income areas and conducting comprehensive large-scale newborn screening for complex diseases and infections.

1.3.2. Laboratory Automation

Laboratory automation has been a crucial driving force behind the advancement of scientific research and development across numerous industries. The increasing demand for high-throughput, precise, and reproducible experimental workflows has led to the development of

technologies such as robotic liquid handling systems, which have revolutionized laboratory processes by enabling the precise and automated dispensing of liquids in various applications [23].

Robotic liquid handlers are sophisticated instruments designed to automate liquid transfers, sample preparation, and assay workflows with unparalleled precision and accuracy. They are indispensable tools in diverse fields such as pharmaceuticals, biotechnology, genomics, proteomics, drug discovery, and clinical diagnostics [24]. These systems have played a major role in accelerating research and development, making it possible to process large volumes of samples efficiently and consistently.

The foundation of robotic liquid handlers lies in their sophisticated engineering, which involves precision robotics, pipetting mechanisms, and advanced software algorithms. The robotic arms equipped with multi-axis movement capabilities enable them to access multiple locations within a laboratory workspace accurately. Meanwhile, various types of liquid handling technologies, such as air displacement and positive-displacement pipetting, ensure precise liquid transfers with minimal risk of cross-contamination.

Modern robotic liquid handlers boast a myriad of functionalities that cater to a wide range of experimental needs. These systems can accommodate various labware formats, such as microplates, tubes, and vials, making them versatile for different assays. They can perform tasks such as liquid dispensing, sample dilution, plate replication, reagent addition, and serial dilutions [23, 24]. Additionally, some robotic liquid handlers integrate features such as temperature control, magnetic bead-based separations, and centrifugation, enabling more complex, complete, and integrated workflows.

The impact of robotic liquid handlers on biomedical research has been extraordinary. These systems have enabled researchers to conduct high-throughput screenings of drug compounds,

genotyping, nucleic acid extractions, and protein quantification with unparalleled efficiency and reproducibility. The automation of such laborious and error-prone tasks has led to significant time and cost savings, allowing scientists to focus on data analysis and interpretation rather than pipetting and stirring.

One of the most critical aspects of robotic liquid handlers is their ability to achieve precise and accurate liquid transfers. With advancements in technology, modern systems can handle volumes ranging from microliters to milliliters, with negligible variation in the dispensing volumes. This precision ensures that experimental results are reliable and reproducible, reducing the risk of experimental errors.

Another vital aspect of robotic liquid handlers is their integration with other laboratory automation equipment, such as plate readers, incubators, and robotic plate handlers. Such seamless integration streamlines the entire workflow, from sample preparation to data analysis, providing an end-to-end solution for researchers. Moreover, these systems often come with customizable software, allowing users to tailor protocols to their specific needs and experimental requirements.

Robotic liquid handlers have emerged as critical tools in modern laboratories, significantly enhancing research productivity, reproducibility, and efficiency [25]. The combination of precision engineering, advanced software, and diverse functionalities has revolutionized laboratory automation, making it possible to tackle complex experiments at an unprecedented scale. As a result, several chapters in this thesis focus on the integration of robotic liquid handlers in enhancing sample preparation and bringing about faster experimental results in the diagnostic world.

1.4.Summary

This thesis focuses on the field of clinical metabolomics, in tandem with workflow simplification and how microsampling can be best utilized for tier-2 metabolomics diagnostic

assay development for reproductive and newborn screening. This includes the investigation of the ongoing clinical metabolomics field in the United States and coming up with possible solution for immediate clinical adaptation.

Chapter 2 provides a potential base matrix solution to develop an assay utilizing passive drooling saliva to simultaneously quantify cortisol and cortisone to detect congenital adrenal hyperplasia (CAH). This study highlights the higher bioavailability of cortisol-cortisone in saliva as opposed to blood and serum, and how easy dilute-and-shoot workflows can still generate highly precise and accurate readouts of these small molecules.

Chapter 3 looks at a more complicated matrix, serum, for an accurate quantitative measurement of four different classes of antidepressants commonly prescribed to combat post-partum depression. The innovation of this work looked at utilizing a microsample of serum, 20 μL, to quantify 8 different analytes accurately and simultaneously, thereby enabling a constant monitoring of different metabolites in the body and prevent them from reaching alarming concentrations to be passed on to the infants via breastmilk. This work also proposed a possible solution of at-home blood sample collection to isolate a minute volume of serum for application, making the monitoring process easier and flexible for mothers tending to newborns.

Chapter 4 and 5 both look at non-derivatized assay development for steroids detection. Chapter 4 showcases the use of electric field to draw four different steroids out of standard DBS samples from adults and introduces the potential of DBS samples as a screening method for early onset development of polycystic ovary syndrome (PCOS), especially for those in limited resource areas where expert healthcare professionals are not easily accessible. Chapter 4 highlights the use of additional optimization of the mass spectrometry parameters to make non-derivatized steroids detection possible in a simple LC-MS/MS workflow. Chapter 5, on the other hand, discusses in

depth the application of the most basic robotic liquid handlers, and their efficacy in sample preparation for total testosterone quantification in human serum. This chapter showcases easy solutions to automate sample preparation protocols for clinical samples, and its ability to improve clinical assay precision.

Chapter 6 highlights a unique application of metabolomics, and tier-2 diagnostic assays can proactively assist qualitative research studies by generating robust quantitative data in a multiplex assay. This chapter provides a confirmatory result to assess the impact of noradrenergic stimulation (oxytocin and yohimbine) on drug concentration availability in patient serum over time. Because patients who abuse opioids are difficult to draw samples from, this work uses 20 μL of serum to quantify six opioids (quantifier and qualifier fragments) in an automated workflow with 3.5 minutes per sample run.

Chapter 7 combines the findings of Chapter 4 and Chapter 6 to introduce a quantitative solution for Neonatal Abstinence Syndrome (NAS) detection. To address sample accessibility and limitation issues, the approach behind this study was to utilize a 3.2 mm DBS sub-punch in a custom 96-array electric-field apparatus to extract five different opioids in a fully automated workflow, and in a process ten-times faster than current gold standard processing methodologies for DBS samples. This specific study establishes the potential of cylindrical electrodes as a driver for biospecimen sample preparation and presents the computational modeling that created the basis of this work.

Unlike the previous chapters, Chapter 8 expands the potential of targeted metabolomics application beyond clinical diagnostics, for organoid platform characterization and improving the *in vitro* pharmacokinetic studies for more accurate *in vivo* extrapolation drug studies (IVIVE), especially for patient-specific tissues. At present, most IVIVE studies depend on theoretical values

to assess the drug efficacy in 3-dimensional tissue aggregates. With our ability to optimize sample preparation methods, we were able to utilize cell culture supernatants to establish the true concentration of drugs reaching breast cancer cell organoids, and how outcomes of current IVIVE analysis may be inaccurate.

Finally, Chapter 9 concludes the thesis with a summary of the work, its immediate impact, future directions and recommendations.

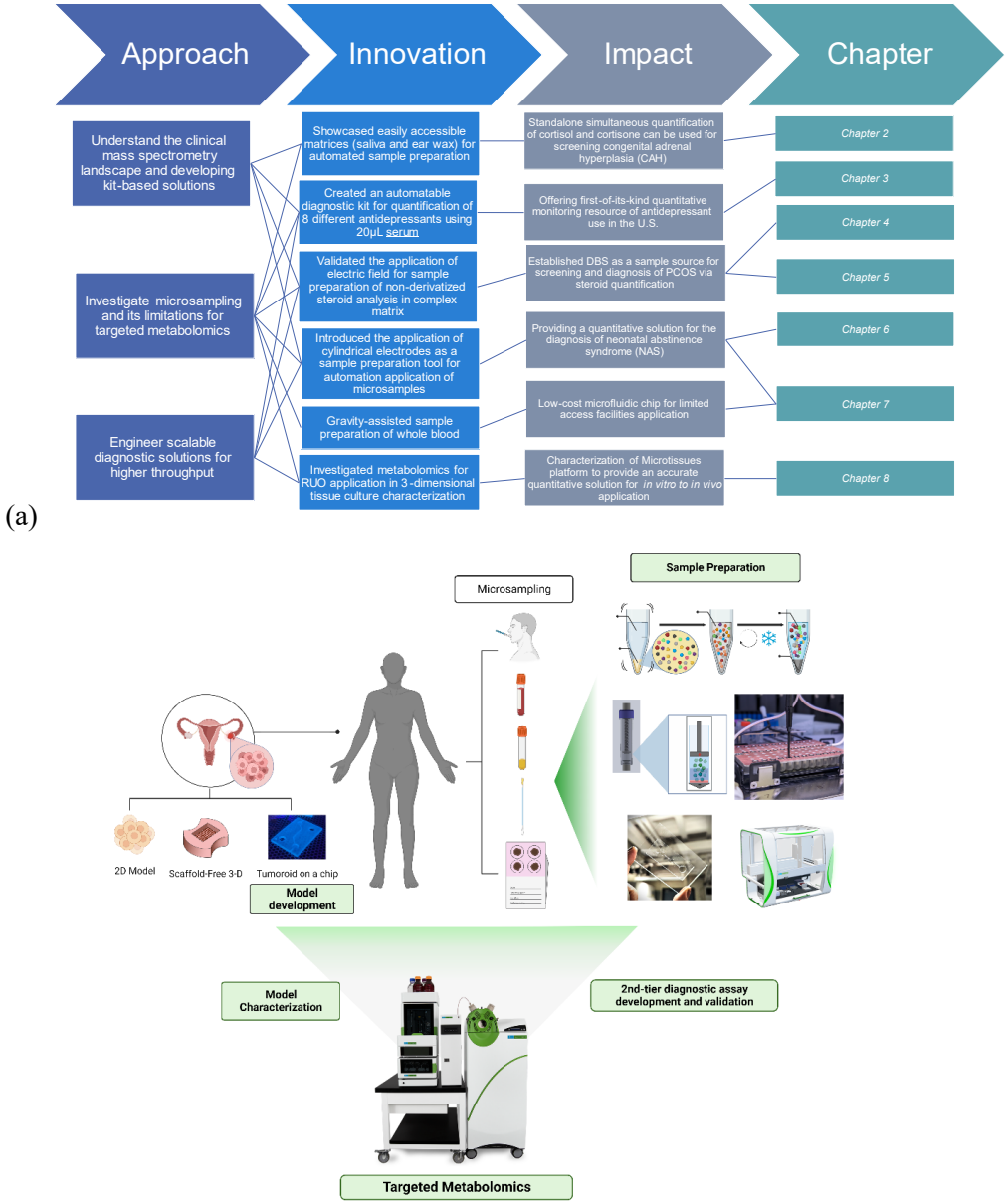

Figure 1 (a) Schematic showing the approach driving the work behind this thesis and its contribution to the field; (b) shows an illustration of 1(a) including showcasing the physical devices created throughout the development process.

Chapter 2: Simultaneous detection of Salivary Cortisol and Cortisone using an Automated High-throughput Sample Preparation Method for LC-MS/MS

Chapter 2 has been published as an original research article.

Fariha, R.[1], Jabrah, M.[1], Hill, C.[2], Spooner, A.[1], Deshpande, P.[1], Tripathi, A.[1].

Simultaneous detection of salivary cortisol and cortisone using an automated high-throughput sample preparation method for LC-MS/MS. *SLAS Technology*. 2022;27(4):237-246.

doi:10.1016/j.slast.2022.01.006

1. Center for Biomedical Engineering, School of Engineering, Brown University, 182 Hope Street, Providence, RI- 02912, USA
2. PerkinElmer Inc., Waltham, MA

2.1.Abstract

High-Performance Liquid Chromatography-Tandem Mass Spectrometry has emerged triumphant over the years as a reliable and high throughput clinical instrument to assess different metabolic irregularities. One of the latest applications of LC-MS/MS has been in the field of quantification of glucocorticoids, such as cortisol and cortisone from saliva, that can be an indicator of abnormalities such as Congenital Adrenal Hyperplasia (CAH), Cushing's Syndrome, and Addison's disease. We have developed and validated an LC-MS/MS-based assay for simultaneous detection of cortisol and cortisone in human saliva, which requires only 20 µL of sample, to measure cortisol across a 0.5 – 70 ng/mL range, and cortisone across a 1.2– 100 ng/mL range, respectively. The developed method exhibits linearity of R2>0.99, for both analytes, inclusive of both MRMs, and a percent coefficient of variation that is less than or equal to 20%. Using dilute-and-shoot for sample preparation, we have exhibited sample accuracy of 100±20 for the assay calibrators, and integrated Needle Wash Solvent Chemistry for minimal sample carryover, making it adaptable for crucial for potential diagnostic use. We have exhibited a method that is simplistic, specific, and highly automatable on liquid handling platforms, such as the JANUS® G3 Workstation. With our innovation, we have introduced a potential to test 81-unknown samples in singlicate within an on-deck plating time of fewer than four minutes. We performed additional verification studies, including an accelerated stability study and a freeze-thaw study showcasing the potential long-term usability of our proposed prototype kit. Overall, this work presents an optimized LC-MS/MS method with automated sample preparation that is ready to be utilized for cortisol-cortisone detection for clinical diagnostic contexts related to Cushing's Disease, among other adrenal and endocrine disorders.

2.2.Introduction

Glucocorticoids (GC), an important class of lipophilic, fat-soluble steroid hormones, regulate a wide variety of physiological functions. GCs modulate numerous processes including mood and cognitive function, growth, reproduction, and development, immune responses, as well as cardiovascular regulation [26, 27, 28]. As a result of this functional diversity, human GC nuclear receptors are expressed ubiquitously throughout the body and in all organs and tissues [29]. Two notable examples of endogenous glucocorticoids are cortisol (**C_F**) and its inactive form, cortisone (**C_E**).

Cortisol, widely known as the stress hormone, is synthesized in, and released from the adrenal cortex, resulting in elevated heart and respiratory rates. These are characteristic of the stress responses, which are triggered because of stressful stimuli that cause the hypothalamus activation of the hypothalamus-pituitary-adrenal (HPA) axis [30]. Elevated levels of cortisol trigger metabolic pathways in the liver, pancreas, and adipose tissue that are responsible for maintaining glucose and protein balance throughout the body [31]. High cortisol signals for increased gluconeogenesis and decreased glycogen synthesis and in the liver and for lipolysis in adipose tissue. Moreover, in the presence of high levels of cortisol, muscle cells decrease glucose uptake and consumption and shift towards increased protein degradation to provide the glucogenic amino acids necessary for gluconeogenesis [32, 33].

Dysregulated levels of cortisol and cortisone may arise from abnormalities in glucocorticoid-activating enzymes such as 11 β-hydroxylase and 21-hydroxylase deficiencies. The latter examples can take place in Congenital Adrenal Hyperplasia (CAH), as well as other inflammatory, psychiatric, and metabolic disorders [34, 35]. Similarly, Cushing's disease and Addison's disease are both prominent adrenal disorders where clinical testing showcases clear signs of irregular levels of corticosteroids [36, 37]. Circulating cortisol-cortisone can therefore

function as biomarkers that allow for the detection and monitoring of chronic stresses, adrenal disorders, and more.

Herein, we have developed and validated a clinical method for metabolic irregularity assessment that utilizes a simple dilute-and-shoot protocol for the analysis of circulating cortisol-cortisone via Liquid Chromatography-Tandem Mass Spectrometry (LC-MS/MS) in saliva. LC-MS/MS is a clinical analytical technique that has matured over the past decade, becoming the gold standard in many biochemical-diagnostics [38, 39]. LC-MS/MS brings many advantages over other analyte detection alternatives, such as ELISA and immunostaining [40]. Among other advantages, LC-MS/MS provides the ability to accurately quantify analytes at low concentrations while maintaining high analyte specificity and exhibits superior sensitivity over other analytical techniques. This is critical in the context of cortisol-cortisone, where high cross-reactivity is frequently observed in immunoassays [41, 42]. The proposed protocol was optimized to measure salivary analyte levels, as salivary cortisol-cortisone levels are similarly indicative of free cortisol in plasma, serum, and urine [43]; however, saliva is easier to obtain and carries fewer disadvantages [44-46]. For example, attempts at quantifying free-cortisol from urine samples encounter heightened matrix effects, due to high amounts of endogenous impurities, leading to ion suppression and loss of sensitivity [46-48]. Plasma samples require more complex sample preparation protocols, often necessitating a solid phase extraction step that reduces high-throughput capacity and increases processing costs per sample. Lastly, simultaneously measuring cortisol-cortisone from plasma may potentially yield misleading results [39], due to the 8:1 ratio of cortisol: cortisone in plasma, as opposed to the 1:2 ratio in saliva [45, 46]. The 11β-hydroxysteroid dehydrogenase in the salivary glands aids the conversion of unbound cortisol to cortisone, leading to this vast difference in abundance. Therefore, saliva is highly indicated as a

diagnostic matrix for rapid diagnosis of diseases affecting the adrenal glands via assessment of circulating glucocorticoids.

Plasma as a means for detecting free cortisol demands a sample preparation process of a higher degree of complexity due to an often-required solid phase extraction procedure that reduces the high-throughput capacity of the proposed method, as well as increases the cost of processing per sample. Lastly, measuring cortisol from plasma may potentially yield misleading results due to its measurement of the total amount of cortisol, including bound cortisol [47]. Ultimately, this encourages the utilization of saliva as a means for rapid recognition, diagnosis, and treatment of diseases affecting the adrenal glands by accurately evaluating circulating glucocorticoid levels.

The present work focuses on optimizing streamlined sample preparation and LC-MS/MS analysis method that avoids the need for error-bound extraction steps (liquid-liquid extraction, solid-phase extraction, etc.) often found in other protocols. This reduces the complexity of the sample preparation process, allowing for a more streamlined and high-throughput automation using conventional robotic liquid handlers, with minimal needed human interaction. Overall, as shown in Table 2, the methodology of this work focuses on a rationalized and simplified approach, while maintaining the linearity of analyte detection with relevant clinical ranges of disease. The proposed method exhibits an excellent range of linearity for established salivary cortisol for CAH, dexamethasone suppression, ACTH stimulation, Syndrome of Apparent Mineralocorticoid Excess (SAME), and other metabolic disorders [48-50]. The proposed protocol has the potential to be utilized as a high-throughput research-only kit, that can measure the free cortisol-cortisone in human saliva with great precision and accuracy using only a 20 µL patient sample volume, across the range of 0.5 to 70 ng/mL ($\mathbf{C_F}$) and 1.2 to 100 ng/mL ($\mathbf{C_E}$) distributed across six calibrators and low and high-Quality Controls (QCs).

Table 1 a) A comparative study of our method against existing literature. It is important to note that our proposed method targets a more clinically relevant range, unlike the other studies.
Table 1. b) Reference range for targeted metabolic disorders for CF and CE, pertaining to genders assigned at birth and infants.

Step	Fariha et al. (2021)	Bakusic et al. (2019)	Magda et al. (2017)	Antonelli et al. (2015)	Fustinoni et al. (2013)
1	Sample Pre-treatment: Thaw samples to room temperature; Centrifuge at 4600 rpm for 10 minutes to collect clear solution	Sample Pre-treatment: Centrifuge at 2000 xg for 5 minutes; store at -80 ºC; thaw before use	Sample Pre-treatment: Centrifuge at 2000 xg for 10 minutes; store at -20 ºC; thaw before use	Sample Pre-treatment: Centrifuge at 2000 xg for 10 minutes; store at -80 ºC; Centrifuge at 2000 xg for 10minutes; thaw before use	Sample Pre-treatment: Centrifuge at 3000 rpm for 5 minutes; store at -20 ºC (in the dark); thaw before use
2	Sample Conditioning: Sample (V=20 µL) + IS (V= 120 µL) [Total V= 140 µL]	Sample Conditioning: Sample (V=200 µL) + IS (20 µL) + Water (V= 800 µL) [Total V= 1020 µL]	Sample Conditioning: Sample (V=250 µL) + IS in ethyl acetate (V= 750 µL) [Total V= 1000 µL]	Sample Conditioning: Sample (V=300 µL) + IS (V= 30 µL) + Methanol (V= 1000 µL) + Water (V= 1000 µL) [Total V= 2330 µL]	Sample Conditioning: Sample (V= 500 µL) + IS (V= 5 µL) [Total V= 505 µL]
3	Dilute and Shoot: Shake at 800 rpm at 50ºC for 10 minutes	SPE via PRiME HLB cartridge [V= 1000 µL]	LLE: Vortex for 2 minutes	SPE via Oasis HLb cartridge [V= 250 µL]	LC-MS/MS (with TurboFlow)
4	LC-MS/MS	Sample Wash: 500 µL water:methanol (95:5 v/v)	5 minutes incubation (room temp.)	Sample Wash: 500 µL water:methanol (80:20 v/v)	N/A
5	N/A	Extraction w/ 500 µL methanol	700 µL separation	Extraction w/ 250 µL methanol	N/A
6	N/A	Extraction w/ 500 µL methanol	Evaporation	LC-MS/MS (with on-line SPE)	N/A
7	N/A	Evaporation	Reconstitution: 700 µL ethanol [+ Derivatization]	N/A	N/A
8	N/A	Reconstitution: water:methanol (50:50 v/v) in 0.1% FA (V= 1000 µL)	LC-MS/MS	N/A	N/A
9	N/A	LC-MS/MS	N/A	N/A	N/A

Results	LoD: C_F = 0.5 ng/mL C_E = 1.2 ng/mL	LoD: C_F = 0.02 ng/mL C_E = 0.02 ng/mL	LoD: C_F = 0.002 ng/mL C_E = 0.005 ng/mL	LoD: C_F = 0.07 ng/mL C_E = 0.04 ng/mL	LoD: C_F = 0.10 ng/mL C_E= 0.10 ng/mL

b)

Clinical Ranges of Cortisol-Cortisone in Different Metabolic Disorders			
Disorder	**C_F (Cortisol)**	**C_E (Cortisone)**	**Reference(s)**
Congenital Adrenal Hyperplasia (CAH)	0.5-2410 nmol/L	0.8-134nmol/L	Bacila, Irina, et al. [42]
Dexamethasone Suppression (Oral Dexamethasone at 0.015 mg/kg body weight for normal-weight individuals)	**Men:** 24.6 ± 7.4 nmol/L **Women:** 25.1 ± 23.2 nmol/L	Not Investigated	Pasquali, Renato, et al. [43]
ACTH Stimulation (250µg administration)	6.7–23.0 nmol/L	Not Investigated	Ospina, Naykky Singh, et al. [44]

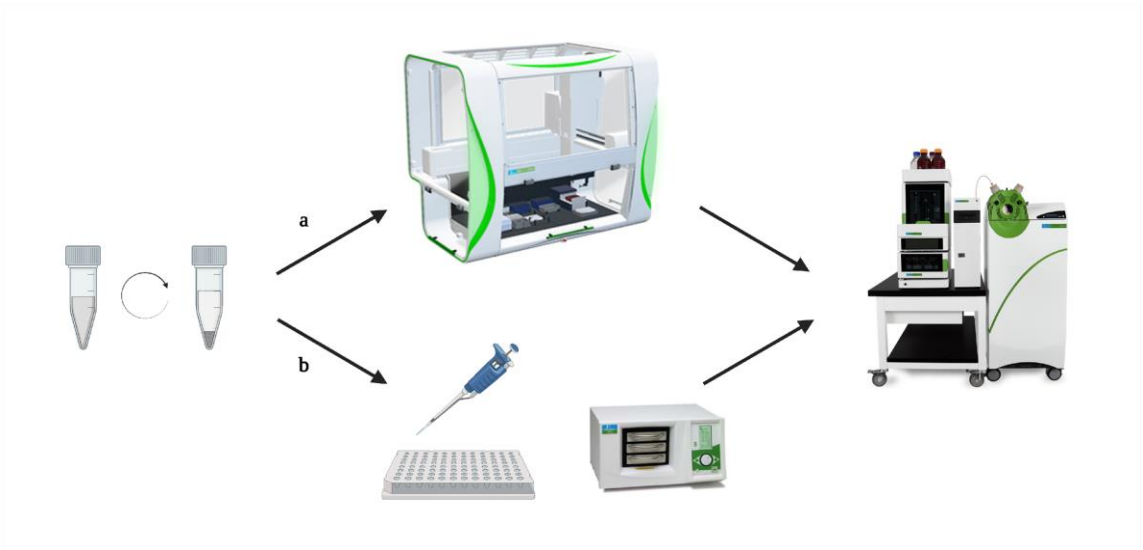

Figure 2. Sample pre-treatment, followed by automated plating (a) and manual plating (b), before LC-MS/MS analysis. For a, every action barring from pre-treatment can be carried on deck, whereas b requires more human input, including utilizing a temperature- controlled shaker.

2.3.Experimental

2.3.1. Chemicals and Reagents

Baker Analyzed HPLC grade water, acetonitrile, and methanol (>99.9% purity) were obtained from VWR for the preparation of calibrators, test samples, and the equilibration of the chromatographic column to avoid particulate matter that might potentially affect LC-MS/MS performance. Ampules of primary analytes of study – Cortisol ($C_{21}H_{30}O_5$, MW= 362.46 amu), Cortisone ($C_{21}H_{28}O_5$, MW= 360.44 amu), Cortisol-D_4 (internal standard) ($C_{21}H_{26}D_4O_5$, MW=366.48 amu) and Cortisone-$^{13}C_3$ (internal standard) ($C_{18}{}^{13}C_3H_{28}O_5$, MW= 363.42 amu) were purchased from Cerilliant Corporation (Round Rock, TX, USA). Reagent grade formic acid was obtained from Sigma-Aldrich. UTak SMX Oral Fluid (Valencia, CA) was used as the base matrix to create the calibrators and QCs.

2.3.2. Preparation of Calibrators, Quality Controls, and Stock Solutions

The cortisol and cortisone stock solutions were initially used to prepare *spike solutions*, using a two-step dilution method. This was done to ensure a 2.5% or less volume percentage of methanol across all calibrators and QCs, yielding five *spike solutions* for cortisol and six for cortisone, respectively. The UTak SMX Oral Fluid was then spiked using these *spike solutions* to create the calibrators and QCs, covering a concentration range of 0.5-70.0 ng/mL (**C_F)** and 1.2-100.0 ng/mL (**C_E**). Calibrators, as well as QCs, were aliquoted and stored at -80°C before starting any system suitability study. Additionally, a temperature-controlled centrifuge step (4°C, at 4600 RPM) was added to the protocol and investigated as a pre-treatment condition to emphasize solid particulate pellet formation, to prevent system clogging after injection of calibrators and QCs in LC-MS/MS.

Daily Working Solution (DWS) was prepared in a 50:50 (v/v) solution of HPLC water to HPLC methanol, with the final concentration at 1.7 ng/mL and 1.3 ng/mL for cortisol and

cortisone, respectively. The DWS was stored at -20°C and was warmed to room temperature prior to each assay.

2.3.3. LC-MS/MS Conditions and Optimized Parameters

The cortisol and cortisone analytes were diluted 10,000- and 1000-fold respectively, in HPLC-grade methanol before being directly infused into the MS to quantify the parent mass, quantifier fragment, and qualifier fragment masses. This was also repeated with the corresponding analyte internal standards, diluted 100 folds in HPLC-grade methanol. The compound transition data, together with the Entrance Voltage (EV), Collision Cell Energy (CC), and Collision Cell Lens 2 (CCL2) values obtained from Multiple Reaction Monitoring (MRM) optimization, are available in Supplemental Table S1.

After MRM optimization, the nebulizer gas pressure, source temperature, HSID (hot surface-induced desolvation) temperature, and drying gas pressure were also optimized to obtain the best relative intensity for both Q3 masses of the analytes and their internal standards. After the Q1 and Q3 masses were detected, the EV, CC, and CCL2 values were re-optimized for the best signal of the analyte quantifier, qualifier, and internal standards. The LC-MS/MS system used was a PerkinElmer QSight® 200-series Triple Quadrupole Mass Spectrometer, equipped with an Electron Spray Injection (ESI) source in using positive ion mode. Integrated to the MS was a QSight LX50 Solvent Delivery Module, QSight LX50 Precision Sampling Module, and QSight® LX-50 Column Stability Module for the column temperature control. The column used was a PerkinElmer Brownlee® SPP C-18 column (2.7 µm, C18, 90 Å, 4.6 x 75mm), set to be 40 °C for the entire assay run, with mobile phase A (inorganic) and mobile phase B (organic) according to an optimized flow profile. The phase was designed with a linear hold, ranging from 100% A to 95% B, and back to 100% A (phase-flow design is available in Supplemental table S2). For

improved carryover mitigation, the Precision Sampling Module needle was put through weak-strong-weak solvent wash cycles, where the weak solvent was 70:30= water: acetonitrile solution and the strong solvent was 100% HPLC acetonitrile. The volume was kept at 250 µL for both wash solvents during the wash cycles. Sample delivery was carried out through a 250 µL syringe, connected to a 10 µL needle and a 20 µL loop, with triple quadruple MS operation at a nebulizer pressure of 200 psi, electrospray voltage of 5850 volts, and a source temperature of 425°C. This produced runs of a total of 2.5 minutes for each sample for simultaneous analyte detection. Afterward, all subsequent chromatographic analyses were performed on the Simplicity™ 3Q (version 1.9) software designed specifically for the QSight instrument.

We performed a phase test with 100 ng/mL concentration of cortisol and cortisone, dissolved in ratios of organic to inorganic solvents ranging from $organic{:}\,inorganic = 95{:}\,5\ to\ 5{:}\,95$. In addition, we performed a 4-parameter test (data not reported) to test the solubility of the analytes in organic solvents (acetonitrile and methanol) and their absolute intensities with respect to two different organic solvents used for mobile phase B. Acetonitrile as mobile phase B yielded the strongest relative signal for each calibrator level and methanol was determined to be a better solvent for dissolving the analytes. The formic acid level was determined to be 0.1% for both mobile phases and the flow rate was held steady at 0.6 mL/min throughout the experiment.

2.3.4. Sample Preparation

Calibrators, QCs, and samples were thawed at room temperature, followed by centrifuging at 4600 RPM for 10 minutes at 4°C. Avoiding the particulate pellet at the bottom, 20µL of the clear solution from the top was added to each well on a large volume 96-well plate, followed by the addition of 120 µL of the DWS to each well. HPLC water was used as blanks. The plate was properly sealed and shaken using the TriNEST™ microplate shaker at 800 RPM for ten minutes

at a controlled temperature of 50°C, before inserting the 96-well plate into the LC-MS/MS autosampler with a Rapid EPS plate seal (BioChromato, Japan) for analysis.

2.3.5. Accuracy, Precision, and Linearity

In order to assess the validity of the proposed LC-MS/MS method, testing of several parameters indicating the assay sensitivity was performed. This was done in a 6-day study, where each calibrator level and QCs were analyzed in triplicates. To confirm method linearity over the specified target range, calibration curves were evaluated from the analysis of the six different calibrator levels on Simplicity 3Q (Version 1.9) software. A standard curve was generated using linear regression with $\frac{1}{x}$ weighting, where the analyte-to-IS ratios were compared against known calibrator concentrations. The series inter-assay linearity was evaluated from this linear regression, with the reported R-Square value as the primary assessment of assay linearity.

Similarly, assay precision was measured as the percent coefficient of variation (%CV), which was obtained from the aforementioned calibration curves for each level within run, between run, and total. Sample accuracy was obtained from the automatically reported analysis from Simplicity 3Q software and averaged for all levels across all runs. For each plate, quality control samples (low= 3 ng/mL for cortisol, 6 ng/mL for cortisone; high= 30 ng/mL for cortisol, 50 ng/mL for cortisone) were run together with the calibrators for further validation of the inter-assay precision.

2.3.6. *Freeze-Thaw*

Information on the developed cortisol-cortisone quantification kit's stability was obtained by performing freeze-thaw testing over multiple cycles. Freeze-thaw stability testing was performed on a full prototype kit, comprising the six cortisol-cortisone calibrators, the two quality controls, as well as the internal standard. Cortisol-cortisone kits were produced and subjected to

six freeze-thaw cycles via transfer from one of two cold reservoirs (-20°C and -80°C) to room temperature and measuring concentration changes of cortisol-cortisone over the six freeze-thaw cycles by analyzing each calibrator level in triplicate.

2.3.7. *Assessing Sample Carry-Over*

To confirm a minimal sample carryover for the proposed sample preparation and LC-MS/MS methodology, the highest calibrator level was injected into the system, followed by triplicate injections of the lowest calibrator level. Any deviation in the measurement of the cortisol-cortisone quantities in the lowest level was observed and recorded, with sample carryover accounting for any significant changes in the analyte concentrations due to the first injection of the highest calibrator concentration.

2.3.8. Evaluating Stability of Prepared Standards

To obtain stability information on the proposed cortisol-cortisone diagnostic kit, we performed an accelerated 14-day accelerated stability study in compliance with the Clinical and Laboratory Standards Institute (CLSI) guidelines for stability testing of *in vitro* diagnostic reagents. Kit calibrators were subjected to extreme temperature changes by being moved across different storage temperatures. Two sets of calibrators were tested for stability, with one being transferred from -80°C to -20°C, and another from -20°C to +30°C; calibrators of the same level were transferred in duplicates. Transfers were staggered and done every two days, for a total of seven transfers over the total period of 14 days.

After the last transfer on the 14th day, samples were harvested and tested against fresh samples to confirm the threshold of stability. Following this accelerated stability study and the confirmation of analyte retention after sample stressing, the following equation (derived from Arrhenius' rate equation) was utilized to obtain an estimate for calibrator stability without any

degradation. This derivation utilizes the ten-degree rule, where the rate of reaction is said to double for every ten degrees Celsius change in temperature.

$$Stable\ Days = (Days\ in\ high\ temperature) \times \left(2^{\frac{\Delta Temperature}{10}}\right)$$

Equation 1 Modified Arrhenius' rate equation for measurement of sample stability.

2.3.9. Automation of Sample Preparation Protocol

To further adapt the cortisol-cortisone quantification kit to clinical applications, the developed sample preparation method was automated and tested for improved high-throughput capacity using the JANUS® G3 Workstation (PerkinElmer Corp., MA, U.S.). The sample preparation process previously described was adapted onto the JANUS® workstation using JANUS® Application Assistant and WinPREP® for JANUS®, via the deck arrangement illustrated in Supplemental Figure 1. To determine the efficacy of this automated sample preparation method, manually prepared samples were compared against automated ones with regards to precision and accuracy.

The JANUS® G3 Workstation is used to automate the sample preparation. The viscosity of the samples was found comparable to water for all standard levels of cortisol-cortisone in oral fluid. Using this information, performance files for liquids with viscosity near or at that of water were used; the details of the performance files for the Blowout Mode, and the Waste Mode can be found in Supplemental Table S3(a) and S3(b), respectively. These performance files ensure that the aspirations and dispenses are accurate and precise each time. Depending on our application and plate layouts, we utilized both Blowout and Waste Mode performance files. For a singlicate dispense, such as the calibrators, we used the Blowout Mode, whereas, for dispenses per aspirate ≥ 2, such as an unknown sample to be tested, we used the Waste Mode. The design of this automation protocol was to maximize the number of unknown samples that could be quantified accurately per assay.

The DWS containing methanol required the addition of a pipette-tip prewetting step and the introduction of transport air gaps into the tip to combat volatile liquid loss. By aspirating and dispensing volume into and out of the pipette tip, the tip becomes ‘prewet’; this action saturates the interior of the pipetting tip with vapors from the solution. When the final aspiration is made, the interaction between the tip and the volatile liquid will no longer create vapor build-up, which is a significant cause of dripping. In addition, air gaps assisted in minimizing the leakage. Aspirating 10 µl of air after initial aspiration and each subsequent dispense was beneficial in combating the dripping of volatile DWS from the pipetting tips.

2.4. Results and Discussion

2.4.1. Blank Matrix Study

For every assay run, L0 (unspiked oral fluid) was injected in triplicate into LC-MS/MS system with the goal of ensuring minimal signal noise. The calculated concentration for both cortisol and cortisone were < 0±0.008 ng/mL, or no peak was observed, demonstrating the absence of either analyte in the blank matrix. The criteria of acceptance for LoD is a signal-to-baseline ratio of 3-to-1, which our LoD met for both cortisol-cortisone (figure 3).

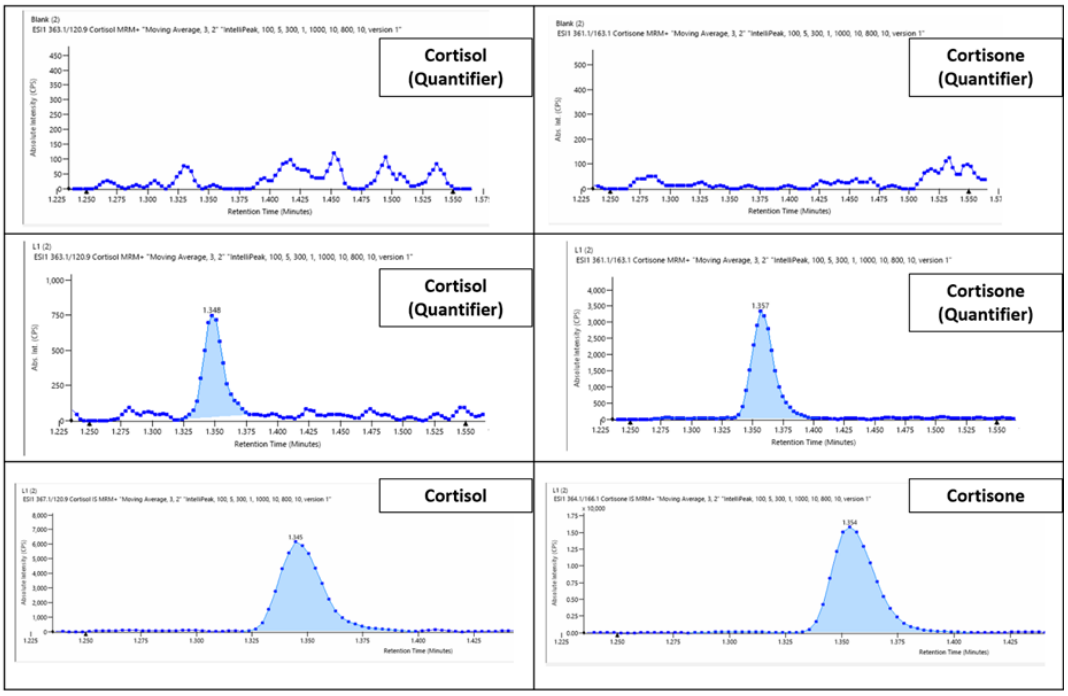

Figure 3. Representative chromatograms showing unspiked salivary matrix (top panel), lowest level of calibrator, L1 (middle panel) and internal standard (bottom panel) for cortisol (left) and cortisone (right). The LoD should be 3:1= signal: baseline for acceptability, and with visible peaks for both analytes when compared to blank, our LoD meets this criterion. The result yielded by the blank matrix was almost identical to HPLC water.

2.4.2. Phase Test and 4-parameter Test

The main purpose of performing the phase test was to obtain the lowest percentage of organic solvent at the end of the final step of the sample preparation, to yield a symmetrical chromatogram with no peak distortion and good signal intensity. An ideal peak should yield a symmetrical Gaussian profile (equation 2), with minimal peak broadening, exhibiting the highest column efficiency.

$$y = \frac{1}{\sigma\sqrt{2\pi}} \exp\left[-\frac{1}{2}\left(\frac{x-\bar{x}}{\sigma}\right)^2\right];$$

where $\sigma = standard\ deviation$, $\bar{x} = mean\ and\ x = \bar{x}\ at\ the\ axis\ of\ symmetry$

Equation 2. Gaussian distribution for chromatogram with no peak distortion

This meant that any percentage of organic and inorganic that produced chromatograms with peak fronting and peak tailing were not considered. Even though the $water: acetonitrile = 55: 45$ ratio gave the best peak shape, upon inspecting the individual MRM intensities, we

observed that $water: acetonitrile = 35: 65$ yielded the highest relative intensity for both the analytes. That said, assessing the signal-to-noise ratio for each analyte was also crucial to the method development process. Both analytes (for quantifier and qualifier) for each $inorganic: organic$ ratio were tested in triplicates and we averaged the MRM intensity and signal-to-noise ratio for each solvent ratio to conclude that $water: acetonitrile = 60: 40$ resulted in a Gaussian peak with the best MRM intensity, along with a high signal, and low noise (selected simplified chromatograms are available in Supplemental figure S2).

2.4.3. True Concentration Test (QC Study)

Because the calibrators were prepared using commercially available cortisol-cortisone in methanol, there was a possibility of the concentration of the actual stock solution not matching the stated theoretical value. Since cortisol and cortisone do not have NIST (National Institute of Standards and Technology) certified material, we had to establish a true concentration of calibrators and quality controls for each manufacturing batch, assuming that the stock solution concentrations measured exactly at 1 mg/mL. As each set of calibrators and quality controls were prepared, each level was analyzed in sextuplets and averaged to obtain the 'true concentration', to avoid error propagation in precision measurements for the following experiments. Figure 6 shows both quantifier and qualifier mass data for both analytes and the 'true concentrations' against the theoretical concentrations.

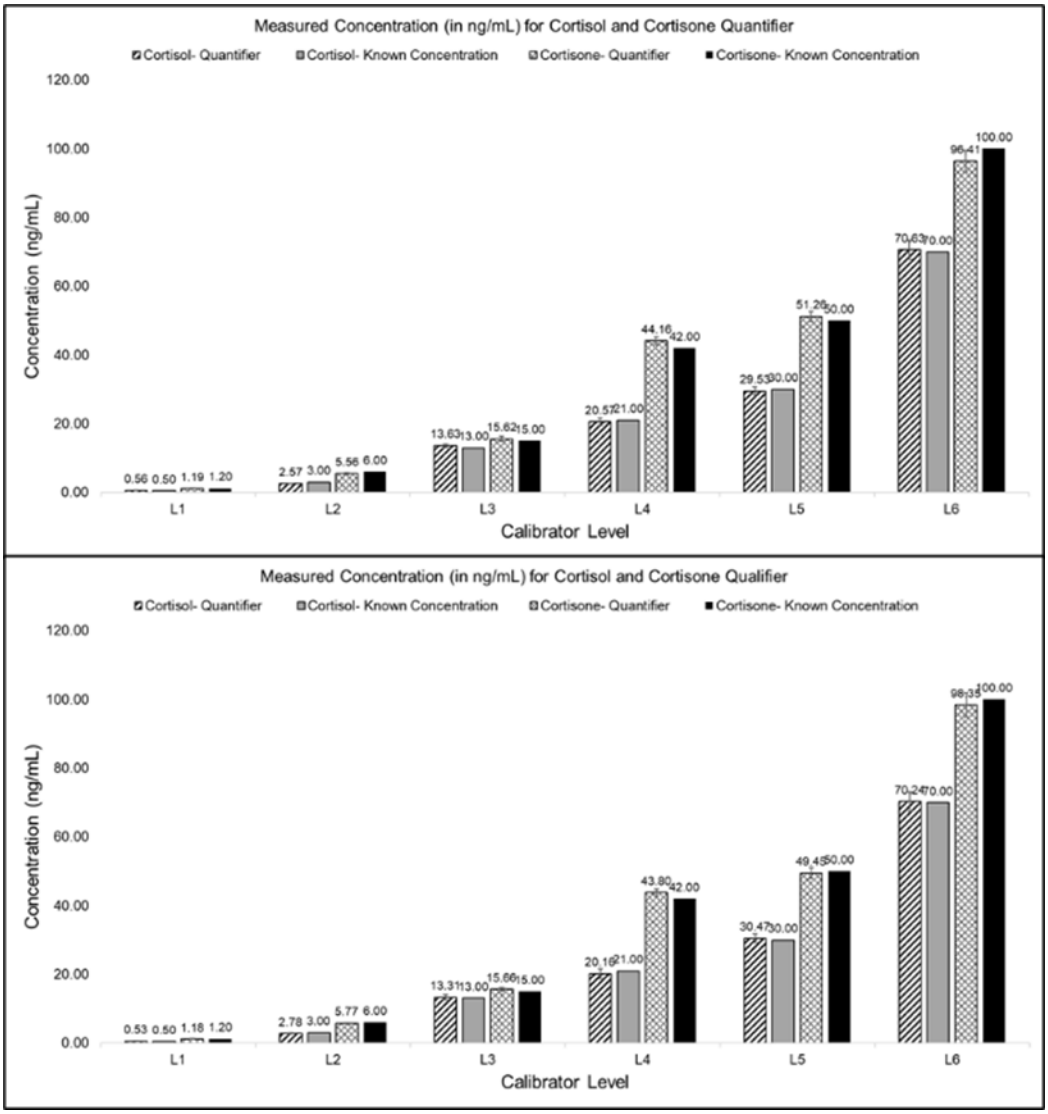

Figure 4 Quantifier (top) and Qualifier (bottom) concentrations measured against the theoretical concentrations for cortisol-cortisone. The measured concentrations were used in the generation of the standard curves for all further tests.

2.4.4. Linearity, Precision, and Accuracy

Cortisol and cortisone calibrators both reported intra and inter-assay precision (%CV) measured at ≤20%. Moreover, for further validation of the results, inter-assay %CV of the QCs of both cortisol-cortisone both reported measurements of ≤10%. Generally, each lab sets the precision threshold for their LC-MS/MS studies, with ±15-20% being standard. Given the absence of NIST-certified materials for cortisol and cortisone, it is challenging to standardize any clinical assay. Hence, we utilized our True Concentration Test to establish the QCs and calibrators such that they can be used to establish the baseline and quantify any QCs for future calibrator manufacturing.

The accuracy for the calibrators was within the 100±20% range for both analytes (table 2). This establishes our method, together with the use of the UTak salivary matrix, to be implemented in clinical laboratory settings for the generation of standard curves for the said glucocorticoid measurements in patient samples. The R-square values were taken as a measure of linearity, generated in Simplicity 3Q software using linear regression. Linearity was calculated by plotting the mean measured analyte concentrations, as a function of the corresponding known enrichment levels and performing linear regression analysis. For both cortisol and cortisone, the R-square value was greater than 0.99 for both MRMs across all 6 days (Supplemental Table S4). In addition, the precision, linearity, and accuracy studies were performed for cortisol-cortisone quantification kits in two storage temperatures: -80°C (reported) and -20°C (not reported). The results obtained for both temperatures were very similar, with the %CV ≤20% for both cortisol and cortisone (inclusive of both MRMs) at both storage temperatures, with n= 18 per level across the study.

Table 2. (Top: Cortisol- Quantifier; Bottom: Cortisone- Quantifier) % CV was used as a measure for precision, determined using 3 replicates per level each day, over a 6-day period (n=18 per level). Samples were found to be within 12% or less for intraday and interday measurements, inclusive of both MRMs for both analytes. The average % accuracy for all calibrators was found to be 100±20, inclusive of both MRMs for both analytes. These values fall well within our ≤20% cut-off value.

Calibrator Level	$\mu_{\bar{x}} \pm \sigma$ (in ng/mL)	% CV	% Accuracy
L1	0.55 ±0.05	8.56	110
L2	2.58 ±0.14	5.61	86
L3	13.44 ±0.55	4.10	103
L4	21.12 ±0.88	4.16	101
L5	30.19 ±0.90	2.99	101
L6	69.61 ±2.00	2.87	99

Calibrator Level	$\mu_{\bar{x}} \pm \sigma$ (in ng/mL)	% CV (Inter-Assay)	% Accuracy
L1	1.13 ±0.13	11.30	94
L2	5.72 ±0.39	6.76	95
L3	15.93 ±0.55	3.44	106
L4	43.83 ±1.75	3.98	104
L5	52.07 ±0.95	1.82	104
L6	95.51 ±2.88	3.02	96

2.4.5. Freeze-Thaw Stability

The concentration of each calibrator and QCs (low and high) for both sets of freeze-thaw cycles (from -80℃ to room temperature and -20℃ to room temperature) were measured and plotted for each run. The data obtained was first observed in JMP Pro 15.2 for outliers. For all six freeze-thaw cycles of both freezing temperatures, the concentration per calibrator level was first compared using a two-tailed Student's paired t-test (α= 0.05) for the technical replicates. No significant difference was observed in the measured concentrations for either temperature across all calibrator levels. In addition, we used the connecting letter report generated by JMP to confirm that the measured calibrators were indeed significantly different from each other and the blank matrix. This is especially important in the context of the lowest-concentration calibrators (L1 and L2) that are only slightly above the background noise level. The connecting letter report indicated the significant difference among all calibrator levels and blanks and showed no significant difference for the same level across runs. This concludes that there is no degradation due to cryopreservation and thawing on the analytes and the same batch of manufactured calibrators can be used for multiple assays over time. The average concentration per calibrator level, per freeze-thaw cycle run is available on Supplemental Figure S3.

2.4.6. Sample Carry-Over

To assess sample carryover, we first established a baseline signal for L1 (lowest calibrator level), followed by one L6 (highest calibrator) injection, followed by 3 immediate injections of L1. MRM analyses of both analytes showcased no statistically significant deviation in the observed L1 measurements from the L1 baseline, indicating that there was no carryover effect in any of the measurements carried out (data spread shown in Supplemental Figure S4). Minimal carryover effect is desirable particularly if this method is to be implemented at a clinical setup. Performing blank washes after each patient sample injection would mean that fewer samples can be tested per plate to accommodate the wash wells. Our method integrates autosampler Needle Wash Solvent Chemistry (as described in the methods section), thus mitigating the sample carryover. This method can be easily transferred for many patient samples tests without the need for any blank insertion after each sample injection.

2.4.7. Kit Stability

For our 14-day accelerated stability study (488 days extrapolated), we ran two plates per temperature point and duplicates per point. The data obtained was first converted to % change (in relation to Day= 0 samples) and then normalized. For both $-20℃$ and $+30℃$ stress temperatures, it was difficult to obtain a conclusive trend for either analyte over the 14-day period. There was a significant difference between the concentration obtained for D=0 and D=14; however, there was no conclusive result for when this decline/degradation began to happen. To take a closer look at this, we ran the D=0, D=2, D=4, D=6 samples for all calibrators for $-20℃$ stress temperature in triplicate. For this run, we looked at the raw concentration values across the 6-days, as well as the % change and the normalized data. This data was then extrapolated to obtain a degradation equation that could be used to plot a trendline. The data obtained from our initial study was plotted against the predicted trendline from the extrapolated data. It was interesting to observe that while

the extrapolated trend predicted a steady 2% decrease in cortisol concentration and a 4% decrease in cortisone concentration, for each day of the accelerated study, the true measured data (in duplicates, across 14-days) exhibited a much slower decline in concentration. Because the predicted values are extrapolated and the experimental values were in duplicates, figure 4 shows no error bars. We then performed a Tukey-Kramer HSD analysis to obtain any statistically significant difference for each level across the six days (measured in triplicates), hoping to reach a conclusion for the stability of the designed 'kit'. The generated connected letter report showed no significant difference in the means of the concentration measured (for both analytes) across the 4-days, stating that the analytes are stable for 8.5 months (256 days) at −80℃ storage. It is important to note that the reported decline is well-within our 20% tolerance for precision and accuracy, and since it is an accelerated study, the stability likely extends beyond the time points tested.

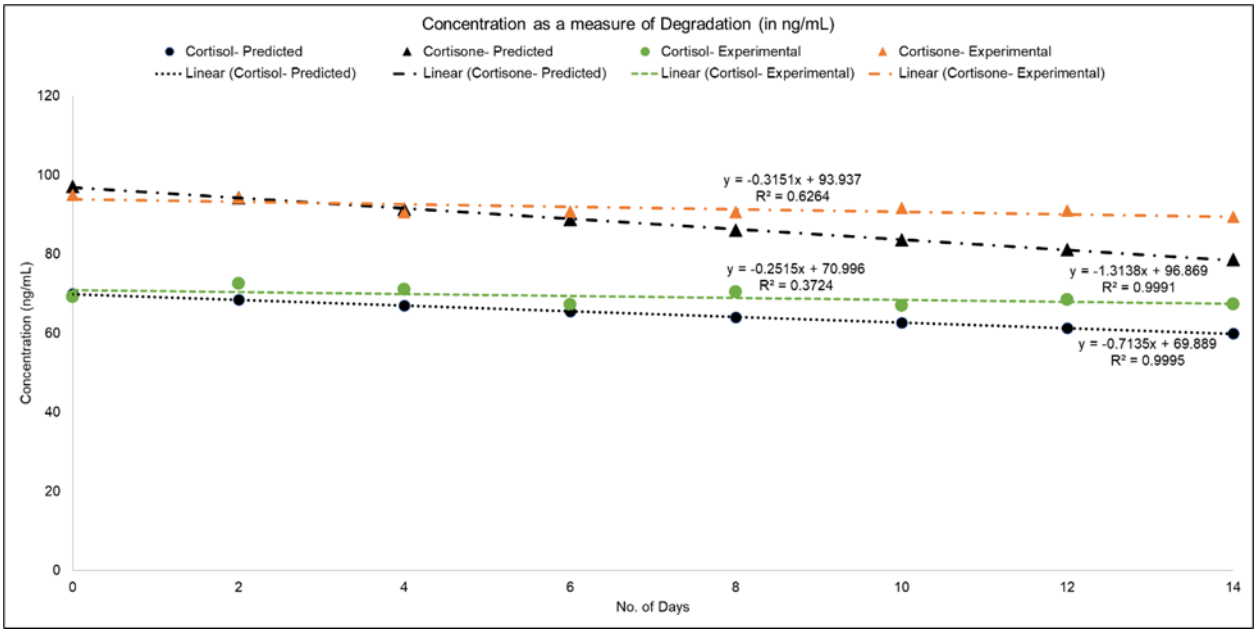

Figure 5. Predicted and experimental concentrations for cortisol and cortisone in the 14-day accelerated stability study. While the predicted trend shows a much sharper decline, experimentally we found both analytes to be stable for a longer time than predicted.

2.4.8. Automation Efficacy, Precision, and Accuracy

Owing to the ease of sample preparation, we were able to quickly adapt the sample preparation protocol to the JANUS® G3 workstation. The established automation protocol demonstrated the capability of completing a precision study on 48 samples in 4.93 minutes, compared to the 6-minute of human plating (human intervention and on-deck actions are illustrated in Supplemental Figure S5). The reported R-Square value for the linear regression for an average of 3 automated runs was ≥0.99, demonstrating that it possesses the required assay linearity. Moreover, automated sample runs reported a considerable improvement in precision (%CV), showcasing a decreased spread in data points across the standard curve (particularly for the higher-concentration calibrators). Since we have already established the overall linearity and accuracy of this assay, we adhered to the use of data points spread in standard curves as a measure of improved precision (figure 6). The automated procedure made the entire assay just above 3-minutes for plating, compared to the human 6-minutes plating. It is important to note that human plating required re-capping the calibrator, QC, and sample vials, to prevent contamination, whereas all the vials could be kept open during the entire duration of plating on the JANUS deck. This action will prove particularly advantageous when translating this method at a high throughput laboratory or clinical setting. Because of the already established assay precision and accuracy, the automation step can be designed for single calibrator injections, leaving the user 81-wells open for at least 81-unknown samples testing in singlicate. Given our study utilizing a small volume (20 µL) sample, small human error in pipetting can magnify, propagate and have a significant impact on the assay precision. That is one avenue where automation greatly helps due to its ability to accurately dispense small volume samples, minimizing error propagation.

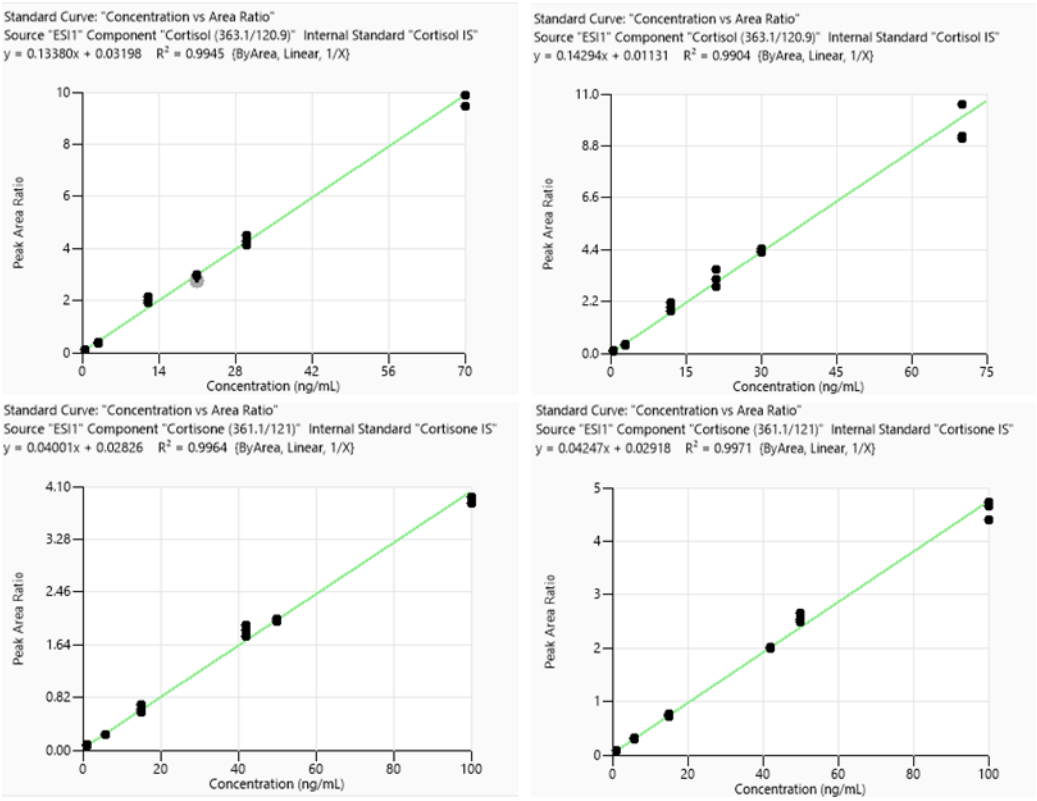

Figure 6. JANUS® G3 Workstation (left) versus human (right) standard curves for cortisol and cortisone (qualifier and quantifier); n=3 per level per plate. The standard curve obtained from JANUS plating showed less spread in the data points compared to the human plate, although the assay linearity was measured at 0.99 and above for both.

2.5.Conclusions

The presented work successfully establishes an optimized LC-MS/MS method for the simultaneous detection of free cortisol-cortisone in saliva. Moreover, a quantification kit for the diagnostic evaluation of cortisol-cortisone was developed. Based on a wide number of assessments performed over the course of this work, the proposed LC-MS/MS method is rapid, sensitive, and precise. The methodology showcased the stability, linearity, and simplicity required for theoretical clinical use. When compared with previous reports, this method and quantification kit additionally showcased a heightened simplicity in the sample preparation process, owing to the lack of expensive and complex phase separation processes required in previous literature. Overall, this allowed for the full automation of the sample preparation process, furthering the usability of this work in the clinical setting. Pending further validation, this quantification kit may be used to provide valuable information in the clinical diagnostic realm for therapeutic monitoring of cortisol

cortisone to elucidate potential adrenal dysfunctions in patients suffering from CAH, Cushing's Syndrome, as well as other endocrine disorders.

2.6.Acknowledgment

We would like to thank Kathryn Sherlock for helping with the automation troubleshooting, and Rudra Maharaj for his valuable insight during the initial phase of this study. We would also like to thank Celeste Welch and Lindsay Schneider for their valuable scientific feedback throughout the study.

2.7.Supporting Information

Figure S1. Deck layout on JANUS G3 for a custom user-defined plate layout with calibrators, QCs and patient samples.

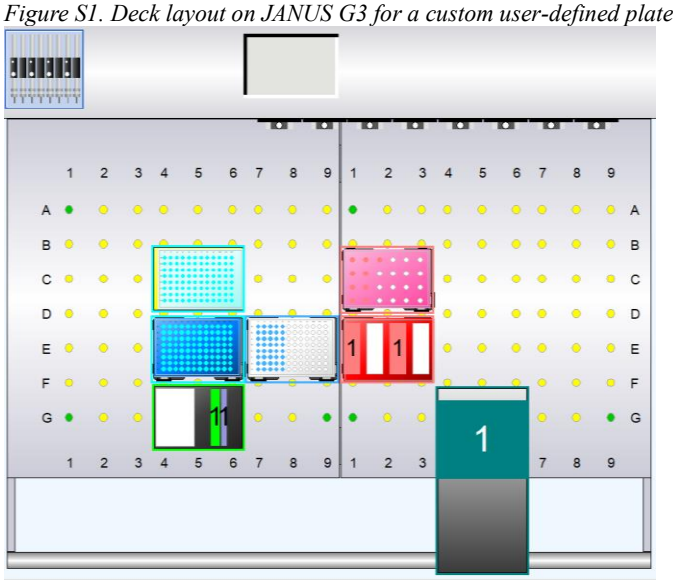

Figure S2. Relative intensity plots for cortisol (top) and cortisone (bottom) for 100 ng/mL of both analytes dissolved in HPLC water, 95% methanol, 55% methanol and 40% methanol. Having a higher percentage of organic solvent displayed a case of peak breakthrough and peak fronting, whereas analytes in greater percentage of inorganic solvent failed to display proper chromatograms.

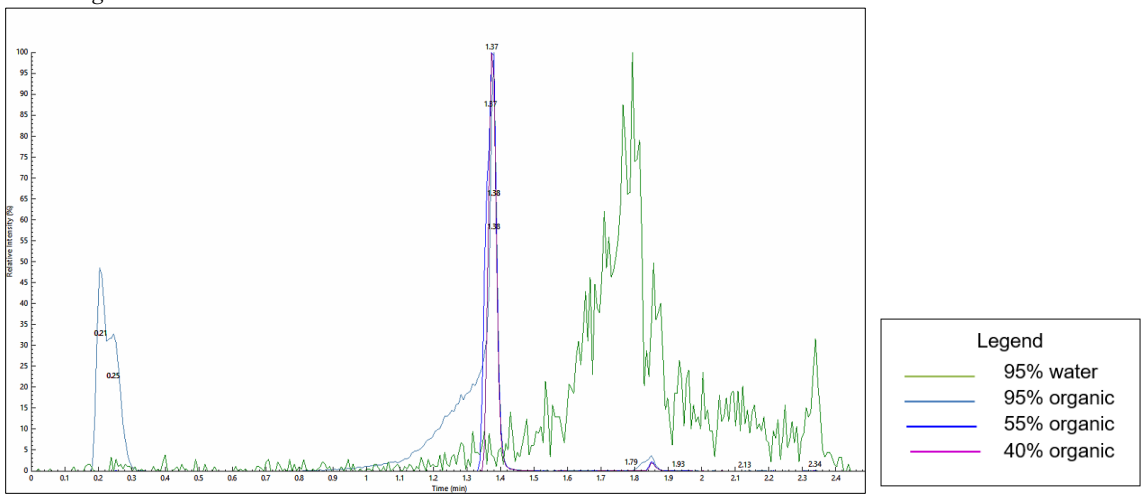

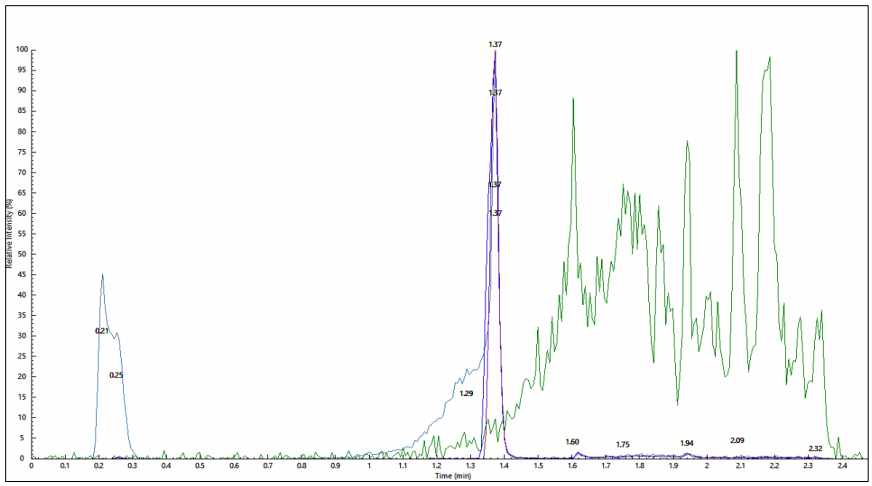

Figure S3. Cortisol and Cortisone concentration (for quantifier) for 6 freeze-thaw cycles from −80°C to room temperature (n=3 per level, per run). Error bars represent standard deviation for the technical replicates. No significant difference was observed in the measured concentration for both analytes over the six cycles, for both MRMs.

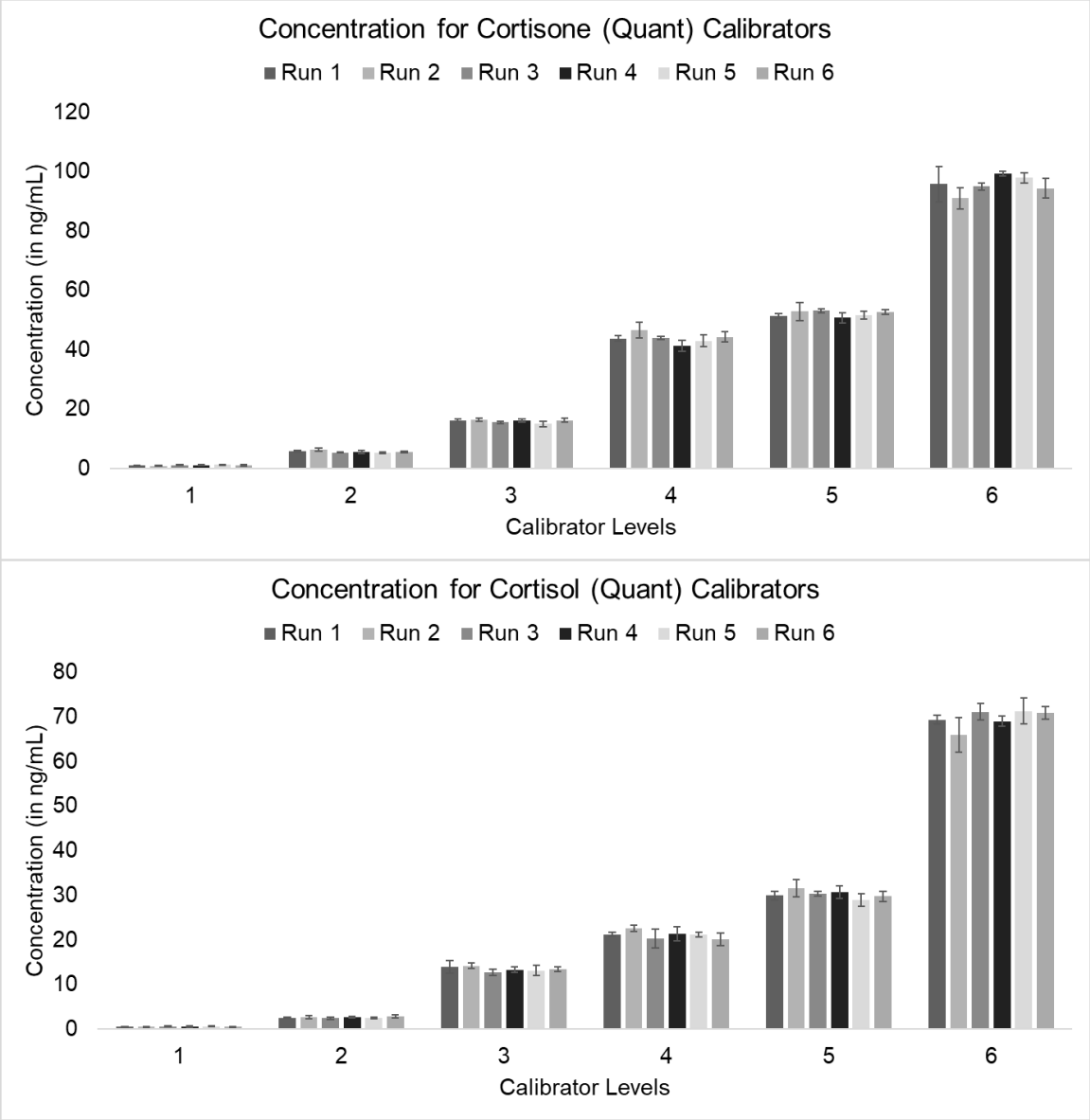

Figure S4. Box-plot diagram showing the spread of the lowest calibrator (L1) for Cortisol (left) and Cortisone (right). There was no significant outlier, and the data spread is within the ±20% range of tolerance for both analytes, both MRMs; n=3 for base, n=24 per analyte, per MRM.

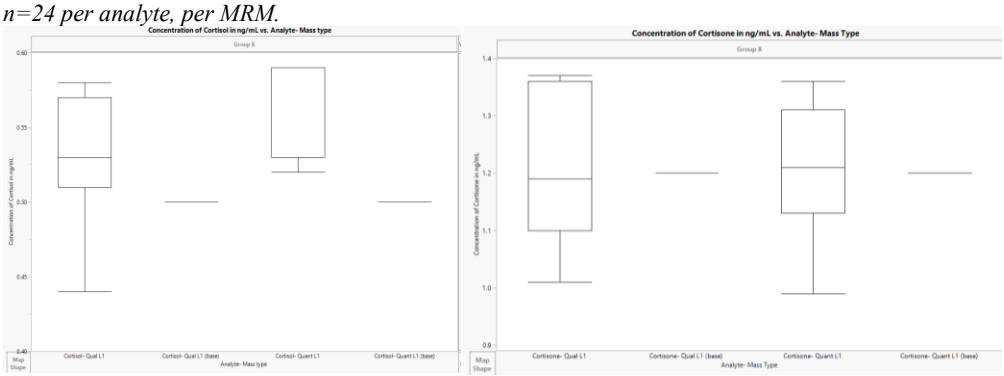

Figure S5. Workflow for automation of sample preparation of Cortisone-Cortisol in oral fluid analyzed by time. Blue boxes signify the steps with human input (off-deck) and green boxes signify the on-deck steps.

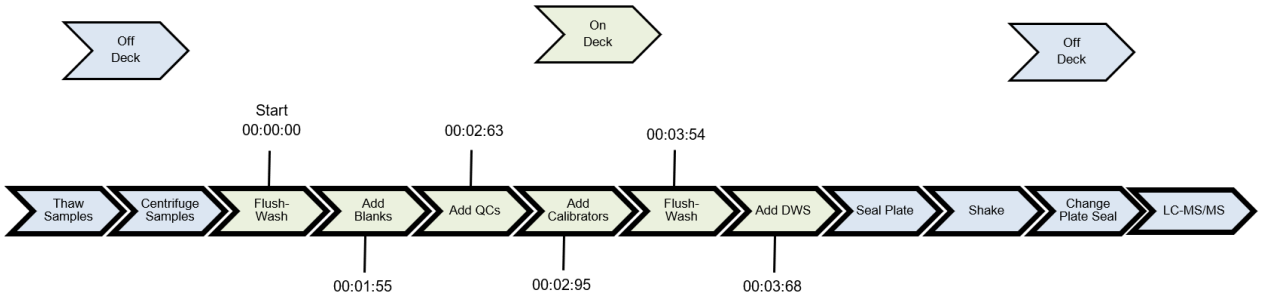

Table S1. Mass transition and parameter table for cortisol, cortisone, and their respective internal standards. Table S2. A phase flow summary for the LC elution.

	Type	Q1 mass	Q3 mass	RT (min)	EV	CC	CCL2
Cortisol (CF)	Quantifier	363.10	120.90	1.34	10	-33	-69
	Qualifier	363.10	327.10		10	-20	-67
	Internal Standard	367.10	120.90		10	-33	-69
Cortisone (CE)	Quantifier	361.10	163.10	1.36	25	-29	-94
	Qualifier	367.10	121.00		25	-44	-92
	Internal Standard	346.10	166.10		25	-29	-94

Time (min)	Flow rate (mL/min)	% A	% B
0.00	0.600	100	0
0.25	0.600	100	0
1.25	0.600	50	50
1.50	0.600	5	95
2.00	0.600	5	95
2.01	0.600	100	0
2.50	0.600	100	0

Table S3.
a) Blowout Mode performance files values used for the automation protocol for singular dispense. This is particularly crucial for high throughput patient sample testing (top row: sample, calibrators, QCs; bottom row: DWS).
b) Waste-mode performance file design for multi dispense, for running samples in replicates (as desired by the user).

Blowout Mode Performance File Values

Volume (ul)	Aspirate Speed (ul/sec)	Aspirate Delay (msec)	Dispense Speed (ul/sec)	Dispense Delay (msec)	Waste Volume (ul)	Waste Volume (% of Asp.)	Blowout Volume (ul)	Blowout Delay (msec)	Transport Air Gap (ul)	System Air Gap (ul)	Slope (ul/ul)	Offset (ul)
20.0	10.0 200	400.0	200 0.0	0.0	20.0 0	3.0	0.0	0.905	-1.079			
120.0	75.0 200	400.0	200 0.0	0.0	20.0 0	3.0	0.0	0.905	-1.079			

Waste Mode Performance File Values

Volume (ul)	Aspirate Speed (ul/sec)	Aspirate Delay (msec)	Dispense Speed (ul/sec)	Dispense Delay (msec)	Waste Volume (ul)	Waste Volume (% of Asp.)	Blowout Volume (ul)	Blowout Delay (msec)	Transport Air Gap (ul)	System Air Gap (ul)	Slope (ul/ul)	Offset (ul)
20.0	10.0	200	400.0	200	5.0	25.0	0.0	0	3.0	0.0	0.973	-0.797
120.0	75.0	200	400.0	200	15.0	10.0	0.0	0	3.0	0.0	0.973	-0.797

Table S4. R ^2- value as a measure of assay linearity, across a 6-day study (−80℃ storage). The R^2 values were >0.99 on each day of testing, for both MRM transitions of Cortisol and Cortisone.

	Day 1	Day 2	Day 3	Day 4	Day 5	Day 6
Cortisol- Quantifier	0.9975	0.9929	0.9967	0.9979	0.9932	0.998
Cortisol- Qualifier	0.9966	0.988	0.9949	0.9953	0.984	0.997
Cortisone- Quantifier	0.9962	0.989	0.9963	0.9983	0.9947	0.9951
Cortisone- Qualifier	0.9956	0.988	0.9969	0.9946	0.9935	0.9952

Chapter 3: An in-depth Analysis on Four Classes of Antidepressants Quantification from Human Serum using LC-MS/MS

Chapter 3 has been published as an original research article.

Fariha, R.[1], Deshpande, P.S.[1], Rothkopf, E.[1] *et al.* An in-depth analysis of four classes of antidepressants quantification from human serum using LC–MS/MS. *Sci Rep* **13**, 2115 (2023).

https://doi.org/10.1038/s41598-023-29229-0

1. Center for Biomedical Engineering, School of Engineering, Brown University, 182 Hope Street, Providence, RI- 02912, USA

3.1. Abstract

Depression is a growing global crisis, with females at a higher rate of diagnosis than males. While the percentage of patients on prescribed antidepressants have tripled over the last two decades, we are still at a crossroad where the discrepancy lies between finding a drug to suit a patient and monitoring the abundance of it in the body to prevent unwanted side-effects. Liquid Chromatography tandem mass spectrometry (LC-MS/MS) has garnered the attention of clinicians as a technique to accurately monitor therapeutic drugs in human serum with high specificity and accuracy. This may be a potential solution, but the challenge persists in the realm of sample preparation, where a method is automatable. We have developed and validated an LC-MS/MS-based assay for simultaneous quantification of 4 different classes of commonly prescribed antidepressants in women that is automated using a JANUS® G3 Robotic Liquid Handler. Our method utilizes a simple sample preparation technique, utilizing only 20 μL of serum sample, to accurately measure Bupropion, Citalopram, Desipramine, Imipramine, Olanzapine, Sertraline and Vilazodone across a range of 1.0 to 230 ng/mL. Our method exhibits a linearity of R2 ≥0.99 when detected in MRM mode and % CV of ≤20% for all analytes across the board. In addition, we have designed a prototype that can be utilized at a clinical mass spectrometry lab, and we have assessed the long-term use of this prototype using an accelerated stability study. Overall, our developed method has the potential to be translated to clinical settings to monitor postpartum depression for a large number of patient samples using automation.

3.2. Introduction

While mental health illness has been prevalent in society for years, with emerging conversations about mental health awareness, more and more people are coming forth to report diagnoses of depression and anxiety disorders. According to a World Health Organization (WHO) report, depression affects about 3.8% of the world's population, tallying at 280 million cases [53].

Pre-existing conditions, ongoing treatments of other ailments, and post-operative phases are also known to contribute to increases in the number of individuals experiencing depression. Of all the patients, female-identifying adults had a higher rate of diagnosis (10.5%) compared to their male counterparts (6.2%) [54]. Additionally, the difference in monoamine functionality between the two biological sexes has also been attributed to the variability in the number of occurrences [55]. Over the last two decades, the percentage of patients on prescribed antidepressants has tripled [56], and of the prescribed classes of antidepressants, Selective Serotonin Reuptake Inhibitor (**SSRI**) leads the count at 53.9%, followed by Tricyclics (**TCA**) at 21.9%, and Norepinephrine and Dopamine Reuptake Inhibitors (**NDRI**), Tetracyclics (**TeCA**), and Serotonin-Norepinephrine Reuptake Inhibitors (**SNRI**) comprising the rest [57]. From a pharmacological standpoint, prescribing antidepressants to female patients is challenging due to liver metabolism rate, drug transport, and clearance rates [55]. Due to the complexity of the disease and interindividual variability in drug metabolism, finding a suitable treatment that works for a patient comes with a long process of trial-and-error, side-effect suitability, and overall treatment efficacy [58, 59]. For example, the antagonistic effects of TCAs on adrenergic, muscarinic, and histaminergic receptors can result in dizziness, memory deficit, and drowsiness [60]. On the contrary, the SSRIs, side-effects are nausea and sleeplessness, and sexual dysfunction [63]. The challenge heightens as patients transition to pregnancy or undergo cancer treatment [62]. As a result, there has been an uprise in the trend to develop effective methods to quantify and monitor a wide range of antidepressants that are prescribed specifically to women. According to Psych Central [61], there are no blood tests available for detecting depression or the effect of antidepressants on a patient. The closest thing to a test available is the pharmacogenomic test to identify how a drug might impact the patient based on their genomic makeup. Because the drugs (and potentially multiple drugs) can lead to the rise

of side-effects with no immediate cure, it is becoming increasingly important to develop blood/serum-based tests for the quantification of different antidepressants in a patient sample. Liquid chromatography-tandem mass spectrometry (LC-MS/MS) has garnered attention in recent times in the clinical realm, especially when paired with automation. LC-MS/MS has been reported as a reliable detection and analytical technique for the simultaneous detection of multiple drugs (such as antidepressants and antipsychotics) with great specificity [62, 63, 64]. The sensitivity of the instrument, together with a relatively shorter run duration, makes it an ideal candidate to develop serum-based diagnostic assays and justifies offsetting the cost of operation in a clinical setting due to its high-throughput ability. Herein, we have conducted an in-depth analysis on four different antidepressant classes (**SSRI**, **TCA**, **NDRI**, and **SNRI**) based on the clinical market analysis of their routine administration in women, especially for treating postpartum depression. This investigation focused on the simultaneous detection of antidepressants from the aforementioned classes from human serum using a triple quad liquid chromatography-tandem mass spectrometry, focusing on i) the development of a prototype kit that utilizes a small sample volume with minimal sample preparation, ii) is easy to automate for clinical application, and iii) is comparable to previously reported studies in terms of precision and accuracy. Figure 7 showcases the molecular motion that takes place in our proposed sample preparation protocol for a small volume analyte extraction. Table 1(a), on the other hand, reports the existing literature for similar studies alongside our prototype kit, as well as a European Commercial Kit (Eureka, Italy). While these studies[10-15] reported promising data, there was no reported ideation of automation of the sample preparation process. Table 1(b) reports the therapeutic ranges for the drugs we have investigated for our study.

Figure 7. An illustration of the antidepressants molecular motion as observed in our sample preparation protocol.

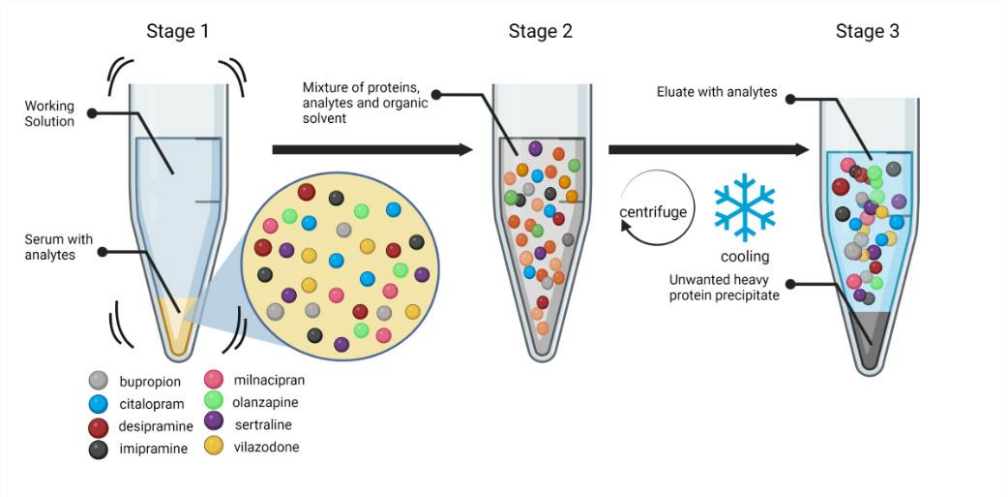

Table 3(a) Method comparison of existing literature.

	Fariha et al. (2022)	**Arantes et al. (2021) [62]**	**Koller et al. (2019) [63]**	**Buhagiar et al. (2019) [64]**	**Wang et al. (2015) [65]**	**Choong et al. (2011) [66]**	**Eureka (Commercial Kit) [67]**
Number of analytes	8	50	9	6	16	5	17
Matrix	Serum	Oral fluid	Plasma	Plasma	Plasma	Plasma	Plasma
Number of Steps for sample preparation	4	6	5	5	6	7	6
Sample Volume (**µL**)	20	500	200	20	180	500	100
Sample Preparation: Step 1	Sample+ 100 µL DWS (with internal standard)	Sample + 25 µL of internal standard + 500 µL sodium tetraborate + 1mL (MTBE)	Sample + 10 µL IS + 800 µL acetonitrile	Sample µL plasma + 20 µL IS	Sample + 20 µL methanol	Sample+ 50 ng of REMO and LIT	Sample + 300 µl of Reagent A (Deproteinization Soln and IS),
Sample Prep Step 2	Shake the plate for 5 minutes at 800 RPM at 25°C	Vortex: 2min at 2500 RPM	Centrifuge: 1400 RPM, 5min, 4°C	Vortex: 10s	Vortex: 30s	Dilution with 4% H_3PO_4	Vortex for 10 sec.
Sample Prep Step 3	Centrifuge: 4600 RPM at 0°C for 10 minutes	Centrifuge: 987g for 5min	Extract Supernatant	Add 200 µL of acetonitrile	Add 1000uL of acidified drug in methanol	Vortex: time not specified	Centrifuge: 14,000 rpm for 10 minutes
Sample Prep Step 4	Collect 50 µL supernatant	Extract Supernatant	Dry supernatant at 45°C	Vortex: 30s	Vortex: 1 min	Wash (3X)	Collect 100 µL of supernatant
Sample Prep Step 5	N/A	Dry supernatant using nitrogen	Reconstitution	Centrifuge: 5 min at 15, 600g	Centrifuge: 10000g, 5min	Add methanol (2X)	250 µL of Reagent B (Diluting Soln)
Sample Prep Step 6	N/A	Reconstitution	N/A	N/A	Separate Supernatant	Dry	Vortex for 5 sec
Sample Prep Step 7	N/A	N/A	N/A	N/A	N/A	Reconstitution	N/A
Run time per sample	7 min	9.5 min	6min	6 min	6min	14min	7 min

Concentration Range	1-230 ng/mL	2.5-250 ng/mL	0.18-3700 ng/mL (drug specific)	0.5-400 ng/mL	2.5-1000 ng/mL (drug specific)	1–2000 ng/mL (drug specific)	1-1,600 (ng/mL)

Table 3(b) Therapeutic ranges for the antidepressants investigated.

Name of the Drug	Class	Therapeutic Range (Adult)	Ref
Bupropion	NDRI	850-1500 ng/mL	Baumann et al. (2005)[73]
Citalopram	SSRI	30-130 ng/mL	Mayoclinic Labs[74]
Desipramine	TCA	100 to 300 ng/mL.	Mayoclinic Labs[75]
Imipramine	TCA	175-350 ng/mL	Medscape[76]
Milnacipran	SNRI	100–150ng/mL	Baumann et al. (2005)[77]
Olanzapine	SSRI	20 to 40 ng/mL	Baumann et al. (2005)[78]
Sertraline	SSRI	30-200 ng/mL	Rao et al. (2001)[79]
Vilazodone	SSRI	Peak plasma conc at 156 ng/mL	Mayoclinic Labs[80]

3.3.Experimental

3.3.1. Chemicals and Reagents

Baker Analyzed HPLC grade water, acetonitrile, and methanol (>99.9% purity) were obtained from VWR for the preparation of calibrators, and operation of the LC-MS/MS. The primary analytes were: Bupropion (BUP B-034), Citalopram (CIT C-095), Desipramine (DES D-906), Imipramine (IMI I-902), Milnacipran (MLN M-209), Olanzapine (OLN O-024), Sertraline (SRT S-021), Vilazodone (VIL (V-076), and the desired internal standards for the analytes were: Fluoxetine D-6 (FLU-D6 F-038), Citalopram D-6 (CIT-D6 C-090), Mirtazapine D-3 (MRT-D3 M-191), Clomipramine D-3 (CLO-D3 C-116), Doxepine (DOX-D3 D-060), Milnacipran D-10 (MLN-D10 M-149), Buproprion (BUP-D9 B-052), Vilazodone D-4 (VIL-D4 (V-028), all purchased from Cerilliant Corporation (Round Rock, TX, USA). Reagent-grade formic acid was purchased from Fisher Scientific to improve ion mobility on the mobile phases. Ultra-low steroid, drug-depleted DDC Mass Spect Gold Serum® was purchased from Sigma-Aldrich and was used as the base matrix to create the calibrators and Quality Controls (QCs). Sodium Azide was purchased from Sigma-Aldrich (used as a preservative).

3.3.2. LC-MS/MS Conditions and Parameters

All antidepressants except OLN and VIL were diluted 1000-folds in HPLC-grade methanol. OLN was diluted 1000-folds in HPLC-grade acetonitrile due to its higher solubility, while VIL was diluted in Methanol:DMSO solvent (90:10 v/v) according to its solubility data from the vendor. All internal standards were diluted 100-folds in HPLC-grade methanol and infused directly into the MS to quantify the parent mass and quantifier fragment masses. The infusion is performed through a direct 1mL gastight Hamilton syringe using a Harvard apparatus at a flow rate of 30 µl/min. All compound transition data, together with the Entrance Voltage (EV), Collision Cell Energy (CC), and Collision Cell Lens 2 (CCL2) values obtained from Multiple Reaction Monitoring (MRM) optimization, are available in Supplemental Table S1.

Upon completing the MRM optimization, the nebulizer gas pressure, source temperature, HSID (hot surface-induced desolvation) temperature, and drying gas pressure were also optimized to obtain the best relative intensity for both Q3 masses of the analytes and the internal standards. After the Q1 and Q3 masses were detected, the EV, CC, and CCL2 values were re-optimized for the best signal of the analyte quantifier, qualifier, and internal standards. The probe positions were also adjusted to obtain the best signal intensity and sensitivity. The LC-MS/MS system used was a PerkinElmer QSight® 200-series Triple Quadrupole Mass Spectrometer, equipped with an Electron Spray Injection (ESI) source in using positive ion mode. Integrated to the MS was a QSight LX50 Solvent Delivery Module, QSight LX50 Precision Sampling Module, and QSight® LX-50 Column Stability Module for column temperature control. The column used was a PerkinElmer Brownlee® SPP C-18 column (2.7 µm, C18, 90 Å, 4.6 x 75mm), set at 40 °C for the entire assay run, with mobile phase A (inorganic) and mobile phase B (organic) solvent. The LC design flow was designed for high sensitivity and low flow rate, with distinct analyte separation. The sample tray holder was kept at a steady 4°C throughout the course of the run. The Precision

Sampling Module needle was put through weak-strong-weak solvent wash cycles between each injection, with 70:30= water: acetonitrile solution as the weak solvent and 100% HPLC acetonitrile as the strong solvent, at 250 µL volume for both solvents. The solvent delivery module was connected to a 10 µL needle and a 20 µL loop, with triple quadruple MS operation at a nebulizer pressure of 300 psi, electrospray voltage of 5850 volts, and a source temperature of 400°C. The drying gas was set to 60, and HSID was set to 320°C. This produced runs of a total of 7 minutes for each sample for simultaneous analyte detection.

3.3.3. Preparation of Calibrators, Quality Controls and Daily Working Solution

All stock solutions were taken through a two-step dilution process in order to obtain the final desired concentrations. Briefly, all the antidepressants stock solutions were diluted 1000-folds, 200-folds, and 20-folds to yield 3 different working solutions (one working solution per dilution, with all analyte stocks combined). Sodium azide was added to the DDC Gold serum at 0.02% (by volume) and stirred at room temperature for approximately 30-minutes. The serum was then aliquoted to individual glass vials, and the working solutions were added to yield a 5-point linearity series (L1-L5), and quality controls (QCs), across the concentration range of: 1 ng/mL to 230 ng/mL for all analytes (theoretically calculated). It was ensured that all working volumes were above 10µL to avoid any small pipetting errors. The calibrators and controls were rocked overnight at 4°C prior to further experimentation. All calibrators were aliquoted and stored at -80°C and thawed before use.

Designing the Daily Working Solution (DWS) included investigating the solvent used, the pH of the solvent, as well as the optimization of the concentration of labeled internal standards that would not lead to false positive signals or large background. For best results, the final protocol had a DWS formulated with acetonitrile, acidified with formic acid with all the internal standards

measuring to 25 ng/mL across the board. The solution was stirred at room temperature for 30-minutes prior to using it for an experiment.

3.3.4. Sample Preparation

The calibrators, QCs, and samples were thawed to room temperature. Each sample was vortexed well prior to plating. To a 96-well v-bottom skirted qPCR plate, 20 µL of calibrator/control/sample was added, followed by 100 µL of the DWS. The plate was then sealed well with aluminum foil and shaken using a TriNEST™ plate shaker at 25°C at 800 RPM for 5-minutes. The plate was then centrifuged at 0°C at 4600 RPM for 10-minutes. Upon completion, the foil was carefully removed and 50 µL of the clear supernatant from the top was collected to a 96-well conical bottom Nunc-polypropylene plate prior to resealing with a Rapid EPS plate seal (BioChromato, Japan) for LC-MS/MS analysis.

3.3.5. Automation

To further adapt the prototype kit for clinical applications, the developed sample preparation method was automated and tested for improved high-throughput capacity using the JANUS® G3 Workstation (PerkinElmer Corp., MA, U.S.). The sample preparation process previously described was automated using the JANUS® Application Assistant and WinPREP® for JANUS®, via the deck arrangement illustrated in Supplemental Figure S1 (a), while Figure S (b) shows the deck arrangement for the Eureka commercial kit. To determine the efficacy of this automated sample preparation method, manually prepared samples were compared against automated ones with regards to precision, measured in %CV. The protocol was created utilizing the specific considerations presented in Table 2. These considerations included factors affecting the aspiration and dispensing of reagents and samples and the pipetting mode (waste or blowout). Pipetting mode selection was determined on a step-to-step basis with the general designation that

waste mode was to be used if the value dispenses per aspirate was > 1 and used in blowout mode when the value was equal to 1. This consideration was also weighed against the individual need of each step with regards to efficiency versus precision. The waste mode can speed up the protocol's timetable but is far less precise in aspirating and dispensing and additionally wastes a small amount of the transferred fluid. Blowout mode in contrast is very precise with no fluid waste however this mode can be slow as well as wasteful of pipette tips as a new tip is utilized on a per aspirate/dispense basis. Therefore, each step was analyzed to balance these factors.

In parallel, an automated protocol for the Eureka Antidepressants in Plasma commercial kit was prepared for a side-by-side comparison of throughput-ability and feasibility- important factors for the integration of such assay kits into the clinical space. The results (discussed later on) have broader implications for the uses of vial and plate-based sample preparation and assay diagnostics.

Table 4. Parameters selected for the automation of the proposed protocol (specific to JANUS® G3 Workstation)

Protocol Step	Volume of Transfer (µl)	Pipette Tip Utilized (µl)	Dispenses Per Aspirate	Pipette Mode	Transfer Gap (µl)	Waste/ Blowout Volume (µl)	Waste/ Blowout Delay (msec)
Standards	20	200	3	Waste	10	5	100
QC's	20	200	4	Waste	10	5	100
Patient Samples	20	200	1	Blowout	10	10	100
DWS	100	1000	9	Waste	15	10	100
Supernatant Transfer	50	200	1	Blowout	10	20	100

3.3.6. DoE and Data Analysis

It is important to note that for the complete study, the Design of Experiment (DoE) was performed using MiniTab® (State College, PA) to optimize the number of samples to be tested for $\alpha = 0.05$ for the multiple variables involved in the study. These variables include: (i) mobile phase B solvent, (ii) organic solvent used to prepare the DWS (methanol versus acetonitrile) and its pH (acidic versus neutral), and (iii) mixing and centrifuge temperature and speed. The statistical power was set to 80% for a full factorial design with three factors. All subsequent chromatographic analyses were performed on the Simplicity™ 3Q (version 3.0) software designed specifically for the QSight instrument. The data was then exported to Microsoft Excel and JMP Pro 16 for visualization and statistical analysis.

3.4.Results and Discussion

3.4.1. *Matrix Effect and Interference*

One of the crucial parts of this study was validating the theoretical design according to the multiple discussed in our previous study[22]. Since this study dealt with a complex matrix like serum, additional studies had to be performed to assess the matrix effect and its impact on ion suppression and the process efficiency. The matrix study was conducted according to the process published by Matuszewski et al.[23], wherein, a set of neat solutions (5 levels) were prepared (using Mobile Phase B, i.e., acetonitrile) and an identical set of solutions was prepared using DDC Mass Spect Gold Serum. The concentration range for this particular study covered 20-1200 ng/mL range. Each level was plated in sextuplets (n= 6 per matrix per analyte) prior to LC-MS/MS analysis. The mean matrix effect range were such that: BUP= 62-101%, CIT= 85-118%, DES= 82-106%, IMI= 71-110%, MLN= 73-109%, OLN= 46-119%, SRT= 71-89%, and VIL= 79-107%. While the matrix effect seemed to be significant based on the upper and lower boundaries of the ranges, the data

obtained is comparable to a previous study by Marchet et al.[24]. Additionally, the concentration range for this study expanded beyond the dynamic range of the standard curve using a linear regression with $\frac{1}{x}$ weighting, plotting the analyte-to-IS ratios. Hence, the solutions were diluted 10-folds (lower level) and 6-folds (upper level) to generate a standard curve with a linear dynamic range. This resulted in an improvement in the matrix effect as well as recovery efficiency (data not reported). The final mean matrix effect is reported to be (82-105) ±20% across all analytes, when measured by peak area. Any value above 100% was interpreted as ion enhancement, whereas anything below indicated ion suppression. Since the analytes do not have certified reference materials that could be held as a standard, it was not possible to perform a value assignment assessment for each analyte due to the matrix effect. However, to rule out any interference from the native serum, we ran triplicates of blank serum on each plate and observed no peaks at the detected retention times for all the analytes. This was important to establish the LOQ values, where a peak was observed for each analyte at their determined Retention Times (RT). Figure 2 illustrates the detected RT for the eight drugs being investigated overlaid on their relative intensity profile. To our greatest surprise, we observed near to no signal for the Eureka antidepressant kit when we ran their calibrators side by side according to the manufacturer protocol (Supplemental Figure S2). This certainly raises concern about the quality of the currently available commercial kits and their application in the clinical diagnostic realm.

Figure 8. Chromatograms showing the Retention Times (RT) of each analyte studied (in serum) and their relative intensity profiles.

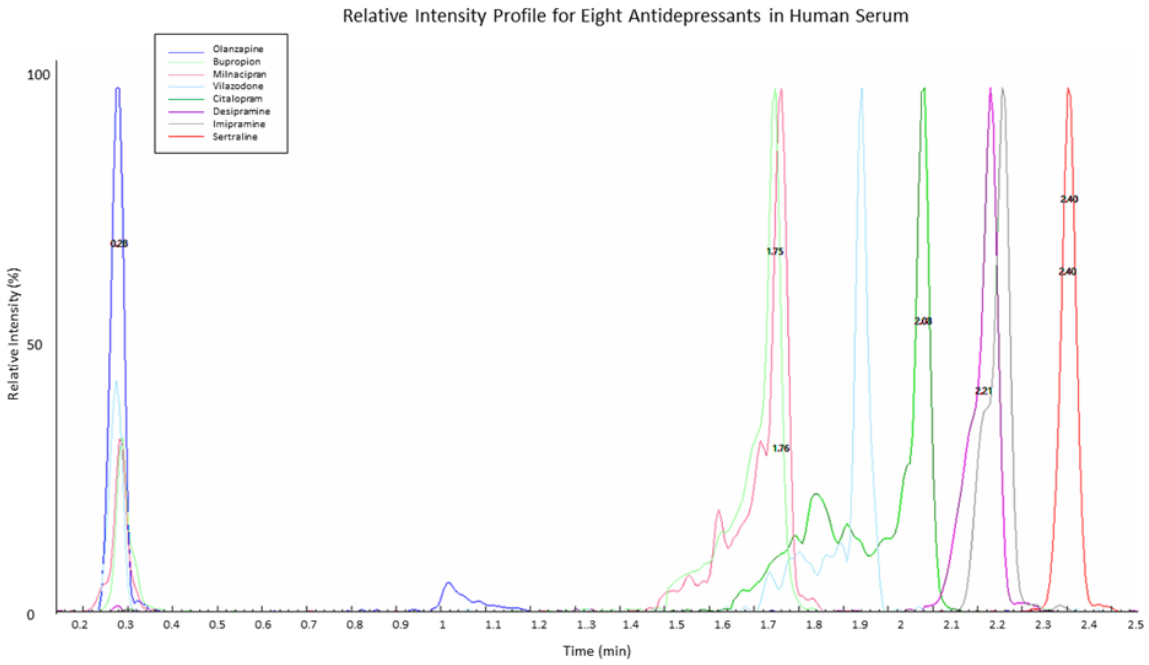

3.4.2. Solvent Analysis: Mobile Phase, DWS, Sample Preparation

A primitive study for a successful chromatographic analysis is to determine an organic solvent that would consistently yield a good signal and be able to elute the desired analytes/fragments with the highest efficiency. Even though methanol was identified as the predominant organic solvent for the antidepressants in the discussion, it was still necessary to determine whether methanol would be an optimized and operational mobile phase B. Additionally, it is important to establish the lowest percentage of organic solvent at the final step of sample preparation that would yield an ideal peak shape, i.e., a Gaussian profile with minimal peak broadening[22]. As a result, we conducted a two-parameter study using methanol and acetonitrile. Both organic solvents were tested as Mobile Phase B, as well as to create neat solutions of 100 ng/mL in $organic{:}\,inorganic = 95{:}\,5$ to $5{:}\,95$ ratios. This resulted in two sets of 19 samples studied in duplicates for acetonitrile as Mobile Phase B and methanol as Mobile Phase B. The entire study was repeated 3-times prior to concluding that acetonitrile serves as the better Mobile Phase B due to the high signal recovery (almost 2-folds higher in average signal intensity for all

eight antidepressants). For the lowest organic solvent percentage, it was determined that a ratio of $organic: inorganic = 60:40$ yielded a Gaussian peak with the best MRM intensity, along with a high signal and low noise, comprehensive across all antidepressants for both methanol and acetonitrile.

While the final ratio of the organic and inorganic solvents was determined, an additional study had to be conducted to assess the performance of the desired internal standards (IS) in the organic solvents[26], as well as the said solvent's efficacy as a protein precipitation solution. To do this, internal standards were all dissolved in: HPLC methanol (with 0.1% formic acid) and HPLC methanol (no acid), and HPLC acetonitrile (with 0.1% formic acid) and HPLC acetonitrile (no acid). This resulted in 4 Daily Working Solutions (DWS) at a concentration of 50 ng/mL across the board for all the antidepressants. These 4 DWS were tested using an identical extraction process: addition to serum, followed by 5-minutes incubation, vortex mixing and centrifugation for separation. For each concentration (calibrators level L1-L5) it was observed that acetonitrile with 0.1% formic acid yielded the highest signal intensity for all analytes (BUP appeared to have a better signal intensity with methanol and 0.1% formic acid, however, the quantified difference was not statistically significant) (data not reported). This study was repeated three times, with n=3 for each calibrator with each DWS to reach a conclusive result. Unlike the previously reported studies[10-14], we shortened the sample preparation protocol by utilizing the effect of pH on the separation buffer. As reported by Lin et al.[25], a better separation occurs for when an acidic buffer is used. Utilizing this, we have innovated the sample preparation technique such that the DWS was acetonitrile measuring at pH= 2.3 at room temperature with the labeled internal standard incorporated in it. For this two-fluid system (as shown on Figure 1), we assumed a thin membrane

formation at the interface of the serum and DWS. That said, the bulk pH of a system like this varies vastly from the surface pH[28], implying the need for an external motion to minimize the effect of membrane separation height, *h*, as shown by Ohshima and Kondo[28] derivation for repulsion, *P*, at the DWS and serum boundary:

$$P_{max} = 4nkT \sin h^2 \left(e^{\frac{\varphi_{DON}}{2kT}}\right) \text{ (eq. 1)}$$

where, φ_{DON} is the Donnan potential. Even though for an almost infinitesimal system like ours with surface pH<3, the bulk pH should not differ too much from the boundary pH, we still incorporated the principles of micromixing[29], for our two-fluid system's homogeneity as explained by the Kolmogoroff microscale equation λ_K (equation 2):

$$\lambda_K = \left(\frac{\nu^3}{\epsilon}\right)^{\frac{1}{4}} \text{ (eq. 2)}$$

where, ν is the kinematic viscosity of the fluid in the system, and ϵ is the power input per unit mass to the bioreactor. In our case, the mixing occurs below the scale of λ_K where molecular diffusion takes place (stage 2 of figure 1). For the third stage, i.e., efficient precipitate separation, we utilized the effect of temperature on organic solvents, where a near 0°C temperature leads to certain protein insolubility[30]. Thus, we have demonstrated the combined effect of centrifugation and temperature at Stage 3 of our separation process, leading to the precipitation of the unwanted proteins and salts, leaving us with a clear and easy-to-remove supernatant, that can be directly injected to the LC-MS/MS for analysis, thereby eliminating the need for sample drying.

3.4.3. Quality Control, Linearity, Precision, and Accuracy

The concentration of each antidepressant for the calibrators was determined by studying the therapeutic ranges (Table 1b). It was important to establish the point of column saturation since there were 8 different antidepressants. Initially, a prototype was designed such that the

concentration varied for each analyte, in order to cover the large therapeutic range of BUP. However, upon investigation, it was concluded that the C-18 column being used would saturate above a 230 ng/mL concentration for all analytes uniformly. This was studied using two different C-18 columns: Perkin Elmer Brownlee SPP C18, and Agilent Poroshell C18, both yielding similar outcomes. Therefore, the final prototype kit was designed to avoid any column saturation. Figure 3 shows the concentration of each calibrator for all eight antidepressants, analyzed in sextuplets, and averaged, and the corresponding theoretical value for that calibrator level. This resulted in measured concentrations at L1= 1 ng/mL, L2= 4 ng/mL, L3= 15 ng/mL, L4= 60 ng/mL, and L5= 230 ng/mL, that were further used to access the assay linearity, precision, and accuracy.

Linearity, precision, and accuracy data were all obtained from the same experiment, where the linearity of the prototype kit was assessed by looking at the R^2-values for each standard curve produced. Precision was reported as %CV measured ±≤20% for intra and inter-assay runs, across 6-days with n=3 for each calibrator level per antidepressant. Table 3 (a-h) show each antidepressant, with their measured concentrations, %CV, %Accuracy and R^2-values. Samples were found to be within 20% for all analytes (except e) for intraday and interday measurements. The sample average sample accuracy was measured at 100±20. The average R^2- values were all above 0.9, indicating assay linearity. Achieving the desired precision for this study was challenging since there were multiple internal standards that would lead to high background noise and impact the precision. The IS concentration for all the drugs had to be optimized (tested concentrations: 1.5 ng/mL, 15 ng/mL, 25 ng/mL, 50 ng/mL) such that there would be no interference leading to a high %CV. It was determined that 25 ng/mL served the best signal without significantly interfering with the assay precision and still producing IS (intrenal standards) curves that were consistent. It is worth noting that the LOQ had a notable high data spread for all the

tested drugs, since the measured concentration was relatively small and only slightly above the background noise produced by blank serum.

Additionally, we faced separation challenges that impacted the assay precision. This was mitigated by investigating and modifying our LC method. We tested three different LC gradients for a partial loop fill. The three separation methodologies tested had the following configurations:

- 3-minutes run time per sample: flow rate from 0.7 mL/min 100% A for one minute, 0.9 mL/min and 95% B, with 30 seconds column equilibration.
- 5-minutes run time per sample: steady flow rate of 0.7 mL/min, 95% A for two minute and 50-seconds, 95% B for one minute, with 2-minutes column equilibration.
- 7-minutes run time per sample: steady flow rate of 0.5 mL/min, 95% A for 50-seconds to 5-minutes, switching to 95% B, and back to 95% A from 5.51 minutes to 7 minutes (equilibration).

Out of the tested separation gradients, the seven-minute method yielded the best analyte separation in tandem with the optimized MS method. This was crucial for the early eluting analyte OLN that would otherwise pass away without undergoing any separation.

Figure 9. Average concentration alongside theoretical concentration of the calibrators. Error bars indicate standard deviation.

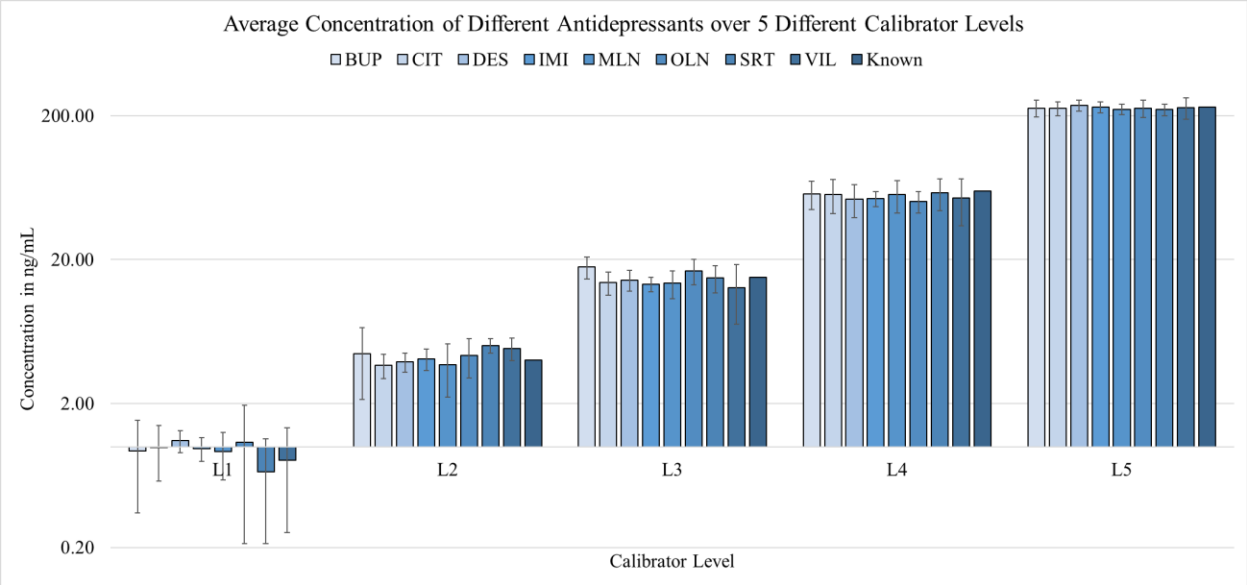

Table 5. *Average measured concentration per calibrator level; %CV as a measure of precision (n=18/level).*

a) BUP

Calibrator Level	$\underline{\mu_x} \pm \sigma$ *(ng/mL)*	*%CV*	*% Accuracy*	*Average* R^2*-value*
L1	0.71±0.11	*15.76*	*64*	*0.986*
L2	4.45 ±0.25	*5.62*	*115*	
L3	17.96 ± 1.20	*6.70*	*125*	
L4	59.37 ± 3.31	*5.58*	*98*	
L5	227.52 ± 2.70	*1.19*	*99*	

b) CIT

Calibrator Level	$\underline{\mu_x} \pm \sigma$ *(ng/mL)*	*%CV*	*% Accuracy*	*Average* R^2*-value*
L1	1.03 ±0.15	*14.7*	*93*	*0.989*
L2	3.59 ±0.35	*9.0*	*104*	
L3	14.70 ± 1.85	*12.6*	*103*	
L4	60.53 ± 1.32	*2.2*	*101*	
L5	229.80 ± 2.75	*1.2*	*100*	

c) DES

Calibrator Level	$\underline{\mu_x} \pm \sigma$ *(ng/mL)*	*%CV*	*% Accuracy*	*Average* R^2*-value*
L1	0.94 ±0.04	*4.1*	*88*	*0.987*
L2	4.23 ±0.14	*3.4*	*109*	
L3	14.43 ± 0.66	*4.6*	*100*	
L4	62.90 ± 0.91	*1.5*	*104*	
L5	227.50 ± 0.57	*0.3*	*99*	

d) IMI

Calibrator Level	$\underline{\boldsymbol{\mu_x}} \pm \boldsymbol{\sigma}$ *(ng/mL)*	*%CV*	*% Accuracy*	*Average* $\boldsymbol{R^2}$*-value*
L1	0.9 ±0.04	*4.2*	*89*	*0.991*
L2	4.33 ±0.12	*2.8*	*109*	
L3	14.88 ± 0.61	*4.1*	*101*	
L4	61.27 ± 0.77	*1.3*	*102*	
L5	228.61 ± 0.58	*0.3*	*96*	

e) MLN

Calibrator Level	$\underline{\boldsymbol{\mu_x}} \pm \boldsymbol{\sigma}$ *(ng/mL)*	*%CV*	*% Accuracy*	*Average* $\boldsymbol{R^2}$*-value*
L1	1.06 ±0.31	*18.82*	*95*	*0.978*
L2	4.30 ±0.64	*14.9*	*120*	
L3	14.78 ± 0.76	*5.1*	*99*	
L4	60.12 ± 1.89	*3.1*	*99*	
L5	229.86 ±1.82	*0.8*	*100*	

f) OLN

Calibrator Level	$\underline{\boldsymbol{\mu_x}} \pm \boldsymbol{\sigma}$ *(ng/mL)*	*%CV*	*% Accuracy*	*Average* $\boldsymbol{R^2}$*-value*
L1	0.89 ±0.03	*3.0*	*92*	*0.988*
L2	4.30 ±0.22	*5.2*	*106*	
L3	16.33 ± 0.85	*5.2*	*108*	
L4	56.50 ± 1.28	*2.3*	*93*	
L5	231.99 ±1.33	*0.6*	*101*	

g) SRT

Calibrator Level	$\underline{\boldsymbol{\mu_x}} \pm \boldsymbol{\sigma}$ *(ng/mL)*	*%CV*	*% Accuracy*	*Average* $\boldsymbol{R^2}$*-value*
L1	0.87 ±0.02	*2.2*	*86*	*0.986*
L2	4.26 ±0.06	*1.5*	*107*	
L3	15.98 ± 0.51	*3.2*	*107*	
L4	60.52 ± 1.13	*1.9*	*101*	
L5	228.38 ±1.11	*0.5*	*99*	

h) VIL

Calibrator Level	$\underline{\boldsymbol{\mu_x}} \pm \boldsymbol{\sigma}$ *(ng/mL)*	*%CV*	*% Accuracy*	*Average* $\boldsymbol{R^2}$*-value*
L1	1.04 ±0.08	*7.4*	*101*	*0.982*
L2	4.14 ±0.30	*7.3*	*104*	
L3	13.47 ± 0.43	*3.2*	*92*	
L4	61.58 ± 3.28	*5.3*	*103*	
L5	229.78 ± 3.19	*1.4*	*100*	

3.4.4. Carryover and Stability

To establish the translatability of this assay at a clinical setting, it was important to assess the carryover effect as well as the long-term stability of the prototype. A minimal carryover is desirable since it would enable the testing of more patient samples, since the number of blank injections between samples can be minimized. Both Carryover and Stability studies were conducted according to our previous work[22]. Despite employing Needle Wash Solvent Chemistry, and advanced autosampler washes, there seemed to be statistically significant sample carryover for all the antidepressants, i.e., %CV of L1 followed by L5 injected exceeded 25% across the board (n=24), when compared to the baseline L1 (injected after blank). Therefore, we recommend performing two blank injections prior to each unknown sample quantification. This data spread is shown in Figure 4a, post-outlier removal.

In addition to assessing sample carryover, we performed a 14-days accelerated stability study (224 days extrapolated), with n=2 per calibrator level per day, storing the samples and -20°C and stressing them at +20°C. We observed about 80% degradation in samples for all analytes at the 14th-day mark, which translates to about 7.5 months at storage temperature. When looking at a concentration by area normalized to 1 to indicate degradation, CIT, DES, IMI, and MLN exhibited a steadier decline, unlike the steep decline of the other drugs. However, when the L5 data for all days and all analytes were used to construct a trendline to predict degradation, only CIT, MLN, and VIL exhibited analyte stability of about 1.1 months (two days, interpreted), as seen in Figure 4b. BUP and OLN showed the highest degradation within two-days, while others overlapped in their degradation trend. Since the number of samples tested were not sufficient, a statistical claim about the stability of all the analytes in the prototype kit inconclusive.

Figure 10. a) Boxplot diagram showing the spread of L1 following L5 injections, and L1-base. Outliers removed; n=24.

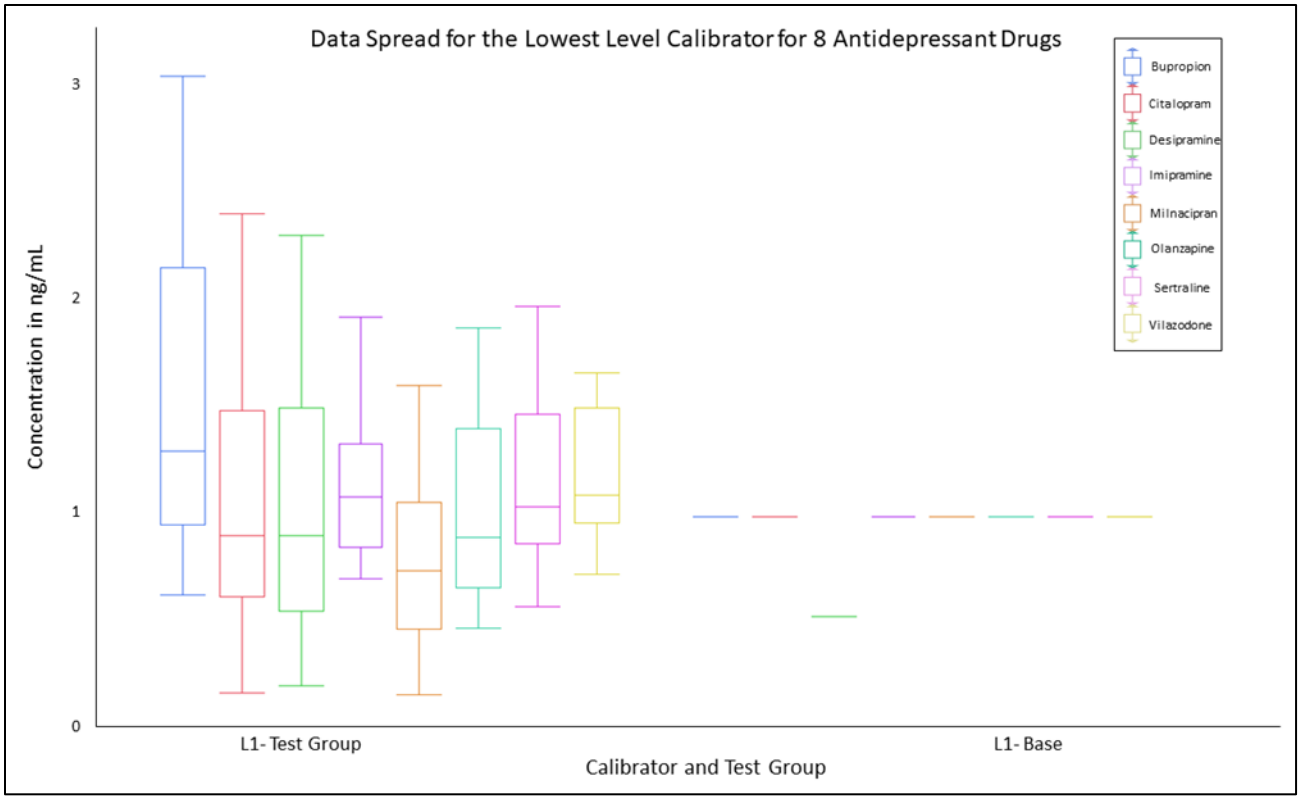

Figure 10. b) Average concentration by area of L5 across 14-days and extrapolated trendlines showing analyte degradation (n=2).

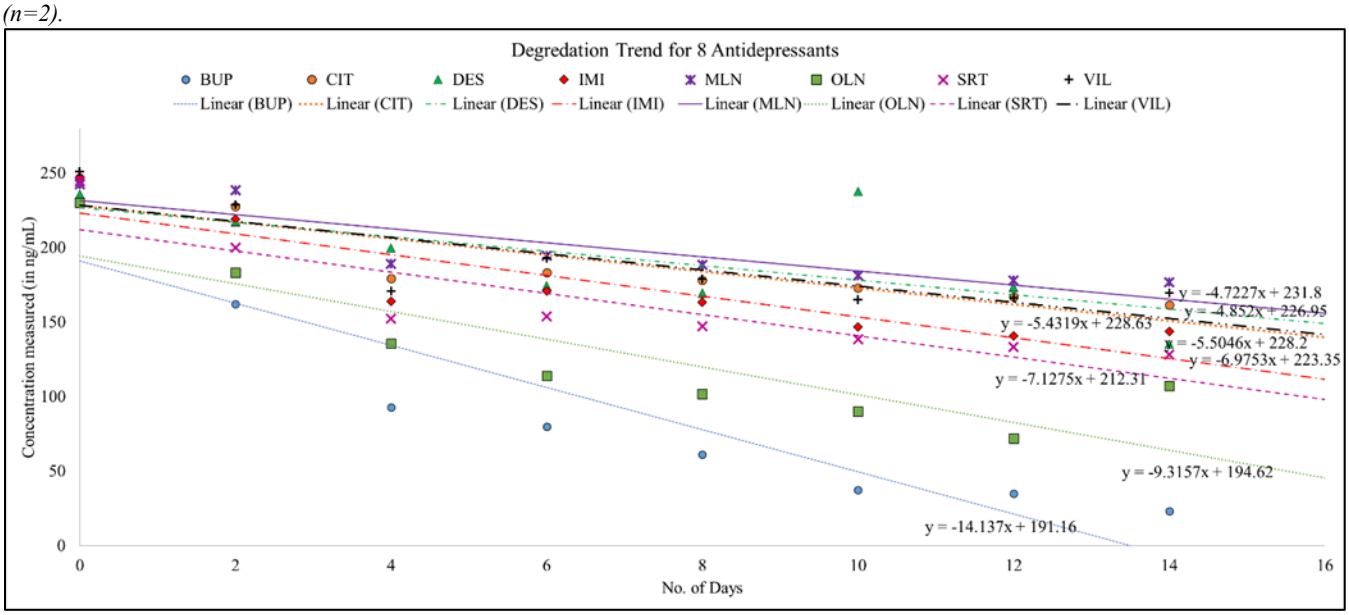

3.4.5. *Ease of Automation*

Mere establishment of an effective protocol for antidepressants monitoring is futile unless it can be translated for a large number of sample testing, enabled by automation. To do this, we

performed a head-to-head analysis for the ease of automation of our prototype kit against the commercial Eureka kit. The parameters investigated included: speed/sample preparation time, automation compatibility, and overall clinical relevance. While both protocols have similar workflows, the commercial kit is less conducive to automation as it relies on a tube-based method rather than a plate-based method and requires 100 µl of sample input. This is a significantly large volume compared to our prototype kit, which requires only 20 µl input. Additionally, tube-based methods decrease the number of patient samples that can be prepared and subsequently analyzed per unit of time. Reported run times for completion of sample preparation automation protocol are reported below in Table 4. Additionally, the feasibility of each of the automation techniques were reviewed with greater ease being seen in the operation of the proposed prototype kit. This means that it has the potential to be a viable option for clinical application, especially those involving low-volume sample collection techniques. Just like our previous study[22], we assessed the efficiency of the automated sample preparation using %CV against manual plating. The results obtained were comparable, with the added advantage of automation to minimize error propagation.

Table 6. Time comparison for the proposed study against a commercial kit.

Sample Preparation Method	Calibrators in triplicate only (mm:ss)	Full plate with triplicate calibrators and 48 patient samples (mm:ss)	Additional Time (Off Deck)	Total Time (Full Plate) (mm:ss)
Proposed Protocol	09:21	17:15	+05:00 Plate Shaker +10:00 Centrifuge	32:15
Eureka	05:26	39:02	+00:10 Vortex +10:00 Centrifuge +00:05 Vortex	49:17

3.5.Conclusion

Even though LC-MS/MS studies have been conducted on human serum to simultaneously quantify different antidepressants, our work here performs an in-depth analysis on 8 different antidepressant drugs from 4-different classes using only 20µL sample volume. Our method is easy and accurate, and more importantly automation friendly. Our study delves into the minute details of establishing and optimizing a prototype kit that can be utilized at a clinical setting, with precision and accuracy comparable to previously established studies. When compared to existing commercial kits available outside of United States, our prototype kit showcased extreme ease for automation adaptability, with minimal sample loss. Owing to the small volume need for our assay, it has the potential to be implemented to quantify the use of antidepressants in postpartum mothers, as well as their infants, to assess the level of drugs that may be passed on during the nursing period.

3.6.Acknowledgments

We would like to thank Collin Hill and Grace Van Der Gugten for their invaluable feedback during the development of this study.

3.7.Supporting Information

Table S4. Optimized Multiple Reaction Monitoring (MRM) parameters for the drugs of interest.

Analyte	Q1	Q3	EV	CC_L2	CC
Bupropion	240.2	131.1	11	-52	-34
Citalopram	325.1	109.1	7	-80	-32
Desipramine	267.2	208.2	28	-80	-29
Imipramine	281.1	86.1	10	-92	-36
Milnacipran	247.3	129.2	15	-36	-34
Olanzapine	313.2	256.1	31	-72	-28
Sertraline	306.1	159.1	16	-88	-33
Vilazodone	442.4	155.1	20	-122	-58
Fluoxetine D6	316.2	154.3	26	-60	-13
Citalopram-D6	331.2	234.2	20	-96	-36
Mirtazapine-D3	269.2	209.1	20	-88	-30
Clomipramine-D3	354.3	100	16	-56	-13
Milnacipran-D10	257.3	110.3	24	-60	-27
Bupropion-D9	249.2	139	19	-60	-38
Vilazodone-D4	446.4	197	23	-110	-39

Figure S1 (a)
Deck layout for the automation of the prototype kit sample preparation developed and reported in this paper. The proposed sample preparation yields a 96-well plate with up to 48 wells containing patient samples as well as a full precision plate for standardization and improved analysis. Patient samples are housed on Columns 1-3, while calibrators were housed on the vial rack in Column 7, row C.

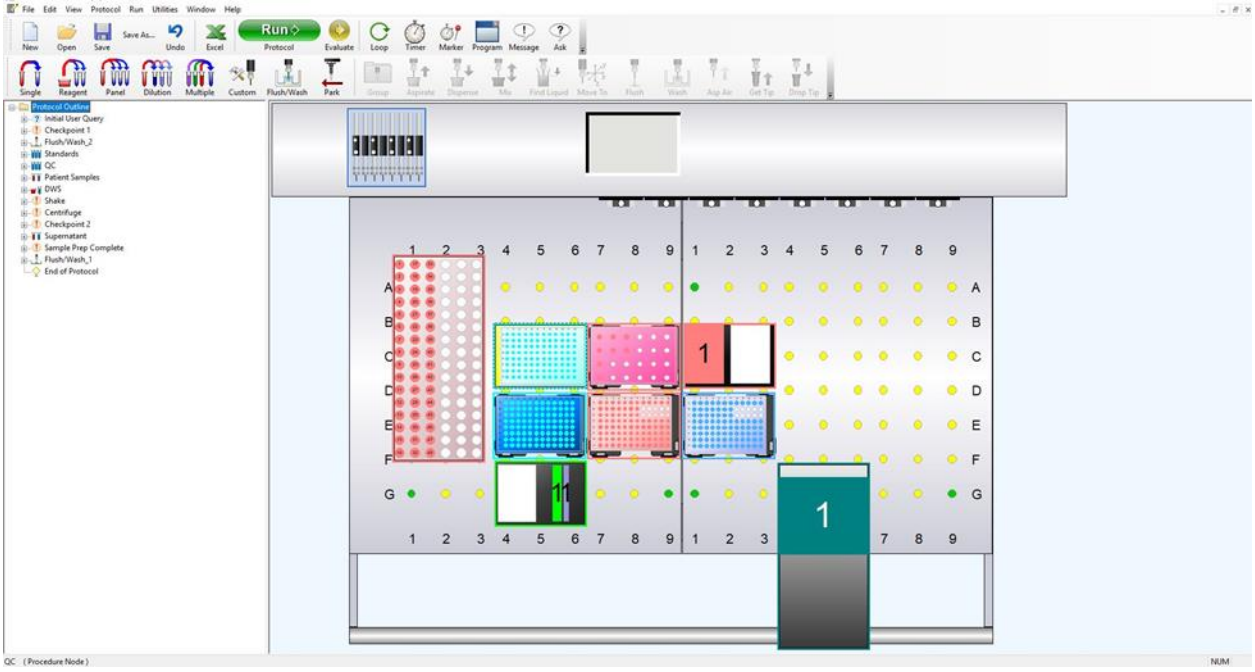

Figure S1 (b) Deck layout for the automation of the ADP sample preparation and analysis kit developed by Eureka (Commercial kit). The protocol shows the layout required for a vial-based protocol. Patient samples are housed on Columns 1-3, while calibrators were housed on the vial rack in Column 7, row B.

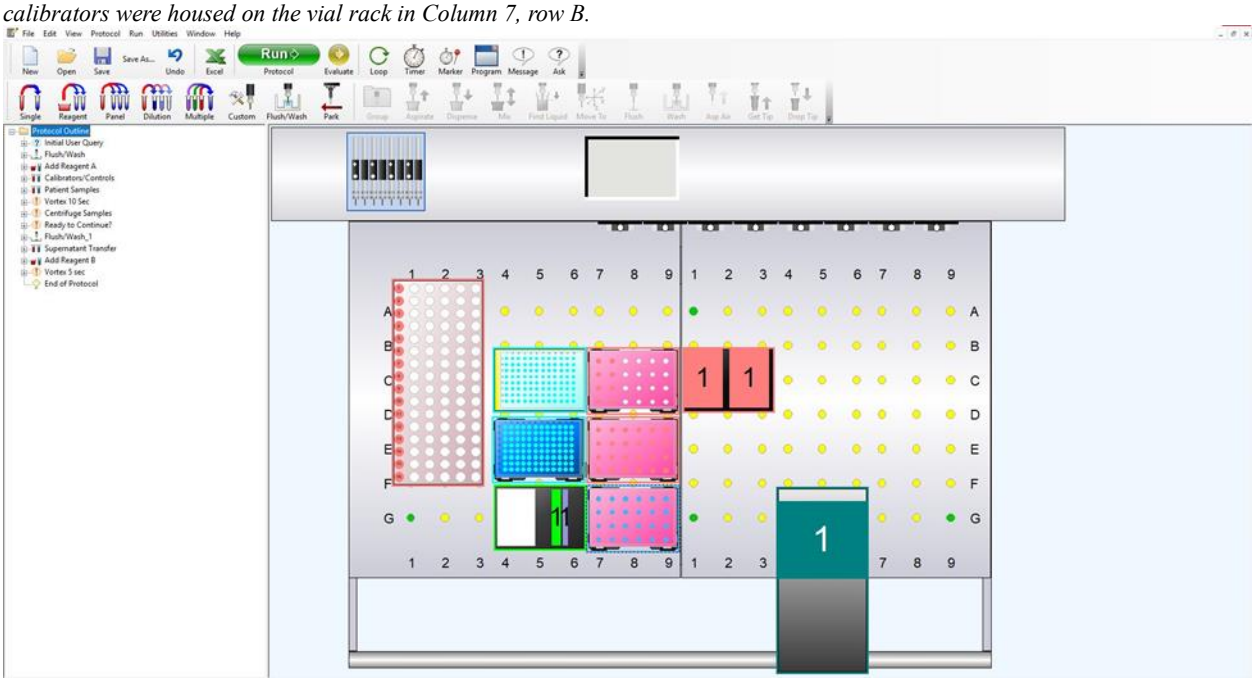

Figure S2. Running samples from the Eureka kit yielded noise when plotted on an overlay for relative intensity. No distinct chromatograms were observed whatsoever.

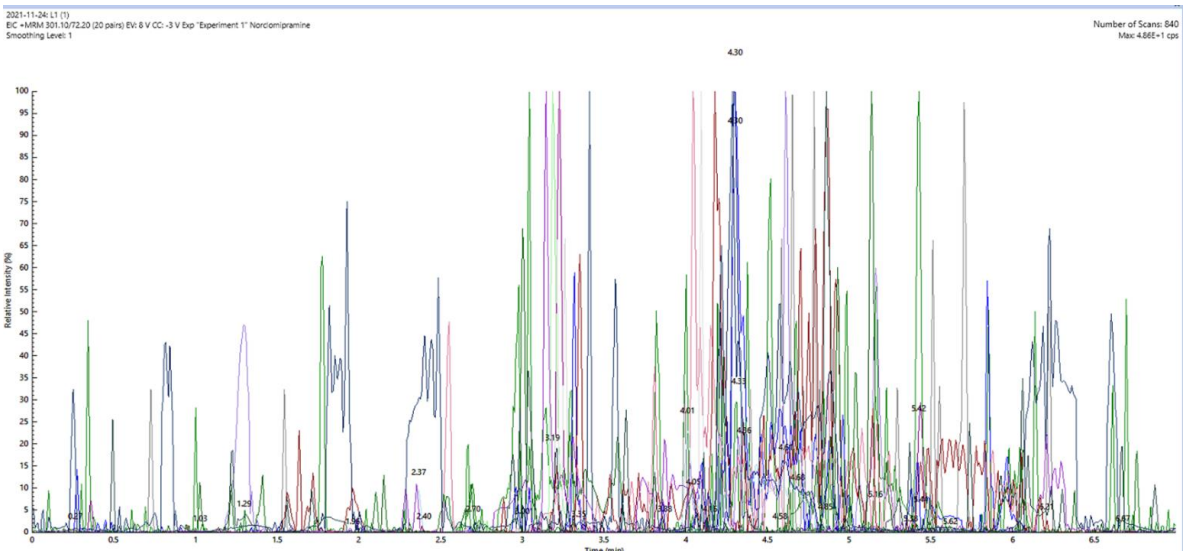

Figure S3. (a) MRM spectra of Bupropion (BUP), Citalopram (CIT), Desipramine (DES), Imipramine (IMI), Milnacipran (MLN), Olanzapine (OLN), Sertraline (SRT), Vilazodone (VIL) over a 3.5-minutes sum scans. Graphs have been superimposed to show parent mass (Q1) in blue and fragments (Q3) in orange (as seen on Simplicit 3Q (version 3.0).

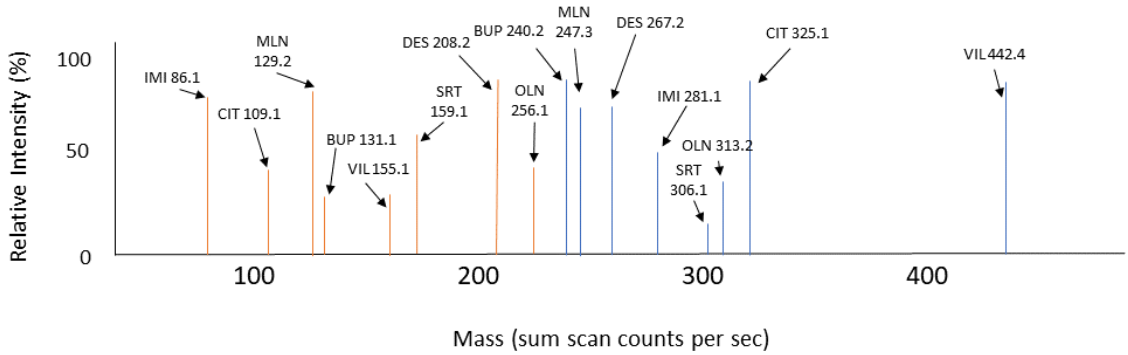

Figure S3. (b) MRM spectra of all internal standards, i.e., labeled analytes, Fluoxetine- D6 (FLU D6), Citalopram-D6 (CIT D6), Mirtazapine-D3 (MRT D3), Clomipramine-D3 (CLO D3), Milnacipran-D10 (MLN D10), Bupropion-D9 (BUP D9), Vilazodone-D4 (VIL D4) over a 3.5 minutes sum scans. Graphs have been superimposed to show parent mass (Q1) in blue and fragments (Q3) in orange (as seen on Simplicity 3Q (version 3.0).

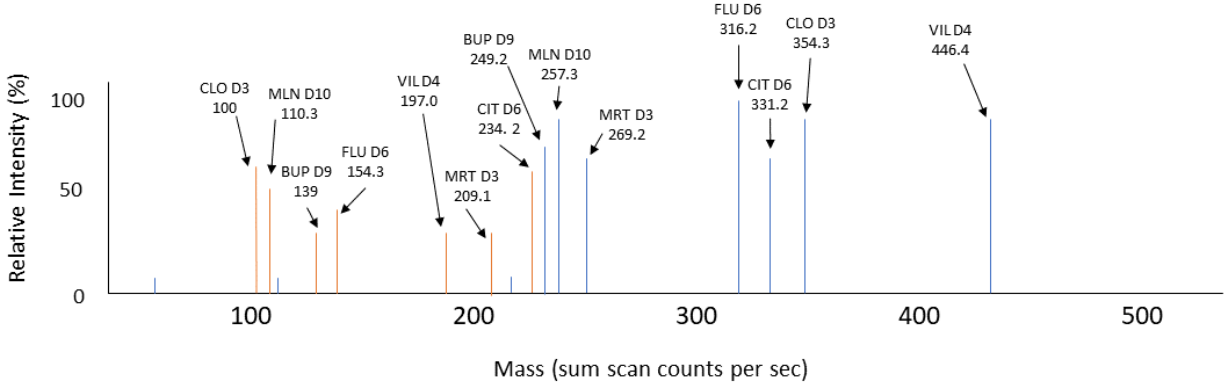

Figure S4. Fragmentation patterns for the analytes as detected on QSight 220 CR (structures and patterns generated using ChemDraw 22.0 (PerkinElmer Inc.)): bupropion, citalopram, desipramine, imipramine, milnacipran, olanzapine, sertraline, vilazodone.

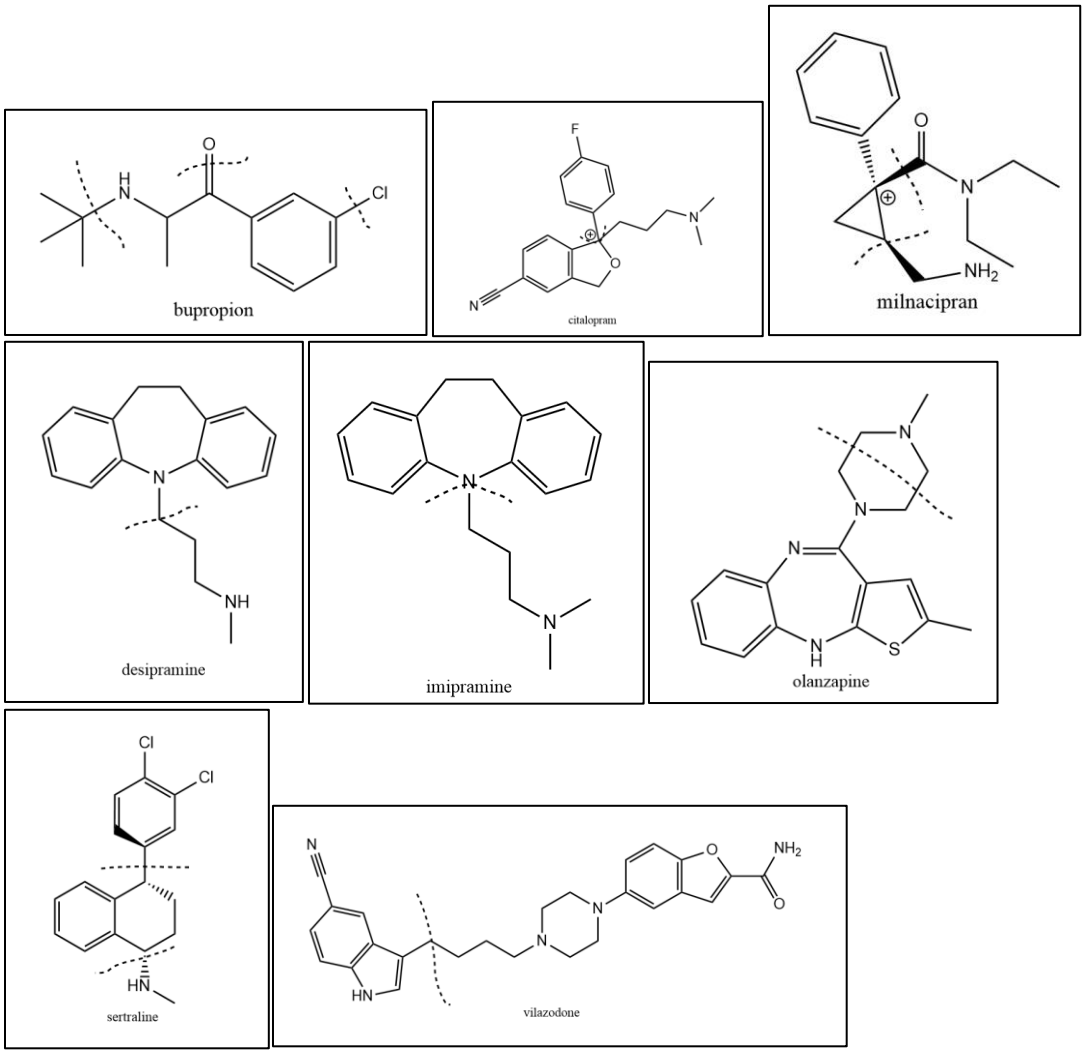

Chapter 4: Electric Field-Assisted Dried Blood Spot Sample Preparation Analysis of Steroids for PCOS Detection using LC-MS/MS

Chapter 4 is under final review to be published as an original research article.

Fariha, R.[1], Rothkopf, E. [1], Murphy, J.[1], Walters, N.[1], Okoh, O.D.[1], Lawandy, N.M.[1],

Tripathi, A.[1*]

1 Brown University Center for Biomedical Engineering

4.1.Abstract

Polycystic Ovary Syndrome (PCOS) is the most prevalent endocrine and metabolic disorder amongst both female adolescents and adults. Despite the prevalence of the disorder, the diagnosis of PCOS is extremely challenging, and the condition often goes un- or underdiagnosed. Hormonal dysregulation is a hallmark of PCOS, but disease detection via hormonal test is inaccessible in limited resource settings. This study addresses the challenges associated with remote sampling by investigating the use of dried blood spots (DBS) samples to quantify four commonly dysregulated hormones in PCOS -- testosterone, 17-hydroxyprogesterone, progesterone, and cortisol -- using liquid chromatography tandem mass spectrometry (LC-MS/MS). In addition to reporting the validation of a whole blood-based linearity series, this study showcases the use of an electric field as a driver of analyte extraction from 50 μL DBS samples. The study also investigates the impact of electric field direction, first through theoretical modeling and then via experimentation using a customized vial setup, ultimately demonstrating that a vertical electric field configuration is able to recover twice the concentration of analytes from DBS compared to a horizontal electric field.

4.2. Introduction

Polycystic Ovary Syndrome (PCOS) is the most common endocrine-metabolic disorder in women of reproductive age [83, 84]. In the United States alone, PCOS affects 5 million women of childbearing age, and annually, the country pours over $4 billion into the identification and management of the disease [84]. On a global scale, PCOS affects approximately 6-10% of women of reproductive age [84], including women in Nepal, Bangladesh, and resource poor countries in Africa, where diagnostic tools such as ultrasound and MRI are limited in availability [85, 86]. While the exact causes of PCOS are still poorly understood, patients commonly present with functional abnormalities of the hypothalamic-pituitary axis [85]. The three most critical symptoms

associated with PCOS are hyperandrogenism, oligo- or anovulation and resultant oligo- or amenorrhea, and polycystic ovary morphology [88-90]. Other signs and symptoms of the condition include enlarged ovaries with cysts, irregular menstrual cycles, pelvic pain, hirsutism, alopecia, acne, acanthosis nigricans, and skin tags [86]. Additionally, PCOS patients are at higher risk for metabolic dysfunction. Considering the infertility challenges and multiple other comorbidities that PCOS patients may encounter as they age, early identification of the disease is crucial. However, patients experiencing these PCOS symptoms tend to present differently with respect to age, posing a challenge to the early identification of the condition when taking an observational or elimination approach to diagnostics [91]. Many women are not diagnosed with the condition until adulthood, even when menstrual irregularities – a common symptom of PCOS – are present during their adolescent years [88]. Such symptoms often go unreported or are ignored, in part out of stigma and in part out of poor patient and physician education surrounding menstrual irregularities such as dysmenorrhea. In fact, as high as 75% of patients overall remain undiagnosed after consulting with a physician [91]. Because of the ambiguity associated with PCOS symptoms, the condition is diagnosed via the elimination of other diseases. Hormonal testing is frequently used to confirm hyperandrogenism or ovarian dysfunction and exclude similar disorders [93]. However, current diagnostic tools lack sensitivity, making the proper assessment of hyperandrogenism difficult. Dried blood spots (DBS) have been extensively studied for multianalyte screening using tandem mass spectrometry for both newborn and adult patient samples[9-13]. Given that DBS can be prepared using non-invasive techniques and can maintain stability in ambient temperatures, we investigated the use of DBS for hormone-based adolescent PCOS diagnostics, particularly for women in low-resource countries [94-105]. We used two different types of DBS cards (standard Whatman 903 Protein Saver cards, and not chemically

coated FTA DMPK-C cards) and for capillary blood collection (finger-prick) to quantify testosterone (T), 17α-hydroxyprogesterone (17-OHP), progesterone (P), and cortisol (C) using liquid chromatography tandem mass spectrometry (LC-MS/MS) [107-117]. Additionally, we address the limitation of analyte recovery [102] of DBS by using an Electric field assisted sample preparation method that is fast, efficient, and relatively inexpensive.

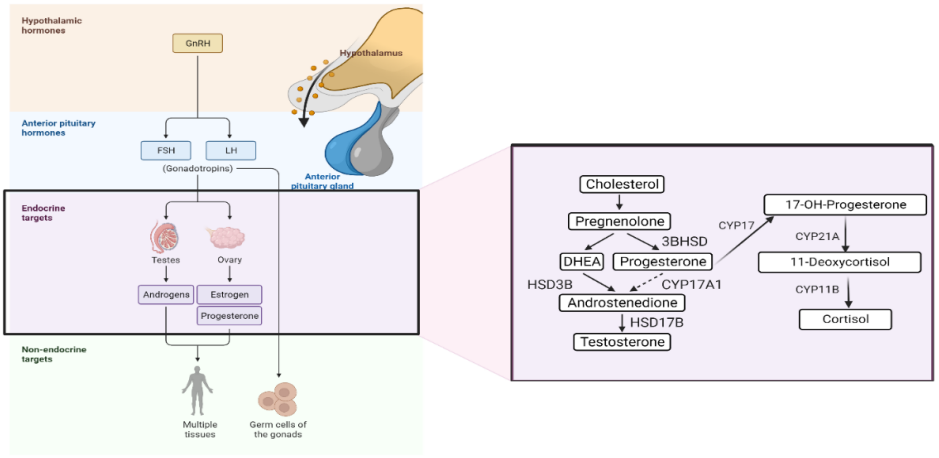

Figure 11 Biosynthesis pathway of the analytes of interest (figure created using Biorender)

4.3. Experimental

4.3.1. Materials and Reagents

Baker Analyzed >99% pure LC-MS grade solvents were purchased from VWR (PA, USA), including water, acetonitrile, and methanol. Testosterone (T-037), Testosterone-2,3,4-13C3 (T-070), Androstenedione (A-075), Androstene-3,17-dione-2,3,4-13C3 (A-084), 17α-Hydroxyprogesterone (H-085), 17α-Hydroxyprogesterone-D8 (2,2,4,6,6,21,21,21-D8) (H-096), Progesterone (P-069), Progesterone-D9 (P-070), Cortisol (C-106), Cortisol-D4 (9,11,12,12-D4) (C-113) Certified Reference Materials were purchased from Cerilliant Corporation (Round Rock, TX, USA). Reagent-grade formic acid (96% pure) was purchased from Fisher Scientific (NH, USA). Blank human whole blood was purchased from UTak (CA, USA). Axygen 96-well 500 µL polypropylene plates were purchased from Corning (NY, US), Nunc 96-Well V-Bottom 250µL

polypropylene plates, and adhesive aluminum foil seals were purchased from ThermoFisher Scientific, and clear Rapid EPS plate seals were purchased from Nacalai USA. Two types of DBS cards used in this study were Whatman 903 Protein Saver Cards and Qiagen FTA DMPK-C cards, purchased from Millipore Sigma (MA, USA).

4.3.2. Electric Field Application

Sterile, disposable electroporation cuvettes (1 mm gap) were purchased from Thomas Scientific (NJ, USA) for the left-to-right (horizontal) electric field application. For the top-to-bottom (vertical) electric field application, we modified 2 mL polypropylene microcentrifuge tubes (with screw caps, Fisher Scientific, NH, US) by first screwing a 6-32 x ¼ Stainless flathead screw (McMaster # 91771A144) into a 0.104" undersized hole drilled into the bottom of the tube. Upon each screw, one 6-32x0.437 aluminum spacer was attached to the countersink side and tightened. This spacer acted as the bottom electrode within our two-electrode system. To construct the top electrode, a 0.140" hole was first drilled into the center of the microcentrifuge tube cap. Then, using the 0.25 mL electrode spacing fixture, a 6.32x1.5 truss head screw (SS McMaster #91770A156) was loaded with one 6-32 x 0.375 aluminum spacer (McMaster #93330A443), the microcentrifuge tube cap, and another 6-32 x 0.375 aluminum spacer, in that order. The spacers were first finger-tightened and then jam locked using 2 pairs of pliers to maintain uniformity in spacing between each vertical-field DBS device. The drawings relevant to this assembly process are shown in Supplemental Figure 2 (a) and (b).

To process six vertical DBS separation samples at once, we also constructed a 6-vial holder. The base of this holder was constructed from ¼" acrylic, upon which two ¼" fuse clips (Digikey 36-3531-ND) were attached using 4-40x 1/2 ph SS screws (McMaster 91 772A110). Each set of two fuse clips was spaced such that one fuse clip held the aluminum spacer located at

the top of the separation apparatus, and the other held the aluminum spacer located at the bottom. On the opposite side of the acrylic sheet, each of the 4-40 x1/2 ph SS screws were loaded with one 18awa #6 pan crime ring connector (Digikey # 298-16802-ND). The screw and the ring connector were then secured in place with a 4-40 Nut SS (McMaster 91841A005). This is shown in Supplemental Figure 2 (c). Preliminary testing was performed using a single tube holder (Supplemental 2 (d)) prior to scaling up for the sextuplet connection (Supplemental 2 (e)).

After complete assembly, the parts were thoroughly cleaned with 70% ethanol, and UV-sterilized overnight.

4.3.3. LC-MS/MS Conditions and Parameters

All analytes and internal standards were diluted 1000-folds and a 100-fold in HPLC-grade acetonitrile, respectively, and used for MS method optimization via direct infusion using a 1mL gastight Hamilton syringe and Harvard apparatus (operating at flow rate 30 μL/min) in Multiple Reaction Mode (MRM). The parent and MRM masses, along with optimized parameters for entrance voltage (EV), prefilter (PF), collision cell lens 2 (CCL2), collision energy (CC), and detector deflector (ID), are listed on Table 1. Additionally, the source parameters were optimized to operate at drying gas= 80, HSID (hot surface-induced desolvation) temperature= 320 °C, nebulizer gas= 200, electrospray voltage= 5850 V, and source temperature= 200 °C (ESI positive). The instrument used was a PerkinElmer QSight 220 CR Triple Quadrupole Mass Spectrometer (with dual source), with LX50 Solvent Delivery Module, Precision Sampling Module, and Column Stability Module.

The column used for the study was ThermoFisher Hypersil Gold C18 (2.1 x 50 mm, with 1.9 μm particle size, and 175 Å pore size) operating at 25°C with a 0.3 mL/min flow rate. The mobile phases were optimized to be water with 0.1% formic acid (A) and acetonitrile with 0.1%

formic acid (B), similar to the method described in our previous study, along with the same Needle Wash Solvent Chemistry optimization strategy[25]. The LC method employed was a 7-minutes long method, with a 2-minutes hold of 30% B, increasing to 50% B for a minute, and increasing to 90% B for 3.5-minutes, before returning to 30%B, while the samples were housed at 4°C in the autosampler.

Analyte	***MRM***	***Q1***	***Q3***	***EV***	***PF***	***CCL2***	***CC***	***ID***
T	*Quant*	*289.4*	*97.2*	*27*	*-17*	*-220*	*-20*	*-120*
	Qual		*109.2*	*32*	*-21*	*-211*	*-10*	*-124*
	IS- 1	*292.0*	*100*	*3*	*-30*	*-63*	*-30*	*-103*
	IS- 2		*112*	*14*	*-36*	*-92*	*-26*	*-104*
17-OHP	*Quant*	*331.5*	*97.1*	*35*	*-17*	*-58*	*-37*	*-111*
	Qual		*109.1*	*36*	*-23*	*-61*	*-39*	*-111*
	IS	*334.3*	*290.2*	*34*	*-12*	*92*	*-27*	*-91*
P	*Quant*	*315.4*	*97.1*	*29*	*-16*	*-215*	*-60*	*-122*
	Qual		*109.1*	*34*	*-17*	*-213*	*-29*	*-122*
	IS	*324.3*	*113.1*	*27*	*-22*	*-64*	*-30*	*-102*
C	*Quant*	*363.1*	*120.9*	*10*	*-15*	*-69*	*-33*	*-133*
	Qual		*327.1*	*10*	*-15*	*-67*	*-20*	*-120*
	IS	*367.1*	*120.9*	*10*	*-15*	*-69*	*-33*	*-133*

Table 6666. Mass parameter table for all the analytes (with both MRMs) and their respective internal standards, operating on ESI positive mode.

4.3.4. Preparation of Calibrators, Quality Controls, and Daily Working Solution

All calibrators and quality controls (QC) samples were made using blank whole human blood as the base matrix, following the 1:1 analyte relationship of wet blood to DBS (whole blood calibrators can be used to establish a standard curve to be used directly to quantify analyte levels in DBS) [38]. Briefly, stock solutions were used to spike the whole blood for levels 1-6 (L1-L6) and QC- Low and High, using two or three-fold dilution methods, ensuring that the percentage of organic solvent in each calibrator was less than 0.5% total. The analytes were added while the blood continuously stirred at room temperature, and post analyte addition, the calibrators were rocked overnight at 4°C, prior to quality analysis. All calibrators and QCs were aliquoted and stored at -80°C in batches and only thawed once for analysis.

The Daily Working Solution (DWS) was the extraction solvent used to process the whole blood calibrators and the dried blood spots. Several formulations of the DWS were tested (data not reported) for efficient protein precipitation and to obtain a proper Gaussian chromatogram. The final DWS formulation was composed of a 1:1.2 acetonitrile to water solution with 0.1% formic acid (to be used ice cold for wet blood, and room temperature for DBS) with the internal standards for T, 17-OHP, P and C at a 10 ng/mL concentration for all the analytes.

4.3.5. Sample Preparation

4.3.5.1.Calibrators and QCs

For the calibrators and QCs in wet blood, 50 µL of each calibrator and QC were plated on to the Axygen plate followed by 150 µL of the DWS and foil sealed prior to shaking in a TriNEST incubator shaker (Revvity, MA, US) at 60 °C at 800 rpm for 5 minutes. The plate was then centrifuged at 4 °C at 4600 rpm for 10-minutes, prior to transferring a 50 µL supernatant on to a Nunc plate (sealed with clear seal) for LC-MS/MS analysis. Caution was observed to ensure that the collected supernatant was clear (red in color) and did not contain any particulates.

4.3.5.2.Dried Blood Spots

To prepare the DBS treatment groups, blank blood was spiked into two groups- low (same concentration as calibrator L2) and high (same concentration as calibrator L5). Then, the two types of cards were spotted with 50 µL of these treatment blood groups and allowed to dry overnight. To minimize the hematocrit levels and punch effect, all the spots were sub-punched to 6.35 mm spots from the center of each spot prior to analysis.

For non-electrical DBS treatment: the DBS were placed in the Axygen plates and processed identically to the wet blood calibrators as mentioned above.

For electrical treatment- horizontal field: DBS punches were placed inside electroporation cuvettes (back of the spot to the negative electrode) with 150 µL DWS (per spot) and connected to a DC power supply (RIGOL DP712) using banana plugs, as described in Machado, M. et al. 2019[39].

For electrical treatment- vertical field: DBS punches were placed inside our custom vials, irrespective of the punch orientation to the bottom electrode, and 150 µL DWS (per spot) was added. The top electrodes we dipped in DWS (on a reagent reservoir) prior to placing inside the vial, so that the top electrode only touches the top of the DWS. The vial was then placed on the custom vial-holder, that was connected to the DC power supply.

For both conditions, the voltage applied was 10V for 180 seconds (3 minutes).

4.3.6. DoE, Computational Model, and Data Analysis

For the entire study, the Design of Experiment (DoE) was performed using JMP Pro 17.0 perform a full factorial design, for power> 80%. All LC-MS/MS data was collected and analyzed using Simplicity 3Q (version 3.0) software for QSight. A computational model of the vertical electric field device was created on COMSOL Multiphysics (version 6.1) using 3D Electric Current model. The data exported was further evaluated using Microsoft Excel, and JMP Pro 17.0

for visualization and statistical analysis (ANOVA, Dunnett's post-hoc test for significance against control (no electricity) and student's t-test for between group comparison for electric field direction). A p-value of 0.05 or less was considered statistically significant.

4.4.Results and Discussion

4.4.1. LC-MS/MS Method Optimization and Validation

While analyzing steroids using LC-MS/MS for clinical application is quite common, it is a standard practice to perform method optimization and validation since they are instrument specific, and there are lab-to-lab variabilities[40, 41]. Our study opted for a rather simplistic sample preparation process (protein precipitation) for future automation adaptability[38, 42]. The limit of blank (LOB), limit of quantitation (LOQ), matrix effect, and interference are defined as described in our previous study[43]. The LOB was <0 for all analytes, inclusive of both MRMs, while the LOQ was the lowest concentration of the linearity series in whole blood, that was reproducible with %CV±20% and (100±20) % sample accuracy. To rule out any native steroid presence, we ran triplicates of blank whole blood on each plate, and consistently observed no peaks at the expected retention times (RT) of the analytes. Blood is a complicated matrix, and it was difficult to obtain uniform dispersion of T, 17-OHP, P, and C across the board [44,45]. As a result, several iterations of the calibrators had to be prepared and analyzed for reproducibility and consistency prior to moving forward with any other testing. Figure 2 shows all the analytes, inclusive of both MRMs, and their RTs in whole blood. The mobile phases used were also optimized like our previous study[43]. For this specific assay, we tested out several percentages of formic acid (0.1%, 0.6%, and 1%) for enhanced ionization, and relied on data (not reported) to move forward with 0.1% formic acid as an additive.

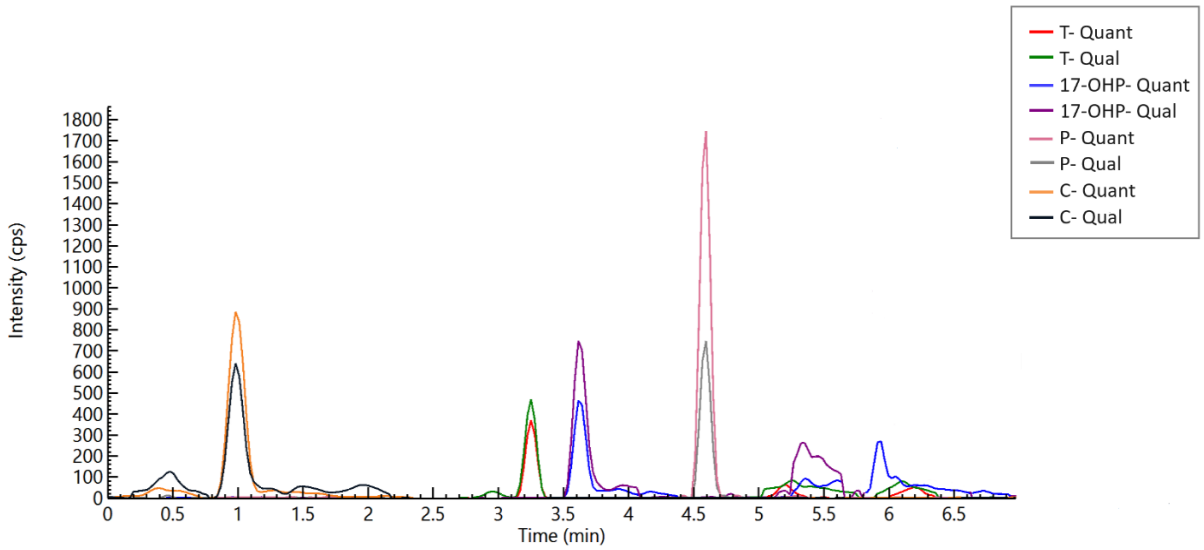

Figure 12 Chromatograms showing absolute intensity profile (e+6 cps) of the analytes in whole blood (MRMs).

Even though studies report a wide range of concentrations of T, 17-OHP, P, and C as an indicator of different stages and age specific PCOS (additional information on Supplemental Table 1), for the simplification of our study, we established the calibrator ranges such that: L1= 0.5 ng/mL, L2= 10 ng/mL, L3= 15 ng/mL, L4= 18 ng/mL, L5= 20 ng/mL, and L6= 25 ng/mL for all four analytes[44-47]. While this may not be reflective of the true range of the analytes in adolescent PCOS patients, for the sake of linearity, assay validation, and reproducibility, we chose to move forward with these concentrations. It is important to note that we additionally explored the potential of urine as an alternative matrix for PCOS detection, however, due to the lack of sufficient clinical data for these specific analytes, we chose to investigate DBS as a noninvasive sample source[48, 50-52]. Figure 3 shows the average concentration (by area) across 9-runs for all four of the analytes, inclusive of both MRMs along with the respective theoretical (known) (each level ran in triplicates per run; no outliers removed). Steroids typically have a high background, especially when analyzed in whole blood, and therefore, the peak for lowest calibrator (L1) had to be manually integrated, since the signal was only slightly above the background. Other than L1, all other calibrators had a %CV ≤20% (cut-off), confirming the reliability and precision of the assay

developed. The inter-assay %CV was 14.50% and 10.80% for T, 8.88% and 18.30% for 17-OHP, 7.80% and 3.46% for P, and 18.93% and 16.92% for C, for quantifier and qualifier, respectively (n=18). A similar trend was observed for accuracy measurement as well (generated by the software). All but L1 showcased % accuracy to be (100±20) % across the board for all MRMs. For each generated standard curve ($\frac{1}{x}$ linear regression weighting), R^2-value was taken as a measure of linearity, which was ≥0.90 for all analytes, inclusive of both MRMs.

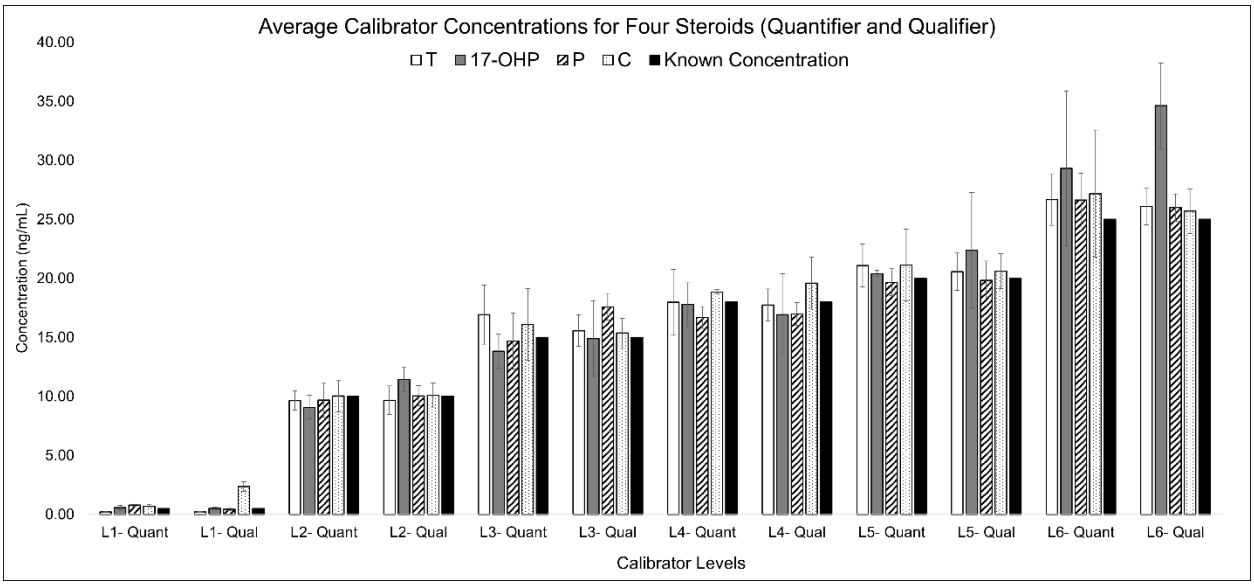

Figure 13 Average concentration for 6 calibrator levels for T, 17-OHP, P, and C (MRMs) along with known concentration (in ng/mL). Error bars represent standard deviation (n=27 per level per analyte)

To avoid analyte overestimation, we also performed a carryover analysis by injecting triplicates of L1 (lowest calibrator) immediately after injecting L6 (highest calibrator) (n=24). No significant spikes were observed in the measured concentration of L1 (cutoff 20%), and hence, it was concluded that there was minimal sample carryover. Figure shows the overall data spread of L1 test group for all the analytes.

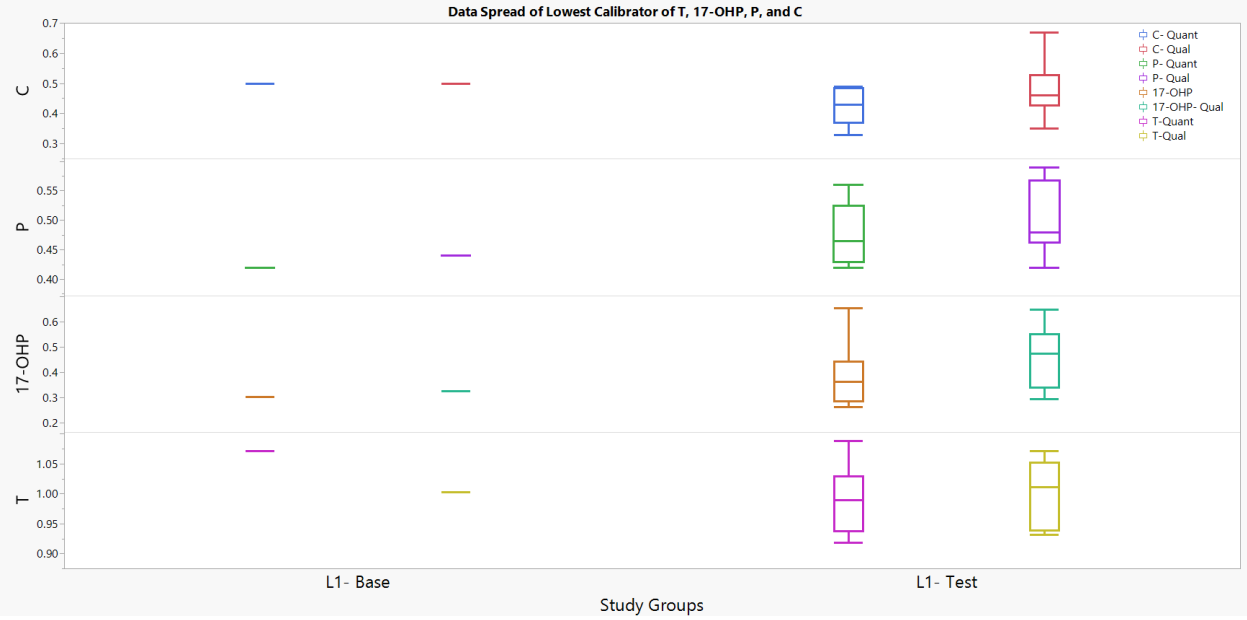

Figure 14. Boxplot spread of L1 against L1 base (injected following three blanks) for all analytes (both MRMs) (n=24 for test group).

4.4.2. DBS Analysis

4.4.2.1. Theoretical Modeling

Building upon the work of Lee at al. to use electric field for gDNA extraction, we chose to expand the electric field application to study hormonal extraction in a method that would be highly reproducible and precise for LC-MS/MS analysis[52, 53]. While using a commercially available electroporation cuvette served as a good starting point, working with DBS for LC-MS/MS sample preparation came with additional challenges, such as limited elution efficiency, associated cost etc.[54-57]. Prior to physical prototyping, we developed a model using COMSOL Multiphysics (3D, electric current, for a time-dependent study) to better understand the transport phenomenon taking place within the system. The idea was to model using materials as close to the true materials that could be utilized in prototyping. The material for the electrodes were the software's built-in Steel AISI 4340, and the fluid was modeled to be deionized water with electrical conductivity, σ= 5.5e-6 S/m, and relative permittivity, ϵ_r= 80 (at 20°C). Modeling the DBS was tricky, since several internal modifications take place within the paper as it stays in the solvent. Hence, the DBS was

modeled by customizing the built-in "Silicon" material, with electrical conductivity, σ= 0.05 S/m (drinking water), and the relative permittivity, ϵ_r= 2.3 (paper [141]).

This is best described using the time-dependent, vector form of the microscopic total current density, J, equation (eq. 1):

$$J = \sigma E + \frac{\partial D}{\partial t} + J_e \text{ (eq. 1)}$$

where, σ is the electrical conductivity (from each material), E is the electric field, $\frac{\partial D}{\partial t}$ refers to the displacement current density (time-varying component), and J_e represents the free current density.

Additionally, the equation used to describe the relation between electric displacement field, D, in this model was:

$$D = \epsilon_0 \epsilon_r E \text{ (eq. 2)}$$

where, ϵ_0 is the vacuum permittivity (constant), ϵ_r is the relative permittivity of each material, and E is the electric

The model depended on the electric field vector, which, in turn, is dependent on the electric potential. Our model consisted of the initial condition of V_0= 0V, and the electric potential, V= 10 V. Figure 5 shows this across time points: (a) t= 0 min, (b) t= 1 min, (c) t= 2 min, and (d) t= 3 min. It is clearly seen that the electric field distribution changes drastically within the first minute (all streamlines representing electric field norm pass through the DBS), while the ISO surface slices show the exact electric field distribution gradient over time on the DBS surface. The increase of electric field norm (t=2 min) followed by the decrease (t=3 min) was taken as an indicator that all the analytes had diffused out of the DBS into the surrounding solution, and running the electric field for longer would not have had an impact on analyte extraction.

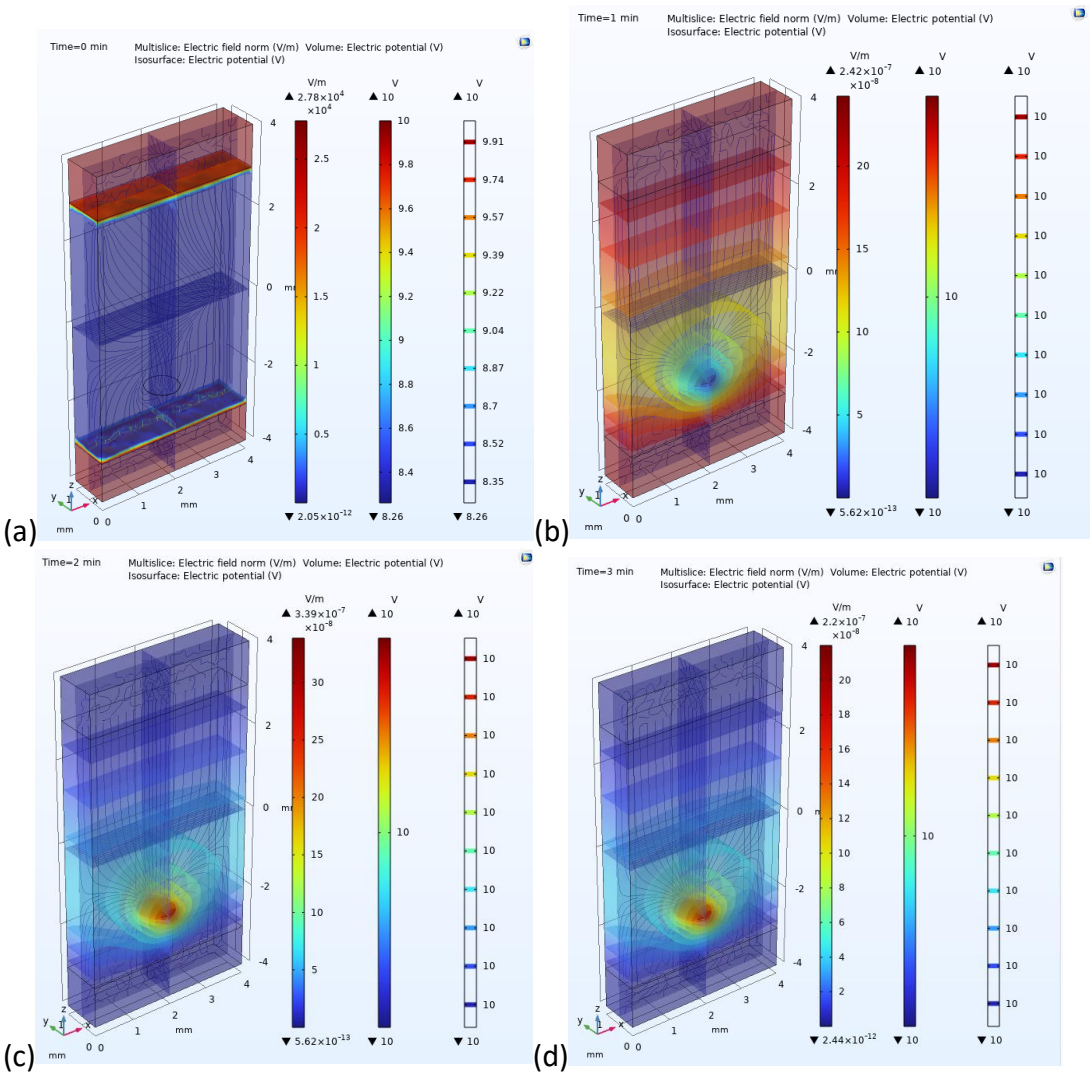

Figure 15. Vertical Electric field vial microenvironment across different time points (a) at t= 0 minute, there was no electric flux in the system, (b) at t= 1 minute, most electric field passed through the DBS, while the surrounding solution experienced increased electric field norm, (c) at t=2 minutes, most of the solution reached an equilibrium while the DBS continued to experience high electric field norm, and (d) at t= 3 minutes, the overall electric field norm declined, showing no further changes taking place within the microenvironment.

The results obtained from the model indicated that the vertical electric field application would be effective and might potentially outperform the traditional electroporation cuvettes. This is because the traditional cuvettes exhibit Helmholtz electronic double layer (EDL) properties resulting in potential drop as the electricity flows from left to right[60]. Overall, the results from the model looked promising when compared against previously reported electric field-assisted sample

extraction methods, especially those that render longer treatment time and complicated setup. Supplemental Table 3 lists some of these findings[53, 61-63].

4.4.2.2.Prototype Design Iterations

The initial iteration of the device (Supplemental Figure 2 (a)) was such that the electrodes would be nichrome wire coils (hand twisted) to sit on a regular plastic tube holder lined with copper tape. However, this idea was quickly discarded due to the lack of reproducibility and inconsistent electric field. A second version of the setup was created (using screws) wrapped with plastic insulation (heat sealed) (Supplemental Figure 2 (b)). While this was an improved iteration, however, the DWS was seen to creep up through the insulation gap, resulting in loss of solution volume in contact with the DBS for extraction. In addition to this, another challenge in this setup was the air trapped on the screw head of the top electrode. To mitigate this, we chose to pre-wet the top electrodes in DWS prior to inserting it inside the tube, thereby minimizing the introduction of air into the vial. Once these issues were resolved, we finalized the working volumes for extraction and accounted for any distance alterations that would arise due to the bottom electrode placement inside the vial. Hence, when we refer to a 0.25 mL spacer, we are really referring to a working DWS volume of 0.15 mL. Figure 6 shows the milieu of the setup, wherein, the circuit was only completed and working when the top electrode touched the DWS solution.

The setup was then tested using the single vial holder setup (Supplemental Figure 3 (d)) prior to scaling up to the 6-vial holder setup (Supplemental Figure 3 (e)). Once sufficient preliminary data was collected to prove our hypothesis (data not reported), the setup was then used to study DBS spots (low and high concentrations groups) using two 6-vial setups (12-spot analysis

at a time), increasing the throughput ability of the entire setup compared to individual electroporation cuvette study.

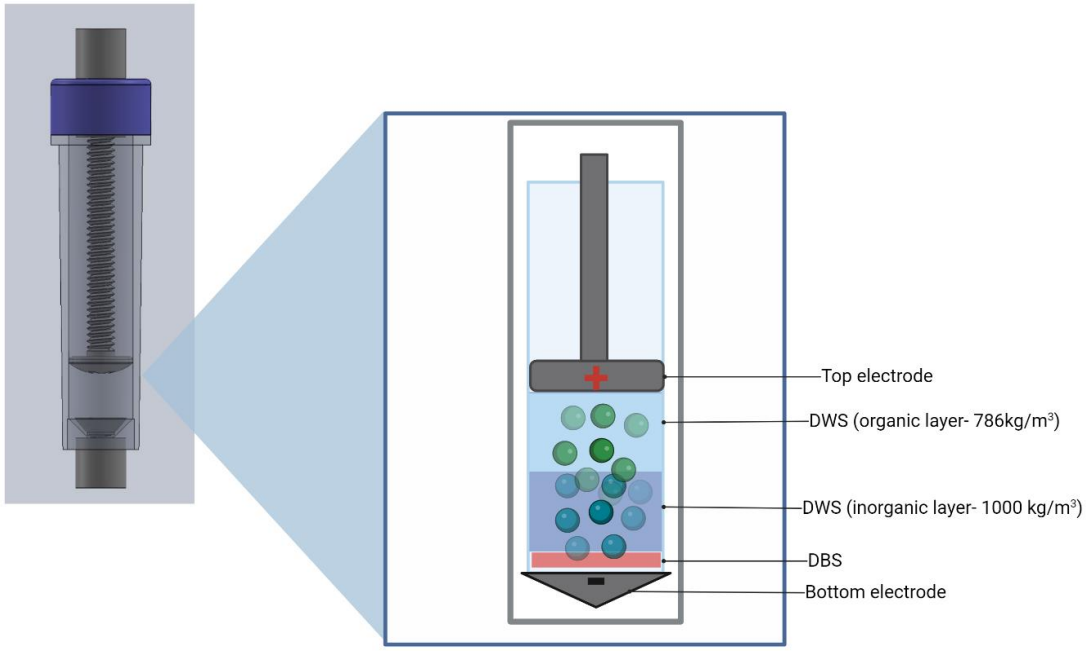

Figure 16. Insight into the vertical electric field setup for analyte movement (organic layer refers to the acetonitrile portion of the DWS and inorganic layer refers to the water layer. The DWS is a clear solution, but for better explaining the fundamentals, they are depicted using different colors in the image) (image created using Biorender).

4.4.3. Experimental Results

For both horizontal and vertical Electric field setups, effervescence was observed across all the spots as soon as the circuit was completed. It is noteworthy to mention that, for the vertical field setup, the 50 µL post-treatment extract was pale pink in appearance and particulate free and was easily collected for LC-MS/MS analysis (the density gradient illustrated in Figure 6 aided the collection process), unlike the horizontal field setup where the extract had to be centrifuged to remove particulates prior to analysis. This added an extra step to the sample preparation procedure and lowered the working volume of the post-treatment extract.

For each card type (Whatman 903, DMPK-C) and concentration (Low= 10 ng/mL, and High= 20 ng/mL), both electrical setups were tested (horizontal electric field- traditional

electroporation cuvette setup, vertical electric field- custom vial setup). Since the DBS cards used for the analysis were spiked in two batches (stored no longer than 24-hours post-drying), there would be batch-to-batch, plate-to-plate variability. Hence, the results obtained (concentration by area) were normalized to the non-Electric field concentration measured per plate, prior to reporting the average recovery in folds change. Figure 7 shows the normalized concentration by area for all four analytes (both MRMs) for all the study groups: (a) DMPK- C cards low concentration, (b) Whatman 903 cards low concentration, (c) DMPK-C cards high concentration, and (d) Whatman 903 cards high concentration. It was evident that all the analytes had significantly better recovery using an electric field within 3-minutes than with a 15-minutes preparation without an electric field. Except C, the other three analytes consistently showed at least two folds or higher recovery with the vertical electric field setup, inclusive of both MRMs. Additionally, the vertical electric field setup reigned superior compared to the horizontal field, since the supernatant obtained post-treatment was particulate free. This elevates its potential for future combination with robotic liquid handlers for sample preparation, since the entire sample preparation procedure can take place within the deck and would not require manual intervention.

(a)

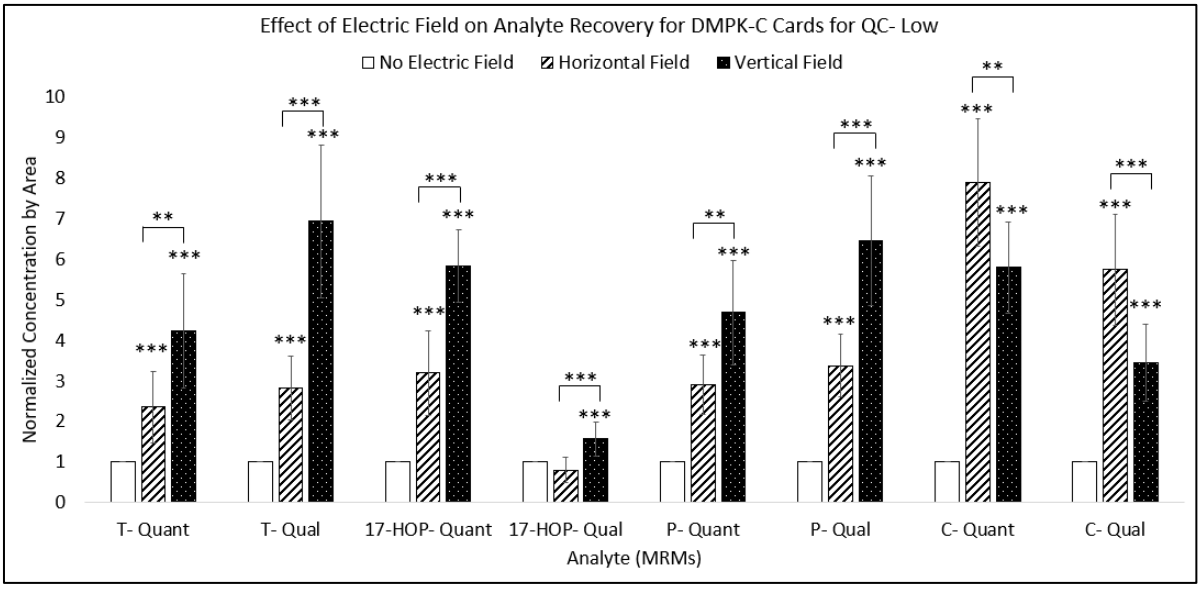

(b)

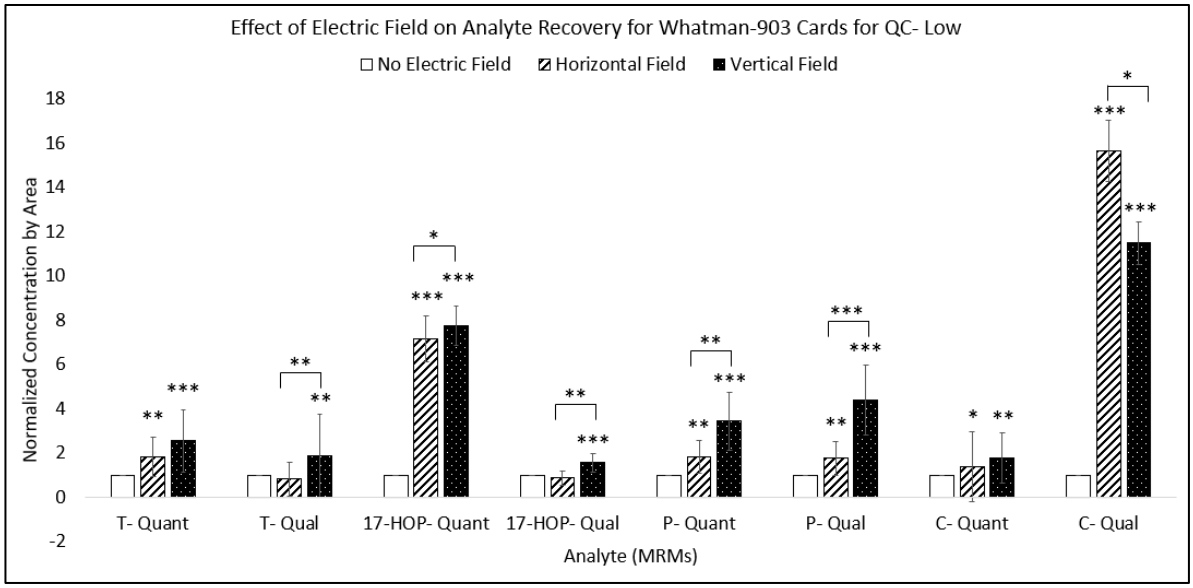
Effect of Electric Field on Analyte Recovery for Whatman-903 Cards for QC- Low
No Electric Field
Horizontal Field
Vertical Field
Normalized Concentration by Area
Analyte (MRMs)
T- Quant
T- Qual
17-HOP- Quant
17-HOP- Qual
P- Quant
P- Qual
C- Quant
C- Qual

(c)

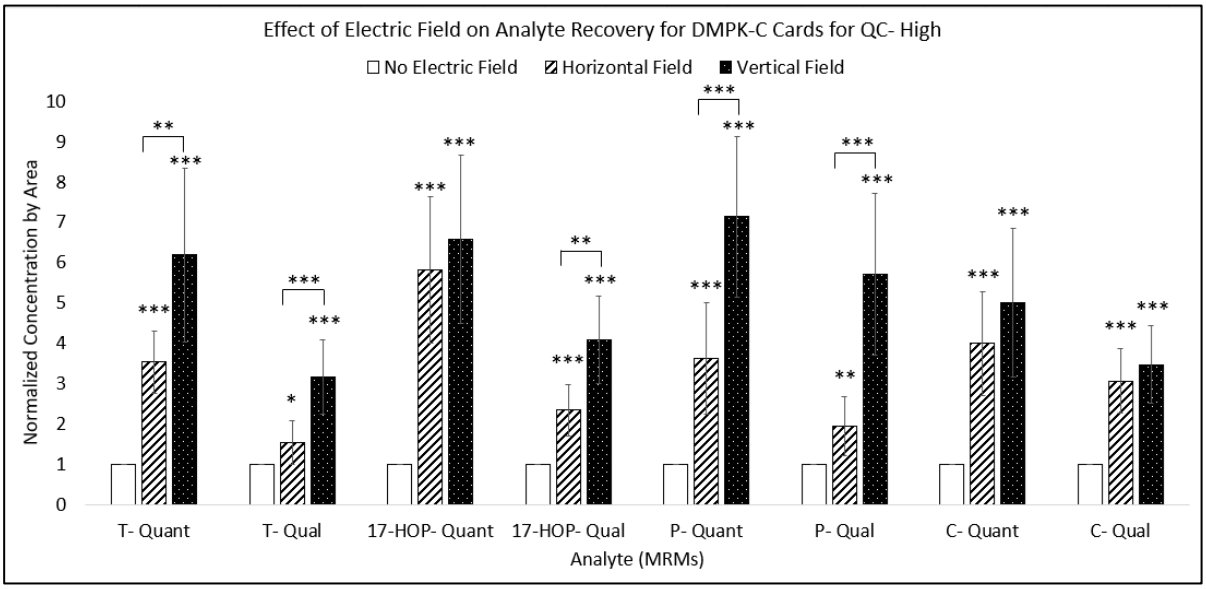
Effect of Electric Field on Analyte Recovery for DMPK-C Cards for QC- High
No Electric Field
Horizontal Field
Vertical Field
Normalized Concentration by Area
Analyte (MRMs)
T- Quant
T- Qual
17-HOP- Quant
17-HOP- Qual
P- Quant
P- Qual
C- Quant
C- Qual

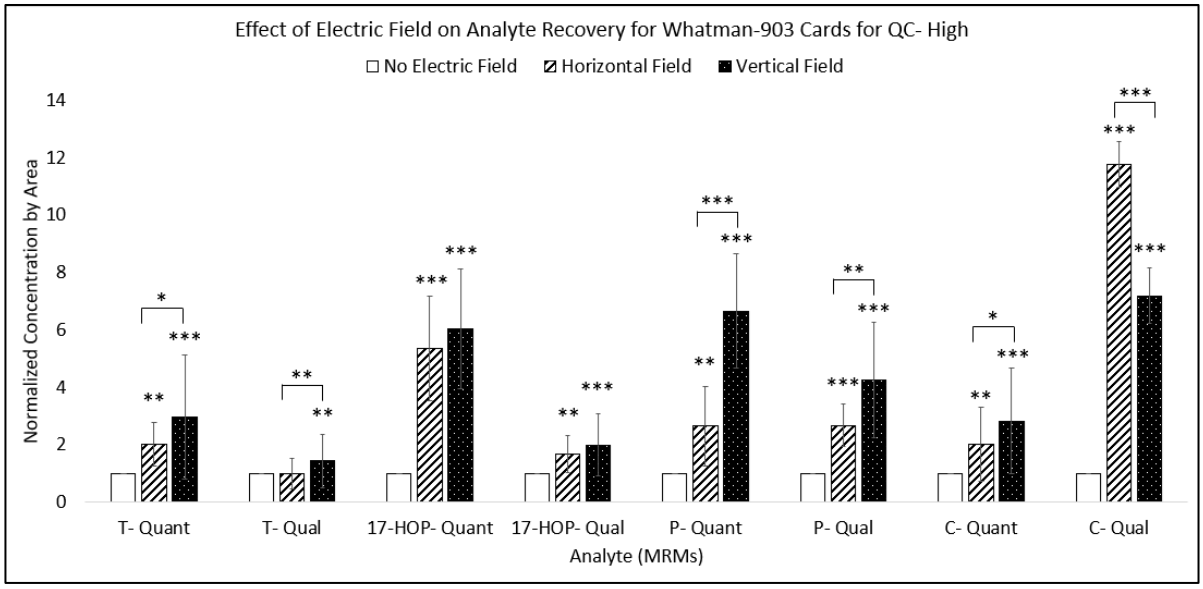

(d)

*Figure 17. Normalized concentration by area (both MRMs) for (a) DMPK-C cards low concentration, (b) Whatman-903 cards low concentration, (c) DMPK-C cards high concentration, and (d) Whatman-903 cards high concentration (n= 24 per study condition, per set of prepared DBS, extreme outliers eliminated); error bars represent standard deviation; statistical significance denoted by: *= p<0.05, **= p<0.01, and ***= p<0.0001 against control, and within groups (indicated in pairs).*

While our customized setup worked and yielded the expected outcomes, it is worth noting that there was no comparison made between the analyte recovery between the two card types, since the changes taking place at the molecular level between the base material of the cards is beyond the scope of this study. Another key factor to note is the spotting technique of the DBS cards[33]. Unlike clinical setups, the cards used in this study were spotted in a laboratory setting inside a biosafety cabinet with accurate 50 µL pipetting on each spot and dried overnight prior to analysis. Hence, the spots were uniform, containing uniform blood volume across the board. This would not be the case for a clinical setup, where the blood volume collected per spot would vary, thereby having varying concentrations of the analytes (higher the volume, greater the analyte). Also, the conception of this study was to assess the potential of remote sampling for preliminary disorder detection. In actuality, the samples would be collected in a remote area and shipped elsewhere for analysis, thereby contributing to analyte degradation during the shipping process. PCOS as a disorder is very heterogenous in nature, with the reported analytes varying in concentration in patients of different age groups, weight group, family history etc. (as showcased on Supplemental

Table 1[2, 44,45,48,64,65]). Therefore, our study merely serves as the basis for potential application of DBS for PCOS detection. A clinician's perspective is crucial to decide the concentration ranges for the analytes to create iterations of the linearity series for a large patient population sample analysis, relevant to specific patient groups and conditions.

4.5.Conclusion

While PCOS remains as the most common endocrine disorder, it deserves more attention for improvement in its early screening and detection, especially for adolescents in low-resource settings where there are financial and cultural hurdles surrounding reproductive health. In our study, we have shown that DBS has the potential to serve as a preliminary detection tool for PCOS, mitigating problems of remote sampling. We have also successfully shown that electric field can serve as the major driver for analyte recovery from the DBS. Additionally, we have showcased a customized vertical electric field setup for a faster and highly efficient analyte extraction, compared to traditional extraction methods.

4.6.Acknowledgment

The authors would like to thank Collin Hill, Grace van der Gugten, Donald Chace and Timothy Garrett for their invaluable input and guidance throughout the course of this study. The authors would also like to thank Mohammad Farhan Haque and Ells Mine Maria St. Paul for being a part of the team and providing experimental support throughout the study.

4.7.Supporting Information

Supplemental Figure 1. Complete experimental setup (image created using Biorender).

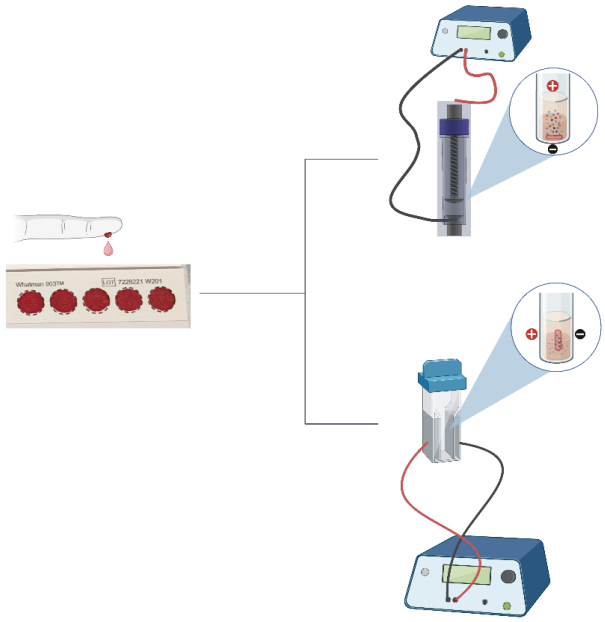

Supplemental Figure 2. (a) Initial iteration of the setup with coils for electrodes; (b) Secondary iteration of the device with

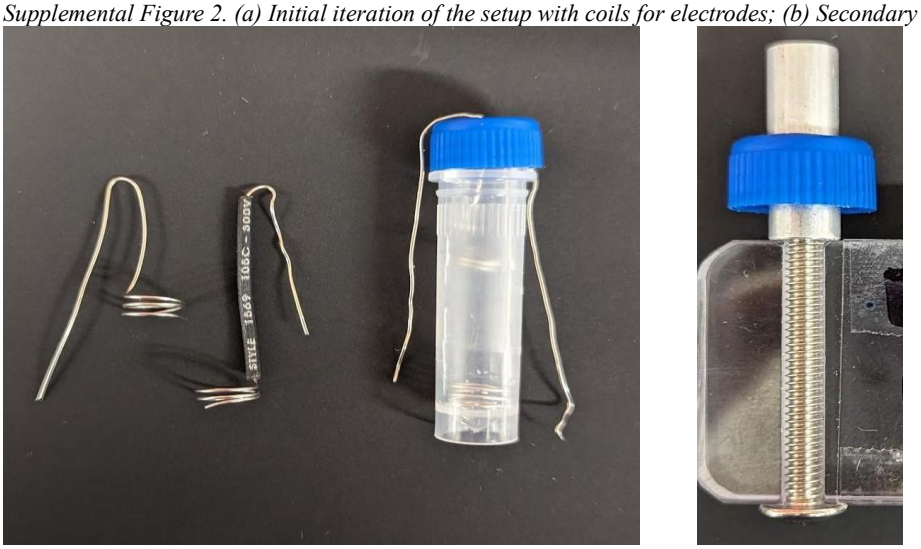

Supplemental Figure 3. Complete assembly (by parts) for vertical electric field.

(a) Bottom electrode assembly for vertical-flow device.

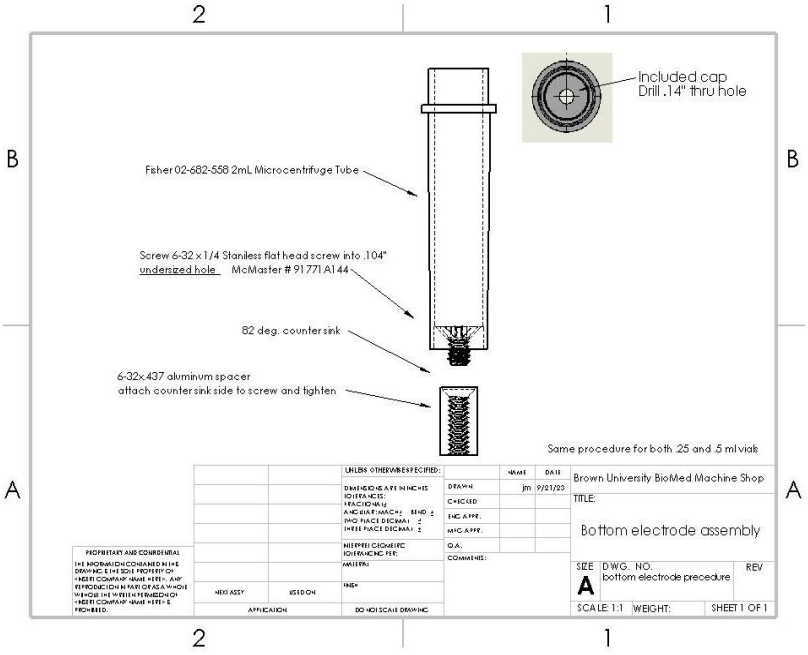

(b) Top electrode assembly for the vertical-flow device using a 0.25 mL spacer.

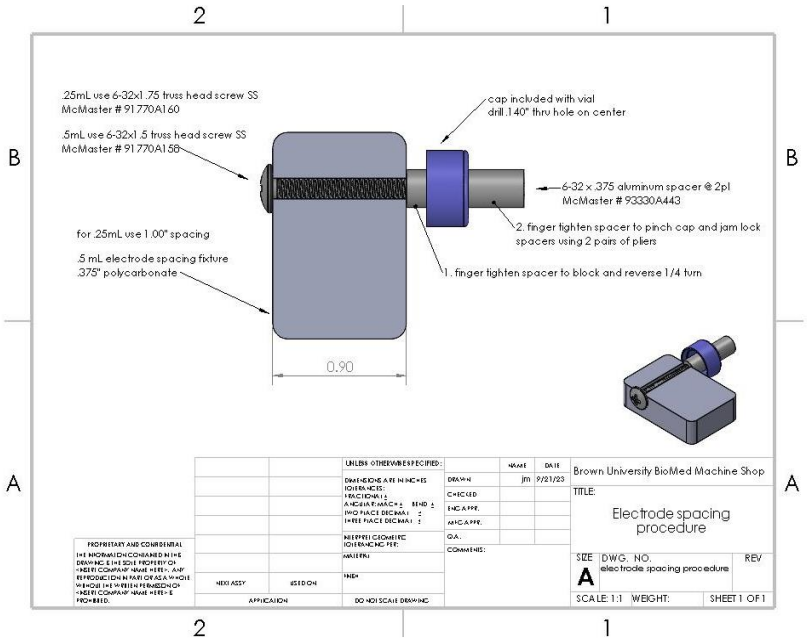

(c) Vertical-flow tube holder parts assembled.

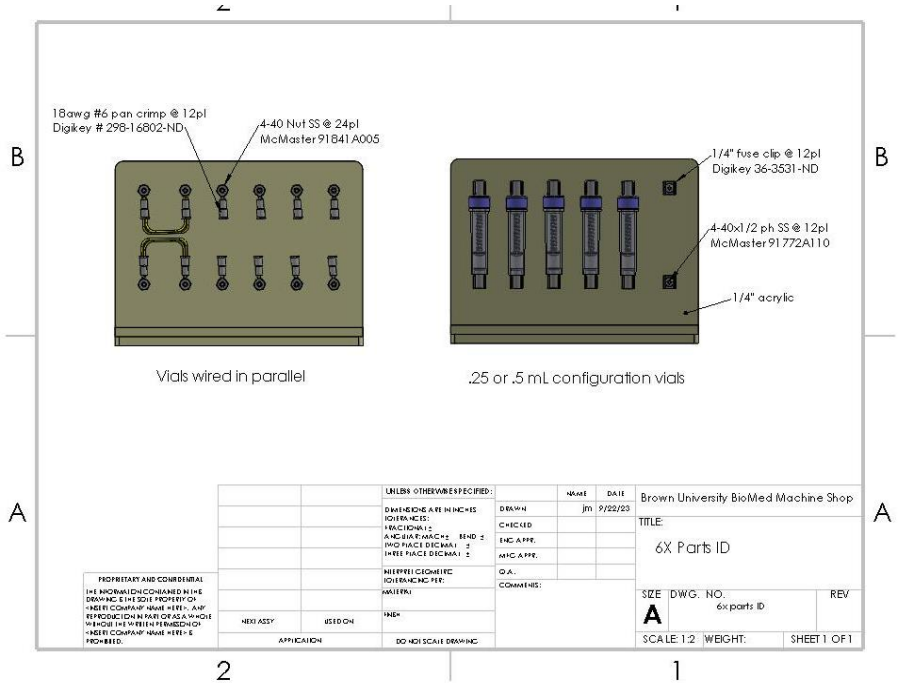

(d) Single vial holder setup (with a 0.5 mL spaced tube).

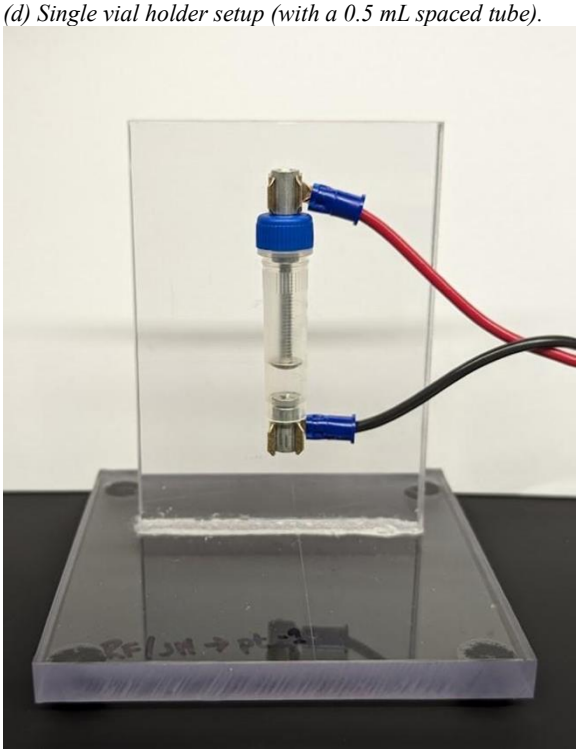

(e) Six-vial holder complete setup (with 0.25 mL spaced tube).

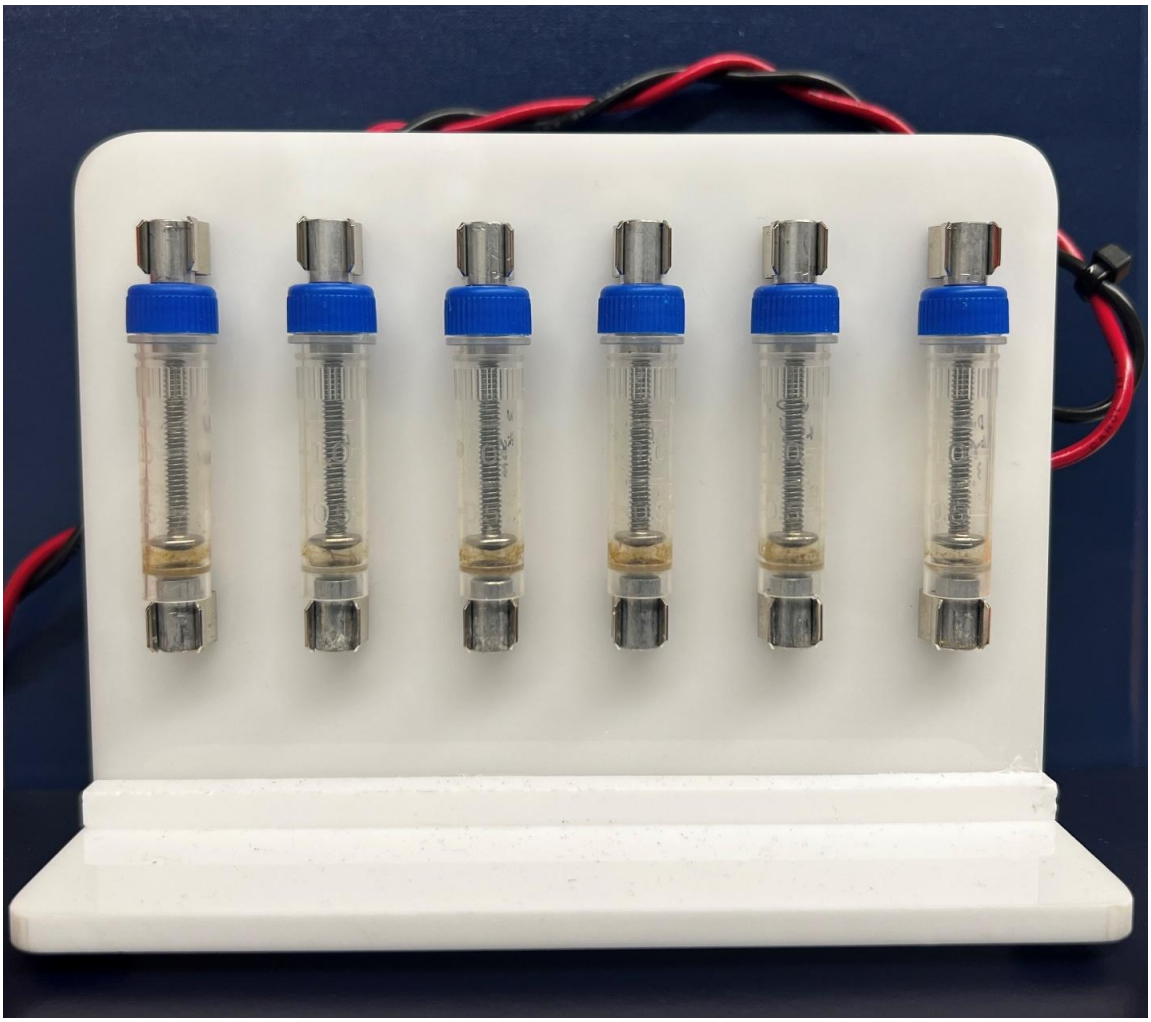

Reference	Testosterone (ng/mL)	17 alpha-OHP (ng/mL)	Progesterone (ng/mL)	Cortisol (ng/mL)
Richardson (2003)[2]	<0.2	2	Not reported	Not reported
Sheehan (2004)[44]	≤1.5	2 to 10	Not reported	2X of normal upper limit
Velija-Ašimi (2013)[45]	0.69	Not reported	3.75	Not reported
Keefe (2014)[64]	0.5 to 1.25	17 to 175.5	0.0012 to 0.0029	0.113 to 0.287
Deng (2017)[48]	0.29 to 0.57	0.1 to 0.6	0.1 to 0.8	56.5 to 114
Pal and Seifer (2022)[65]	1.4 to 1.7	<2	>15	<180

Supplemental Table 1. Hormone ranges for PCOS reported in serum and blood across different age groups and conditions.

2)

Testosterone

	Quant	Level	Average Concentration	CV%	Inter-assay %CV
		L1	0.21± 0.02	9.98%	14.50
		L2	9.65± 0.82	14.85%	
		L3	16.93 ± 2.52	8.47%	
		L4	17.98± 2.79	15.50%	
		L5	21.10 ± 1.81	8.57%	
		L6	26.69 ± 2.19	8.20%	
T					
	Qual	Level	Average Concentration	CV%	Inter-assay %CV
		L1	0.22± 0.02	7.96%	10.80
		L2	9.67± 1.21	8.51%	
		L3	15.56± 1.32	12.55%	
		L4	17.75± 1.34	7.57%	
		L5	20.56± 1.59	7.74%	
		L6	26.11± 1.58	6.03%	

17-OHP

	Quant	Level	Average Concentration	CV%	Inter-assay %CV
		L1	0.59± 0.19	31.79%	8.88
		L2	9.08± 1.01	10.24%	
		L3	13.84± 1.42	11.08%	
		L4	17.80± 1.83	10.27%	
		L5	20.40± 0.27	1.32%	
		L6	29.33± 6.55	22.32%	
17-OHP					
	Qual	Level	Average Concentration	CV%	Inter-assay %CV
		L1	0.52± 0.11	20.47%	18.30
		L2	11.44± 1.06	21.42%	
		L3	14.90± 3.19	9.28%	
		L4	16.92± 3.44	20.36%	
		L5	22.39± 4.88	21.81%	
		L6	34.63± 3.63	10.49%	

Progesterone

	Quant	Level	Average Concentration	CV%	Inter-assay %CV
		L1	0.80± 0.08	10.16%	7.80
		L2	9.69± 1.47	16.24%	
P		L3	14.70± 2.38	15.16%	
		L4	16.69± 0.93	5.55%	
		L5	19.67± 1.14	5.82%	

		L6	26.63± 2.28	8.56%	
	Qual	Level	Average Concentration	CV%	Inter-assay %CV
		L1	0.44± 0.13	29.60%	3.46
		L2	10.04± 0.85	6.40%	
		L3	17.60± 1.13	8.49%	
		L4	16.99± 0.96	5.64%	
		L5	19.83± 1.64	8.25%	
		L6	26.01± 1.15	4.43%	

Cortisol

	Quant	**Level**	**Average Concentration**	**CV%**	**Inter-assay %CV**
		L1	0.70± 0.12	17.28%	18.93
		L2	10.04± 1.35	18.75%	
		L3	16.10± 3.02	13.47%	
		L4	18.85± 0.19	1.02%	
		L5	21.13± 3.02	14.27%	
		L6	27.19± 5.39	19.83%	
C					
	Qual	Level	Average Concentration	CV%	Inter-assay %CV
		L1	2.37± 0.39	16.57%	16.92
		L2	10.11± 1.02	8.15%	
		L3	15.39± 1.25	10.08%	
		L4	19.60± 2.21	11.26%	
		L5	20.61± 1.49	7.24%	
		L6	25.71± 1.89	7.35%	

Supplemental Table 2. The average measured concentration per calibrator level for T (a), 17-OHP (b), P (c), and C (d). %CV used as a measure of precision (n=27/calibrator level; n=18 for inter-assay measurement).

3)

Reference	Ferreira Avelar et al., (2021)[61]	Nauruzbayeva et al., (2020)[62]	Wuethrich et al., (2016)[56]	Voloshin et al., (2016)[63]
Electrical input characteristics	Electrophoresis source connected to a multimeter with a RS-232 communicator - 300V input	Uniform electric field as high as ~2000 V/cm (0-2000 V/cm tested) - Voltage source range: 0-10kV	Solid Membrane: 300V Liquid Membrane: N/A Electrophoretic concentration: 0.4-1.3 kV & 0.5-2kV	Tested 4.6 V/cm pk-pk at frequencies from 100-400 kHz
Electrical Input: Duration	10 minutes	Not reported	Solid Membrane: 10 minutes Liquid Membrane: 10 minutes Electrophoretic	72 hours

			concentration: 30 minutes	
Matrix Analyzed	Synthetic and human oral fluid	Water	Urine and environmental waters	Tumor cells
Sample Volume required	1 mL	- 200 µL - 10-20µL droplets & 50µL tested - Faraday cage: 1 mL reservoir	Not reported	Not reported

Supplemental Table 3. Electric field applications for sample preparation from literature.

Chapter 5: Understanding Sample Preparation Workflow: Semi-Automated Preparation of Serum Testosterone for Detection Using LC-MS/MS

Chapter 5 is under review to be published as an original research article; preprint available online.

Fariha, R.[1], Hill, C.[2], Jabrah, M.[1], Spooner, A.[1], Tripathi, A.[1]

1. Center for Biomedical Engineering, School of Engineering, Brown University, 182 Hope Street, Providence, RI- 02912, USA
2. Revvity Inc., Waltham, MA

5.1.Abstract

High-Performance Liquid Chromatography-Tandem Mass Spectrometry has been pivotal to recent clinical advancements in the detection and monitoring of the progression of different metabolic disorders. Such systems have been used to routinely monitor serum testosterone levels in patients, to both mitigate side effects of different medications, as well as diagnose androgen-associated disorders. The present study develops and validates an LC-MS/MS-based assay for the detection of total serum testosterone from only (100µL) of sample volume. To increase the high throughput capability of the developed diagnostic kit for clinical use on patient samples, the proposed method was streamlined via semi-automation on a JANUS® G3 Workstation liquid handler. The proposed diagnostic kit showcased high detection precision (CV<5%) as well as sample accuracy (93-108%), within a clinically relevant range of testosterone serum concentrations (5-1500ng/dl). Moreover, the assay showcased LoD of 5 ng/dl, which is significantly comparable to commercially established diagnostic tools. The developed method also exhibited high linearity over the specified testosterone serum range, with an obtained linearity of R^2>0.99 using both manual as well as automated sample preparation. Overall, the work shown presents an optimized, automatable LC-MS/MS-based testosterone diagnostic assay for the routine evaluation of patient testosterone levels in serum for clinical and research use.

5.2.Introduction

The measurement of total testosterone (T) in human serum at very low levels is pivotal in the clinical practice of diagnostics, treatment, and prevention of a variety of sex-hormone related disorders. This includes the diagnosis of hypogonadism and androgen deficiencies in men and Polycystic Ovarian Syndrome (PCOS) in women, as well as various types of cancers. Abnormally excessive or deficient T levels in patients may be associated with doses and side effects of patient medications and prescriptions [148-151, 155, 156]. Hence, clinical diagnostic and therapeutic

studies require accurate monitoring of patient T levels, to ensure both patients' improved long-term healthcare and quality of life.

Advances have been made in the field of quantification and screening of low or elevated T levels using immunoassays [153]. However, such assays suffer from notable discrepancy in results that limit their utilization within wider diagnostic uses [154]. Due to its increased detection specificity when detecting analytes at significantly lower concentrations [152, 157, 159] liquid Chromatography (LC) Tandem Mass Spectrometry (MS) approaches were alternatively investigated in the screening of patient T levels. Despite being widely studied, limitations exist [158] specifically in terms of repeatability in regards to sample preparation procedures, LC separation conditions, and MS signal-to-noise optimizations at very low levels. Several studies have been performed[8-12] with various combinations of parameters and protocols for each of the three steps to seek improvements in the sensitivity, accuracy, efficiency, and cost of the T assays. Sample preparation procedures are critical to achieving the success criteria, as they isolate, concentrate, and separate the analyte of interest from the biological sample into an LC-MS compatible matrix. This sample preparation workflow is primarily governed by the sample volume added for testosterone quantification, the method of testosterone extraction (different solutions used for protein precipitation, and the impact of pH on pellet formation), method of plating (semi-automated vs. manual), and sample reconstitution solvent. Additionally, the ease of automation increases the reproducibility and throughput ability of the assay. Table 7 is a summary of various sample preparation protocols for LC-MS/MS testosterone detection. It showcases the unified approach to the selection of organic liquids, the volume ratios, ideal pH, as well as the different optimizations of the time of incubation and temperature conditions to primarily improve analyte extraction efficiency from other studies.

In this study, we discuss a sample preparation workflow that utilizes robotic liquid handlers for sample preparation automation, integrated with LC-MS/MS analysis for the quantification and monitoring of testosterone in human serum, a popular matrix in the clinical setting. The proposed sample preparation methodology takes into account a minute optimization of i) the choice of microplate used, based on plate area and sample volume ratio, ii) the time taken for sample incubation and phase-separation, iii) sample drying gas and temperature, iv) optimization of Multiple Reaction Mode (MRM) in mass spectrometry, v) method of plating, vi) choice of column and mobile phases, and vii) LC ramping. Finally, based on the optimized method and workflow, a highly sensitive, reliable prototype kit for the precise measurement of testosterone in patient samples using LC-MS/MS for clinical application was manufactured.

# Steps	**Fariha et al.**	**Sun et al.(2020)[8]**	**Zhou & Wang (2019)[12]**	**Häkkinen et al.(2018)[9]**	**Schofield et al. (2017)[11]**	**Thienpont et al. (2008)[10]**
1	**Sample Conditioning** Sample (V= 100uL) + Acetonitrile (with 0.1% Formic Acid) mixed with Internal Standard (V= 200 uL)	**Sample Conditioning** Sample (V = 100uL) + Calibration Liquid (V= 100uL) 15min Mix + 0.5mol/L Ammonium Acetate (V= 100uL) pH = 5.5 120min mix RT	**Sample Conditioning** Sample (V = 200uL) + Acetonitrile (mixed with internal standards) (V= 400uL)	**Sample Conditioning** Sample (V = 150uL) + Calibration Liquid (V= 20uL) 15min Mix	**Sample Conditioning** Sample (V = 500uL) + Calibration Liquid (V= 50uL)	**Sample Conditioning** Sample (V = 200uL) + Calibration Liquid (V= 20uL)

2	**Protein Precipitation** Shake= 10 min at 25°C Centrifuge= 20 min at 4°C Decantation V= 150 uL	**LLE extraction** nHexane+ethylacetate V = 200uL+300uL 2x	**LLE extraction** Vortex = 10min Freeze at −20°C 10 min Vortex = 10min Centrifuge 10min	**LLE extraction** Toluene V = 1000uL 10min	**LLE extraction** hexane:ethyl acetate (9:1) V = 2500uL Centrifuge = 2min Freeze at −80°C 15 min	**LLE extraction** Methyl t-Butyl Ether V = 1000uL
3	**Evaporation** Organic Phase T= ~60°C	**Evaporation** Organic phase	N/A	**Evaporation** Organic phase	**Evaporation** Organic phase T = 35°C	**Evaporation** Organic phase T = 50°C
4	**Reconstitution** 100 uL 70:30 (v/v) Acetonitrile: Water (with 0.1% Formic Acid)	**Dissolve** Sodium Carbonate V = 200uL c = 0.2mol/L pH = 9.8	**Dissolve** 200uL supernatant + water (1:1) V = 200 uL	**Dissolve** 30% Acetonitrile V = 50uL	**Dissolve** Methanol:water (1:1) V = 150 uL	**Dissolve** 0.7 mol/L Hydroxylamine in 3:7 Methanol/water V = 50uL T = 70C 15 min
5	N/A	**LLE extraction** nHexane V = 500uL 2x	N/A	N/A	N/A	N/A
6	N/A	**Evaporation**	N/A	N/A	N/A	N/A
7	N/A	**Dissolve** Methanol V = 100uL	N/A	N/A	N/A	N/A
8	**LC-MS**	**LC-MS**	**LC-MS**	**LC-MS**	**LC-MS**	**LC-MS**
Results	LOD= 5 ng/dl Linear Range= 5- 1500 ng/dl CV< 5% Accuracy ~ 93-108%	LOD = 0.5ng/dl Linear Range = 1 - 1000 ng/dl CV < 3.5% Accuracy = 94%-108%	LOD = 1ng/dl Linear Range = 1 -2000 ng/dl CV < 3% Accuracy ~ 93-104%	LOD = 0.4ng/dl Linear Range = 0.4 -384 ng/dl CV < 8% Accuracy = 81%-98%	LOD= 1 ng/dl Linear Range= 1-1170 ng/dl CV < 7% Accuracy ~ 97- 107%	LOD = 0.5ng/dl Linear Range = 1 -2500 ng/dl CV < 10% Accuracy ~ 89%

Table 7. Method development comparison of the proposed protocol against protocols in literature.

5.3.Experimental

5.3.1. Chemicals and Materials

Ultra-low steroid DDC Mass Spect Gold Serum® was purchased from Sigma-Aldrich and Testosterone (T-037 and T-070) in Acetonitrile were obtained from Cerilliant (RoundRock, TX, USA). Baker Analyzed HPLC grade water, Acetonitrile (>99.9% purity), and Ethanol (>99.9% purity, gradient grade) were obtained from VWR. Formic Acid for LC-MS was obtained from Honeywell. Sodium Azide used was purchased from Sigma-Aldrich.

5.3.2. Quality Control

To ensure the linearity series prepared for the assay functioned as expected, National Institute of Standards and Technology (NIST) approved Standard Reference Material 971a- Hormones in Frozen Human Serum was used. SRM 971a (Male) was used in the development of the assay, with the testosterone measuring at 580.8±9.0 ng/dL mass concentration. SMR 971a was stored at -80°C and thawed to room temperature when ready for testing. The internal standard for the assay was prepared by diluting the Cerilliant T-070 Testosterone (at 1 mg/mL) ($^{13}C_3C_{16}H_{28}O_2$ (MW= 291.40)) two-hundred folds in HPLC grade ethanol (500 ng/mL). This solution was further diluted one-hundred folds in acetonitrile with 0.1% formic acid solution to prepare the Daily Working Solution (DWS).

5.3.3. Phase Testing

The isotopically unlabeled testosterone was dissolved at 10 ng/mL concentration at varying ratios of HPLC water and acetonitrile at from 100% to 0% v/v ratio of the solvents and injected in the LC-MS/MS system for analysis. Figure 1 shows the Relative Intensity (RI) overlay plot from this test, that helped identify a water: acetonitrile= 70:30 v/v ratio as the optimum condition for sample injection and analysis.

Figure 18. Relative Intensity (RI) overlay plot for different organic to inorganic solvent ratio used for T dissolution. Red line shows premature elution when T was dissolved in 100% acetonitrile. Green line shows a delay in retention time (RT) when T was dissolved in 100% water. Lines blue (Water:Acetonitrile= 65:35) and indigo (Water:Acetonitrile= 70:30) show the best chromatogram shapes with highest RI (~200000). Water:Acetonitrile= 70:30 ratio was chosen due to the lower signal-to-noise ratio.

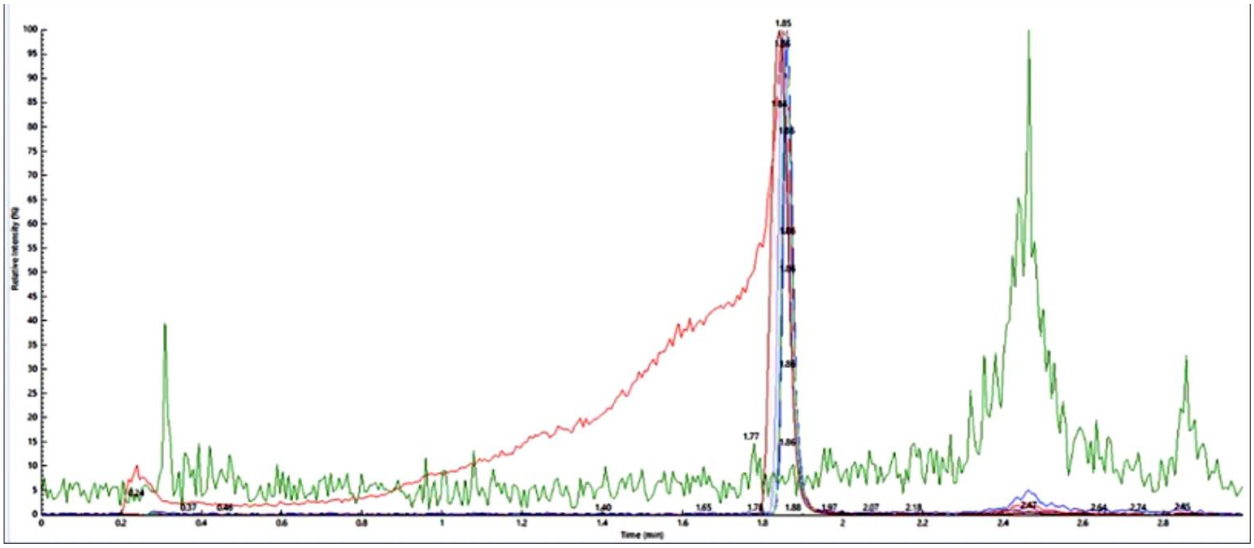

5.3.4. Calibrator Preparation

Sodium azide (0.05%) and thawed DDC Mass Spect Gold Serum® were used as the base for the calibrators. Two intermediate 'bulk' solutions were prepared using the isotopically unlabeled T-037 testosterone solution purchased from Cerilliant (at 1 mg/mL) ($C_{19}H_{28}O_2$ (MW= 288.42)). This solution was diluted to 500 ng/mL and 12.5 ng/mL in gradient grade ethanol to form Bulk Solution A and B, respectively. These bulk solutions were added to spike the gold serum base to form six-concentration calibrators via overnight rocking.

5.3.5. Sample Preparation

All samples were brought to room temperature, and on a large volume conical bottom Axygen shallow 96-well plate, 100 µL of the calibrators were added to 200 µL of DWS. This step was investigated with deep well v-bottom 96-well plates, standard v-bottom 96-well PCR plates, as well as vial-based preparation techniques. The role of the well-depth and shape on the automation of the procedure is further discussed in the results sections. The DWS consisted of acetonitrile, with 0.1% formic acid, as well as an internal standard. The samples were shaken using the

TriNEST™ microplate shaker at 700 RPM for ten minutes, and then centrifuged at 4600 RPM at 4°C for twenty minutes. The organic layer was decanted to a separate shallow conical bottom 96-well Nunc plate, evaporated to dryness at ~60°C with a constant airstream, and then reconstituted with 100 µL of HPLC water: acetonitrile (70:30 v/v) in 0.1% formic acid solution. The plate used for decantation was also investigated with standard v-bottom 96-well PCR plate, as well as a vial-based method. Additionally, the reconstitution solvent was tested for the effect of pH, with no acid, 0.1% formic acid and 1% formic acid over 3-runs. The samples were given a final ten-minute shake at the TriNEST™ at 400 RPM before being injected to the LC-MS/MS.

5.3.6. Carryover

Carryover for the study was performed by first establishing baselines for the highest and lowest concentrations of the calibrators. Following running working solutions, the highest calibrator (single injection) was injected into the system immediately followed by injection of the lowest concentration of the calibrator (in triplicate). Any significant change in the measured concentration of testosterone was taken as an indication of carryover. The measured concentration of the lowest calibrator concentration was equated as a measure of sample carryover, running it in the same plate following the injection of the highest calibrator concentration, in triplicates for seven different sets.

5.3.7. LC-MS/MS Equipment and Conditions

The PerkinElmer QSight™ 200 MassSpec triple quad liquid chromatography system, together with the QSight™ LX-50 Pump, QSight™ LX-50 Oven and QSight™ LX-50 Autosampler, was used with an ESI source. HPLC column (3 µm, C18, 100 Å, 50 x 3.0 mm) with guard column (2.7 µm Brownlee SPP) were used with the system. The triple quad mass spec was operated with the nebulizer gas pressure at 200 psi, electrospray voltage of 5850 volts, and a source temperature of 425°C. The total run time for each sample was 3 minutes, with 429 scans, with the system being

operated in Multiple Reaction Monitoring (MRM) mode. Analytes were resolved by reverse-phase HPLC prior to mass spectrometry analysis to reduce the level of interfering compounds and provided a characteristic chromatograph with retention time for each analyte. The first quadrupole (Q1) was set to filter out all ions except for the precursor (analyte or internal standard). Q3 filtered out all but one selected testosterone ion, thus a signal was only detected when a selected precursor generated a specific fragment (MRM transition). Analyte and internal standards specific to MRMs were monitored sequentially during chromatographic separation. Signals were quantitated only if the specified MRM was recorded at the correct analyte retention time. Thus, quantitation in this MS/MS method is very specific. 'Quantifier' corresponds to testosterone with Q3 mass= 97 amu, and 'Qualifier' corresponds to testosterone with Q3 mass= 109 amu and will be referred to as such throughout the paper. For the method developed, the retention time for each sample was 1.84 minutes (with the matrix). The LC method for this study was established such that there was a fast full-loop flush at 2.00 mm needle height from the bottom of the well at 14 µL flush volume. With HPLC water as the weak solvent (Mobile Phase A) and LC-grade acetonitrile as the strong solvent (Mobile Phase B), the analytes were loaded at a flow rate of 0.600 mL/min flow rate initially. Table 2a and 2b illustrate the optimized MRM parameters, and the optimized conditions for the LC method applied in this study, respectively. The setpoint temperature for the samples was maintained at a steady 4°C. The column was maintained at a steady temperature of 40°C for the duration of the analysis. The data was collected using the Simplicity 3Q software made for QSight, version 2016-2019.

Table 8:
Table 8 a) *Mass parameter table for T (quantifier and qualifier) and their respective internal standards. RT refers to the retention time (in minutes).*
Table 8 b) *Solvent flow rate for weak and strong solvents used in the mobile phases for the LC-MS/MS extraction and analysis of testosterone.*

Analyte	Type	Q1 mass	Q3 mass	RT (min)	EV	CC	CCL2
Testosterone	**Quant**	289.20	97.00	1.84	20	-34	-56

	Quant IS	292.00	100.00	1.84			
	Qual	289.20	109.00	1.84	20	-37	-64
	Qual IS	292.00	112.00	1.84			

Time (min)	Flow rate (mL/min)	% A	% B
0.00	0.600	70	30
1.00	0.600	70	30
2.00	0.600	50	50
2.10	0.600	5	95
2.50	0.600	5	95
2.51	0.600	70	30
3.00	0.600	70	30

5.3.8. Automation

To further adapt the testosterone prototype kit for a robust research application, a semi-automated sample preparation method was created using the JANUS® G3 liquid handler (PerkinElmer Corp., MA, U.S.). The sample preparation process previously described was adapted onto the JANUS platform using the Janus Application Assistant and WinPREP® for Janus® software. Figure 2a showcases the finalized deck layout of the sample preparation protocol, while Figure 2b shows the on-deck and off-deck steps, color-coded by human interaction. Owing to the complexity of some of the steps in the sample preparation process (albeit as simple as protein preparation), the plate had to be taken off-deck several times for shaking, centrifugation and drying, thus the use of the "semi-automated" terminology. Finally, to determine the efficacy of this automated sample preparation method, manually plated samples were compared via LC/MS analysis against automated plates with regards to precision as well as preparation speed.

Figure 19.
(a) Automated Sample Preparation Deck Layout
(b) Sample preparation automation workflow analyzed by time for both on and off deck protocol steps. Blue boxes represent the on-deck steps while grey boxes represent the off-deck steps. Times staggered above and below the workflow indicate times in Minutes: Seconds: Milliseconds measured with a stopwatch.

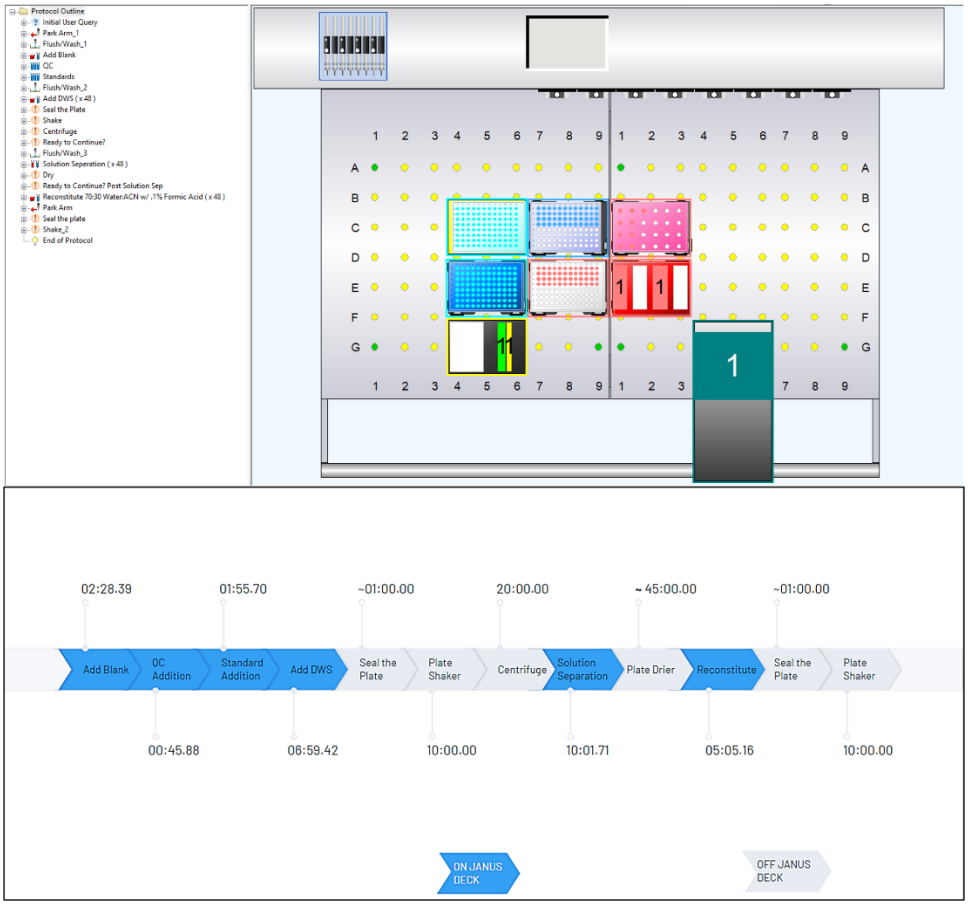

For all the studies, statistical significance was established using a student's t-test, where p-value<0.05 was considered statistically significant between averaged concentrations measured. For the carryover study, the result was investigated further using a box-plot diagram to identify any outliers (none identified), and for the accelerated stability study, the normalized concentrations were compared by generating a comparative letter report using Tukey's HSD post-hoc test. All statistical analysis were performed using JMP 15 Pro software.

5.4.Results and Discussion

5.4.1. Method Validation

At the beginning of the study, it was important to confirm that the manufactured calibrators were indeed giving the expected readouts before any further studies could be performed. Therefore, the calibrators were plated in sextuplicate for quantification and validated against the NIST material. Supplemental S1 shows the average concentrations measured for each calibrator level and the

NIST material alongside the known concentration. The NIST material measured very close to the theoretical value (5.80±0.01), and the same was observed for the calibrators prepared, even for the lowest concentration of 0.05 ng/mL. Once the concentrations were established, the calibrators were then used as 'standards' for the other experiments, moving forward. Upon multiple studies, it was established that the Axygen 96-well conical bottom plates were ideal for the initial plating, and the larger surface area of the Nunc 96-well plate made it ideal for the drying and reconstitution step (data for two of the plates used are reported in Supplemental Figure S2, along with Supplemental Table TS1 outlining the difference in preparation methodologies).

5.4.2. Precision, Linearity and Accuracy

Linearity, accuracy, and precision were performed over a 6-day study, where each calibrator level was plated in triplicates, and the data was obtained from a 6-point calibration curve using the Simplicity 3Q software. Calibrator analyte/IS ratios were plotted (y-axis) against the calibrator concentrations (x-axis), and a standard curve was generated using linear regression with $\frac{1}{x}$ weighting. Standard curve fitting via linear regression was also performed on Simplicity 3Q, which was then utilized to determine both inter-assay linearity as well as sample accuracy, allowing for the measurement of individual analyte coefficient of variation (CV). Total precision was calculated as %CV for each level within run, between run, and for all 6 runs. Table 3 shows the average concentration for the calibrators, the %CV, and % Accuracy for quantifiers (top) and qualifiers (bottom) for the full study. For each plate, quality control samples (low= 2 ng/mL; high= 10 ng/mL) were run together with the calibrators for method validation. These quality control samples were prepared with the calibrators from the same standard reference material lot and tested with the NIST material. The R-square values were taken as a measure of the linearity based on a

standard linear regression curve. Figure 3 illustrates the observed linear trend (for automated and manual sample preparation), where R-Square values measure at 0.99 and above for both runs. Sample accuracy was similarly obtained from the Simplicity 3Q software and averaged for all the plates across the study days.

Table 9: *(Top: Quantifier; Bottom: Qualifier) % CV was used as a measure for precision, determined using 3 replicates per level each day, over a 6-day period (n=18 per level). Samples were found to be within 6.2% or less for intraday and interday measurements, inclusive of both MRMs. The average % accuracy for all calibrators was found to be 100±20, inclusive of both MRMs as well. These values fall well within our ≤20% cut-off value.*

Calibrator Level	$\mu_{\bar{x}} \pm \sigma$ ***(in ng/mL)***	***%CV***	***% Accuracy***
L1	**0.05±0.005**	**5.6**	**90.6**
L2	**0.28±0.005**	**3.7**	**107.3**
L3	**2.00±0.060**	**2.1**	**97.5**
L4	**5.32±0.060**	**1.7**	**106.9**
L5	**9.77±0.119**	**1.9**	**99.5**
L6	**14.67±0.227**	**1.4**	**98.3**
Calibrator Level	$\mu_{\bar{x}} \pm \sigma$ ***(in ng/mL)***	***%CV***	***% Accuracy***
L1	***0.05±0.003***	**6.1**	**89.1**
L2	***0.29±0.020***	**5.5**	**109.4**
L3	***1.98±0.052***	**2.5**	**96.7**
L4	***5.39±0.080***	**1.7**	**107.3**
L5	***9.83±0.129***	**1.8**	**99.3**
L6	***14.67±0.283***	**1.7**	**98.3**

Figure 19. Standard curve comparison, to illustrate performance differences between manual vs. automated plating of calibrators L1-L6 in triplicates (n=3 per calibrator per plate). Both plates were run on the same day, with the results showcasing comparable performance.

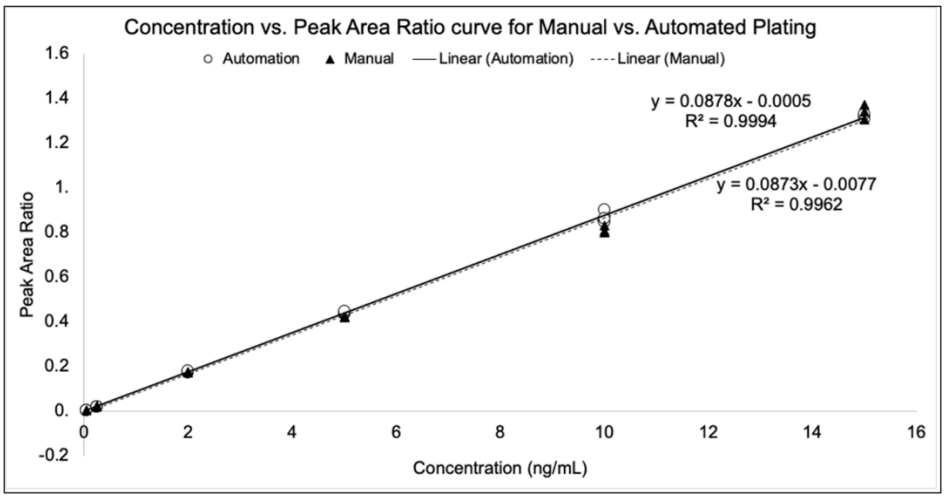

5.4.3. Accelerated Stability

The stability of the calibrators was tested via an accelerated stability study where the samples were subjected to extreme temperature changes (from -20°C storage to 30°C) at two-day intervals, over a period of 14 days. Using the equation:

$$Stable\ Days = (Days\ in\ high\ temperature) \times (2^{\frac{\Delta Temperature}{10}})$$

Equation 1. Modified Arrhenius' Equation

we were able to identify how long the calibrators would be stable without any degradation. This was important in the design process of a prototype kit that can be used in clinical settings. Duplicates of calibrators were transferred from -20°C storage to 30°C every two days, and on the 14th day, samples were harvested. All the samples were then tested against fresh (Day 0) samples. Samples were mainly stable over the 14 days (as seen in Supplemental S2), and from the stability approximation obtained from equation 1, the calibrators are expected to be stable for up to 488 days. Calibrator 1 had no specific trend, and it was also only slightly above the background. Therefore, by virtue of the trends observed for all other calibrators, it was assumed that Calibrator 1 had the same trend.

5.4.4. Freeze-Thaw

Once results were obtained for precision, linearity, and accuracy, prototype kits were produced using the calibrators (six concentrations of testosterone, two quality control calibrators, and an internal standard vial), that were stored at -20°C. The prototype kit was subjected to six freeze-thaw cycles (between -20°C and room temperature), and changes in the measured concentration of testosterone calibrators over the freeze-thaw cycles after thawing to room temperature in triplicate were obtained (Figure 4). No significant degradation was observed in any of the measured testosterone values over the six freeze-thaw cycles.

Figure 20. *Average testosterone concentration for quantifier and qualifier for different calibrator levels and quality control (low and high) samples. No significant difference was observed in the measured value of testosterone for all the different calibrators over six freeze-thaw cycles.*

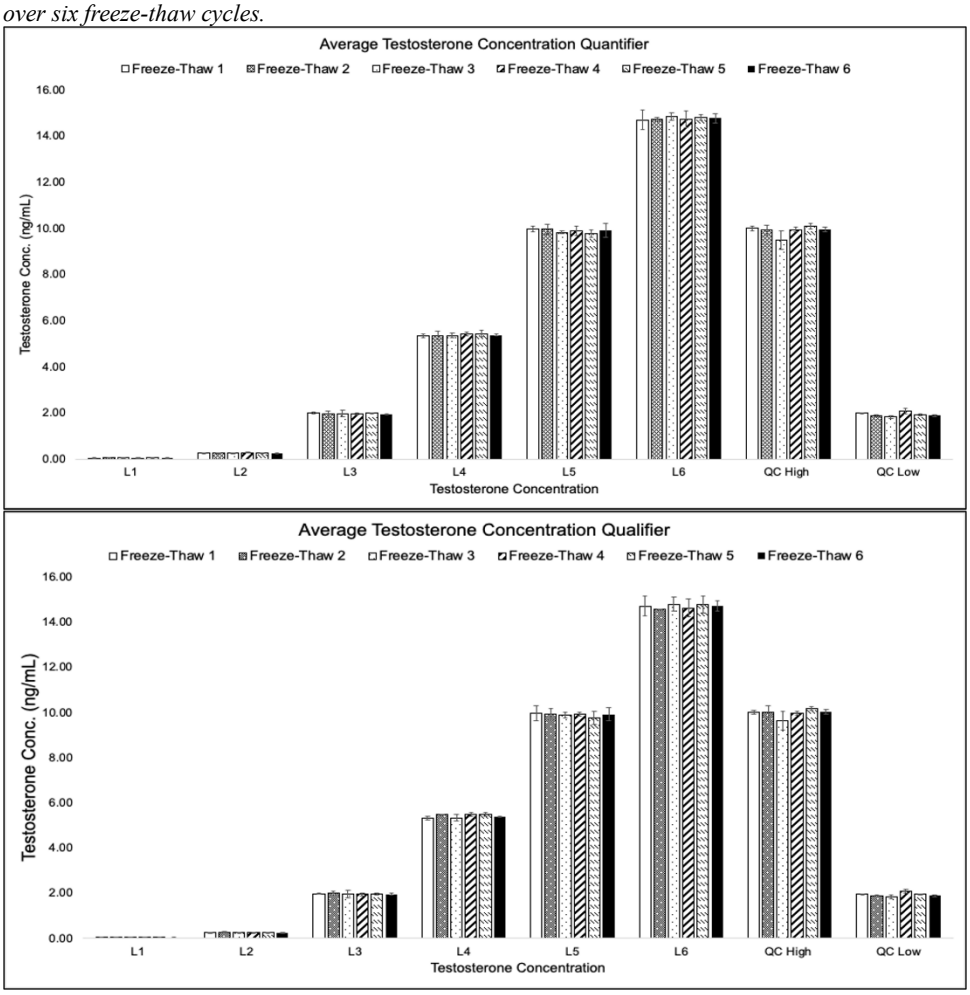

5.4.5. Automation

To assess the proposed prototype kit's adaptability for large-scale sample testing, the developed semi-automated sample preparation process was tested against manual plating. Overall, automation efficacy was directly observed by comparing the necessary plating time, as well as overall plate performance (linearity, precision, and accuracy with regards to the calibrators plated in triplicate against a manually prepared plate). The semi-automated protocol yielded an overall runtime of 27 minutes 16 seconds (including off-deck actions), compared to the manual plating time of 17 minutes, obtained over an average of 6 runs. As mentioned previously, the automated protocol's runtime is increased due to the complexity of serum as a matrix, that required additional air gaps to be created within each pipetting tip used. This required the protocol to be programmed with 10 μL of air aspirated pre-aspiration and post-dispense of the calibrators and samples, before discarding the tip. This additional step was part of both the initial calibrator and sample pipetting step, as well as post-centrifugation supernatant separation step. For the first step, it was observed that human serum, when shaken (resulting from sample transportation and handling) or vortexed (for calibrators and QCs, once thawed to room temperature and prior to pipetting) almost always formed a thin film towards the opening of the container, which the robotic liquid handler's sensing technology would often misinterpret as the starting liquid height. Hence, this issue was mitigated by enabling the 'Ultra' sensing option for the liquid search height instead of 'High' sensing option with a liquid height verification feature, in addition to the air aspirations. For the latter step, i.e., supernatant separation, the viscosity and volatility of the serum was impacted due to the addition of the organic solvent present in DWS, which resulted in significant sample dripping- a critical challenge observed when using multichannel pipettes for manual preparation as well. Adding the air aspiration step provided an easy solution to this problem, which is not possible to apply for manual preparation. For the other steps, i.e., adding the DWS and the reconstitution solvent,

significant time was added due to the pre-wetting steps. Both aforementioned solvents were composed of volatile liquids leading to significant dripping, which was mitigated using 3 cycles of pre-wetting the tips, with 150% of the aspirating volume. This not only prevented the dripping, but also ensured accurate volume dispenses per individual sample, even with multiple tips in action. Additionally, some of the off-deck tasks in the protocol included sample shaking, centrifugation, as well as drying, which are not readily available features for conventional liquid handlers, and upgrades to include them would make the process expensive. As shown in Figure 3, the performance of the automated plating was similar to that of manual plating, with a reported R-Square value for the observed linearity of $R^2 = 0.9994$ for the automated plate, and $R^2 = 0.9962$ for the manual plate, with no statistically significant difference. The high linearity of the standard curves showcases both the proposed assay's linearity over the required range of testosterone concentrations, as well as the automatability and the high-throughput capacity of this kit and increasing applicability of its utilization in clinical settings with patient samples.

5.5.Conclusion

Herein, this study successfully establishes a chromatographic assay with LC-MS/MS analysis for testosterone detection in serum using a prototype kit with automation incorporation for clinical adaptability. This can play a pivotal role in screening for hormonal disorders, as well as for research purposes when developing treatments for said hormonal disorders. Overall, the improvements this study proposes for testosterone is of tremendous value to the scientific community for better understanding of a rather simplistic workflow for sample preparation.

5.6. Acknowledgments

We would like to thank Joe Trometer and Cel Welch for their valuable insight during the initial phase of this study.

5.7.Supporting Information

Supplemental Figure S1. Average measured concentration of testosterone (quantifier and qualifier) for the calibrators and NIST material. Standard deviation was used as a measure for error bars.

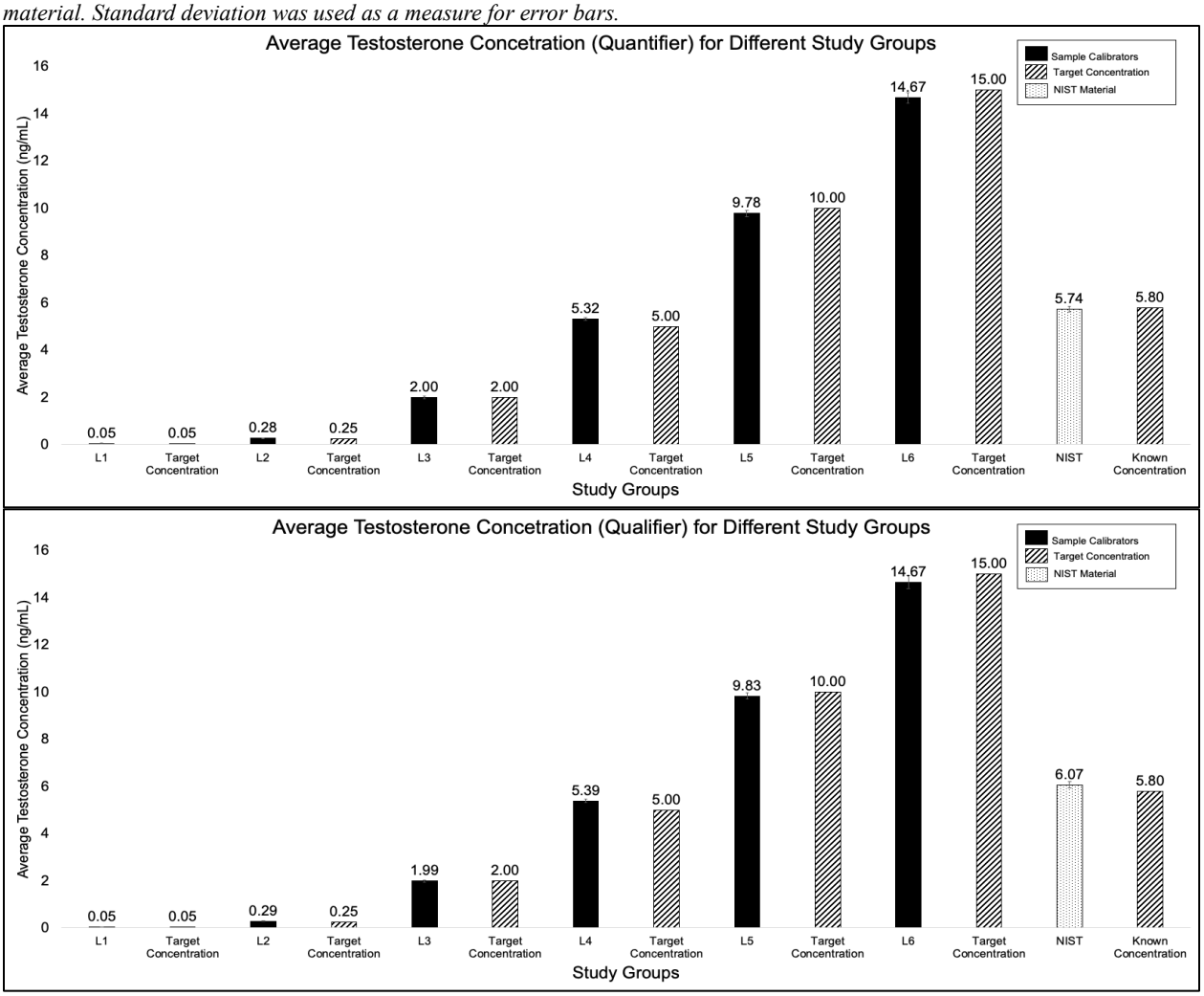

Table TS1. *Two different sample preparation methods, by plate size, shape, and type of plate seal used.*

Method 1	Method 2
Plate 1: 800 µL conical bottom	Plate 1: 450 µL v-bottom
Aluminum Foil Seal	Plastic Plate Cover mat
Plate 2: Standard 96-well qPCR plate (Surface area ~ 30 mm^2)	Plate 2: Nunc 96-well clear plate (Surface area ~ 52.8 mm^2)

Surface Area to Sample Volume Ratio = 1:5	Surface Area to Sample Volume Ratio = 1:2.8
Final Plate Seal: X-Pierce Plate Seal	Final Plate Seal: Rapid EPS Plate Seal

Supplemental Figure S2. *Average (measured) testosterone concentration for two different sample preparation methods listed on Table S1.*

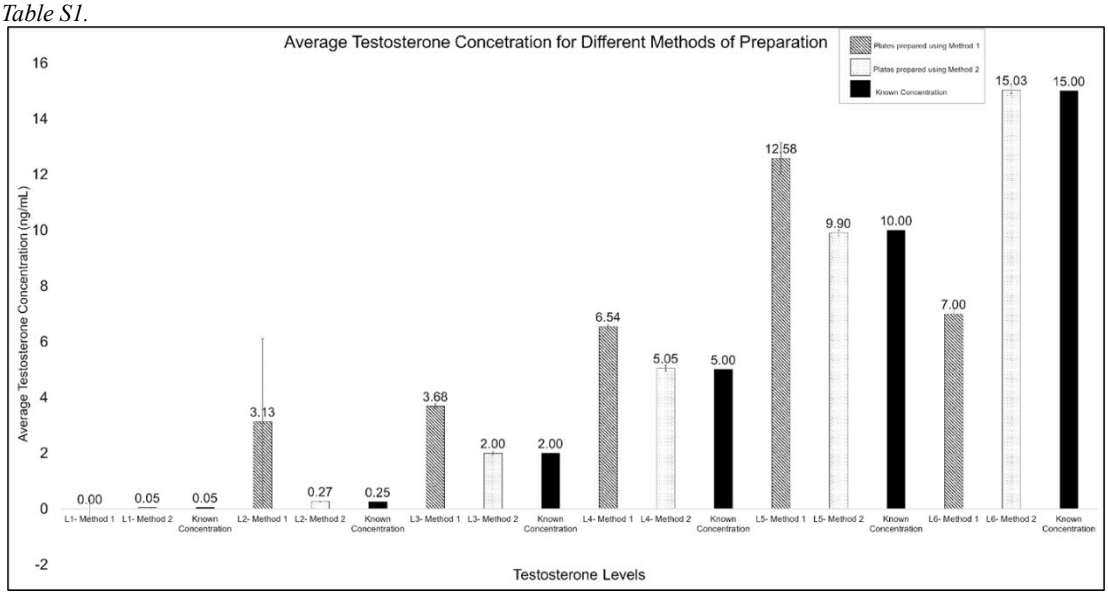

Supplemental Figure S3. *Normalized (to Day 0) average testosterone concentration for quantifier over 2-day intervals up to Day=14. Samples were mostly stable over the 14 days.*

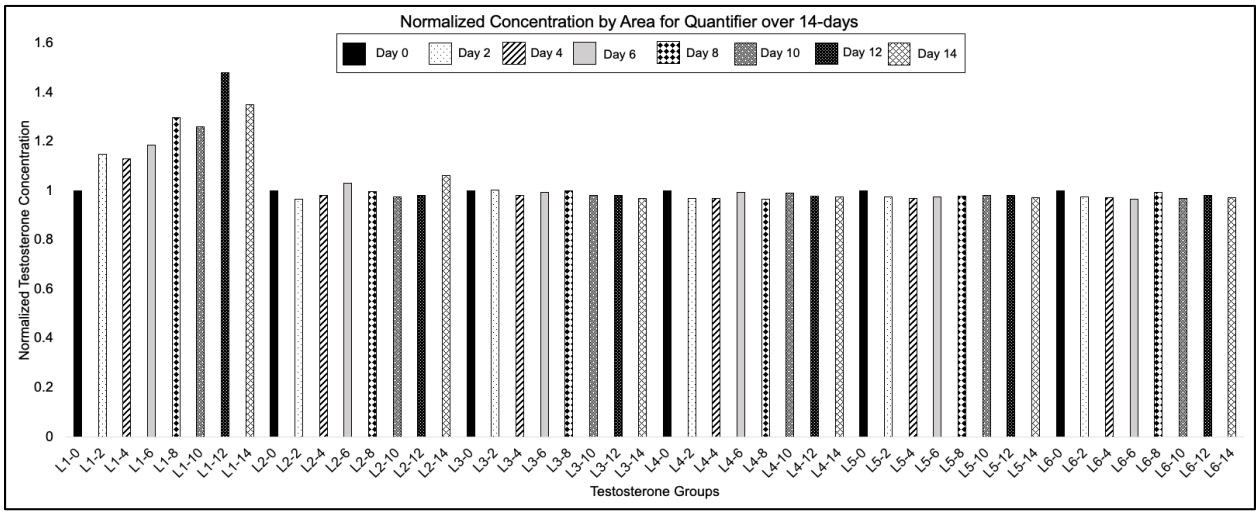

Supplemental Figure S3. Average measured concentration of testosterone (quantifier and qualifier) for no formic acid, 0.1% formic acid and 1% formic acid during reconstitution step. Results obtained for 0.1% formic acid and 1% formic acid were not statistically significant.

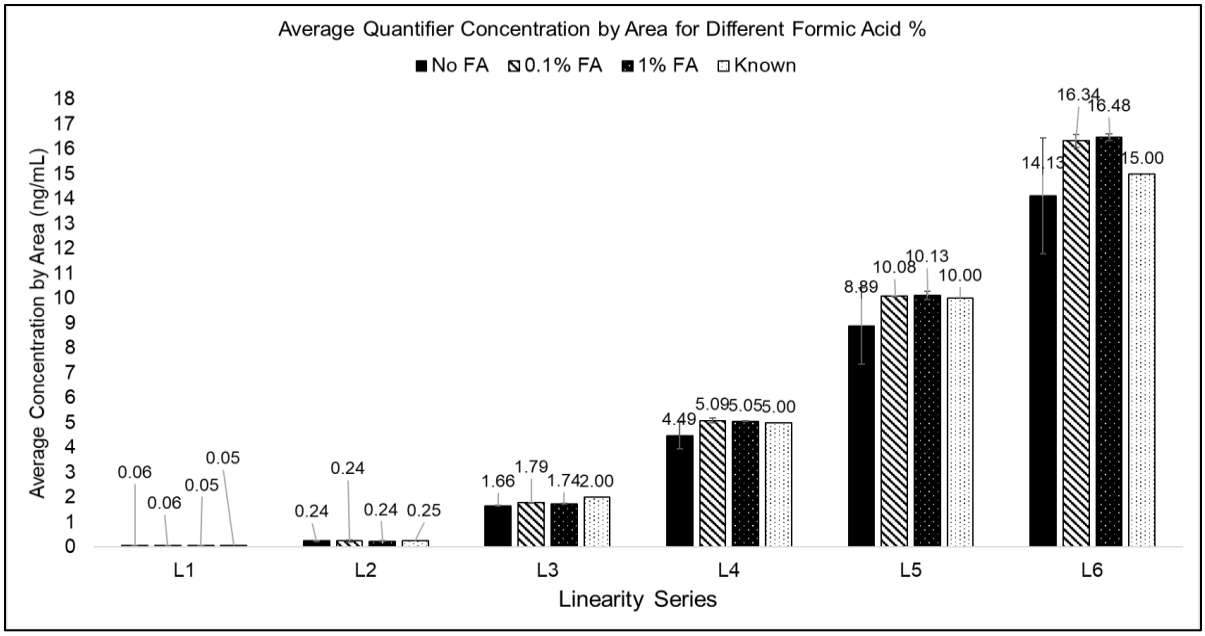
Average Quantifier Concentration by Area for Different Formic Acid %
No FA
0.1% FA
1% FA
Known
Average Concentration by Area (ng/mL)
Linearity Series
L1
L2
L3
L4
L5
L6
0.06
0.06
0.05
0.05
0.24
0.24
0.24
0.25
1.66
1.79
1.74
2.00
4.49
5.09
5.05
5.00
8.89
10.08
10.13
10.00
14.13
16.34
16.48
15.00

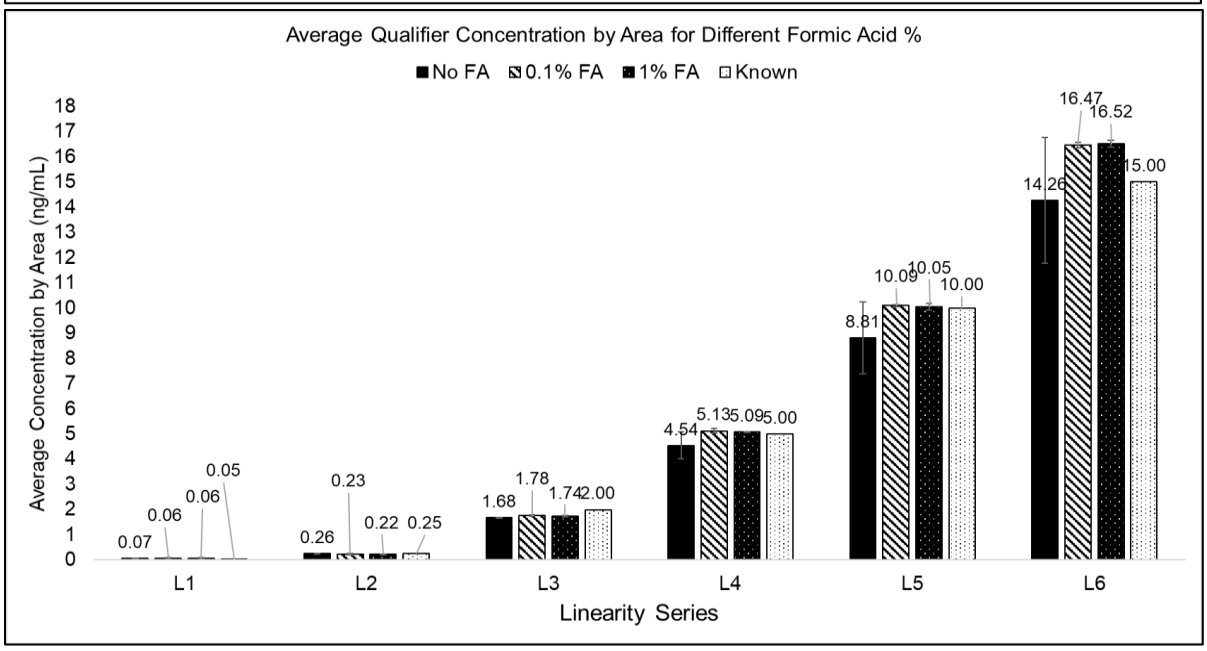
Average Qualifier Concentration by Area for Different Formic Acid %
No FA
0.1% FA
1% FA
Known
Average Concentration by Area (ng/mL)
Linearity Series
L1
L2
L3
L4
L5
L6
0.07
0.06
0.06
0.05
0.26
0.23
0.22
0.25
1.68
1.78
1.74
2.00
4.54
5.13
5.09
5.00
8.81
10.09
10.05
10.00
14.26
16.47
16.52
15.00

Chapter 6: Opioid Quantification via Microsampling Techniques to Assess the Impact of Noradrenergic Activation

Chapter 6 is currently under review to be published as an original research article.

Fariha, R.[1], Rothkopf, E. [1], Haass-Koffler, C.[2], Tripathi, A.[1*]

1. Brown University Center for Biomedical Engineering

2. Brown University Department of Psychiatry and Human Behavior, Alpert Medical School

6.1.Abstract

Despite progress in neurobiological studies with human subjects, sample availability remains a challenge. Urine samples, widely used for screening, suffer from false-positive results due to immunoassay cross-reactivity. Serum, used for confirmatory testing, offers advantages but faces limitations in collection due to stigma, and safety concerns. Microsamples, with a working volume less than 50 μL, present an ideal strategy for robust quantitative data collection in investigations and preclinical studies. We developed, validated, and automated a serum-based LC-MS/MS assay for accurate quantification of six opioids using only 20 μL of patient samples. Our method, applied in a clinical trial involving oxytocin and yohimbine stimulation, identified six different opioids, undetected by urine strip tests, potentially influencing behavioral data outliers. Our high-throughput, automated approach surpasses existing methods in literature, enhancing efficiency in multi-matrix studies.

6.2.Introduction

Even though COVID-19 pandemic was regarded to be one of the biggest challenges the United States had to combat with in recent times, it is important to note that just in 2021 alone, there were 80,411 reported deaths in the country associated with opioid overdose [160]. As a result, much attention is given to research focusing on drugs of opioids in the form of the HEAL initiative by the National Institutes of Health (NIH) [161], including understanding the noradrenergic system and its relationship to addiction [162]. Over the last decade, researchers have conducted animal testing as well as preclinical investigations to assess the impact of oxytocin (OT) administration in substance abuse craving or withdrawal [163-166]. OT, a well-established neuropeptide produced by the hypothalamus, plays a crucial role in the stress and anxiety regulation, social bonding, reproductive behavior etc. In addition to OT, Yohimbine (Y), an alkaloid-derived from

the Pausinystalia yohimbe tree, has also been investigated for its modulating ability on opioid withdrawal [167, 168]. Both OT and Y have been regarded as molecules of key interest in the noradrenergic system modulation, wherein they dictate the drug-seeking behavior, and hence, have an impact on addiction [167, 169, 170]. Despite the progress in neurobiological studies with human subjects, one of the pressing challenges that is pertinent to the success of these studies is sample availability. While urine samples are widely used for a preliminary screening, the number of false-positive screens are fairly high due to the antibody cross-reactivity in the immunoassays [171]. Serum, on the other hand, is often used for confirmatory testing, with its advantages of providing a shorter detection window, presence of parent compound, and fewer external contaminants. However, due to the associated stigma, unpredictable behavior, as well as safety concerns, the serum sample collection for multivariable analysis- including mass spectrometry-based analysis- from the subjects remains a limiting factor [173-175]. Utilizing microsamples- samples with a working volume less than 50 μL- can be an ideal strategy for collecting robust quantitative data from such investigations and preclinical studies. Multiplex metabolomics assays for liquid chromatography tandem mass spectrometry (LC-MS/MS) for opioid quantification can prove to be crucial for its ability to screen and quantify any of the metabolites of analytes of interest in addition any other compound the subject may have in his/her system with great sensitivity and specificity [176, 177]. Herein, we have developed, validated, and automated a serum-based assay for LC-MS/MS application for an accurate quantification of six different opioids using only 20 μL of patient sample. Additionally, we have used our protocol to test patient samples from a clinical trial involving OT and Y stimulation prior to cue reactivity, and how any behavioral data outlier observed might have resulted from the presence of different opioid metabolites in the subject's system that could not be detected via a urine strip-test. Our method hails superior to several others

reported in the literature (Table 10) (multi-matrix studies) due to its high throughput ability via automation.

	Fariha et al. 2024	Liao et al., 2022	Swortwood et al., 2016	Mathias et al., 2014	Kim et al. 2011	Kacinko, 2008
Number of Analytes	6 opioids	24 opioids	1 opioid (buprenorphine and 6 of its metabolites)	3 opioids and their metabolites (total 20)	12 drugs	1 opioid (buprenorphine and 3 of its metabolites)
Matrix	Serum	Urine	Plasma and breastmilk	Urine	Plasma	Urine
Number of Steps for Sample Preparation	5	5	15	3	4	10
Sample volume required	20 µL	Not specified	100 µL	100 µL	20 µL	200 µL
Sample Preparation Method	Protein Precipitation and Dilution	Dilute-and-Shoot	Protein Precipitation and Solid Phase Extraction (SPE)	Dilute-and-Shoot	Protein Precipitation and Dilution	Solid Phase Extraction (SPE)
Sample Preparation: Step 1	Add 80 µL extraction solvent (acidified acetonitrile and methanol solution with 2.5 µg/L IS)	Urine samples centrifuged for 1 min at 17,000 rpm.	Add IS (50 µg/L)	Urine samples centrifuged for 1 min at 17,000 rpm.	Add IS and reserpine	Add IS
Sample Preparation: Step 2	Shake at 700 rpm at 45 °C for 5 minutes	10 µL of supernatant was diluted with 90 µL water	Add 300 µL of ACN	Add IS (in 4 different combinations and volumes, concentration not specified)	Add 1000 µL acetonitrile	Acidification of mixture
Sample Preparation: Step 3	Centrifuge at 0 °C for 10 minutes	Add IS	Centrifuge at 8000 g at 4 °C for 10-minutes	Dilute and analyze	Mix (30 seconds)	Vortex
Sample Preparation: Step 4	Extract 50 µL supernatant, add 167 µL DWS (acidified water with 2.5 µg/L IS)	Foil heat seal	Supernatant transfer and acidification	N/A	Centrifuge (1400 g for 5 minutes) and analyze	SPE- Addition to cartridge
Sample Preparation: Step 5	Shake at 400 rpm at 25 °C for 30	Centrifuge and analyze	Vortex	N/A	N/A	SPE- Wash (1)

	seconds and analyze					
Sample Preparation: Step 6	N/A	N/A	SPE- Addition to cartridge	N/A	N/A	SPE- Wash (2)
Sample Preparation: Step 7	N/A	N/A	SPE- Wash (1)	N/A	N/A	SPE- Dry (1)
Sample Preparation: Step 8	N/A	N/A	SPE- Wash (2)	N/A	N/A	SPE- Wash (3)
Sample Preparation: Step 9	N/A	N/A	SPE- Dry (1)	N/A	N/A	Nitrogen drying of eluents
Sample Preparation: Step 10	N/A	N/A	SPE- Wash (3)	N/A	N/A	Reconstititue and analyze
Sample Preparation: Step 11	N/A	N/A	Nitrogen drying of eluents	N/A	N/A	N/A
Sample Preparation: Step 12	N/A	N/A	Reconstititue	N/A	N/A	N/A
Sample Preparation: Step 13	N/A	N/A	Vortex	N/A	N/A	N/A
Sample Preparation: Step 14	N/A	N/A	Centrifuge (1)	N/A	N/A	N/A
Sample Preparation: Step 15	N/A	N/A	Centrifuge (2) and analyze	N/A	N/A	N/A
Injection Volume	10 µL	10 µL	50 µL	Not Specified	1 µL	15 µL
Instrumentation Type	LC-MS/MS	LC-MS/MS	LC-MS/MS	LC-MS/MS	LC-MS/MS	LC-MS/MS (ion-trap)
Run Time Per Sample	3.5 minutes	26 minutes	8 min	8 minutes	6 minutes	20 minutes
Concentration Range	10-2000 µg/L	10-10,000 µg/L	2µg/L to 100µg/L	N/A	0.1 µg/mL-10 µg/mL	5−1,000 µg/L

Table 10: Direct method comparison highlighting major differences between the described assay against methods published in literature.

6.3. Experimental

6.3.1. Chemicals and Reagents

All of the solvents used were Baker Analyzed, LC-MS grade, and with a purity of >99% (from VWR). Such solvents include water, acetonitrile, and methanol used for the preparation of calibrators and LC-MS/MS operation. The analytes for the study were purchased from Cerilliant Corporation (Round Rock, TX, USA). The analytes used were Buprenorphine (Bup B-044),

Codeine (Cod C-006), Hydrocodone (Hd_Cod H-003), Methadone (Meth M-007), Morphine (Morph M-005), Oxycodone (Oxy O-002). The internal standards for the analytes were Buprenorphine-D4 (B-901), Codeine-D3 (C-005), Hydrocodone-D3 (H-005), Methadone-D3 (M-008), Morphine-D3 (M-003), and Oxycodone-D3 (O-005). Fisher Scientific reagent-grade formic acid (96% pure) was purchased for improved ion mobility in the mobile phases. Sigma-Aldrich ultra-low steroid, drug-depleted DDC Mass Spectrum Gold Serum was used for the creation of the calibrator and Quality Control (QC) base matrices. Sigma-Aldrich Sodium Azide (≥99.5%, ReagentPlus) was purchased to be used as a preservative.

6.3.2. LC-MS/MS Conditions and Parameters

All analytes and internal standards were diluted 1000-folds and a 100-fold in HPLC-grade methanol, respectively, and used for MS method optimization via direct infusion using a 1mL gastight Hamilton syringe and Harvard apparatus (operating at flow rate 30 μL/min) in Multiple Reaction Mode (MRM). The parent and MRM masses, along with optimized parameters for entrance voltage (EV), prefilter (PF), collision cell lens 2 (CCL2), collision energy (CC), and detector deflector (ID), are listed on Table 11. Additionally, the source parameters were optimized to operate at drying gas= 60, HSID (hot surface-induced desolvation) temperature= 320 °C, nebulizer gas= 300, electrospray voltage= 5850 V, and source temperature= 200 °C (ESI positive). The instrument used was a PerkinElmer QSight 220 CR Triple Quadrupole Mass Spectrometer (with dual source), with LX50 Solvent Delivery Module, Precision Sampling Module, and Column Stability Module.

The column used for the study was the Restek Raptor Biphenyl C18 (2.1 x 50 mm, with 2.7 μm particle size, and 90 Å pore size) operating at 40°C with a 0.25 mL/min flow rate, on a fast partial loop fill. The mobile phases were optimized to be water with 0.1% formic acid (A) and

acetonitrile with 0.1% formic acid (B). The final LC method used for the study was a 3.5-minutes long method, with a 30-seconds flow of 2% B, followed by a 1-minute hold of 50% B, and another 1-minute hold of 100% B, followed by 30-seconds of column equilibration, while the samples were housed at 4°C in the autosampler. To alleviate the carryover impact, different combinations of needle wash solvents were tested. This included combinations of (i) 70:30= acetonitrile: water, 100% acetonitrile, 70:30= acetonitrile: water wash (data not reported), (ii) 100% water, 100% methanol, 100% water wash (data not reported), (iii) 50:50= methanol: water, 100% methanol, 50:50= methanol: water, and (iv) 70:30= methanol: water, 100% methanol, 70:30= methanol: water wash. Combination (iv) resulted in the least sample carryover and was used for the entirety of the study.

Analyte	MRM	Q1	Q3	EV	PF	CCL2	CC	ID
Bup	Quant	468.50	55.20	43	-18	-183	-61	-110
	Qual		187.00	43	-15	-222	-50	-108
	IS	472.60	59.00	42	-27	-223	-64	-112
Cod	Quant	300.30	199.10	25	-23	-151	-40	-110
	Qual		171.10	22	-23	-151	-49	-111
	IS	303.30	165.10	22	-22	-151	-57	-111
Hd_Cod	Quant	301.30	200.10	47	-25	-110	-37	-114
	Qual		172.00	55	-25	-132	-52	-108
	IS	303.30	241.10	40	-24	-54	-39	-117
Meth	Quant	310.30	105.20	11	-27	-87	-37	-112
	Qual		91.10	5	-25	-90	-51	-104
	IS	313.30	105.20	5	-26	-95	-41	-101
Morph	Quant	286.30	165.10	14	-25	-120	-50	-109
	Qual		153.10	15	-24	-128	-52	-110
	IS	289.30	165.10	11	-25	-116	-54	-110
Oxy	Quant	316.30	241.10	13	-27	-138	-35	-117

	Qual		212.10	7	-26	-144	-53	-111
	IS	319.30	244.10	8	-25	-145	-39	-114

Table 11. Optimized MS parameters for each opioid (quantifier and qualifier fragments and internal standard).

6.3.3. Preparation of Calibrators, and Daily Working Solution

Sodium azide (0.02% by volume) was added to DDC Mass Spect Gold Serum (ultra-low steroids, analyte stripped, blank) and stirred at room temperature for ~30 minutes. This was then used to create an eight-point linearity series of 10- 2000 µg/L concentration range. The calibrators went through two step dilution process (L1 used a 10,000-fold diluted solution, L2 and L3 used a 1000-fold diluted solution, and L4-L8 used a 10-fold diluted solution) and were rocked overnight at 4 °C prior to being aliquoted and stored at -80 °C. All calibrators (except freeze-thaw and accelerated stability analysis) and patient samples were only thawed once prior to experiments.

The Daily Working Solution (DWS) determined for the entire study were- an acidified (0.1% formic acid) 50:50= acetonitrile: methanol solution with 2.5 µg/L of the internal standards (IS) (DWS- 1), and an acidified (0.1% formic acid) HPLC water with 2.5 µg/L of the internal standards (DWS- 2).

6.3.4. Sample Preparation

All calibrators and patient samples were thawed to room temperatures and pleated in 400-µL v-bottom axygen plates and sealed using an aluminum foil seal. To 20 µL serum sample, 80 µL DWS-1 was added and shaken at 700 rpm at 45 °C for 5-minutes using a TriNEST plate shaker. The plate was then centrifuged at 4600 rpm for 20-minutes at 0 °C. 50 µL of the clear supernatant was collected on a separate plate, to which 167 µL DWS-2 was added and pipette mixed prior to analysis. The blanks used were HPLC water.

6.3.5. Automation

Once the sample preparation protocol was finalized, it was then adapted on the JANUS® G3 Workstation (PerkinElmer Corp., MA, U.S.). Building upon our previous work with serum on the platform, the JANUS® Application Assistant and WinPREP® for JANUS® were used to automate the protocol for this study, especially for the patient samples. Briefly, the deck layout (Supporting Information Figure 1) was used, with the patient samples housed on the left side of the deck in 75-mm tube racks. Caution was observed to ensure there was no sample dripping and cross contamination, while maintaining a %CV equal to or better than a manually prepared plate by an experienced researcher. The calibrators were pipetted for triple dispense using the 200 µL conductive tips, whereas all patient samples were pipetted using 75 µL conductive tips for single dispense- even if a sample were to be tested in triplicate. This was done to prevent cross contamination across samples collected since the stimulation profiles were different even for the same patient. DWS-1 was pipetted using 200 µL conductive tips for single 80 µL dispenses once all samples were plated. The 1000 µL tips were tested to increase the speed of the protocol, however, since DWS-1 is purely an organic solution, there was significant solution dripping, despite modifying the transfer gaps. Table 12 showcases all the labware definitions and modifications used for the final experiment. For the mixing step, clean, empty 1000 µL tips were used with "pre-aspirate mixing" function once all the solutions had been added to the final plate.

Table 12. *Parameters selected for the automation of the proposed protocol (specific to JANUS® G3 Workstation)*

Protocol Step	Volume of Transfer (µl)	Pipette Tip Utilized (µl)	Dispenses Per Aspirate	Pipette Mode	Transfer Gap (µl)	Waste/ Blowout Volume (µl)
Calibrators	20	200	3	Waste	10 (before and after aspirate)	5
Patient Samples	20	50	1	Blowout	10 (before and after aspirate)	0
DWS- 1	80	200	1	Blowout	30	10
Supernatant Transfer	50	75	1	Blowout	20 (after)	5
DWS- 2	167	1000	4	Waste	10 (after)	5

Even though the automated plating protocol took 7 minutes and 22 seconds longer than a manual plating protocol (excluding capping/re-capping time, and deck preparation), the automated protocol was regarded superior because of ease of sample tracking, as well as consistent particulate-free supernatant transfer each time.

6.3.6. DoE and Data Analysis

Design of Experiment (DoE) for the protocol and assay validation study was performed using JMP Pro 17.0 perform a full factorial design, for power> 80%. All LC-MS/MS data was collected and analyzed using Simplicity 3Q (version 3.0) software for QSight. The data exported was further evaluated using Microsoft Excel, and JMP Pro 17.0 for visualization and statistical analysis (ANOVA, Dunnett's post-hoc test for significance against control (baseline) and Tukey-Kramer HSD test for comparison among different groups). A p-value of 0.05 or less was considered statistically significant. Graphpad Prism 9 was strictly used to generate illustrations based on all the statistical analysis performed on JMP Pro.

6.4.Results and Discussion

6.4.1. Matrix Effect, Interference, and Solvent Analysis

Similar to our previous investigations, it was important to establish that all analytes were visible in an intricate diagnostic material like serum. As a result, an eight-point calibrator set in methanol was prepared along with the serum calibrator set and ran to assess any ion suppression taking place. The calculated matrix effect (ME) threshold was set to be ±20%, i.e., any value less than 80% would indicate significant ion suppression. The final mean matrix effect was reported to be (83.5-98) ±20% across the board for all the MRMs, when measured by peak area. Any value above 100% represented ion enhancement, which was only observed for methadone (average 118.9% for 10 μg/L). To rule out any interference from the native serum, we ran triplicates of blank serum (L0) on each plate and observed no peaks at the detected retention times for all the

analytes. For this study, the LOD was defined as the quantifiable lowest concentration distinguishable from blank serum (2 µg/L) and LOQ was defined to be the lowest calibrator level that met the precision cutoff (i.e., L1= 10 µg/L). Figure 20 (a) shows the blank serum with internal standard, while figure 1 (b) shows L1 in serum with internal standard.

Figure 20. Representative chromatograms showing unspiked serum (top) and, lowest level of calibrator, L1 (bottom) for buprenorphine. This is was consistent for all the other analytes, inclusive of both MRMs.

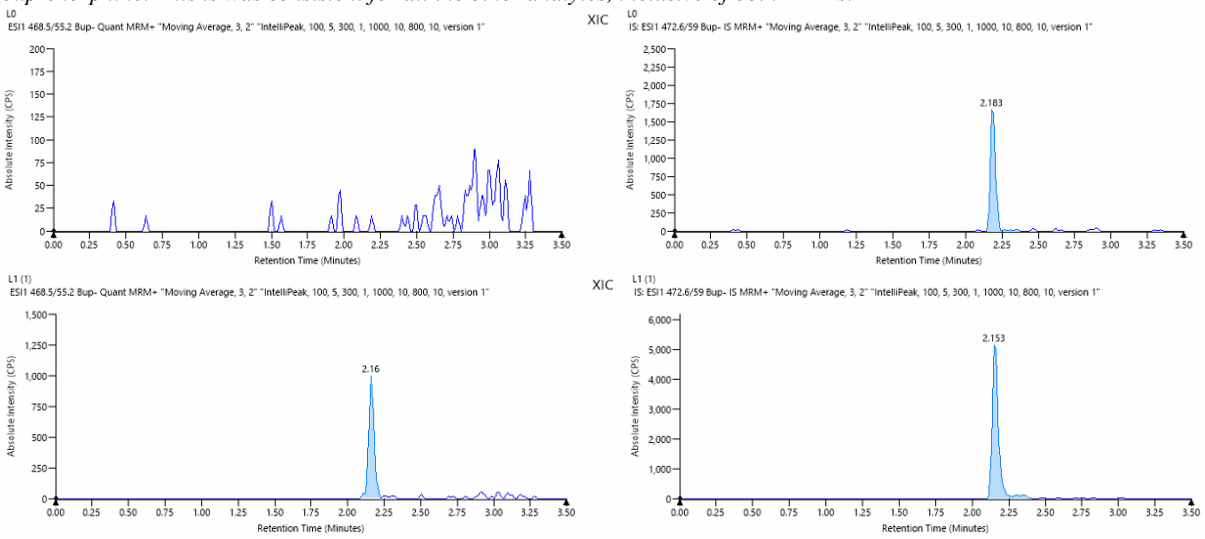

In addition to assessing the ME, it was important to establish that each analyte showcased distinguished peaks for their respective, consistent retention times (RT). Figure 21 illustrates the detected RT for the six opioid quantifiers, overlaid on their absolute intensity profile (in serum). This was consistent with our overall experimental findings, where methadone displayed higher analyte recovery across the board compared to all the other analytes, even though they were all visible, and had independent chromatographic separation.

Figure 21. Chromatogram overlay showing absolute intensity for all six opioid quantifiers in serum and their respective retention times.

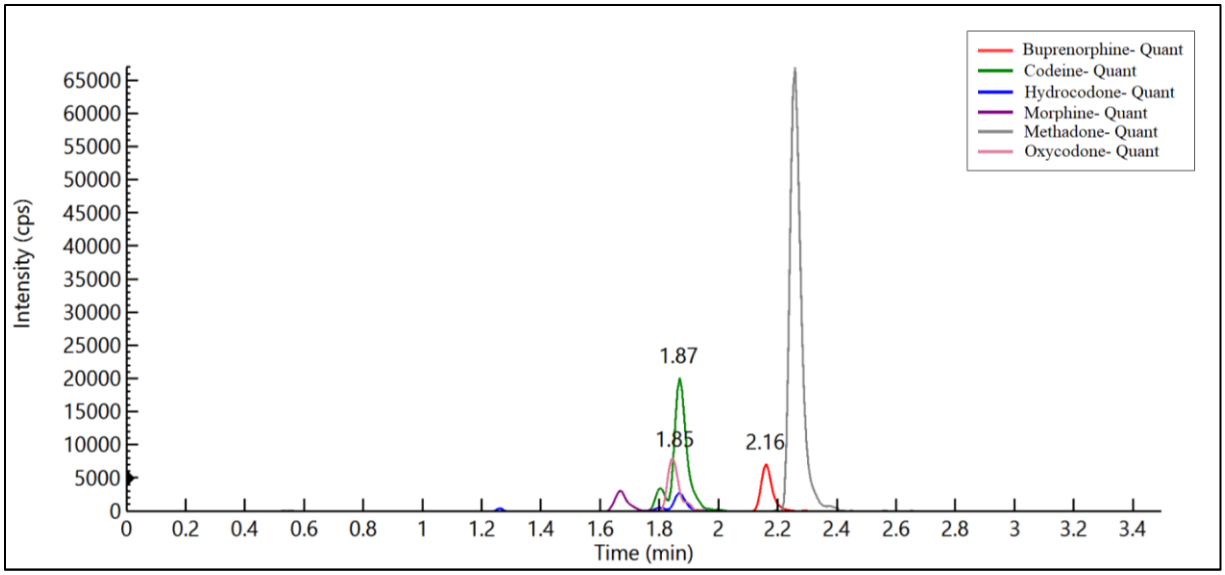

One interesting finding from the chromatography setup was the mobile phase B flow percentage and how the slightest change in the value can impact the separation of the analytes. One of the initial methods tested used a 5% mobile phase B initially, unlike the 2% of the final method used, and it significantly impacted the separation of morphine. Over 5 repeated runs, ranging mobile phase B from an initial 10% to 2%, only the absolute resolution of morphine (both MRM) in serum was affected, while all other analytes had distinct peaks resolved irrespective of the percentage of mobile phase B flown through the column initially. The chromatography method used for the entirety of the study has been previously described in the experimental section.

Additionally, we conducted a phase-test like our previous studies, where we determined the final inorganic-to-organic solvent ratio for a proper Gaussian peak without any significant loss of signal. For the six opioids of interest, it was determined that 70% inorganic content was required for the desired chromatography shape. This dictated the sample preparation procedure to be a two-step extraction and dilution process, instead of a single solution for simultaneous protein crash and dilution. Even though most traditional protocols would call for either methanol or acetonitrile to be used for protein crash, we investigated their individual and combined impact on the

microenvironment of the system. Even though the opioids reference materials used in this study have a greater solubility in methanol (manufacturer protocol), the pellet formation caused by methanol only was visually not compact, and therefore, made the automation process challenging. For an efficient automation process, it is crucial that the protein pellet formed each time is uniform, compact, and roughly the same height from the well-bottom, because the robotic handler had to be programmed to account for the pellet size to prevent accidental aspiration of the particulates. As a result, we extrapolated the findings of Roy and Flynn [19] for the solubility of morphine.

$$pK_a' = pH + \log\left(\frac{C_T - [B_S]}{[B_S]}\right) \text{ (eq. 1)}$$

where, pK_a' is the dissociation constant, C_T is the total concentration of a saturated solution, and B_s is the free-base solubility. Using eq. 1, Roy and Flynn determined the dissociation constant of morphine, and additionally showcased that the solubility of morphine increases in the presence of a weak acid, with no degradation of the molecule at a higher temperature (45 °C). Therefore, following the addition of DWS-1, the sample solution was exposed to a higher temperature with mechanical mixing, accelerating the convection process of the analytes, and immediately then put through separation by temperature assisted centrifugation. This resulted in the opioids leaving the serum solution to the DWS and staying put while the water and protein content from the serum settled at the bottom of the plate. This produced a tight ~2.8 mm protein pellet consistently for all the samples, aiding the automation of the protocol.

6.4.2. Quality Control, Linearity, Precision, and Accuracy

Upon finalizing the methods, the calibrators were run in sextuplets and averaged to obtain their initial spike value (to be used for later experiments). Figure 3 showcases the theoretical spike values (striped) against the measured concentrations (solid) in a log scale for the opioid quantifier fragments.

Figure 22. Average calibrator concentrations post-bulk production of the calibrators against theoretical spike concentrations. Error bars represent standard deviation.

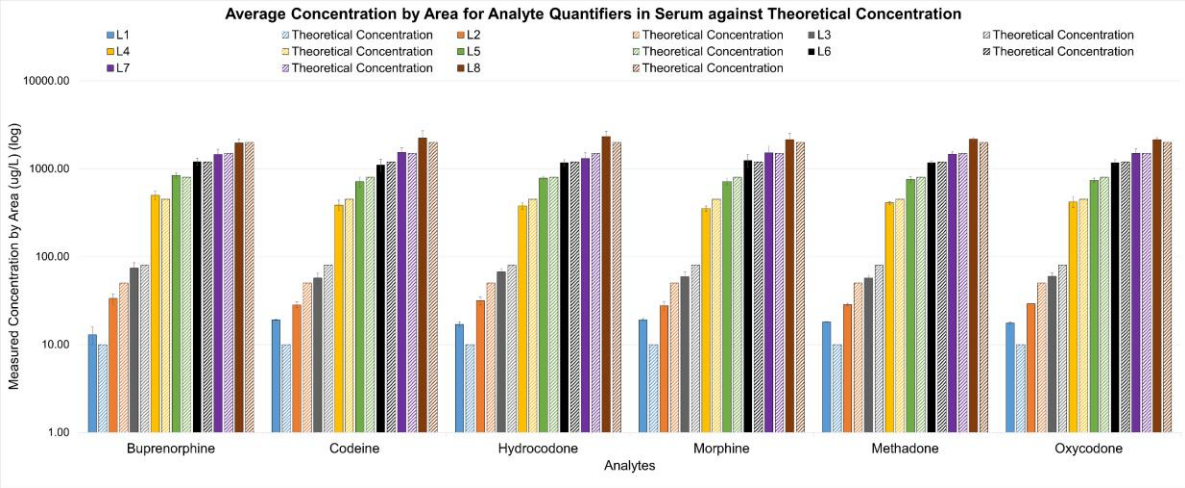

Linearity, precision, and accuracy data were all obtained from the same experiment, where the linearity of the calibrators was assessed by looking at the R^2-values for each standard curve produced, which reported to be 0.95 and above for all analytes, inclusive of both MRMs. Precision was calculated as %CV measured ±≤20% for intra and inter-assay runs, across 6-days with n=6 for each calibrator level per analyte. Even though the %CV was below 20% for all the analytes, the sample accuracy measurements were off. This is because the accuracy values were off from on the quality control run (against theoretical/entered values), and therefore, those values simply carried over (the batch runs were saved as templates with previously entered theoretical measurements). Table 13 (a-f) shows the measured concentration with standard deviation, %CV, and % accuracy for all the analyte quantifiers. This is representative of both MRMs for the specific analyte.

Table 13. *Average measured concentration per calibrator level; %CV as a measure of precision (n=36/level).*

a) Buprenorphine

Calibrator Level	$\boldsymbol{\mu_{\underline{x}} \pm \sigma}$ *(ng/mL)*	*%CV*	*% Accuracy*
L1	12.8 ± 1.6	*12.7*	*128.5*
L2	33.4 ± 4.5	*13.3*	*66.9*
L3	74.1 ± 10.9	*14.6*	*92.7*
L4	498.2 ± 55.4	*11.1*	*110.0*
L5	836.3 ± 50.6	*6.0*	*104.5*
L6	1209 ± 104.7	*8.7*	*100.7*
L7	1455.7 ± 216.5	*14.9*	*98.0*

L8	1969.9 ± 219.9	*11.2*	*98.5*

b) Codeine

Calibrator Level	$\underline{\boldsymbol{\mu_x}} \pm \boldsymbol{\sigma}$ *(ng/mL)*	*%CV*	*% Accuracy*
L1	19.0 ± 0.3	*1.21*	*190.3*
L2	28.3 ± 2.1	*7.6*	*56.6*
L3	57.2 ± 8.2	*14.4*	*71.5*
L4	385.5 ± 52.1	*13.5*	*85.6*
L5	709.8 ± 95.3	*13.4*	*88.7*
L6	1113 ± 174.9	*15.7*	*92.7*
L7	1537.1 ± 184.0	*11.9*	*102.5*
L8	2240.1 ± 462.0	*20*	*112*

c) Hydrocodone

Calibrator Level	$\underline{\boldsymbol{\mu_x}} \pm \boldsymbol{\sigma}$ *(ng/mL)*	*%CV*	*% Accuracy*
L1	16.9 ± 1.2	*7.2*	*169*
L2	31.5 ± 3.3	*10.7*	*63.0*
L3	67.2 ± 6.2	*9.3*	*84.0*
L4	379.0 ± 36.8	*9.7*	*84.3*
L5	784.2 ± 32.4	*4.1*	*98.1*
L6	1176 ± 101.0	*8.6*	*98.0*
L7	1306.5 ± 210	*16.1*	*87.1*
L8	2328.5 ± 340.4	*14.6*	*116.4*

d) Morphine

Calibrator Level	$\underline{\boldsymbol{\mu_x}} \pm \boldsymbol{\sigma}$ *(ng/mL)*	*%CV*	*% Accuracy*
L1	18.9 ± 0.7	*3.6*	*189*
L2	27.7 ± 2.9	*10.4*	*55.4*
L3	59.4 ± 6.9	*11.5*	*74.3*
L4	352.7 ± 25.4	*7.2*	*78.4*
L5	716.3 ± 62.7	*8.7*	*89.5*
L6	1250.5 ± 201.1	*16.1*	*104.2*
L7	1518.7 ± 283.1	*18.6*	*101.3*
L8	2145.6 ± 390.2	*18.2*	*107.3*

e) Methadone

Calibrator Level	$\underline{\boldsymbol{\mu_x}} \pm \boldsymbol{\sigma}$ *(ng/mL)*	*%CV*	*% Accuracy*
L1	18.1 ± 0.1	*1.0*	*181*
L2	28.5 ± 1.2	*3.8*	*57*
L3	57.2 ± 4.2	*7.4*	*72.0*
L4	408.8 ± 15.2	*3.7*	*90.8*
L5	759.1 ± 52.2	*6.8*	*94.9*
L6	1178.8 ± 36.0	*3.1*	*98.2*
L7	1469.1 ± 76.8	*5.2*	*97.9*
L8	2170.3 ± 105.3	*4.8*	*108.5*

f) Oxycodone

Calibrator Level	$\boldsymbol{\mu_{\underline{x}} \pm \sigma}$ *(ng/mL)*	*%CV*	*% Accuracy*
L1	17.6 ± 0.6	*3.2*	*175*
L2	29.1 ± 1.9	*6.5*	*58.4*
L3	59.7 ± 5.1	*8.5*	*74.6*
L4	421.2 ± 58.1	*13.7*	*93.7*
L5	741.5 ± 44.8	*6.0*	*92.7*
L6	1174.0 ± 90.3	*7.7*	*97.8*
L7	1499.2 ± 187.9	*12.5*	*99.9*
L8	2147.3 ± 103.3	*4.81*	*107.4*

6.4.3. Carryover, Stability, and Freeze-Thaw

Assessing sample carryover is a key feature of a protocol and method validation, especially if it has automation adaptation, as well as clinical sample testing. Both Carryover and Stability studies were conducted according to our previous work [124]. Figure 23 (a) shows five of the analytes (both MRMs) (except Buprenorphine) where the lowest calibrator, L1, was injected in triplicates right after injecting L8 (L1- Carryover). The baseline L1 was established by injecting L1 at the beginning of the run right after blank injections. The data obtained for the L1-Carryover group had no outliers, and the data spread was well within the desirable limit. Hence, it was concluded that there was no statistically significant carryover (Dunnett's test was performed against L1- Baseline) for the specified five analytes. Buprenorphine (not shown) had statistically significant increase in L1 post-L8 injection, and therefore, all the patient sample tested included two blank injections between different patients and different stimulation conditions.

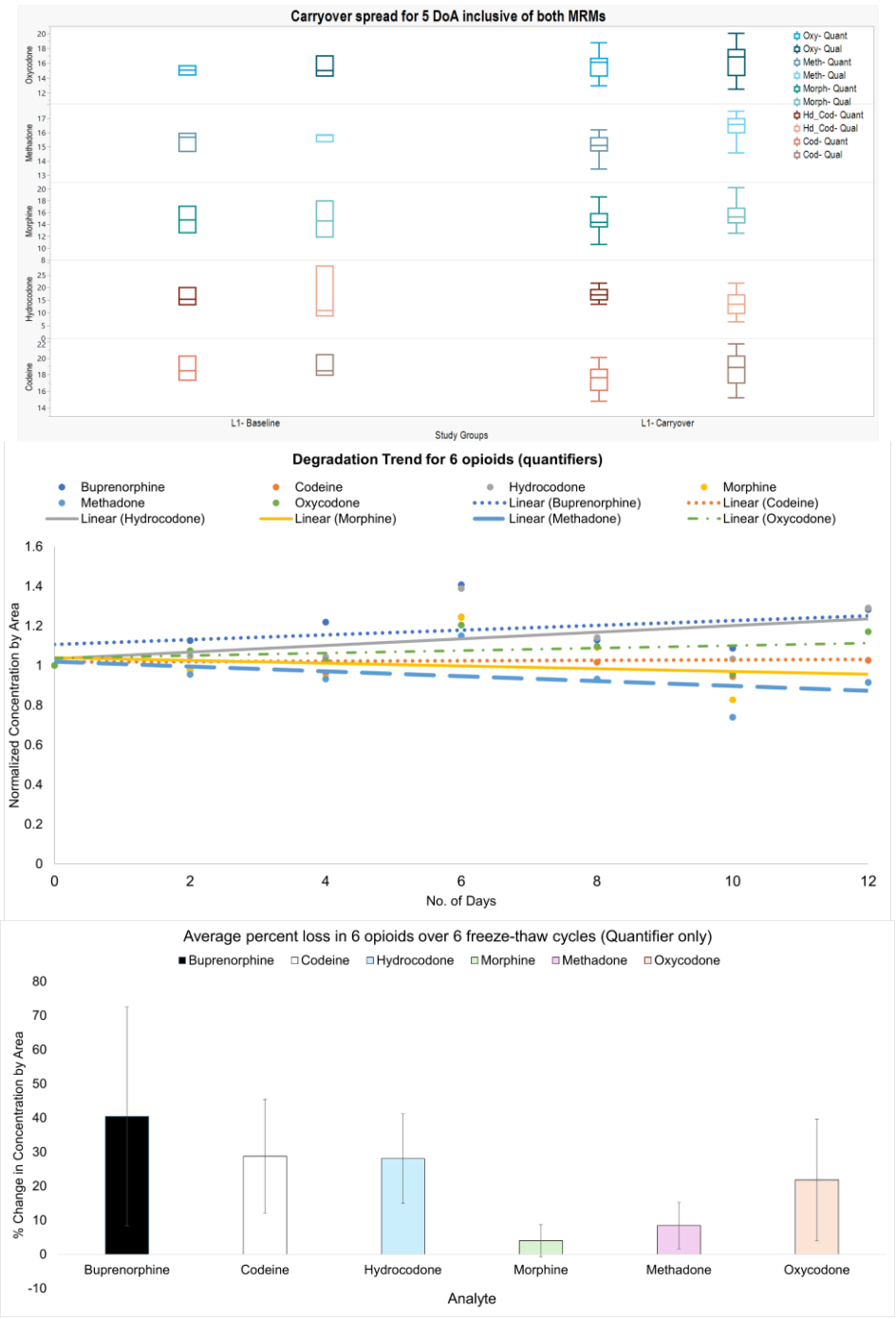

Figure 23 (a). Carryover spread for baseline L1 (following blank) for all analyte (MRMs) except buprenorphine, against carryover study group (followed by L8 injection) (n= 24; no significant outliers were observed).
(b) Representative accelerated stability (12-days) trend for all six analytes (n=3, with 3 technical replicates). Out of all the analytes, methadone showcased statistically significant decrease after Day 4 (21-days extrapolated), and thus, this was the determining factor for all the calibrator stability.
(c) Average percentage change in analyte concentration over 6 freeze-thaw cycles (n= 48 total; 6 per level). Because of 40% and higher loss of concentration of buprenorphine, the calibrators were only thawed once.

In addition to assessing sample carryover, we performed a 12-day accelerated stability study (63 days extrapolated), with n=3 per calibrator level per day, storing the samples at -20°C and stressing them at +4°C. Figure 23 (b) shows the stability trend of the different six analytes for one of the calibrator quantifiers. This is representative of the trend observed for all the calibrators for all analytes, inclusive of both MRMs. This trend showcases that the calibrators are stable at a storage temperature of -20°C for 21 days extrapolated.

Figure 23 (c) shows the average percentage loss (averaged for all calibrators) in analyte for six opioid quantifiers over six freeze-thaw cycles (-20°C to +25°C). All analytes except morphine and methadone exhibited a 40% decrease in analyte concentration. While morphine and methadone both showcased approximately 10-15% loss in analyte, these values were, indeed, significant, and will impact the repeated use of the calibrators. Therefore, the calibrators were frozen right after bulk manufacturing smaller aliquots and thawed only once for each use.

6.4.4. Ease of Automation

Owing to the nature of the sample preparation employed as described in section 6.4.1, automating this method was fairly straightforward, with the programmed human interactions. This was due to the limitation of the workstation in the facility itself, where an on-deck shaker or centrifugation were not available. For more expensive and sophisticated automation platforms, this protocol can be fully automated without needing any manual interaction. Additionally, it must be noted that the serum samples, once thawed, often form a thin air film halfway through the sample container (in this case, a 2 mL microfuge tube). When automating the protocol, caution must be taken when applying the liquid tracking features, since the instrument might send the thin film as the top of the fluid and start sample aspiration. This will lead to precision issues. Therefore, for all serum samples, the aspirate height was set to be 2 mm above the well bottom, with the liquid

tracking feature turned off. On the contrary, for the supernatant collection step, the well bottom was defined to be higher than the physical dimension, accounting for the pellet size, with the liquid tracking and clot detection features enabled, so that in the event of uneven pellet formation, the system is able to identify any protein pellet should it come to contact with one.

The key reason for pushing the automation of the method is the working sample volume. Even though researchers are comfortable with pipetting small volumes, the biggest challenge of microsample for clinical application is the need for accuracy. Granted the motivation behind this work is to be able to access the smallest serum volumes from volunteers to assess the impact of noradrenergic stimulation on cue reactivities, scaling up the volume to minimize pipetting error will defeat the purpose of the study. Additionally, the underlying thermodynamic principles may not hold true if the scale of the study is to be increased. Therefore, the key driving factor behind this method development was the simplification of the workflow for easy automation.

6.4.5. Patient Data Report

Prior to exposing the participants to any noradrenergic stimulation, all participant baseline serum and urine were collected. The urine was tested using a lateral flow assay (LFA) (Cliawaived Inc. methadone and buprenorphine dip tests) to identify the presence of methadone or buprenorphine in the system. Interestingly, a lot of the participants tested positive for buprenorphine in urine but did not show any buprenorphine in serum. One of the possible reasons behind this discrepancy is the chemical nature of buprenorphine, which is extremely light-sensitive. Previous studies of this compound involving LC-MS/MS reported measures including wrapping the autosampler door and working with the samples in the dark. While the calibrators continued to show buprenorphine even for lower concentrations due to the caution maintained during manufacturing and handling, the patient samples did not show any significant presence of

buprenorphine for any of the samples, for they had been collected and exposed to light prior to LC-MS/MS quantification. Interestingly, the patients did test positive for buprenorphine on the LFA. This is likely because the LFA has been designed to detect buprenorphine and any of its metabolites, especially norbuprenorphine and norbuprenorphine glucuronide, whereas our LC-MS/MS assay only quantified buprenorphine. One of the advantages, however, of our assay was the ability to detect any of the other drugs present in the patients' body that they may not have reported or could not be detected using the LFA. For the final reported data, any outliers were removed, and any values above or below 3-SD were eliminated prior to grouping the obtained data from the patients by condition. It can be seen that patients on methadone exhibited statistically significant decline in drug concentration when exposed to yohimbine pill (both MRMs). For oxytocin, however, this group showed no statistical significance. Interestingly, though, none of the participants reported the use of hydrocodone, morphine, or oxycodone, although they were quantified in their systems. For both MRMs of hydrocodone, there was a slight but statistically significant decrease in the drug concentration for the placebo group (both oxytocin and yohimbine placebo). For both MRMs of morphine, there was a statistically significant decrease in the drug concentration for oxytocin exposure, while there was an increase in drug concentration for yohimbine pill (quantifier), both oxytocin spray and yohimbine (qualifier). The only conclusive result from this study would be that yohimbine stimulation certainly declined methadone concentration in serum, since the other drugs detected in the system were not disclosed/reported by the participants. An important finding from looking at individual data points was the reported adverse effect in some of the patients. One of the participants on placebo for both oxytocin and yohimbine reported adverse effects, and upon looking at the data, it was seen that the patient had significant quantities of morphine and hydrocodone in the system. Additionally, two other

participants on yohimbine pill but placebo for oxytocin spray reported adverse effects, and they both also had high quantities of morphine in their serum. This raises questions regarding the accessibility of morphine for abuse, as well as the possible cross reactivity of yohimbine administration to those on morphine dosage.

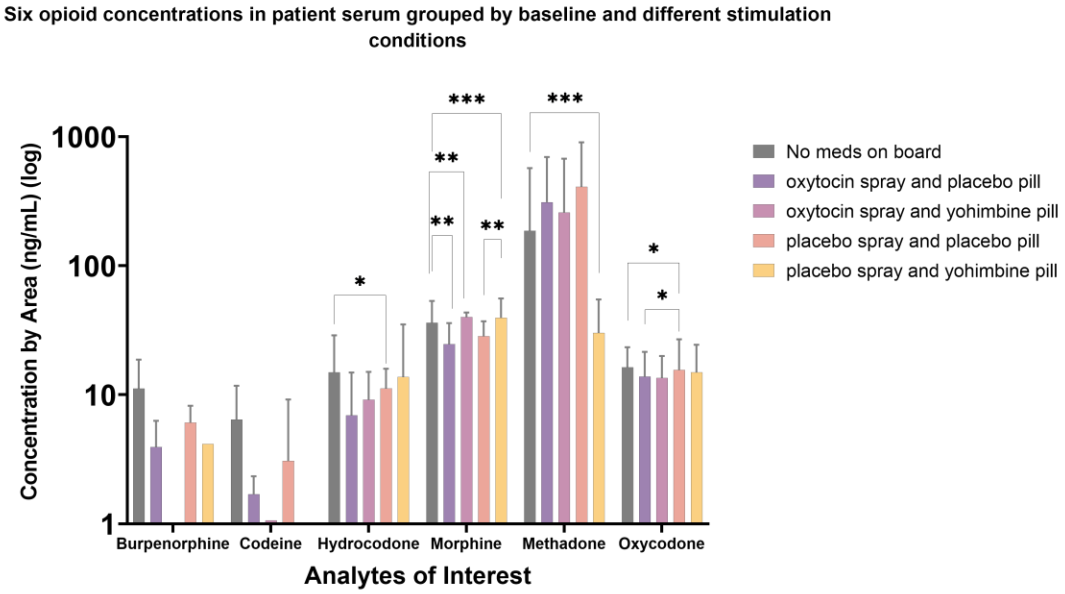

(a)

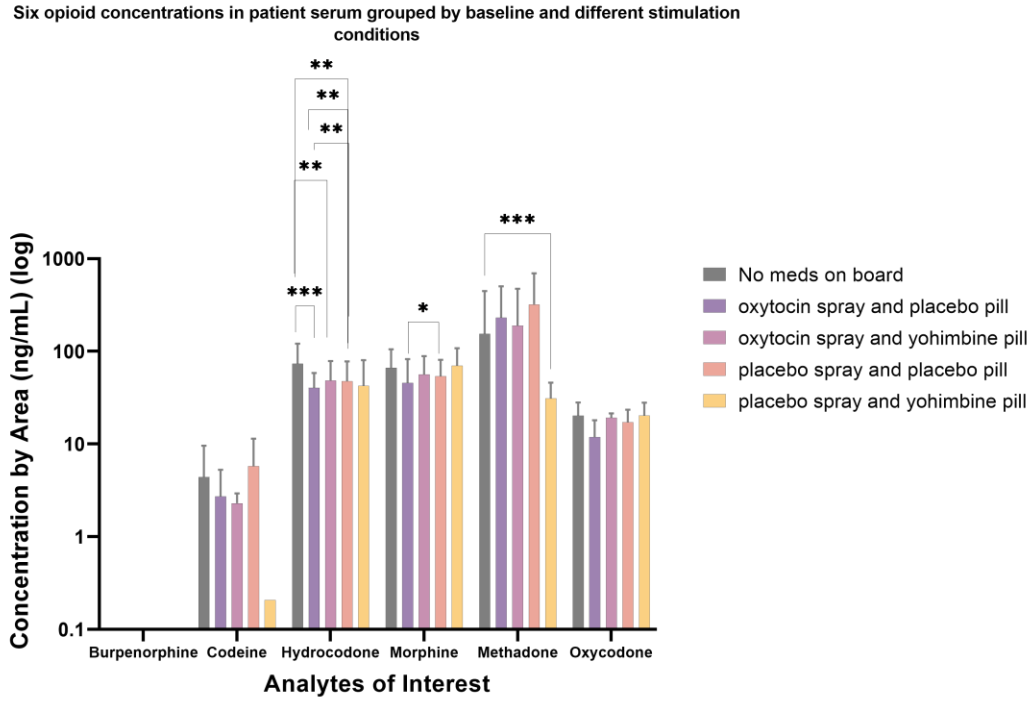

(b)

*Figure 24. (a- Quantifier, b- Qualifier) Average concentration by area for different patient groups (n=19 patients total) for 6 opioids for different stimulation conditions (error bars represent standard deviation; statistical significance denoted by: *= p<0.05, **= p<0.01, and ***= p<0.0001 against control, and within groups (indicated in pairs)).*

6.5.Conclusion

Multiplex metabolomics assay can play a vital role in supporting ongoing research studies to assess noradrenergic stimulation on opioid abuse. Microsampling, together with automation, can provide a solution to working with limited sample volumes while generating robust and participant-specific data to ensure the accuracy of the derived conclusions. We have demonstrated that our validated assay can effectively quantify six different opioids in clinical samples to confirm the finding that yohimbine pill administration can effectively reduce methadone abuse in humans.

6.6. Acknowledgements

The authors would like to thank Collin Hill (Revvity Inc.) for his guidance. The authors would also like to thank Zoe Brown for her help with patient sample collection, and Nondi Walters for her help with sample transportation. This work used patient samples supported by the National Institute of Health (NIH) grant *Oxytocin to Reduce Stress-Induced Craving in Individuals with Opioid Use Disorder* to the Haass-Koffler lab.

6.7.Supporting Information

Supplemental Figure 1. JANUS deck layout for calibrator and patient sample plating, together with extraction steps, and supernatant.

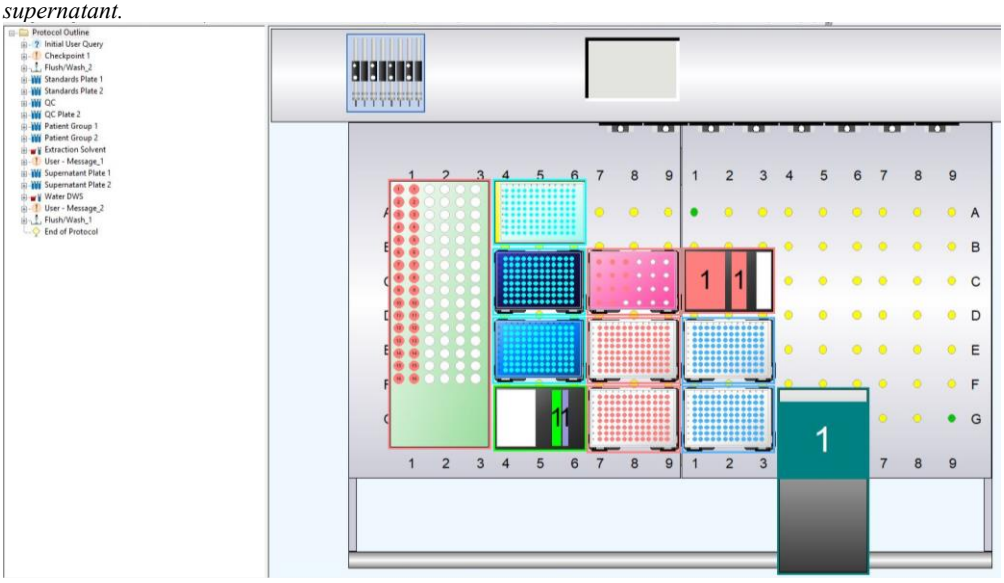

Supplemental Figure 2. Raw individual patient data for six opioids (MRMs), grouped by oxytocin and yohimbine treatment (-1= placebo for both, 0= placebo for the given condition, 1= stimulation for both).

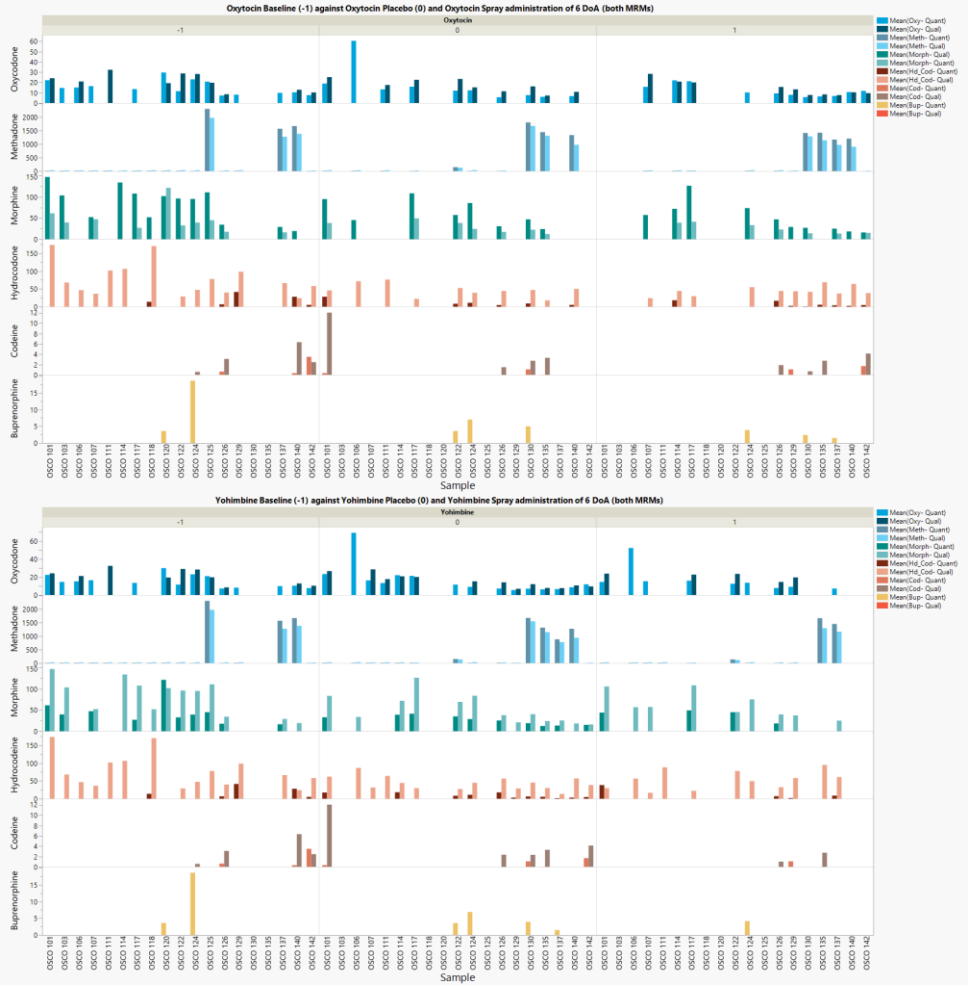

Chapter 7: Revolutionizing Neonatal Abstinence Syndrome Research: Precision through Electric-Field Assisted Automatable High Throughput Sample Preparation of Dried Blood Spots (DBS)

Chapter 7 is under review to be published as an original research article; preprint available online.

Fariha, R.[1], Murphy, J.[1], Walters, N.[1], Rothkopf, E. [1], Okoh, O.D.[1], Lawandy, N.M. [1,] Tripathi, A.[1]

1. Brown University Center for Biomedical Engineering

7.1.Abstract

In the United States, approximately one in five pregnant women self-reports opioid abuse, and in utero exposure to opioids, a consequence of maternal misuse, results in Neonatal Abstinence Syndrome (NAS), characterized by withdrawal symptoms in newborns. Current diagnostic approaches for NAS rely on visible signs, with the Finnegan Neonatal Abstinence Scoring System (FNASS) serving as the gold standard. Pharmacological treatments, often involving morphine administration, contribute to extended hospital stays for affected infants. However, challenges in obtaining biological samples from infants impede efficient NAS diagnosis.

This paper introduces a groundbreaking approach utilizing a device with cylindrical electrodes for opioid extraction from 3.2 mm diameter Dried Blood Spot (DBS) samples in a fully automated workflow. The study involves method development using Liquid Chromatography Tandem Mass Spectrometry (LC-MS/MS) for opioid quantification in whole blood. The research highlights the potential of DBS microsamples as a quantitative diagnostic material for the rapid and efficient detection of NAS in infants. This innovative approach offers a promising avenue for enhancing diagnostic accuracy and expediting turnaround times, addressing current limitations in NAS diagnosis and contributing valuable insights to maternal and infant healthcare.

7.2.Introduction

Maternal and infant health are often impacted by lifestyle choices and socioeconomic influences. This includes the exercise of unhealthy behavior such as smoking, or use of illicit drugs, including opioids. According to the Centers for Disease Control and Prevention (CDC), 1-in-5 pregnant woman reported the misuse of opioids [180, 184]. And this is just the self-reported number. According to the World Health Organization (WHO), the environmental cues, financial need, and lack of education usually trigger the need for engaging in opioid misuse [182]. In utero exposure to illicit drugs, especially opioids, lead to a condition called Neonatal Abstinence Syndrome

(NAS), where neonates showcase a spectrum of clinical manifestations as a result of withdrawal from the drugs. Reports from the Healthcare Cost and Utilization Project (HCUP) states that approximately one baby is diagnosed with NAS every 24 minutes in the United States, and cases of NAS increases are reported nearly in all states and demographic groups [183]. The signs and symptoms of NAS in newborns include tremors, seizures, vomiting, jaundice, and in extreme cases, sudden infant death syndrome (SIDS), and these signs vary greatly depending on the extent of which a single or multiple substances were abused [185,188]. A 2023 work by Anbalagan and Mendez highlighted how the NAS clinical diagnosis is strictly based on visible signs and relies heavily on material history (if available) [186]. The current gold standard of NAS diagnosis is the Finnegan Neonatal Abstinence Scoring System (FNASS), where scoring an eight out of 21 clinical signs in the system will cause an actual treatment regimen to begin [186,187,192]. A typical pharmacological treatment of NAS includes dosing an infant with maximum 0.2 mg/kg dose of morphine, every three to four hours, which often leads to prolonged hospital stays. The main reason behind a score-based screening and pharmacotherapy without performing any biological testing is the access to patient samples. Obtaining samples from an infant is challenging, especially in the case of NAS where blood or serum would be the most accurate diagnostic source material [185,190]. Even though heel pricks are collected on dried blood spot (DBS) cards, they are mainly used for tier-1 diagnostic tests by the government for conditions such as phenylketonuria (PKU), sickle cell disease, or spinal muscle atrophy. Therefore, even though samples are collected within the window for which quantitative NAS screening is possible, there is still a limit on the volume and availability of the DBS spots that can be used [189]. Even if a DBS is available for quantitative screening of NAS, the turnaround time for the diagnosis is typically five to seven days due to sample processing and analysis. One of the greatest challenges of working with DBS is analyte

recovery even for highly specific and sensitive liquid chromatography tandem mass spectrometry (LC-MS/MS) tier-2 diagnostic assays [190,193,194]. Herein, we have demonstrated the application of a novel device utilizing cylindrical electrodes for opioid extraction using 3.2 mm diameter DBS spots in a fully automated workflow. This study highlights the method development on LC-MS/MS for five opioid quantification in whole blood, and the application of DBS microsamples as a quantitative diagnostic material for NAS detection in infants.

7.3. Experimental

7.3.1. Chemicals and Reagents

All of the solvents used were Baker Analyzed, LC-MS grade, and with a purity of >99% (from VWR). Such solvents include water, acetonitrile, and methanol used for the preparation of calibrators and LC-MS/MS operation. The analytes for the study were purchased from Cerilliant Corporation (Round Rock, TX, USA). The analytes used were Codeine (Cod C-006), Hydrocodone (Hd_Cod H-003), Methadone (Meth M-007), Morphine (Morph M-005), Oxycodone (Oxy O-002). The internal standards for the analytes were Codeine-D3 (C-005), Hydrocodone-D3 (H-005), Methadone-D3 (M-008), Morphine-D3 (M-003), and Oxycodone-D3 (O-005). Fisher Scientific reagent-grade formic acid (96% pure) was purchased for improved ion mobility in the mobile phases. Analyte free fresh whole blood (female donors) was obtained from Research Blood Component LLC (Watertown, MA, US) that were used in the manufacturing for calibrators and test samples. Two types of dried blood spot cards were purchased: Whatman-903 Protein Saver Cards (Cytiva, MA, US) and QIACard DMPK-C (Qiagen, MD, US).

7.3.1. LC-MS/MS Conditions and Parameters

The LC-MS/MS parameters were identical to our previous work. Briefly, the standard reference materials were diluted 1000-folds (base analyte) and 100-folds (internal standards) in methanol and injected directly into the QSight 220 mass spectrometer using a Harvard apparatus for MS

optimization. Once the mass parameters were optimized, the electrospray ionization (ESI) positive source parameters were optimized. Finally, ~5 mL whole blood was spiked to 500 ng/mL opioid concentration, extracted and injected into LC using the previously optimized method to establish the matrix-specific Retention Time (RT).

7.3.3. Device Prototyping

Sterile Axygen 96-well clear v-bottom 500 μL polypropylene plates were purchased from Corning (NY, US) and 0.104" diameter holes were created on four corners of the plate to tighten and place 6-32x5/16 flathead screws (McMaster #91771A145). At the bottom of the axygen plate, a copper PCB FR4 0.62, 3.20x4.9" (trimmed to fit the plate) was placed, and the screws were tightened through both using 6-32 nuts (McMaster #90730A007) (holes drilled at 0.14"). This was done for all 96-wells, and the screws served as the bottom electrode of the apparatus. For the top electrode, 96 holes were drilled on a copper PCB FR4 0.62, 3.20x4.9" to fit stainless steel press fit PEM spacers (McMaster #SOS63212-18-8). The mechanical connection between the PEM spacers and the PCB established the electrical connection, thereby making the cylindrical PEM spacers serve as the top electrodes. Once all 96-wells were populated with top and bottom electrodes, electrical wires soldered on both sides of the top and bottom PCBs and insulated with 4" wide tape. After complete assembly, the parts were thoroughly cleaned with HPLC methanol and UV-sterilized overnight prior to use. The bottom electrode assembly drawing can be seen on supplemental figure 1.

Low-cost Chip Fabrication: An additional investigation we undertook was looking at alternative methods for analyte whole blood recovery in a cost-effective platform. To do this, a microfluidic chip model was first developed on COMSOL Multiphysics, that was then laser cut (Universal

Laser Systems) on to 1/8th thick Acrylic plexiglass plastic (NIUBEE) to 10-cm chip sizes with bases, and glued together by acrylic-on-acrylic adhesive.

7.3.4. Calibrators Preparation

A seven-point calibrator set was manufactured using the blank whole blood in a 2-step dilution process, covering a range of 1 to 1000 ng/mL concentration. Caution was observed when adding the spiking solution (reference material stock solution dilutions) keeping the blood constantly stirring at body temperature (37 °C) at 200 rpm. Similarly, a batch of 'treatment' blood was made that was used to spot the DBS cards. They were then rocked overnight at 4 °C before being aliquoted into smaller batches and stored at -80 °C. These aliquots were only brought to room temperature once for each experiment.

7.3.5. DBS Preparation

Using the 'treatment' blood made, both Whatman-903 and DMPK-C cards were spotted inside a biosafety cabinet. 50 µL blood was added to each spot (5 spots for Whatman-903 cards and 4 spots for DMPK-C cards), and the cards were allowed to dry overnight at room temperature prior to using. The oldest spots used at any point of the study were only 72-hours old. Anything older than that was discarded, and a fresh batch was prepared. This was done because it is the window between sample collection and NAS symptoms appearance in an infant. For an actual clinical case, the oldest DBS that would be used for this application would be 72-hours old. Once the spots were dried, they were sub-punched using an automatic DBS puncher (Revvity Inc., MA, US) with a 3.2 mm punch head. Each spot was sub-punched 4-times (supplemental figure 2), and a single spot was then used for analysis. This meant that samples from the same spot, same card, and same batch could be used for preparation method testing simultaneously, eliminating batch-to-batch and card-to-card variation. The spots were directly punched into the standard Axygen plates for testing using

the automated puncher, however, the E-DBS apparatus had to be used without the top-electrode since the DBS puncher could only punch into standard plates. The top-electrode was replaced once the wells were populated with DBS prior to the experiments.

7.3.6. Sample Preparation

Just like our previous study, a two-step extraction method was developed for the calibrators, where 80 µL of Daily Working Solution- 1 (DWS-1) prepared with 50:50 v/v methanol: acetonitrile with 0.1% formic acid and 2.5 ng/mL of internal standard was added to 50 µL of whole blood in v-bottom Axygen plates. After mixing at 45 °C for 5-minutes at 700 rpm, the plate was then centrifuged at 0 °C for 20-minutes prior to extracting 50 µL of clear supernatant. To the supernatant, 167 µL of Daily Working Solution- 2 (DWS-2) made of HPLC water and 1% formic acid was added, and plate was shaken at 400 rpm at 25 °C for 1-minute before LC-MS/MS analysis.

For *regular DBS* sample preparation, 80 µL DWS-1 and 167 µL of DWS-2 were simultaneously added to each DBS spot and shaken at 45 °C for 10-minutes at 700 rpm. The plate was then centrifuged at 25 °C for 20-minutes, prior to collecting the supernatant LC-MS/MS analysis.

For the *sonic DBS* sample preparation, spots were placed inside 2 mm microfuge tubes with 80 µL DWS-1 and 167 µL of DWS-2, and pulse vortexed for 30-seconds. The tubes were then sonicated at 25 °C for 10 minutes. The supernatant was then analyzed.

For the *E-DBS* sample preparation, 80 µL DWS-1 and 167 µL of DWS-2 were added to the spots placed inside the device, and an electric field was applied for 3-minutes (negative electrode on top), prior to collecting the supernatant for analysis.

The sample preparation workflows are shown in Figure 25.

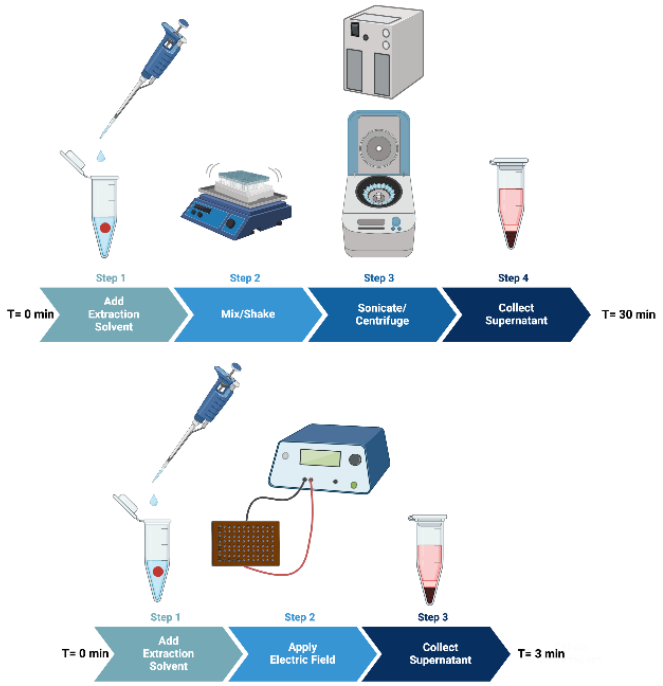

Figure 25. Sample preparation workflow for DBS (top: regular, bottom: E-DBS)

7.3.7. Automation

The entire workflow for whole blood calibrators, regular DBS treatment and E-DBS were all automated using the JANUS® G3 Workstation (PerkinElmer Corp., MA, U.S.), with the software JANUS® Application Assistant and WinPREP® for JANUS®. Because whole blood is a much more viscous fluid than serum or water, with the tendency to drip, the calibrators had to be plated using a single-dispense blowout mode, making the calibrators plating process longer than working with other less-viscous fluids (liquid handler optimized parameters for this protocol is available on Supplemental Table 1). The whole blood and regular DBS workflows both had human interventions programmed, together with off-deck steps.

For E-DBS apparatus, the protocol was completely automated, and all the steps took place on-deck without needing any human interventions. However, prior to using the device on-deck, a new labware definition had to be created to account for the dimensional changes of a standard v-bottom Axygen plate. This included updating the well bottom height to account for the bottom electrode,

and redefining the plate edges, and well diameters. It is important to note that the JANUS® tips used were all electrically conductive, and therefore, the well bottom was purposefully defined to be slightly higher than the actual top of the bottom electrode. The dispense height was also modified such that the tips would dispense at the center of the top electrodes without crashing, or dispensing in the air and missing the wells entirely. The plate definition and schematic on the JANUS® is shown in supplemental.

7.3.8. Computational Modeling and Data Analysis

Computational modeling of the electric-field application was performed using three-dimensional time-dependent electric current (EC) on COMSOL Multiphysics version 6.1. Device prototypes were sketched and visualized using SolidWorks. LC-MS/MS data was generated and preliminary analyzed on Simplicity 3Q (for QSight 220) and exported to Microsoft Excel for further analysis. All statistical analysis was performed using JPM Pro 17 (t-test, ANOVA, Dunnett's post-hoc test and Tukey-Kramer HSD test). A p-value of 0.05 or less was considered statistically significant. Graphpad Prism 9 was strictly used to generate illustrations based on all the statistical analysis performed on JMP Pro.

7.4.Results and Discussion

7.4.1. LC-MS/MS Method Validation

Since no quantitative data was available in literature regarding the concentration of opioids in infants suffering from NAS, the linearity series was designed to cover a wide range of concentrations. Hence, calibrator L1 for all the analytes was set to be 1 ng/mL whereas L7 was set to be 1000 ng/mL (theoretical). Even though we have previously studied the same group of opioids in serum, blood is more complicated as a matrix, and was likely to cause greater ion suppression. Similar to our previous work, the Matrix Effect (ME) was evaluated. In whole blood, all 5 opioids exhibited a recovery of 57.3% to 65.8% with our working volume of 50 µL whole blood. Figure

26 shows the absolute intensity profile overlay of the analytes in whole blood for calibrator L5. This is certainly lower than the absolute intensity profiles obtained for lower calibrators in serum. But the observation aligns with previously reported work in the literature [195-198], and therefore the sample preparation method for the calibrators was finalized and used for the rest of the study.

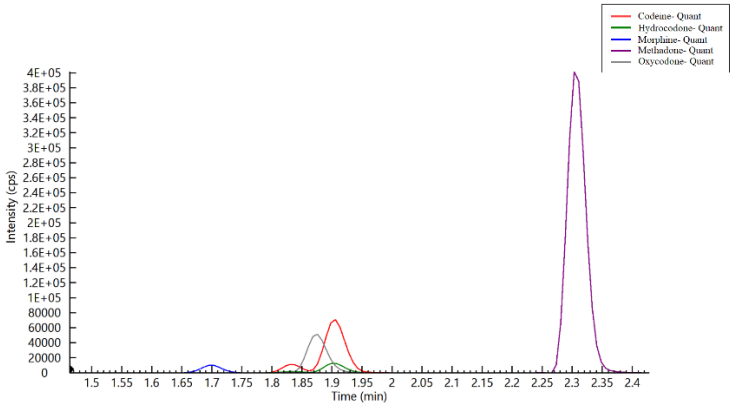

Figure 26. Absolute intensity profile (overlay) of the five opioid quantifiers in whole blood, showing the analyte elution on their respective retention times.

Selecting the internal standard concentration to be higher (2.5 ng/mL) than the lowest level of calibrator (L1= 1 ng/mL) posed the question of false positive for a tier-2 diagnostic application, and therefore, blank whole blood (L0) was run each time to ensure there was no false signal due to the internal standard. Figure 27 shows L0 and L1 for methadone against their internal standards. The E-DBS protocol was initially tested for 1 ng/mL concentration of internal standard but because the internal standards remained in a potent fluid form during the electric-field application, there was possible analyte degradation. Hence, a slightly higher concentration of internal standard was tested and chosen moving forward. After manufacturing each set of calibrators, they were run in sextuplets to determine the actual concentration, based on which they were re-used for the rest of the study.

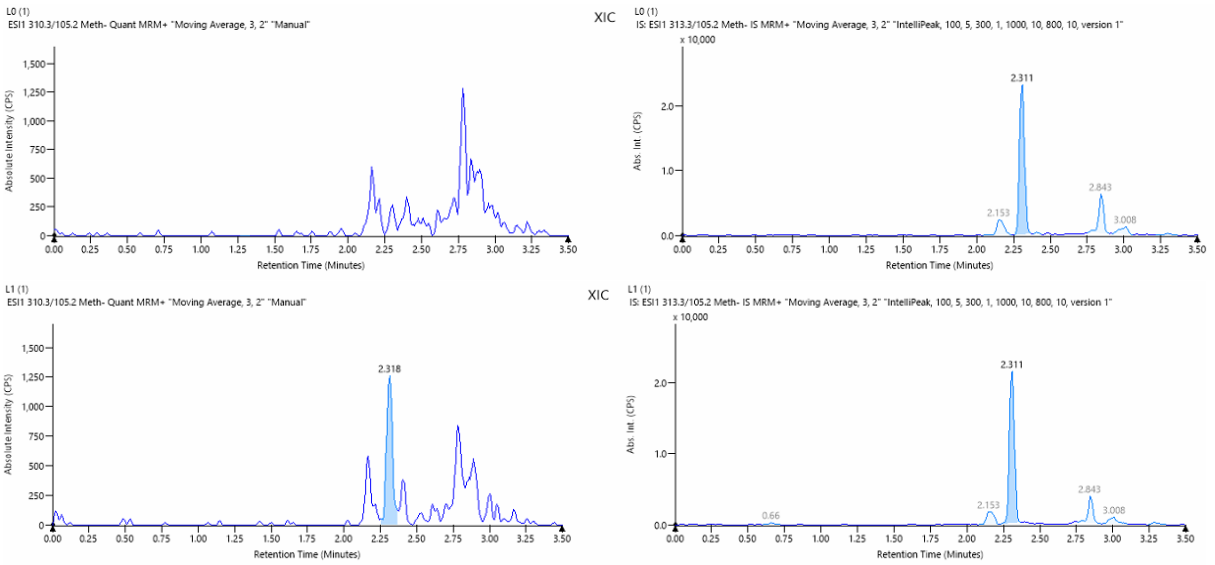

Figure 27. (a) Blank whole blood (left) with internal standard (right) for methadone; (b) calibrator L1 (left) with internal standard (right) for methadone.

Carryover was assessed by injecting triplicates of L1 right after injecting L7. For all 5 opioids, inclusive of both MRMs, there was no significant carryover observed. Linearity was assessed by looking at the R-square value of all the analyte MRMs, which were reported to be 0.9 or higher. Precision and accuracy were assessed similar to our previous studies, where %CV ±≤ 25% was considered good assay precision, and analyte accuracy (reported from the software) had to be between (80±20) % for good accuracy. The assay precision, linearity and accuracy were performed after the measured concentrations were established. Table 14 (a-e) lists all the mean concentration with standard deviation, %CV and %accuracy for all the analyte quantifiers (n=18 per calibrator, tested over 6-runs).

Table 14. (a-e) Data from whole blood calibrators for analyte quantifier from the iteration used for the DBS method validation study (over the course of the study, three total iterations of the calibrators were prepared for testing).

a) Codeine

Calibrator Level	$\mu_{\underline{x}} \pm \sigma$ *(ng/mL)*	*%CV*	*% Accuracy*
L1	0.99 ± 0.08	*8.76*	*79*
L2	7.89 ± 1.4	*18.9*	*74*
L3	23.2 ± 1.8	*8.1*	*107*
L4	288.5 ± 54.5	*18.9*	*90.7*
L5	539.3 ± 63.5	*22.0*	*85.5*
L6	*975.8* ± 111	*20.6*	*80.5*

L7	*1105.6* ± 201	*20.6*	*91.9*

b) Hydrocodone

Calibrator Level	$\underline{\mu_x} \pm \sigma$ *(ng/mL)*	*%CV*	*% Accuracy*
L1	0.73 ± 0.1	*15.7*	*69.3*
L2	7.25 ± 1.9	*26.1*	*95.8*
L3	32.2 ± 6.2	*19.3*	*89.1*
L4	331.7 ± 49.4	*14.9*	*95.4*
L5	459.6 ± 70.1	*15.4*	*85.6*
L6	*805.1* ± 108	*23.6*	*93.6*
L7	*1248.5* ± 90	*11.3*	*102.8*

c) Morphine

Calibrator Level	$\underline{\mu_x} \pm \sigma$ *(ng/mL)*	*%CV*	*% Accuracy*
L1	0.71 ± 0.1	*16.9*	*83.5*
L2	11.23 ± 1.7	*15.4*	*82.4*
L3	33.8 ± 7.6	*22.7*	*94.4*
L4	390.2 ± 65	*16.9*	*87.5*
L5	667.6 ± 89	*20.6*	*101.4*
L6	*908.6* ± 96	*14.5*	*86.1*
L7	*1119.9* ± 208	*22.9*	*98.0*

d) Methadone

Calibrator Level	$\underline{\mu_x} \pm \sigma$ *(ng/mL)*	*%CV*	*% Accuracy*
L1	1.05 ± 0.09	*8.6*	105
L2	9.60 ± 1.04	*10.8*	96.0
L3	29.3 ± 2.5	*8.5*	97.5
L4	324.8 ± 44.2	*13.6*	108.3
L5	579.0 ± 80	*18.4*	97.1
L6	*756.5* ± 100	*17.4*	96.5
L7	*11103.7* ± 60	*7.91*	89.0

e) Oxycodone

Calibrator Level	$\underline{\mu_x} \pm \sigma$ *(ng/mL)*	*%CV*	*% Accuracy*
L1	0.73 ± 0.1	*18.9*	*93.7*
L2	6.70 ± 1.5	*22.3*	*95.1*
L3	27.9 ± 4.4	*15.9*	*82.6*
L4	322.8 ± 55	*17.3*	*87.4*
L5	609.1 ± 26.9	*4.41*	*89.9*
L6	*745.6* ± 117	*19.3*	*103.0*
L7	1000 ± 92	*12.4*	*99.7*

7.4.2. An Alternative for Whole Blood Sample Preparation

Although evaluating microsampling with DBS was invaluable for this study, the cost of constituent cards for this medium is prohibitive for most limited access facilities. This obstacle is

exacerbated by the cumbersome laws and regulations surrounding the use of DBS samples. As a result, we also developed a gravity-assisted low-cost sample preparation microfluidic chip for whole blood sample preparation. As previously mentioned, obtaining true parental history for NAS is challenging. Hence, an additional solution that can provide us with an insight into the parental opioid abuse history would be a low-cost, single-use chip ($10 a piece Capitainer qDBS cards against $1.50 per chip). These chips function using capillary flow action assisted by gravity at limited access facilities (i.e. areas where sophisticated laboratory equipment are inaccessible). Once the extraction solvent has been added to its respective reservoir, the analyte in question can be separated from ~50 μL of maternal blood and the pale-brown supernatant can be subsequently sent out for analysis.

The fundamental basis of this chip was established via time-dependent laminar flow finite element analysis of the chip design, where whole blood was modeled as a custom material (ρ= 1060 kg/m^3, and μ= 0.03 Pa.s) and the extraction solvent was modeled as ethanol (built-in material). This is shown in Supplemental Figure 4. Through capillary flow action and gravity assistance (the chip is to be operated at a 45° angle), the analytes were mixed and subsequently flowed from the sample reservoirs to the collection channel in about 2.5 minutes. For method validation of these chips, we tested a vial of blood spiked with methadone head-to-head against the 30-minutes regular preparation protocol. We evaluated a total of 16 single-use chips, and the differences in analyte recovery from the chip versus a standard whole blood preparation failed to reach statistical significance (p-value= 0.698). Figure 28 shows methadone quantifier recovery for off-chip versus on-chip protocol with the data spread. Although the results of this study were novel and certainly informative, additional replicates (n= 64) are required to establish the robustness of these findings.

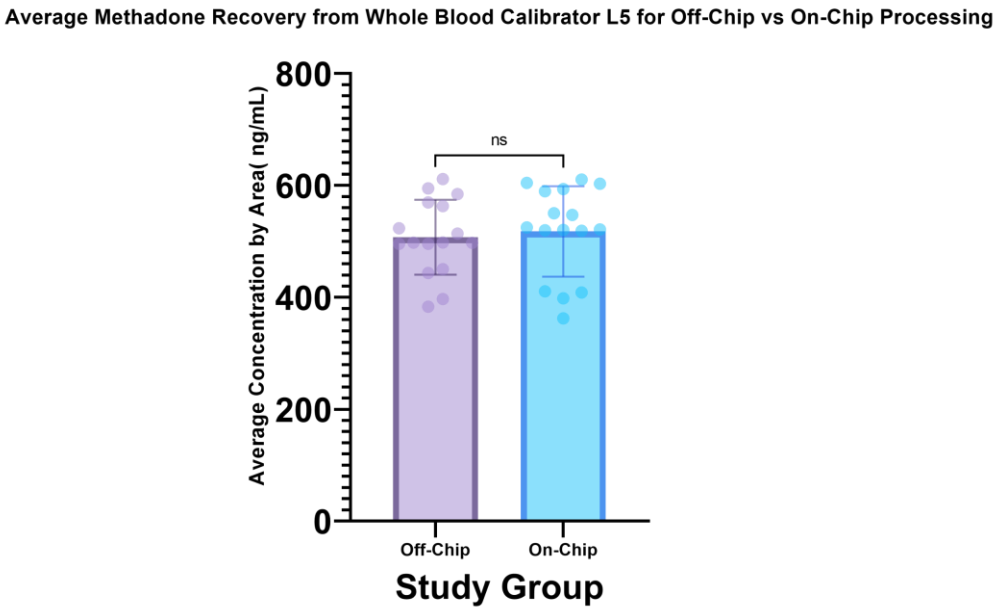

Figure 28. L5 analyte recovery for methadone quantifier (n= 16).

7.4.3. Electric-Field Apparatus for DBS

We had previously developed a time-dependent study model on COMSOL Multiphysics for vertical electric field across a dried blood spot, however, the previous model was a closed system with a solid top electrode. The high throughput E-DBS apparatus utilizes hollow cylindrical spacers, wherein, there is air in the middle of the electrode itself, with the potential for loss of electric field. Even though the governing equation is still the vector form of the microscopic total current density, J (eq. 1), the material type for this specific model was nonsolid to account for the hollow interior of the top electrode.

$$J = \sigma E + \frac{\partial D}{\partial t} + J_e \text{ (eq. 1)}$$

where, σ is the electrical conductivity (from each material), E is the electric field, $\frac{\partial D}{\partial t}$ refers to the displacement current density (time-varying component), and J_e represents the free current density. The material selection domains are available in Supplemental Figure 4. Briefly, the electrodes were assigned the built-in Steel AISI 4340, while the surrounding was assigned deionized water at 20 °C with specified electrical conductivity and relative permittivity (σ= 5.5e-6 S/m, ϵ_r= 80).

The DBS was assigned the built-in material silicon. Our model consisted of the initial condition of V_0= 0 V, and the electric potential, V= 30 V. For elevated accuracy, the mesh used for the model was ‘extremely fine’.

Figure 29 (a) shows the electric potential of the entire system at time, T= 1 min. This shows that despite the hollow core, the electric potential of the entire system becomes uniform within the first minute of the electric field application, and it stays that way for the rest of the exposure time. On the other hand, Figure 29 (b) shows only the DBS in solution at T= 1 min. This was a separate model to independently inspect the behavior of the DBS in a solution when it is sitting on the electrode (i.e., a two-material system). This shows that even though the field lines become sporadic as time passes, the field lines through the DBS are rather uniform. This is further demonstrated in Figure 29(c), where the red arrows represent current density. This magnified image of the DBS in the complete system (3-material system) shows that even at T= 3 min, the current density is much larger within the DBS, as opposed to the surrounding, drawing more analytes out of the spot faster.

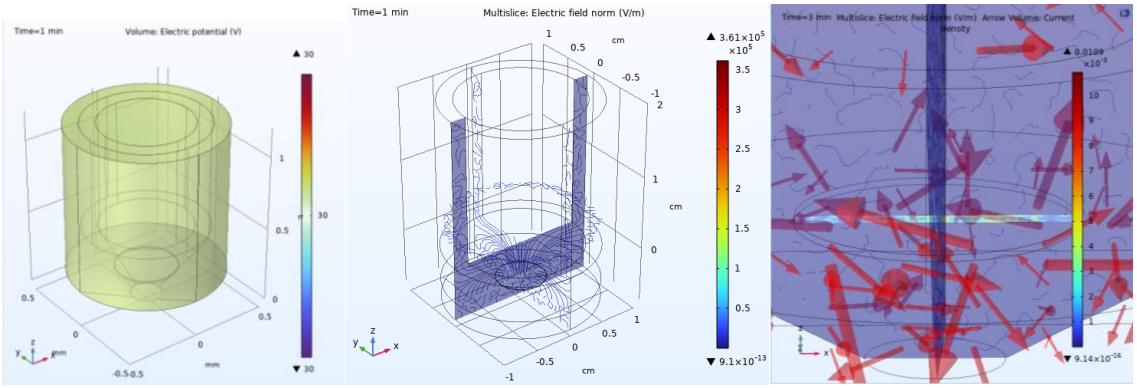

Figure 29 (a) Electric potential across the electrodes (modeled for a single well), extraction solution and DBS at T= 1 minute; (b) an isometric view of the electric field across DBS in fluid; (c) magnified x-z slice of the current density across the DBS at T= 3min.

These computational models and results laid the foundation of the E-DBS device prototype. It is important to note that the computational model used the electrode height for shorter PEM spacers, whereas the actual prototype used slightly longer PEM spacers.

7.4.4. Device Iterations

One of the initial prototypes of the device used PEM spacers shorter than the final device (final spacers were $\frac{3}{8}^{\text{th}}$ of an inch). The idea was to use it for both whole blood calibrators as well as the DBS. However, the reusability issue of the device was an important consideration since the PEM spacers for the prototype had to be deburred manually to prevent DWS flow creeping up the top electrode. A key feature of this device is that it can be placed on a robotic liquid handler platform, and the circuit is not completed until there is fluid in the well in contact with both the top and the bottom electrode. Working with DBS for metabolomics application is challenging because the theoretical starting volume to work with is the diameter of the DBS spot that gets diluted in the extraction solvents (in this case, DWS- 1 and 2). Shorter spacers would require a larger volume of extraction solvent to be used, thereby diluting the analytes further. As a result, the overall signal from the extracted sample would have been lower, making it difficult to quantify above the baseline. Hence, instead of increasing the extraction solvent volume, longer spacers were utilized.

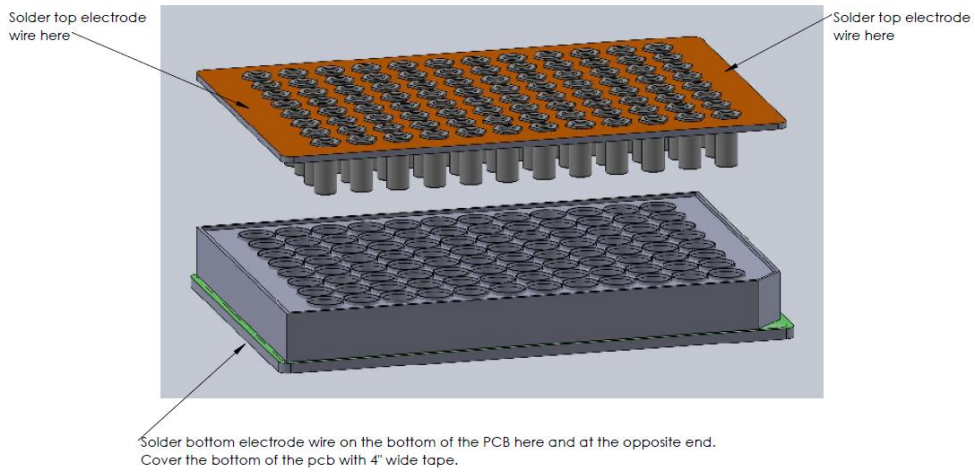

Figure 30. Complete E-DBS device assembly by parts, showing top and bottom electrodes.

Another challenge was the diminishing electric field effect. An earlier prototype used single electric wire for both top and bottom electrodes (Supplemental Figure 5). This was noticed when spots in wells closer to the wire reported readouts ~1000 ng/mL higher than those further away.

This was resolved in the final version by soldering two electrical wires on both top and bottom electrodes. Figure 30 shows the device design in its entirety, indicating the locations of electrical wire placement.

For preliminary testing, single rows of the top electrode populated with PEM spacers, and they did not impact the shape of the PCB copper. However, once all the 96 spots were populated, the top electrode exhibited significant warping on the shorter edges. This warping was significant and impacted the uniformity of the electric field across the place. To mitigate this, metal pieces with threaded holes were place in the four corners wells, with fastener screw tops. This left the final device with 92 functional wells instead of 96 but the warping for the metal no longer impacted the electric field distribution or the functionality of the device in its entirety. For the purpose of this study, we fashioned three identical devices that were re-used after alternating water- methanol-water rinses post-experiment. For the large-scale applicability of this device, the manufacturing method needs to be modified to be less labor intensive, lowering the overall cost per device, and turning them into single-use consumables.

7.4.5. Dried Blood Spot Protocol Optimization

While a computational model and a testable prototype serve as a good starting point for method testing, the E-DBS protocol had to be optimized for opioids. The behavior of opioids in an electric field has not been studied for the context of metabolomics diagnostics. As a result, optimization of the E-DBS protocol had to be performed prior to conducting high throughput testing using the JANUS. The DBS spots were tested against a regular 30-minutes recovery protocol for against several electrical conditions of 3-minutes exposure time. Over nine different test runs (n=36 spots per run per condition) with multiple batches of spotted DBS, 30 V direct current (DC) for 3-minutes outperformed all other conditions (differentiated by connected letter report on Tukey-

Kramer HSD analysis). These conditions included 30 V alternating current (AC) of frequencies 0.56 Hz to 5.6 Hz, and 20 V AC at 0.56 Hz and 5.6 Hz. Supplemental Figure 6 showcases the normalized concentration by area of the DBS for different electrical conditions (normalized to regular no electrical processing) for the 5-opioids, inclusive of both MRMs in Whatman-903 cards. The error bars for the study groups are larger because all the data of the spots were pooled and grouped together by condition. This includes the different batches of the spiked blood made (same protocol and volumes, but different days), as well as different manufacturing lots of the DBS cards used.

Studies have often regarded DMPK-C cards superior to Whatman 903 cards for bioanalysis because in theory, they are not processed with chemicals that would interfere with the analysis report. However, the Whatman 903 cards are the most widely used and accepted cards for newborn sample collection. As a result, we investigated both card types for opioid analyte recovery with both non-electrical and electrical workflows. Figure 31 (a) shows the difference in analyte recovery for the quantifiers using a regular 30-minutes procedure, while 31 (b) shows the data for E-DBS processing (n= 72; 12 spots per card type for 6-repeated study). The Whatman 903 cards consistently performed significantly better than DMPK-C cards. This proves to be advantageous, because had DMPK-C cards performed better, this would have raised the ethical question of double sampling an infant specifically for NAS applications. The superior performance of Whatman 903 cards means that any 3.2 mm sub-punched spot from an already collected sample for newborn screening can be used for opioid quantification.

Additionally, we repeated the same study for the same number of samples using regular filter paper 31 (c). While the scope of the material used to create the sample collection cards is beyond the scope of this study, it was important for us to establish that the electrical processing

theory was valid, irrespective of the additives or manufacturing practices of the DBS cards. The spiked whole blood used to spot these cards were much higher in concentration than the one used to test Whatman 903 and DMPK-C cards, since there was no available documentation on the behavior of the opioids on regular filter papers (especially the molecular binding of the analytes to the polymer network in the card). The regular filter paper spots were much thinner and discolored much faster than the Whatman 903 or DMPK-C cards. At the end of the electrical processing, the residual filter paper spots were ivory, while the spots had disintegrated by the end of the 30-minute regular processing. The regular processed filter paper spots had to be centrifuged prior to supernatant collection to prevent any paper particulates from clogging the LC-MS/MS.

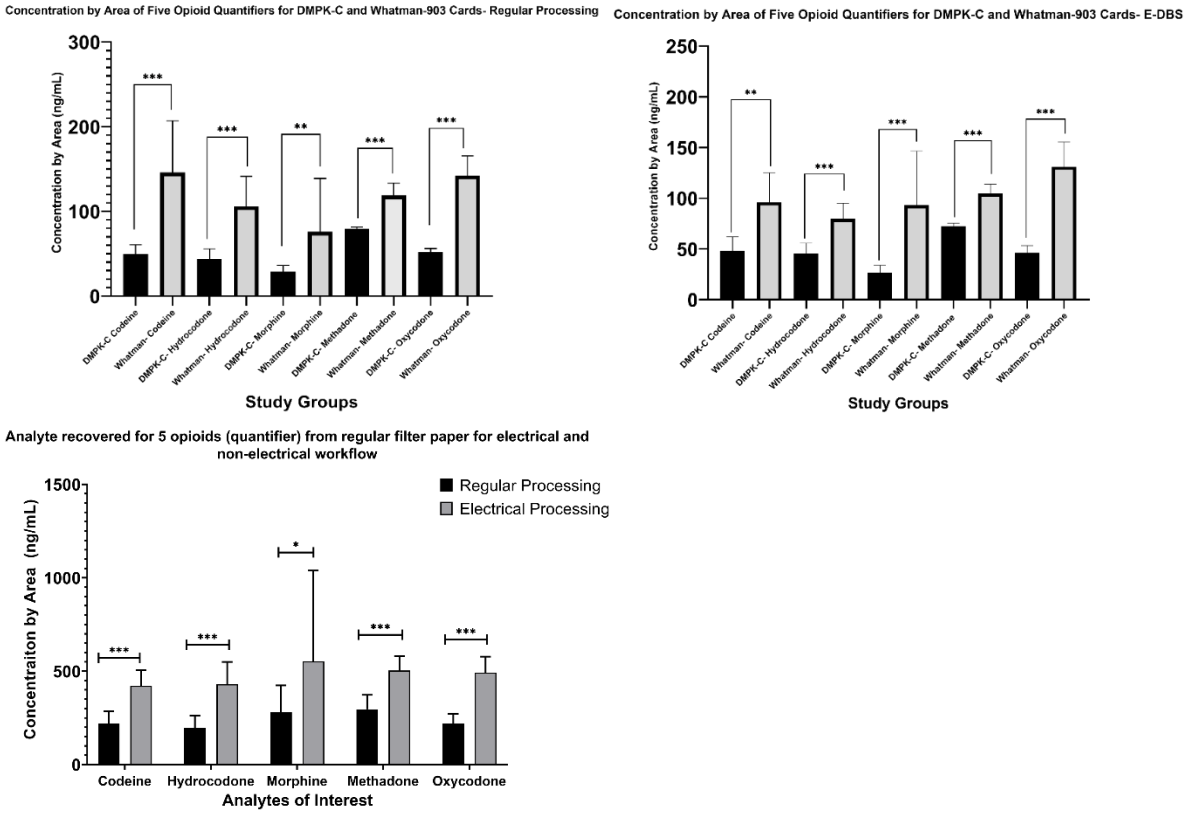

*Figure 31 (a) Average analyte (quantifier) recovery for DMPK-C and Whatman 903 DBS cards for non-electrical 30-minutes processing workflow and (b) E-DBS processing workflow (n= 72; 12 spots per card type for 6-repeated study); (c) regular vs. electrical processing of regular filter paper sports (n= 63 spots, for 3-repeated runs) (error bars represent standard deviation, statistical significance is indicated by: *= p< 0.05, **= p< 0.01, and ***= p<< 0.01).*

7.4.6. Total Laboratory Automation

One of the key features of this innovation is its ability to perform in a fully automated workflow without the need for off-deck procedure or human interventions. Most DBS studies regard sonication as the gold standard for complete analyte recovery. However, sonicating the samples hinders the high throughput ability of a protocol, especially one that would require a quick turnaround time. To assess the performance our device in a clinical laboratory, we not only automated the E-DBS method, but we also automated the calibrator preparation steps (every experiment would require running the calibrators for accurate measurements of the analytes in DBS). We also tested the regular DBS processing workflow using the JANUS to get a head-to-head measurement on the time taken to perform the assay and the subsequent analysis. For the sonication method, the spots had to be individually placed in microfuge tubes, adding to the time taken per sample, and the entire process had to be manually performed. Table 15 shows the time taken for each process (12-samples). It is important to highlight that for the sonic DBS, the analyte recovered was inconsistent, with some of the samples showing close to no recovery (over 3 repeated experiments).

Sample Preparation Method	Number of Steps on deck	Time taken for on deck steps (mm:ss)	Additional Time (Off Deck)	Total Time (12 samples) (mm:ss)
Whole Blood	4	32:21	30:00	62:21
Regular DBS	3	12:36	30:00	42:36
Sonic DBS	N/A	N/A	22:68	22:68
E-DBS	2	12:36 (for plating) + 3 minutes electric treatment	N/A	15.36

Table 15. Total time taken to plate 12-samples using each of the workflow. The regular and E-DBS process have identical DWS addition steps (12:36 minutes), that have been paced to ensure no extraction solvents drip on any of the surrounding wells. Off-Deck reported time does not include plate removal, sealing, seal removing etc. steps. Total time for the sonic DBS workflow does not include capping and re-capping time.

While this may also mean that the sonication protocol may have needed optimization, its inconsistent performance against the 30-minutes regular processing was certainly alarming. Overall, the 3-minutes E-DBS processing reigned superior not only in terms of consistency and

throughput ability, but also in terms of ease of automation. Figure 32 (a) shows the average analyte concentration from all the runs of all the DBS tested for method comparison. For sonic, n= 36 (12 samples, 3-repeated runs), while n= 288 for regular processing (48 samples, 6-repeated runs), and n= 552 (92 samples, 6-repeated runs) for E-DBS processing. Figure 32 (b) shows a snapshot of DWS-1 addition to the E-DBS device.

Note that this study does not report any of the findings from the preliminary device iterations or experimental runs.

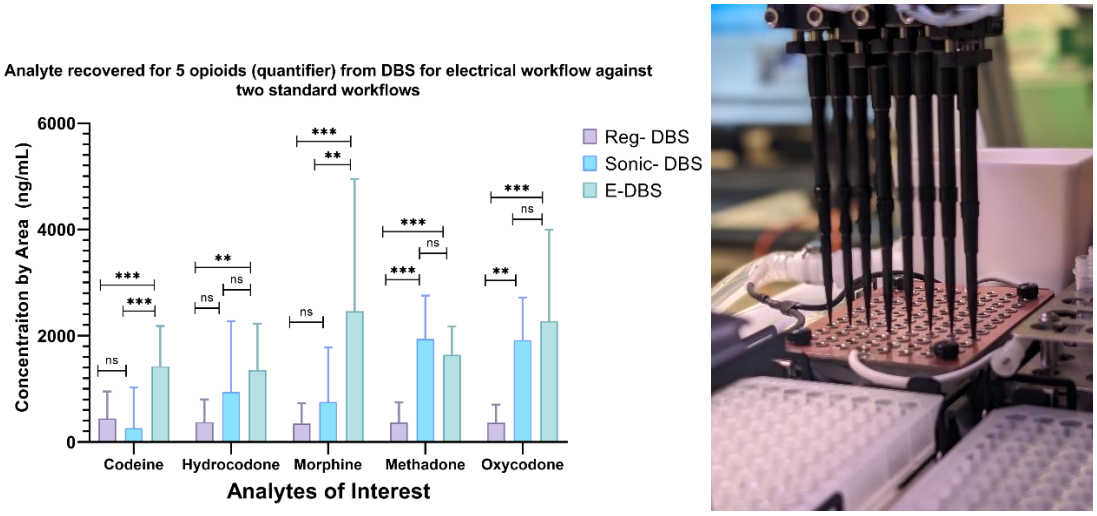

*Figure 32. (a) Average analyte (quantifier) recovery for three different workflows (error bars represent standard deviation, statistical significance is indicated by: *= p< 0.05, **= p< 0.01, and ***= p<< 0.01). Outliers (beyond 3 SD measure) were removed.*

7.5. Conclusion

In conclusion, the prevalence of opioid abuse among pregnant women in the United States underscores the urgent need for improved diagnostic methods and interventions to mitigate the impact of Neonatal Abstinence Syndrome (NAS) on newborns. Current diagnostic approaches reliant on visible signs and prolonged pharmacological treatments present challenges in effectively diagnosing and managing NAS. This paper presents a pioneering solution that utilizes an electric field as a driver for opioid extraction from DBS samples in a fully automated workflow. The utilization of DBS microsamples as a quantitative diagnostic material represents a significant advancement, potentially revolutionizing NAS diagnosis by enhancing diagnostic accuracy for

Tier-2 diagnostics, and expediting turnaround times. By addressing current limitations in NAS diagnosis, this innovative approach holds promise for significantly improving maternal and infant healthcare outcomes.

7.6.Acknowledgements

The authors would like to thank Collin Hill for his guidance in developing solutions for NBS.

7.7.Supplemental

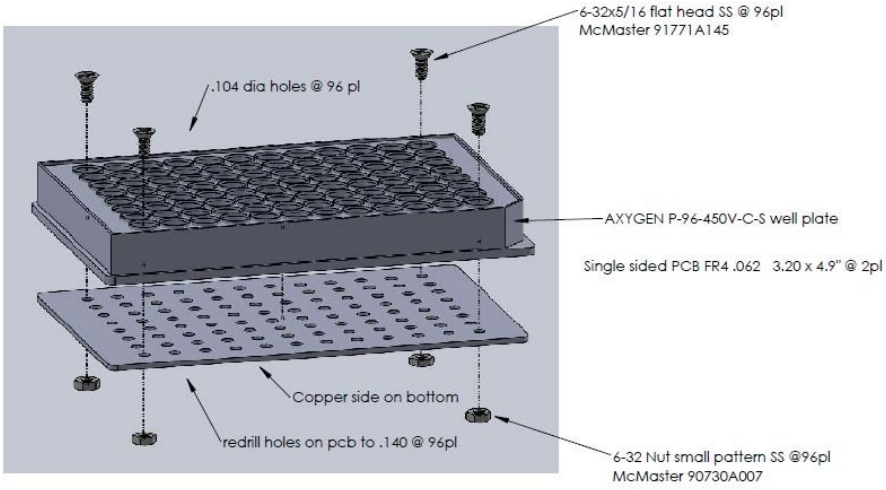

Supplemental 1 Bottom electrode assembly drawing

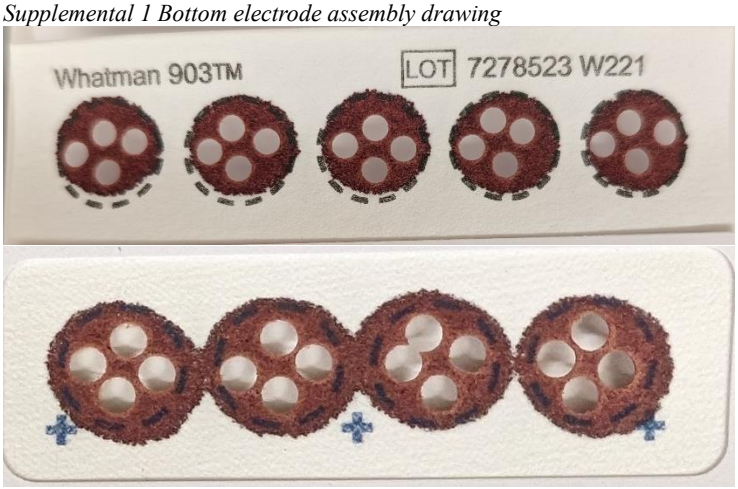

Supplemental 2(top) Whatman 903 cards after sub-punching; (bottom) DMPK-C cards after sub-punching

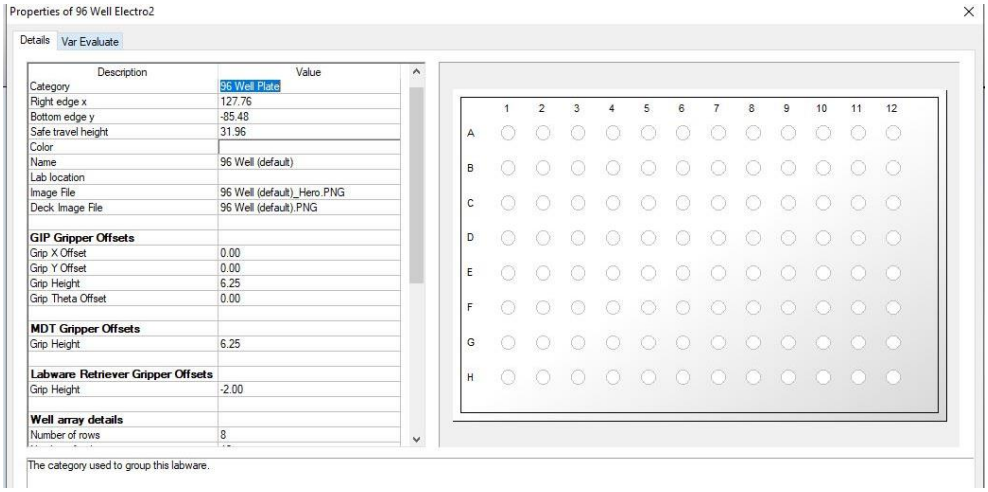

Supplemental 3 E-DBS plate labware definitions.

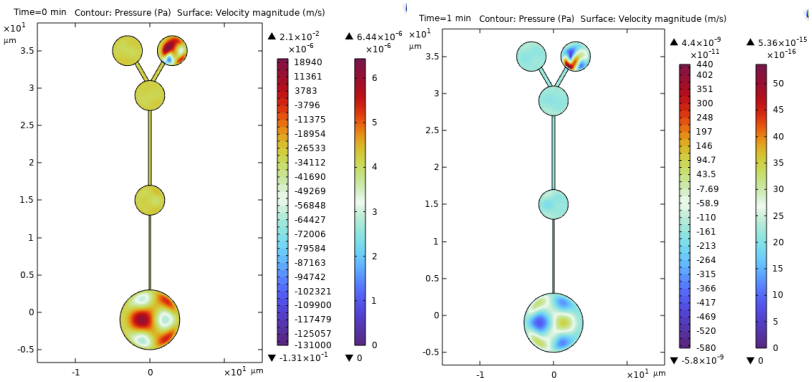

Supplemental 4. Pressure and velocity profiles of gravity-assisted microfluidic chips

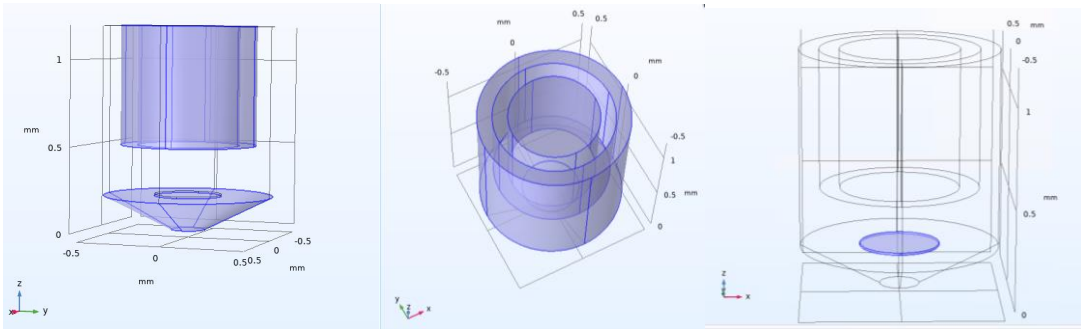

Supplemental 5. (a) Material 1 (steel) assignment for electrodes, (b) Material 2 (water) assignment for the extraction solvent, and (c) Material 3 (silicon) assignment for the DBS.

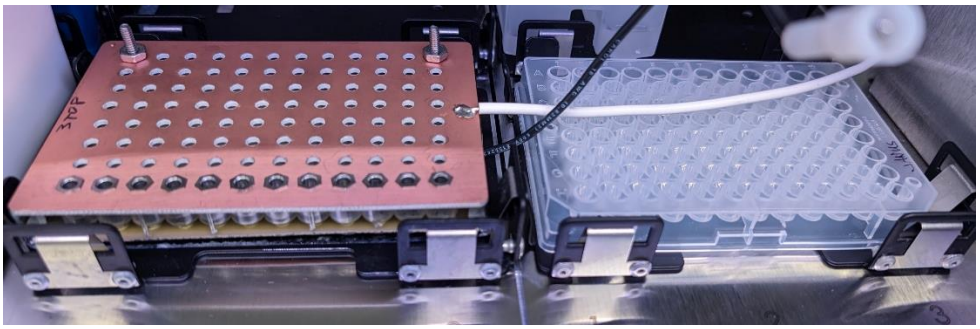

Supplemental 6 Initial device prototype (left) with single electrical wire connectivity, next to a regular Axygen 96-well plate.

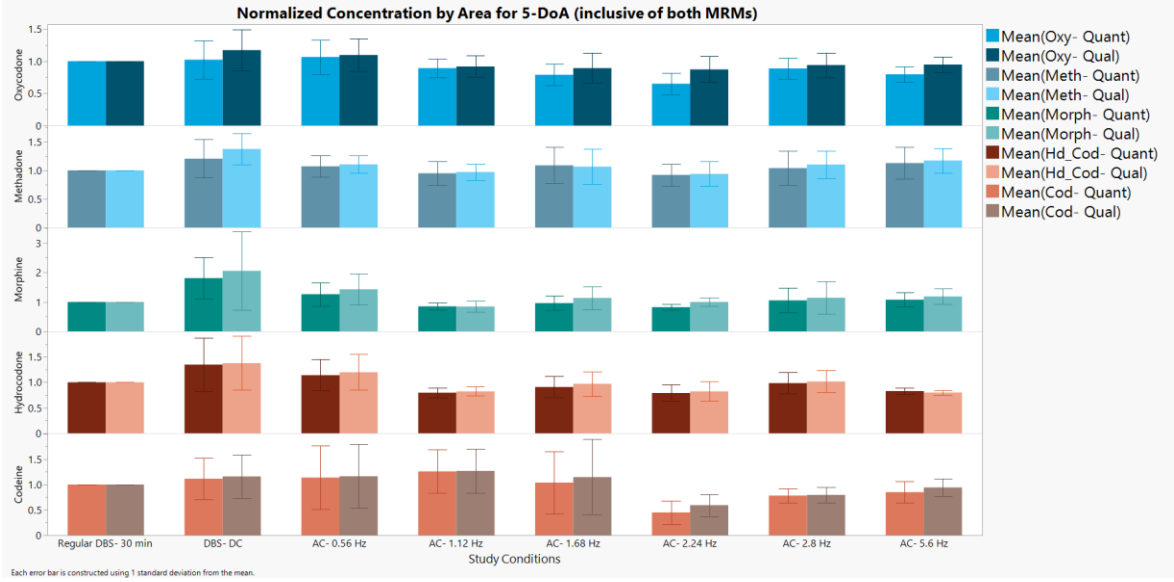

Supplemental 7. Normalized concentration by area for the analytes of interest (inclusive of both MRMs) for different electrical conditions. Significance bars are not shown.

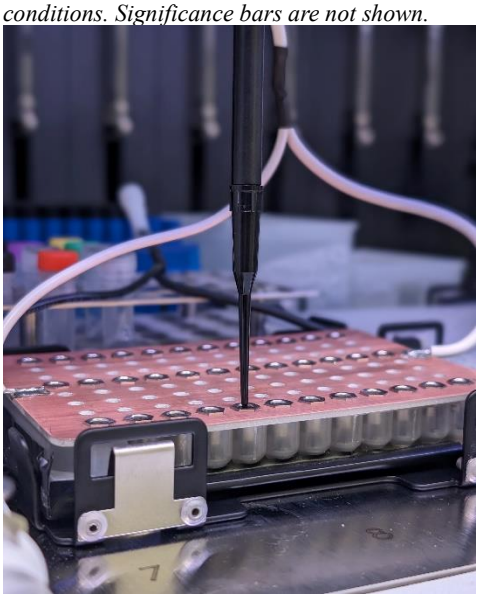

Supplemental 8. Cross section of an early device iteration showing in the middle of supernatant separation step.

Supplemental 9. JANUS deck layout for calibrators, treatment condition and calibrator whole blood plating, and E-DBS preparation used for the final study. Empty rows indicate where sonicated sample supernatant plating.

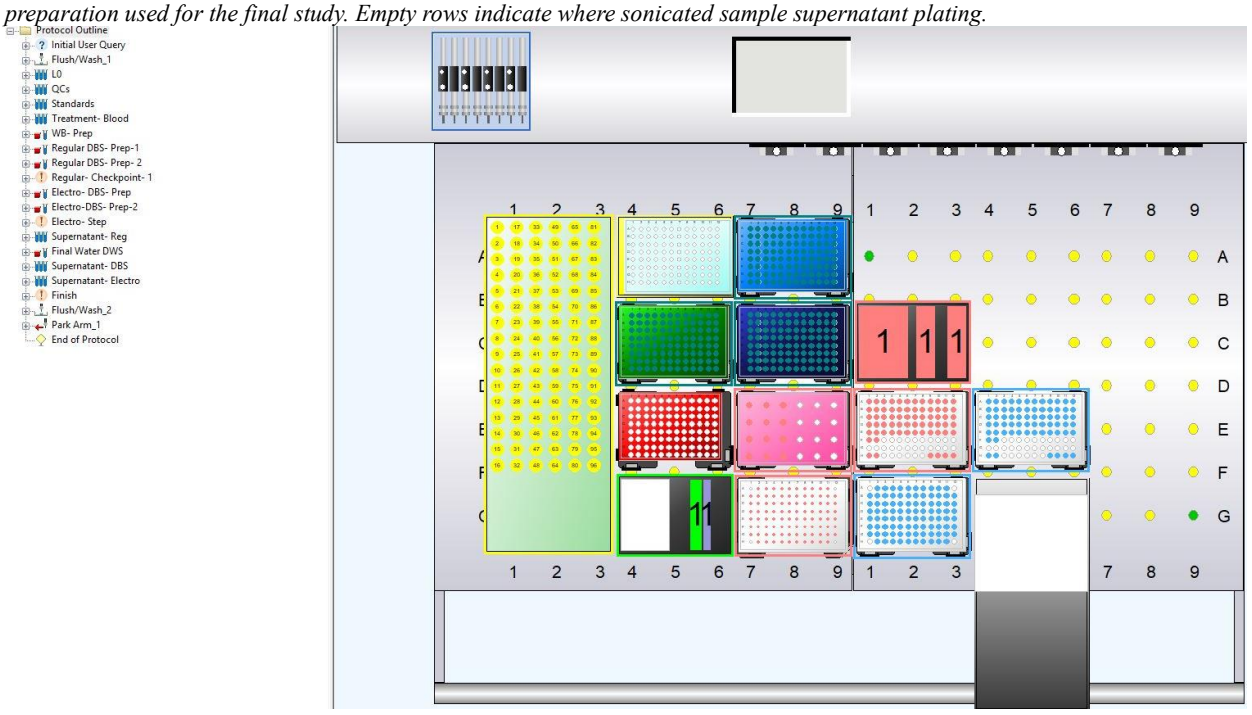

Protocol Step	Volume of Transfer (µl)	Pipette Tip Utilized (µl)	Dispenses Per Aspirate	Pipette Mode	Transfer Gap (µl)	Waste/ Blowout Volume (µl)
Whole Blood Calibrators	50	200	1	Blowout	10 (before) and 30 after aspirate	10
DWS- 1	80	200	1	Blowout	30	10
Supernatant Transfer	50	75	1	Blowout	20 (after)	5
DWS- 2	167	1000	4	Waste	10 (after)	5

Supplemental Table 1. Liquid handling parameters used for the automation of calibrators and regular DBS.

Chapter 8: An Insight into Microtissues: LC-MS/MS application for Drug Monitoring in an Organoid Microenvironment

Chapter 9 is under final review to be published as an original research article.

Fariha, R.[1], Okoh, O.D.[1], Hamze, J.[2], Rothkopf, E.[1], Tripathi, A.[1]

1. Center for Biomedical Engineering, School of Engineering, Brown University, 182 Hope Street, Providence, RI- 02912, USA
2. Department of Biology and Medicine, Brown University, Providence, RI- 02912, USA

8.1.Abstract

While 2D in vitro cell culture models have been used over the years, 3D cell culture technique is becoming increasingly popular due to its ability to replicate the in vivo tumor environment better. Out of the existing 3D cell culture techniques, Microtissues has garnered attention due to its scaffold-free nature and high-throughput ability. However, traditional cell culture assessment techniques are unable to characterize this platform due to limitations of quantifying trace amounts of absorption taking place within these molds. By optimizing the sample preparation technique (liquid-liquid extraction in tandem with protein precipitation), our strategy utilized a small volume of cell culture media to accurately quantify the drug adhesion to the Microtissues molds, with an LoD of 0.03 μM, optimized for cellular microenvironment with relevance for extrapolation to patient application. The overall assay exhibited a linearity of R-square>0.99 inclusive of both MRMs, and a percent coefficient of variation that was less than or equal to 10%. Our study expands the use of LC-MS/MS to quantify the absorption of Paclitaxel by the 3D Microtissues molds, and its subsequent impact on MCF7 breast cancer tissue viability for an in vitro to in vivo extrapolation analysis. This work has the potential for precision medicine application since the entire procedure can be catered to produce patient-specific tissues and generate reliable data to assess drug efficacy.

8.2. Introduction

Breast cancer is the second most common cause of cancer-related deaths in women, accounting for 30% of newly diagnosed female cancers annually [199]. Given its prevalence and impact, extensive research efforts have been dedicated to understanding and treating breast cancer at the cellular and molecular levels [200]. This research journey typically begins with two-dimensional cell culture studies on the laboratory bench, progressing to experiments using animal models. The tumor microenvironment, which plays a crucial role in tumor growth and

angiogenesis, has been a focus of researchers attempting to recreate its complex characteristics in a laboratory setting [203-206]. *In vitro* drug testing has historically used assays optimized for a two-dimensional platform as an initial step in the research and development of drugs and disease characterization [207]. Over time, *in vitro* cell culture models, particularly two-dimensional cultures, have been widely employed and refined, becoming the gold standard for studying cell behavior in a laboratory setting. However, these two-dimensional models have limitations in terms of accurately representing cellular behavior, functions, and drug responses observed in a living organism, as indicated in Table 16 [208-210].

To overcome the limitations of two-dimensional cell cultures, researchers have made significant advancements in cell culture techniques, with the recent development of three-dimensional tissue spheroids and organoids representing a significant leap toward achieving more realistic in vitro modeling of the cellular environment [211-213]. Three-dimensional tissue spheroids create an environment conducive to cell-cell and cell-matrix interactions, thereby better mimicking the *in vivo* conditions within an *in vitro* construct [214,215]. This is because in a three-dimensional construct, cells are surrounded by other cells and an extracellular matrix (ECM), resembling the natural environment of the body. The ECM plays a critical role in regulating various biological processes, including cellular differentiation, homeostatic regulation, and wound repair [209,216,217]. Two-dimensional monolayer cultures fail to replicate the complex architecture and cell-specific composition of the ECM. Consequently, testing compounds in the absence of the ECM and the intricate cell microenvironment often yield responses that may not be observed in the true cellular milieu. Recognizing the limitations of two-dimensional cell culture and the growing popularity of three-dimensional cell culture, especially in disease modeling, researchers are increasingly adopting different techniques to create three-dimensional cultures [218]. There

are many different techniques including matrix-based spheroid and organoid growth (both on and embedded within scaffolds) and scaffold-free spheroid formation, as indicated in Supplemental Table S1. Even with the recent developments with three-dimensional cell culturing techniques there are constraints such as randomized and uncontrolled cell growth, which ultimately leads to the formation of necrotic cores, rendering them unreliable for apoptotic drug studies and disease models [204,206,218,219].

To counteract the various drawbacks found in other models, *Microtissues* offer a non-adhesive three-dimensional cell culture platform that utilizes the concept of self-assembly to facilitate more controlled growth of three-dimensional cells and the formation of structures like spheroids, honeycombs, and toroids [220,221]. By manipulating various parameters, such as seeding density, researchers gain greater control over the size of the three-dimensional tissue or a microtissue produced for their studies [220, 221]. When it comes to disease models and drug studies that involve monitoring drugs over specific exposure times and regimens, the assays conducted can be time-sensitive and reliant on the penetration rate within a three-dimensional structure [217,222,223]. A thorough literature search found the widespread use of Paclitaxel for in vitro studies of MCF7 breast cancer cells, both in two and three-dimensional formats, as standalone treatments or in combination therapies. It is logical to utilize a known drug to investigate the potential of a technology for assessing cell viability [224,225,226]. For our study, we wanted to choose a well-researched combination on the *Microtissue* platform, such as MCF7 and Paclitaxel [244], to validate or challenge the hypothesis. Typically, most three-dimensional cell culture assays execute drug studies based on the theoretical assumption that the concentration of drug reaching the cell clusters is exactly what is calculated [224]. However, this may not be the case. Liquid Chromatography tandem Mass Spectrometry (LC-MS/MS) can play a significant role in

accurately quantifying not only the amount of drug delivered to a three-dimensional tissue but also providing insights into patient-specific treatment regimens [225,226,227]. Our study highlights the application of LC-MS/MS to precisely quantify the true concentration of drug (Paclitaxel, in this case) reaching the MCF7 spheroids in culture over different time points. To our knowledge, this is the first quantified drug absorption analysis performed for the *Microtissues* platform. The results obtained proves invaluable for the application of the *Microtissue* molds for patient-specific drug regimen analysis down the line.

	Characteristics	2D Cell Culture	3D Cell Culture
1	Cell Morphology	Cultures deform cell shape due to growth on a flat 2D surface	Actual shape is maintained with spheroid, organoid and other 3D cell culturing models
2	Cell Proliferation	Growth of cells is too rapid and therefore is unable to mimic that of in vivo growth	Growth of cells under 3D conditions is better able to replicate actual cell growth in vivo
3	Cell and ECM proliferations	Growth on a flat surface is not an appropriate replication of the actual environment of a tissue due to lack of ECM and cell interactions.	Due to the 3-dimensional structure, cells and ECM are able to interact replicating what occurs in vivo.
4	Cell-Cell Interactions	The multi-cells interactions occurring are unable to accurately depict what occurs in native organ environment	Multi-cell interactions in varied 3D cell culturing models are able to replicate native environments
5	Cell Differentiation	Unable to accurately mimic native tissue	Better resemblance of differentiation in native tissue with markers expression more similar to native tissue
6	Drug Response efficacy	Unable to see proper drug efficacy due to plastic substrate environment that cells are maintained within	More predictable due to the similarity's due in vivo environment
7	Apoptosis and viability (tumor models)	More sensitive relative to what occurs in vivo when studying target drugs	Higher resistance to anti-cancer target drugs, better resembling what occurs in vivo.
8	Physiological relevance	Not relevant due to lack of recapitulation of tumor microenvironment	Feasible to make physiologically relevant nutritional and oxygen conditions

9	Experimentation and analysis	Simple to use and very replicable data	Relative to 2-dimensional models, they are more complicated to use and harder to replicate
10	Characterizations	Ease of characterization regardless of instrument. Further, techniques are reviewed and readily available	More difficult to characterize due to the necessity of certain instrumentation as well as more time-consuming
11	Cost	More well-established and relatively inexpensive	More expensive and less standardization due to lack of studies.

Table 16. Comparison between 2D and 3D cell culture models (compiled from literature).

8.3.Experimental

8.3.1. Chemicals and Reagents

All solvents used were LC-MS grade, Baker Analyzed, with a purity >99.9% (obtained from VWR) including water, acetonitrile, and DMSO used in the preparation of calibrators, and operation of the LC-MS/MS. Reagent-grade formic acid (96% pure) was purchased from Fisher Scientific. Paclitaxel (PTX) (10 mM in DMSO) was obtained from AdooQ Bioscience and Docetaxel (DOC) (10 mM in DMSO) was obtained from MedChem Express. Dulbecco's Modified Eagle Medium (DMEM), Penicillin-Streptomycin, 1x PBS, and Fetal Bovine Serum were Gibco Manufactured, and purchased from ThermoFisher Scientific (North America). Cell culture grade agarose was purchased from Sigma Aldrich, and Microtissue molds were purchased from Microtissues Inc.

8.3.2. Cell Culture Conditions

Microtissues were created using 2% agarose solution (in 1x PBS), on the reusable 24-96 small spheroid micro-molds, and equilibrated in serum-free DMEM (with L-glutamine, phenol red, and sodium pyruvate) supplemented with 1% penicillin/streptomycin for at least 24-hours prior to all experiments. Human epithelial MCF7 breast cancer cells were obtained from American Tissue Culture Collection (ATCC, Rockville, MD), and cultured using DMEM with L-glutamine, phenol red, and sodium pyruvate, supplemented with 10% FBS and 1% penicillin/streptomycin at

5% CO_2 and 37 °C. Cells were expanded (P8-10) using a standard Trypsin protocol: one Versene solution wash, followed by three 1x PBS washes, and ~0.05% trypsin in PBS for 5 minutes, quenched with serum containing media, centrifuged at 125 g for 5 minutes, prior to resuspension and counting. Cells were continued in 2D culture flasks at no more at 1.2 million cells per well, and the spheroids were seeded at 500 cells per spheroids, i.e., 4.8×10^4 cells per well with media exchanged every at DIV= 3 prior to PTX exposure. PTX solutions were made using DMEM with L-glutamine, phenol red, and sodium pyruvate, supplemented with 10% FBS and 1% penicillin/streptomycin media (also referred to as complete media hereafter) in varying concentrations (as described throughout the study). The control samples had DMSO concentration <0.05% for consistency in all the samples across the board.

8.3.3. Drug treatment Protocol and Empty Microtissue Study

In tandem with spheroid culture, Microtissues were made and plated, and taken through the same equilibration process as described above. Once equilibrated, these Microtissues were not seeded with cells, and rather exposed to PTX solutions over 6, 12, 24, and 60 hours. The same drug solution prepared to treat the empty Microtissues were placed on empty culture wells (within the same plate) and analyzed alongside the empty Microtissues samples. Additionally, all prepared drug solutions were run on the LC-MS/MS each time to determine the true starting concentration for each experiment for future data normalization.

8.3.4. LC-MS/MS Conditions and Parameters

PTX and DOC (as internal standard) were diluted 250-fold in HPLC-grade acetonitrile and infused directly into the MS to quantify the parent mass and quantifier fragment masses. The infusion was performed using a Harvard apparatus at a flow rate of 30 µl/min. All compound transition data, together with the Entrance Voltage (EV), Collision Cell Energy (CC), and Collision

Cell Lens 2 (CCL2) values were obtained by Multiple Reaction Monitoring (MRM) optimization. Upon completing the MRM optimization, the nebulizer gas pressure, source temperature, HSID (hot surface-induced desolvation) temperature, and drying gas pressure were also optimized to obtain the best relative intensity for both MRMs of the analytes and the internal standards. After the Q1 and Q3 masses were detected, the EV, CC, and CCL2 values were re-optimized for the best signal of the analyte quantifier, qualifier, and internal standard as listed on Table 17 (a). The probe positions were also adjusted to obtain the best signal intensity and sensitivity. The system used was a QSight 220 CR Triple Quadrupole Mass Spectrometer with LX50 HPLC front (PerkinElmer, Waltham, MA), equipped with an Electron Spray Injection (ESI) source in positive ion mode. The optimized MS parameters were: nebulizer pressure of 80 psi, electrospray voltage of 5850 volts, and a source temperature of 425°C. The drying gas was set to 60, and HSID was set to 220°C. An Agilent Zorbax RRHD C-18 column (1.8 µm, 2.1 x 50 mm), set at 25 °C with mobile phase A (water with 0.1% Formic Acid) and mobile phase B (acetonitrile with 0.1% formic acid) was used. The final LC gradient profile was designed for a high sensitivity and a low flow rate (0.4 mL/min linear flow), with a 3-minutes run time per sample (Table 17 (b)).

The sample tray holder was maintained at 10°C. The autosampler needle was put through weak-strong-weak solvent wash cycles between each injection, with 70:30 = water: acetonitrile solution as the weak solvent and 100% HPLC acetonitrile as the strong solvent, at 250 µL volume for both solvents. The solvent delivery module was connected to a 10 µL needle and a 20 µL loop, with a solvent injection volume of 10 µL, 2 mm from vial bottom.

Table 17: (a) Optimized MS parameters for PTX and DOC (IS) on the QSight
(b) LC gradient flow design for the elution of PTX and DOC.

	Q1 mass	Q3 mass	EV	CC	CCL2
Paclitaxel-Quantifier	876.4	308.2	32	-48	-376
Paclitaxel-Qualifier	876.4	531.2	41	-30	-210

Docetaxel- IS	830.4	549.1	33	-34	-209

Time (min)	Flow rate	% A	% B
0	0.4	95	5
0.25	0.4	37	63
0.9	0.4	27	73
1	0.4	5	95
1.5	0.4	5	95
1.51	0.4	27	73
2	0.4	37	63
3	0.4	95	5

The stock PTX (10 mM) was taken through a two-step dilution process to yield a 6-points linearity series and quality controls (QC- Low and QC- High) in *complete media* (as described above). Briefly, 15 mL of *complete media* aliquoted in individual glass vials with stir bars and diluted PTX solutions were added to each vial, stirred for about 15 minutes at room temperature prior to overnight rocking at 4°C. All working volumes were greater than 10µL to avoid small volume pipetting errors, and DMSO was normalized by volume across all calibrators and quality controls, and L0 (*complete media* only, with DMSO). The Extraction Solvent was designed for the best layer separation and PTX adhesion, in addition to maintaining a pH suitable for the column. The final extraction solvent consisted of acidified acetonitrile (to be used ice cold) (0.1% formic acid) with DOC diluted 10,000 folds, integrated well by stirring in room temperature for at least 30 minutes.

The entirety of the study rendered four iterations of the linearity series, and each series was individually quantified in bulk prior to using it for any experimentation. Additionally, all the calibrators after bulk production were aliquoted in 2 mL microfuge tubes for single use (200 µL per level per experiment) and stored in -20°C. Samples for freeze-thaw analysis were stored in larger volumes (1600 µL) and samples for stability analysis were stored separately under different temperature conditions.

8.3.5. Sample Preparation

The sample preparation optimization took place in several stages. The finalized protocol used a liquid-liquid separation technique between the *complete media* and the Extraction Solvent, mixed in 1:2 ratio, vortex mixed and centrifuged at 0°C for 10 minutes at 4600 rpm. The final supernatant collected was from the top layer, carefully avoiding the DMSO micropartition that separated the phenol red and FBS serum proteins from PTX and the organic solvent. The final extract was placed in Thermo Fisher 2 mL screw top autosampler vials for analysis.

8.3.6. Validation against Immunoassay

To assess cellular viability, Live/Dead cytotoxicity kit for mammalian cells (Thermo Fisher) was used. The kit contained 4 mM Calcein-AM (for viability) and 2 mM ethidium homodimer-1 (for cell death). The tissues (with MCF7 spheroids growing in them) were taken through 3 washes of serum-free media, with ten minutes incubation between each wash. Once the washes were done, the manufacturer protocol was adjusted and optimized for the 3D spheroids and used for the assay. The wells were imaged using the Zeiss Axio Observer Z1 connected to an XCite fluorescence lamp (series 120 Q). The controls used were *Complete Media* for live and 70% ethanol for dead, and the EGFP (green) and dsRed (dead) channel exposures were normalized to the controls for the experimental groups.

8.3.7. DoE and Data Analysis

For the entire study, the Design of Experiment (DoE) was performed using JMP Pro 16 to optimize the number to be tested for statistical significance ($\alpha = 0.05$) for the multiple conditions (number of samples per round of drug exposure, number of samples for assay validation etc.). All

LC-MS/MS data was collected and analyzed using Simplicity 3Q (version 3.0) software for QSight. The data exported was further analyzed using Microsoft Excel, JMP Pro 16, and GraphPad Prism for visualization and statistical analysis.

8.4.Results and Discussion

8.4.1. Method Development and Optimization

Prior to starting any type of cell culture sample collection, it was important to develop an assay method that would enable the accurate quantification of PTX from the cell culture supernatant media consistently across different runs. As a result, an assay was developed utilizing the MS and LC parameters described in the *Experimental* section, and the Mobile Phases were tested in two independent runs HPLC water with 0.1% formic acid to be Mobile Phase A, and two different Mobile Phase B -acetonitrile with 0.1% formic acid, and methanol with 0.1% formic acid. The signal intensities (data not reported) observed were much greater for acetonitrile as Mobile Phase B, that was then used for the rest of the study. Following this test, PTX dissolved in organic solvents was tested in varying percentages of organic solvent (5 to 95% acetonitrile and methanol) and water, to determine the optimal ratio of organic solvent required in the sample for a proper chromatogram shape (data not reported). It was observed that PTX can yield proper bell-shaped chromatograms without any statistically significant decline in signal intensity for up to $2:1 = acetonitrile:water$ ratio mixture. Additionally, we injected varied concentrations of DOC to identify the optimal concentration of the drug required to serve as the IS. For our study, this concentration was identified to be 0.001 nM DOC in acidified acetonitrile. PTX is unstable in alkaline and methanolic solutions as established in the literature [234,235, 237], therefore the use of acidified acetonitrile proved to be a better choice for the subsequent mixing and temperature dependent centrifugation step after adding the extraction solvent. Additionally, the concentration of DOC internal standard was optimized such that there were no false peaks or large background

noise. This is shown in Figure 33, for the lowest level of calibrator, and blank media with no PTX and only DOC internal standard.

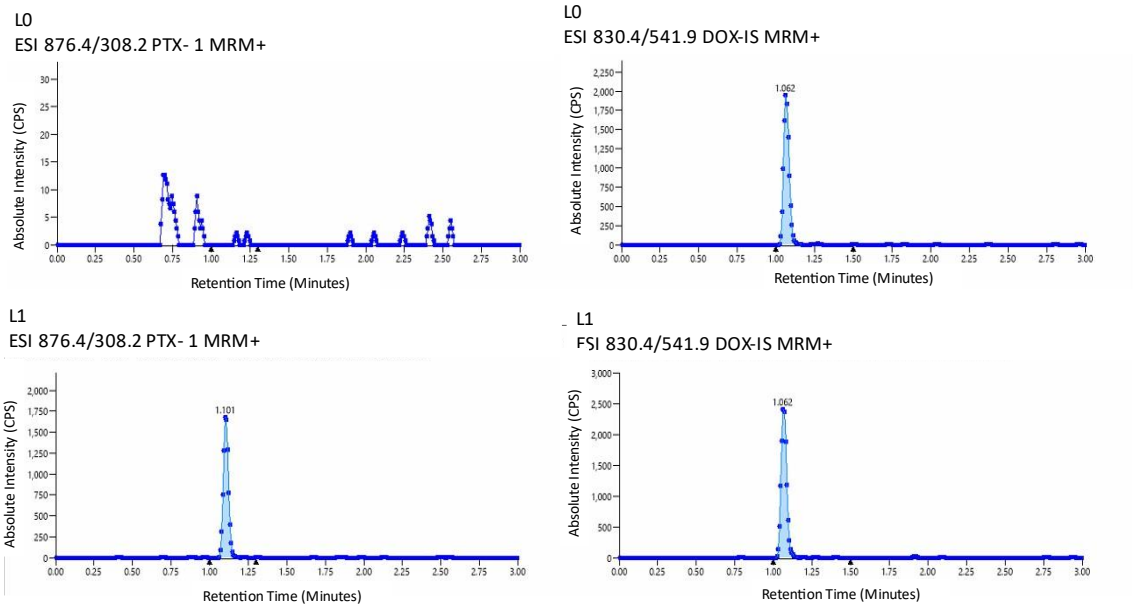

Figure 33. (top) Blank media (L0) with no PTX and only internal standard produced no peak for the PTX but showed a signal for DOC (as expected), while (bottom) lowest calibrator level (L1) produced a significant peak for PTX while also showing a signal for the DOC internal standard.

The extraction method utilized was based on the extensively reported literature on the nature of PTX and its solubility on different solvents, and the impact of temperature and pH on it [37,38,39,40]. For this study, we were able to identify the infinitesimally small partition that results due to the DMSO in which the initial PTX stock was dissolved it, separating the aqueous (*Complete Media*) and organic (extraction solvent) phases at bulk. The partition coefficient (K_D) of this entire system was determined by equation 1, where A_1 refers to the extraction solvent and A_2 refers to the *Complete Media* (per convention) [236], and the DMSO layer was ignored, rendering this a two-phase system.

$$K_D = \frac{[A]_1}{[A]_2} \qquad \text{(Equation 1)}$$

And while equation 1 was held true for a more simplistic approach, the presence of DMSO could not be ignored (especially due to its clear visibility post-centrifugation due to the phenol red indicator in *Complete Media*). Therefore, equation 2 [235] was employed, assuming that the chemical potential of PTX at bulk (extraction solvent) and surface (DMSO partition) were equal. In this equation, $\bar{A}$ (area per molecule) is considered to be approximately equal for all solvent species, and this subsequently led to the understanding that the PTX molecules reached the surface (DMSO) from bulk (*Complete Media*) due to greater solubility and the underlying physical interpretation, and due to equal assumption between the DMSO and extraction solvent layer, the PTX molecules underwent a relatively easy transition to the organic phase with ease (rose to surface). This is visually represented in the finite element analysis model in Figure 34 (created using COMSOL Multiphysics, version 6.0, for three-dimensional Transport of Diluted Species, in a time-dependent study).

$$\omega = \exp\left[\frac{\gamma^{lv}_{extraction\ solvent} - \gamma^{lv}_{DMSO}}{k_B T}\right]\bar{A} \quad \text{(Equation 2)}$$

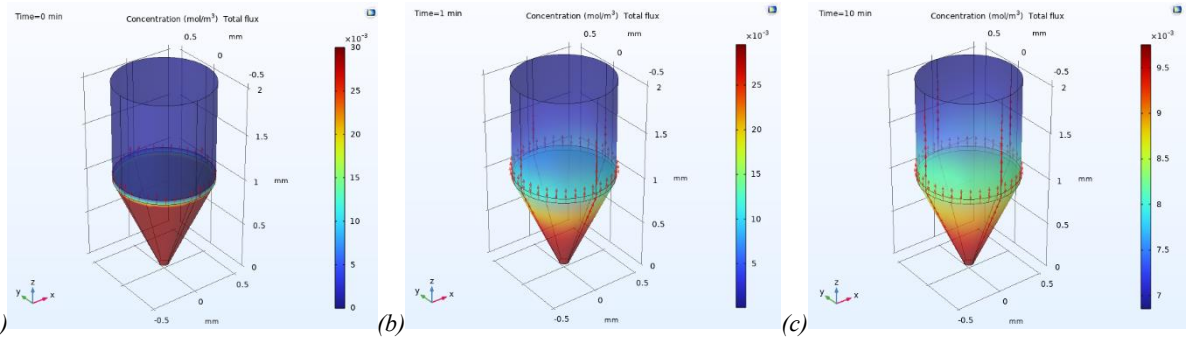

(a) *(b)* *(c)*

Figure 34. Computational model showing the concentration flux within the vial over time, visually represented with PTX in Complete Media (bottom), DMSO layer (middle) and extraction solvent (top); (a) at T=0 min, prior to mixing, PTX is concentrated at the bottom layer (as expected), (b) at T=1 min, mixing already takes place, with migration of PTX molecules towards the extraction solvent; (c) at T=10 min, the concentration gradient shift is evident within the DMSO layer, with arrows indicating the flux flow (majority towards the extraction solvent). The model was created to reflect the total time of the system, i.e., including mixing and centrifugation, prior to the layer removal at T= 10 min.

8.4.2. Calibrator Validation

To continue this investigation, the aforementioned *Complete Media* was used to create a linearity series that would consistently yield standard curves between 0.02 µM to 15 µM values per run, so that unknown samples could be run against these standards to quantify the drug absorption. This also meant that the linearity series generated had to be validated for robust use throughout the course of the study and tested for its potential for future applications. The validation study resulted in four iterations of the linearity series (data only reported for one of the iterations), each resulting in similar results for all validation steps across the board. The measured concentration, along with the %CV (as a measure of precision), and the accuracy are reported in Table 18. This is the iteration of the linearity series that was used for the rest of the experiments.

The linearity series generated had the following concentrations: L1= 0.03 µM, L2= 0.2 µM, L3= 2.9 µM, L4= 6.8 µM, L5= 8.9 µM, and L6= 13.6 µM (for the reported iteration), and this was used to perform all additional analysis needed for validation (shown in Figure 35). The linearity of the assay was assessed by looking at the R-Square value generated for both MRMs for all linearity series iterations, across multiple runs (n=3 per level per run, and a total of 6-runs were performed per linearity series). All values observed were greater than or equal to 0.9 demonstrating that the assay was linear, irrespective of the manufacturing iteration.

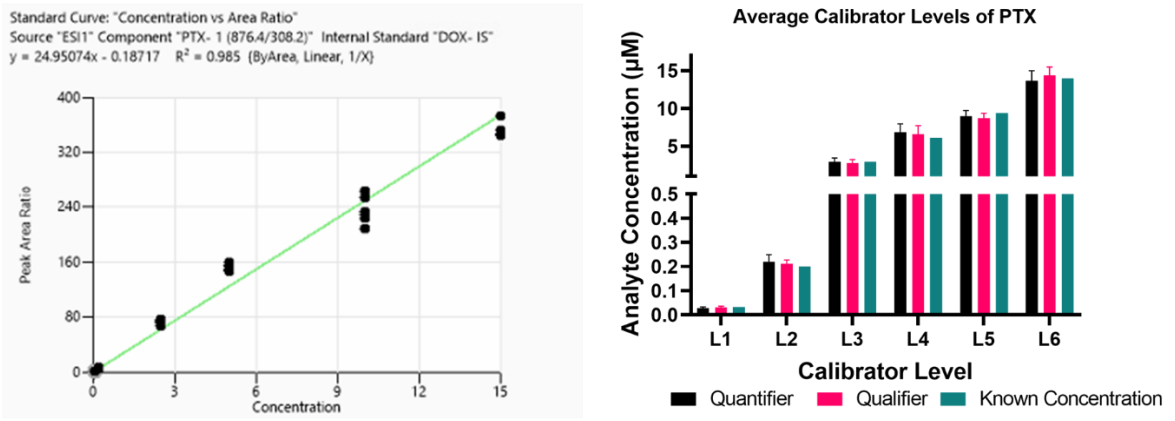

Figure 35. (left) Standard curve for PTX calibrator from one of the runs, showing an R-square value of 0.985; (right) Average analyte concentration measured per calibrator across three different runs from the same linearity series.

The %CV was looked at as a measure of the assay precision, with ±20% or less being the passing criteria, for individual, as well as inter and intra-assay precisions. Similarly, the % accuracy cutoff was 100±20%, and the assay exhibited high precision and accuracy consistently for all four manufactured linearity series (data only reported for one of the iterations).

Table 18. ((a) quantifier (b) qualifier) Average concentrations, standard deviation, %CV and % accuracy for PTX calibrators (n=3 per level, per run; total number of runs= 6).

(a)

Calibrator Level	$\mu_{\bar{x}} \pm \sigma$	***%CV***	***%Accuracy***	***Interassay %CV***	***Intra-assay %CV***
L1	0.03 ± 0.01	*17.8%*	*83%*	*16.7%*	*8.9%*
L2	0.22 ± 0.03	*13.2%*	*110%*		
L3	2.93 ± 0.50	*17.0%*	*101%*		
L4	6.82 ± 1.3	*16.6%*	*111%*		
L5	8.97 ± 0.76	*8.4%*	*95%*		
L6	13.66 ± 1.34	*9.8%*	*97%*		

(b)

Calibrator Level	$\mu_{\bar{x}} \pm \sigma$	***%CV***	***%Accuracy***	***Interassay %CV***	***Intra-assay %CV***
L1	0.03 ± 0.01	*17.2%*	*102%*	*12.5%*	*8.2%*
L2	0.21 ± 0.01	*6.91%*	*96%*		
L3	2.80 ± 0.42	*15.2%*	*97%*		
L4	6.56 ± 1.2	*17.5%*	*109%*		
L5	8.72 ± 0.62	*7.2%*	*92%*		
L6	14.40 ± 1.07	*7.4%*	*101%*		

8.4.3. Carryover and Stability Analysis

To optimize the number of samples and replicates that could be run each time, we investigated the carryover of PTX, by injecting a L1 in triplicates following an L6 injection without incorporating any blank samples in between (repeated in a set of triplicates for seven times). Figure 36 (a) shows the known concentration (theoretical value), and the base value (L1 measured in triplicates after two blank injections), and the carryover spread. No significant outlier was observed for any of the repeats, and carryover spread was well within a ±20% range.

PTX has been widely investigated for its stability for *in vitro* testing [239, 240], with most studies recommending the creation of a new batch of treatment each time prior to the application of the drug for treatment regimen. However, the long-term stability of PTX in the context of LC-

MS/MS application, and how stable a linearity series might be in an aqueous solution. Thus, each calibrator in duplicates were stored at -20°C and stressed too +4°C over 8-days, at 2-day intervals, as described in detail on our previous studies [242,243]. At the end of the eighth day, each calibrator was run in triplicates and averaged to get the final concentration of each calibrator for each day. Once compiled, the data obtained was normalized to D=0 for both MRMs, and a paired student's t-test was performed to identify statistical significance. Figure 36 (b) shows the normalized concentration for all calibrators over 8-days for the quantifier (the qualifier produced an identical trend), and all calibrators except L5 yielded similar results, i.e., they were stable across all eight days. Ignoring the outlier (L5), all levels measured lower than D=0 at D=4, with L2, L3 and L6 reporting a p-value< 0.05. Therefore, the results obtained can be interpreted to showcase that the calibrators are stable for 11-days when stored in -20°C despite being in an aqueous solution.

(a)

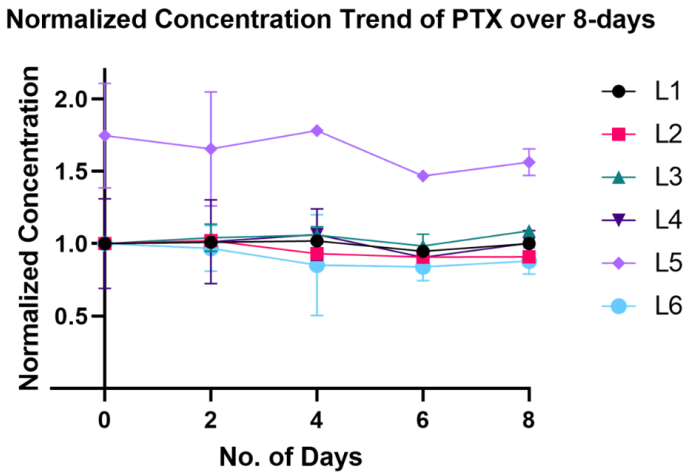

(b)

Figure 36. (a) Carryover spread of L1 calibrator level for PTX MRMs (n= 3, triple injection per sample, in sextuplet groups). (b) Normalized PTX concentration (quantifier) for all calibrator levels (n= 2 per calibrator with triplicate injections).

8.4.4. Drug Treatment

Once the assay had been optimized and validated, the *Microtissue* mold testing took place. The treatment regimen took place as described in the experimental section and is also illustrated in Figure 37. It was interesting to observe that the amount of PTX absorbed by the mold was nearly half of the treatment concentration for anything below a 1 µM treatment during the first 24-hours. However, for anything above 1 µM of a treatment concentration, the absorption by the molds were about 25-30% even by the end of the 60th hour of exposure, as shown in Figure 38 (a) (the difference between two treatment concentrations for both MRMs). The empty wells with no mold in them showed little to no absorption of the drug. This study was repeated in four rounds for each time point, with triplicates of tissue for each concentration at each time point, and the collected supernatant were prepared in triplicates and triple injected (n=12 per concentration, per time-point, with 3 technical replicates). Not only was there a significant difference between the treatment concentrations, but the amount of drug absorbed by the mold over different time points was also an important finding, because time-dependent dose analysis is often the primary experiment

conducted for most novel drug development studies. The absorption data obtained from different time points were scrutinized using Tukey-Kramer HSD analysis, and the connecting letters report solidified that the amount of drug absorbed by the molds were statistically significant (as shown in Figure 38 (b)). While time H= 0 is not shown in the figure, all studied time points were significantly different than the initial treatment concentration. This data establishes the basis for all future *in vitro to in vivo extrapolation* studies, by bringing to attention the phenomenon of analyte absorption by the mold, even for a scaffold-free model, like *Microtissues*. Additionally, the absorption trend may be different for the different molecules being studied, for instance, the analyte absorption may be higher or lower for Tamoxifen- a hormone-based anticancer treatment, compared to PTX for the same *Microtissue* mold created using the same composition of agarose. This means that future *in vitro to in vivo extrapolation* studies must investigate and account for the drug absorbed by the model platform for the different concentration ranges being studied, as well as the times of exposure being studies, since the absorption values are different for each time point.

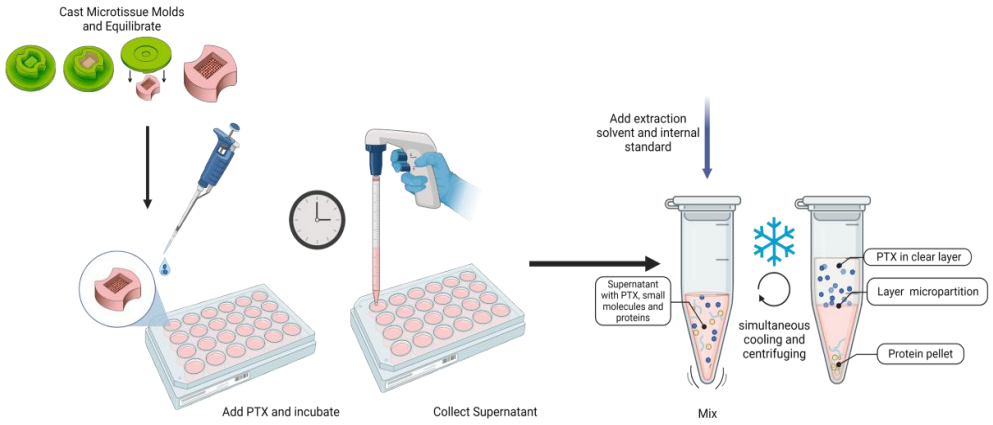

Figure 37. Microtissue casting, drug treatment, and post-treatment sample separation technique.

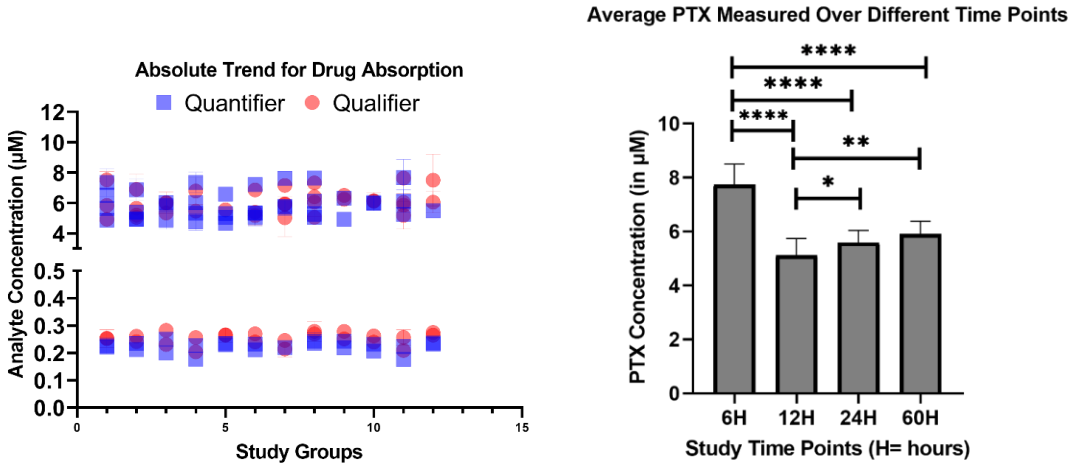

(a)
(b)

Figure 38. (a) PTX absorption trend for 0.5 µM treatment group and 5 µM treatment groups for both MRMs (n=12 Microtissue mold for the reported data); (b) Average PTX concentration measured by Microtissue molds at different time points (n=12 per time point).

8.4.5. Qualitative Validation

Once all findings and conclusions were drawn from empty *Microtissue* studies, we chose to further validate the findings against the current gold-standard to understand spheroid viability for cell culture models. Briefly, we seeded the *Microtissue* molds with MCF-7 cells and allowed them to self-aggregate into spheroids and exposed them to PTX for 24-hours. This was tested alongside a plate of empty *Microtissue* molds, and the drug absorbed by the mold was accounted for when compiling the live-dead images (Figure 39). Live-Dead assay is a qualitative measure, and in accordance with our quantitative data obtained, we noticed that the lower PTX concentration had more live cells (green) than the higher PTX concentration. Figure 39 shows the theoretical concentration of the drug supplied along with the actual LC-MS/MS measured concentration of the treatment. For the 5 µM theoretical concentration group, more dead spheroids (red) were seen, as the absorption taking place at this dose was insufficient to cause a drastic drop in viability, while the other two groups showed more live spheroids (green). Traditionally, this qualitative data would suffice as an end-point assay, however, now we know that it will generate inaccurate data for an *in vitro* to *in vivo* extrapolation study. Additionally, most traditional cell culture methods

are either qualitative or optimized for 2-dimensions, and LC-MS/MS can provide a solution by yielding quantitative outcomes, irrespective of the dimensions of the culture (easily adaptable for 2D and 3D methods). This can be visualized as a closed system, as shown in supplemental figure S2.

Theoretical Concentration	Media	70% EtOH	5 µM	0.5 µM	0.05 µM
Actual Concentration	Media	70% EtOH	4 µM	0.2 µM	0.02 µM

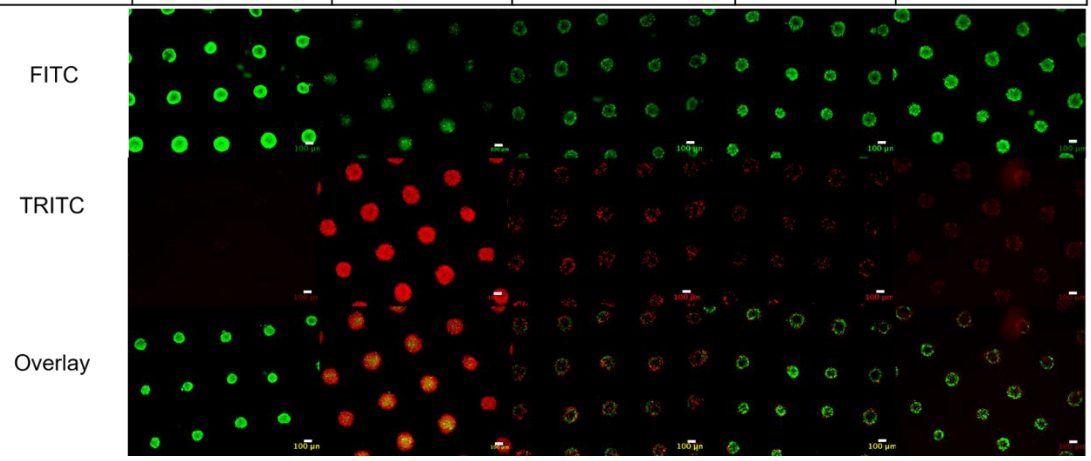

Figure 39: Representative live (FITC- green) and dead (TRITC- red) channel images of the MCF7 spheroids for theoretical and actual concentrations (accounting for mold absorption) (n=3 Microtissue molds per condition, only one section of one of the Microtissues for each condition is included in this panel). Since less absorption takes place below a 1 µM concentration, more live spheroids (green) were seen for the 0.05 and 0.5 µM theoretical concentration study groups.

8.5.Conclusion

In vitro to in vivo extrapolation studies are extremely important to researchers to better understand and establish the reliability and relevance of preclinical data. Understanding and characterizing these studies are necessary for personalized medicine, toxicity profiling, and time-dependent drug studies among other applications. Our study showcases an enhanced application of LC-MS/MS for better understanding *Microtissues* technology, an emerging solution in the field of *in vitro to in vivo extrapolation studies.* We have not only quantified and established the importance of accounting for PTX absorption by the *Microtissues* mold, but this study aims to highlight the absolute necessity of investigating all analyte absorptions for different 3D cell culture techniques in the future.

8.6.Acknowledgment

This work was in part supported by Revvity's research grant to Brown University. The authors would like to thank Zahra Ahmed and Dr. Vikas Srivastava for all their logistical support for this study. The authors would also like to thank Dr. Jeffrey Morgan for his guidance in using the Microtissues.

8.7.Supporting Information

	Microtissues	Spontaneous Aggregation	Liquid Overlay Cultures	Scaffold based cultures	Gyratory and Spinner Flasks	Pre-engineered collagen composite scaffolds	Rotary Cell Culture System
Cost	Relatively inexpensive	Inexpensive	Inexpensive	Expensive	Inexpensive	Expensive	Expensive
Ease of Use	Easy to prepare and use	Easy to prepare and use	Easy to prepare and use	Easy to prepare and use	Easy to prepare and use	Easy to prepare and use	Easy to prepare and use (quick)
Spheroid Rigidity	Well-defined controlled spheroids	Cluster and not well-defined spheroids	Concave bottom results in defined spherical shape	well-defined controlled spheroids	uncontrollable size and not well-defined spheroids	forms well-defined sepheroids with temperature alteration	well-defined controlled spheroids
Throughput Ability	High	Relatively Low	Low	Low	Relatively Low	High	High
ECM Support	Scaffold-Free	Successfully mimics in vivo ECM	High when Hyaluronan present	Cells grow on thick layer of ECM resulting in cell differentiation	Use natural and synthetic ECM mimicking hydrogels	Mimics in vivo ECM well	Mimics in vivo ECM well

Supplemental Table S1. The advantages and disadvantages of existing 3D cell culture techniques against Microtissues [236-239].

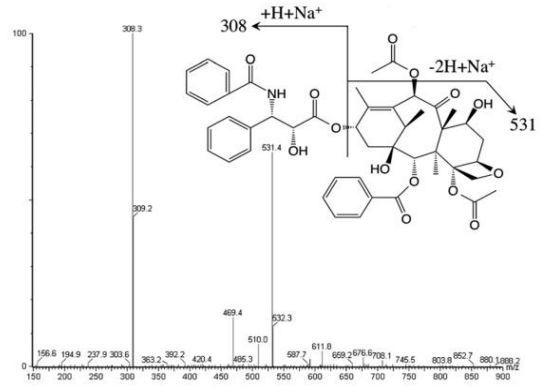

Supplemental Figure 1. MS spectra showing the mass fragments identified and used for this study.

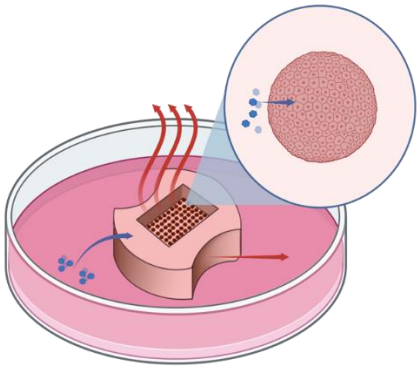

Supplemental Figure 2. Closed in vitro system of PTX in Complete Media penetrating and entering the Microtissue mold, while equilibration media diffuses out of the mold to the surroundings. PTX has to overcome the mold barrier to finally reach the spheroids, and depending on the time of the study, some media evaporation also occurs.

Chapter 9: Conclusion

9.1. Summary

This dissertation started out with an investigation of a rather simple matrix with the goal of minimizing the sample volume required for a tier-2 quantitative assay for small molecule detection. Over the course of the study, the work has evolved to include more complex matrices, such as serum, whole blood, and dried blood spots. The overarching goal was to simplify the sample preparation workflow for all these matrices to reduce the turnaround time for multiple clinical metabolomics analyses. During the investigation, we innovated novel treatment protocols and devices with immediate translatability in clinical settings, while maintaining the overall assay precision despite lowering the volume of samples required. The biggest driver behind this work was the ability to expand the use of DBS as a diagnostic source material for metabolomics analysis, for adult and neonatal health. Additionally, we automated our assays on a standard robotic liquid handling platform, with minimal attachments, while still retaining the throughput ability. Because of our collaborative work, we were able to test patient samples using our assays and devices, shedding light on the possibility of immediate translatability of the findings.

9.2.Conclusions and Future Directions

All the work featured in this dissertation were tied together by 3 key ideas: use of microsamples, clinical application of LC-MS/MS for the microsamples, and the automation potential of developed protocols. In Chapter 2, we showcased that for a condition like CAH, passive saliva collection can be beneficial and provide an alternative diagnostic matrix to serum for this disorder detection. Additionally, we utilized artificial saliva to create a prototype kit that was extensively validated for linearity, accuracy, precision, carryover, and stability. The future of this specific study would be to expand and test the protocol across different clinical laboratories throughout the country and obtain any relevant data for inter-facility discrepancies. Additionally,

I would like to utilize this protocol to start gathering information from infant saliva and build a database to more comprehensively characterize cortisol-cortisone dysregulation.

Chapter 3 garnered a lot of attention due to its novel nature of simultaneous quantification of eight different antidepressants used to treat postpartum depression. The high throughput nature of this protocol deems it ideal for immediate testing in clinical facilities, and this can be expanded beyond postpartum depression monitoring. One ideal future milestone for this protocol would be to monitor for residual antidepressants remaining in an individual's system following prescription alteration. Furthermore, this approach is agnostic to any demographic information, such as gender, age, or health (smoking versus non-smoking status).

Chapter 4 introduces the ability to expand DBS sampling for steroid analysis to screen for PCOS, and how electric field can be utilized to draw steroids out of DBS cards faster than a traditional mechanical workflow. This study initially started with investigating the potential of urine as a diagnostic matrix to detect early onset PCOS, however, lack of clinical data to curate targeted metabolite calibrators rerouted the study to investigate DBS. Even though steroids dysregulation has been widely reported as a disease phenotype of PCOS, due to the heterogeneity of the disorder, it is nearly impossible to establish a single set of calibrators encompassing the prowess to accurately predict PCOS outcome across a diverse array of DBS samples. The vastly distinct concentrations of steroids present in each patient further complicate this problem. Additionally, as more predictors of this disorder are identified, the number of analytes to be quantified in this approach is projected to increase exponentially. Increasing the process complexity in this manner is essential to improving assay robustness and detection sensitivity to ameliorating ease of processing at the bench and clinical outcomes respectively.

Chapter 5 highlighted strategies that can be utilized to quantify total testosterone in human serum using a semi-automated workflow. Instead of employing large, expensive instruments, the innovation focused on exploiting a simpler contraption for high throughput sample preparation. Prototype kits for this particular study were manufactured at Brown and shipped to Revvity Inc. research facilities in Texas, US. This study, at its present state, is ready for clinical adaptation.

Chapter 6 was a collaborative work with the Haass-Koffler lab for Behavioral and Social Sciences wherein participants were exposed to different noradrenergic stimulations over a set period. Even though the patients tested negative for all other opioids except buprenorphine and methadone on a urinary lateral flow assay, employing LC-MS/MS quantification of the patient samples revealed trace elements of other opioids in their system. We were able to look at individual patient data in addition to their stimulation conditions and identify possible reasons behind reported adverse effects. Moreover, we were able to identify that yohimbine stimulation certainly has an impact on drug consumption over time. There is a lot that can be done with this study. Firstly, the data can be evaluated against the salivary cortisol measurements of the patients, and we can potentially extrapolate the behavioral trend for craving or withdrawal. Additionally, we can start collecting patient DBS spots and build an Atlas correlating the opioid bioavailability in serum against whole blood.

Chapter 7 not only introduced an entirely new device and application of electric field, but it also provides enough evidence that 3.2 mm DBS sample spots from infants can alter the landscape of NAS screening. We fashioned a 96-array device that efficiently draws five different opioids out of a DBS sample in 3-minutes on a total laboratory automation workflow. We optimized the electrical conditions needed for this experiment and compared it against two current gold-standard sample preparation methods. Additionally, we introduced a low-cost gravity-

assisted microfluidic chip for maternal whole blood processing during this investigation. This work resulted in the application of a provisional patent for the use of hollow cylindrical electrodes for biospecimen sample preparation, and the application of this apparatus can extend beyond metabolomics. For the future direction of this specific work, I would like to see the application of this device in genomic DNA and RNA extraction from DBS samples. While it is ready for further testing as a standalone consumable for metabolomics at its current state, it will be interesting to add genomics to its application profile and expand the value proposition. Furthermore, I want to utilize this device to begin collecting a wide variety of demographic data alongside clinical measurements from DBS. These metrics will serve as the basis of follow up analysis leveraging statistical and machine learning techniques to project individualized patient outcomes.

Chapter 8, unlike the other chapters, focused on the RUO application of metabolomics for tissue engineering. We highlighted the inaccuracies of current *in vitro to in vivo* (IVIVE) studies, wherein, final patient-specific pharmacokinetic data are extrapolated based on theoretical measurements. We have showcased that cellular supernatant from 3-dimension Microtissue molds can deliver inaccurate drug quantities (paclitaxel in this case) to MCF7 spheroids, and thus, for a patient-specific study, the extrapolated measure of drug dosage can prove to be insufficient. The future possibility of this study is infinite. This study can be expanded to testing any scaffold-free tissue culture platform for any drug study (e.g. chemotherapeutics, PARP-inhibitors, and beta blockers, to name a few). Moreover, this introduces the amalgamation of targeted metabolomics for complete characterization of *in vitro* microenvironments.

Overall, this dissertation presents key developments in the domain of clinical metabolomics, which push the boundary of what it can achieve. Despite this, it is irrefutable that this field, much like the rest of science, is constantly changing at a rapidly increasing pace. For

example, the original "complete genome" was generated in 2003, it was not until two decades later that the whole genome was properly sequenced as part of the telomere-to-telomere project, which leveraged long-read sequencing platforms that were only made available a decade prior. Likewise, metabolomics will undoubtedly experience its own landmark accomplishments of similar gravity. Relative to transcriptomics and genomics, metabolomics is a comparatively immature domain. However, with additional research and funding, I expect metabolomics to become part of routine diagnostic practices. Hardware advances that reduce the footprint of LC-MS/MS instrumentation will only accelerate this transition. As this development occurs in tandem with the artificial intelligence and machine learning revolution, software solutions can be improved to predict patient conditions directly from raw intensity profiles, rendering the cumbersome process of data extraction and analysis obsolete. Engineering solutions can be developed alongside software improvements to construct a new system leveraging the advantages of high resolution of mass spectrometry and triple quadruples, an innovation which would enable a single sample run to obtain multiomics data from microsamples. Technological advancements can push these capabilities even further, such as in the case of standard candles at Matterworks (MA, US), where a single calibrator set can be used to study multiple metabolites of different classes. Although this premise is novel and certainly innovative, additional research is required to standardize single calibrators and sample preparation methods for distinct diagnostic matrices across a wider range of metabolites. Finally, as multiomics approaches to clinical diagnostics gain traction within academia and the private sector, metabolomics will play a critical role alongside its more mature counterparts, genomics and transcriptomics.

9.3.Contributions of this Dissertation

9.3.1. Contributions to the field

To the field of diagnostics and metabolomics, this dissertation has the following contributions:

- Encourages clinical chemists to think beyond most traditional sample preparation methods (LLE, SPE etc.), and instead focus on enhancing simpler sample preparation workflow for automation.
- Provides method development insight into liquid chromatography tandem mass spectrometry applications and promotes the use of kit-based approaches for clinical sample quantification.
- Offers a profound comprehension of microsample milieu of different diagnostic matrices for a variety of metabolite quantification.
- Development of electric field for metabolite extraction from dried blood spots with novel devices for a high throughput turnaround time.

This dissertation emphasizes the importance of translational research and how modern engineering improvements combined with a thorough comprehension of fundamental scientific principles can transform the sample preparation operations for clinical metabolomics. The opportunity of working on such diverse projects incorporating public health interests and fundamental research question (for example, organoid growth and development) to be answered by quantitative solutions leveraging my background as an engineer with my passion to change the world, was truly one of a kind. I am proud of the strides I have made, and I look forward to watching these innovations become widely used technology in the near future.

9.3.2. Contributions to the Scientific Community

This dissertation has several contributions to the scientific community at Brown University, and the global scientific community at large. The research findings have been presented at several conferences and scientific settings, catered to those interested in the clinical application of LC-MS/MS, and to those interested in high throughput engineering solutions. A number of articles, including those from Science Daily, Healthnews, and AAAS's EurekaAlert, as well as a feature by the Brown Daily Herald, also emphasized various aspects of the research to both a lay audience and the larger scientific community (https://www.brown.edu/news/2023-02-10/monitoring-antidepressants and https://www.browndailyherald.com/article/2023/03/brown-researchers-create-improved-automated-system-for-antidepressant-drug-detection). Throughout the course of these studies, eight students—four undergraduates, three master's, and one high school student—were mentored, advancing their ability to perform in cross-disciplinary teams, empowering them with benchtop and automation rigor, and aided in their growth and development as scientific communicators through journal writing and conference presentations. As a first-generation scientist in my family, and the first Ivy League graduate from my hometown, I am honored that my scientific findings reached a global audience, and I hope it inspires the next generation of scientists, especially the first-generation, underrepresented women from small towns (https://www.prothomalo.com/lifestyle/im8k0p1qug and https://www.tbsnews.net/feature/pursuit/narayanganj-ivy-league-113575).

I hope my work and contributions in advancing the biomedical engineering landscape encourages others like me to dream and chase their dreams. It is truly rewarding when you can shatter the glass ceilings to achieve beyond the limitations dictated by social norms.

References

1. World Health Organization. Quality Health Services. Accessed March 8, 2024. https://www.who.int/news-room/fact-sheets/detail/quality-health-services
2. World Health Organization. Improving Quality of Care. Accessed March 8, 2024. https://www.who.int/southeastasia/activities/improving-quality-of--care
3. Centers for Disease Control and Prevention, National Center for Health Statistics. National Vital Statistics System, Linked Birth / Infant Deaths on CDC WONDER Online Database. Data are from the Linked Birth / Infant Deaths Records 2017-2021, as compiled from data provided by the 57 vital statistics jurisdictions through the Vital Statistics Cooperative Program. Accessed at http://wonder.cdc.gov/lbd-current-expanded.html on Mar 8, 2024 2:10:06 PM
4. Babu, M., & Snyder, M. Multi-Omics Profiling for Health. *Molecular & Cellular Proteomics*, 22(6), 100561 (2023). doi:10.1016/j.mcpro.2023.100561
5. Ritchie, M. D., Holzinger, E. R., Li, R., Pendergrass, S. A., & Kim, D. Methods of integrating data to uncover genotype–phenotype interactions. *Nat Rev Genet*, 16(2), 85-97 (2015). doi:10.1038/nrg3868
6. Ding, J., & Feng, Y-Q. Mass Spectrometry-Based Metabolomics for Clinical Study: Recent Progresses and Applications. *TrAC Trends in Analytical Chemistry*, 158, 116896 (January 2023). https://doi.org/10.1016/j.trac.2022.116896.
7. Van Roekel, E. H., Loftfield, E., Kelly, R. S., Zeleznik, O. A., & Zanetti, K. A. Metabolomics in epidemiologic research: challenges and opportunities for early-career epidemiologists. *Metabolomics*, 15(1), 9 (2019). doi:10.1007/s11306-018-1468-z
8. Trifonova, O. P., Maslov, D. L., Balashova, E. E., & Lokhov, P. G. Current State and Future Perspectives on Personalized Metabolomics. *Metabolites*, 13(1), 67 (2023). doi:10.3390/metabo13010067
9. Metabolomics-Based Methods for Early Disease Diagnostics: A Review - PMC. Accessed March 14, 2024. https://www.ncbi.nlm.nih.gov/pmc/articles/PMC3890417/
10. Microsampling tools for collecting, processing, and storing blood at the point-of-care - PMC. Accessed March 14, 2024. https://www.ncbi.nlm.nih.gov/pmc/articles/PMC10013775/
11. Hüttenhain, R., Choi, M., Martin De La Fuente, L., et al. A Targeted Mass Spectrometry Strategy for Developing Proteomic Biomarkers: A Case Study of Epithelial Ovarian Cancer. *Molecular & Cellular Proteomics*, 18(9), 1836-1850 (2019). doi:10.1074/mcp.RA118.001221
12. Ferreira, C. R., Yannell, K. E., Jarmusch, A. K., Pirro, V., Ouyang, Z., & Cooks, R. G. Ambient Ionization Mass Spectrometry for Point-of-Care Diagnostics and Other Clinical Measurements. *Clinical Chemistry*, 62(1), 99-110 (2016). doi:10.1373/clinchem.2014.237164
13. Fleming, K. A., Naidoo, M., Wilson, M., et al. Box 11.2, Definition of Laboratory Tiers. Published November 27, 2017. Accessed March 14, 2024. https://www.ncbi.nlm.nih.gov/books/NBK525286/
14. Geaghan, S. Diagnostic Test Sample Volume: How Much Is Too Much?: Leveraging Point-of-Care Testing to Reduce Sample Volumes, Iatrogenic Anemia, and Transfusion Requirement in Adult Populations. *Point of Care*, 10(4), 157 (2011). doi:10.1097/POC.0b013e318238cbd5
15. The healthcare diagnostics value game. Published online 2018.
16. Process control— introduction to quality control. (n.d.). In Laboratory and Quality Management System.
17. The evolution of blood-spot newborn screening - PMC. Accessed March 14, 2024. https://www-ncbi-nlm-nih-gov.revproxy.brown.edu/pmc/articles/PMC4729101/
18. Little to give, much to gain – what can you do with a dried blood spot? - PMC. Accessed March 14, 2024. https://www-ncbi-nlm-nih-gov.revproxy.brown.edu/pmc/articles/PMC7500853/
19. Whittaker, K., Mao, Y. Q., Lin, Y., et al. Dried blood sample analysis by antibody array across the total testing process. *Sci Rep*, 11(1), 20549 (2021). doi:10.1038/s41598-021-99911-8.
20. Velghe, S., Delahaye, L., & Stove, C. P. Is the hematocrit still an issue in quantitative dried blood spot analysis? *Journal of Pharmaceutical and Biomedical Analysis*, 163, 188-196 (2019). doi:10.1016/j.jpba.2018.10.010
21. Demirev, P. A. Dried Blood Spots: Analysis and Applications. *Anal Chem*, 85(2), 779-789 (2013). doi:10.1021/ac303205m
22. AbuRuz, S., Millership, J., & McElnay, J. Dried blood spot liquid chromatography assay for therapeutic drug monitoring of metformin. *Journal of Chromatography B*, 832(2), 202-207 (2006). doi:10.1016/j.jchromb.2005.12.050
23. Gaisford, W. Robotic liquid handling and automation in epigenetics. *J Lab Autom* 17, 327–329 (2012). https://doi.org/10.1177/2211068212457160

24. Ortiz, L., Pavan, M., McCarthy, L., Timmons, J., & Densmore, D. M. Automated Robotic Liquid Handling Assembly of Modular DNA Devices. *J Vis Exp* (2017) doi: 10.3791/54703.
25. Chory, E. J., Gretton, D. W., DeBenedictis, E. A., & Esvelt, K. M. Enabling high-throughput biology with flexible open-source automation. *Mol Syst Biol* 17(3), e9942 (2021). doi: 10.15252/msb.20209942.
26. Timmermans, S., Souffriau, J., & Libert, C. A general introduction to glucocorticoid biology. *Front Immunol* 10, 1545 (2019).
27. Stephens, M. A. C., & Wand, G. Stress and the HPA axis: Role of glucocorticoids in alcohol dependence. *Alcohol Res: Curr Rev* (2012).
28. Ehlert, U., Gaab, J., & Heinrichs, M. Psychoneuroendocrinological contributions to the etiology of depression, posttraumatic stress disorder, and stress-related bodily disorders: the role of the hypothalamus–pituitary–adrenal axis. *Biol Psychol* 57, 141-152 (2001).
29. Nicolaides, N. C., Galata, Z., Kino, T., Chrousos, G. P., & Charmandari, E. The human glucocorticoid receptor: molecular basis of biologic function. *Steroids* 75, 1-12 (2010).
30. Ramamoorthy, S., & Cidlowski, J. A. Corticosteroids: mechanisms of action in health and disease. *Rheum Dis Clin North Am* 42, 15-31 (2016).
31. Kuo, T., McQueen, A., Chen, T.-C., & Wang, J.-C. Regulation of glucose homeostasis by glucocorticoids. In Glucocorticoid Signaling, 99-126 (2015).
32. Exton, J. Regulation of gluconeogenesis by glucocorticoids. *Monogr Endocrinol* 12, 535-546 (1979).
33. Olgemöller, B., Roscher, A. A., Liebl, B., & Fingerhut, R. Screening for Congenital Adrenal Hyperplasia: Adjustment of 17-Hydroxyprogesterone Cut-Off Values to Both Age and Birth Weight Markedly Improves the Predictive Value. *J Clin Endocrinol Metab* 88, 5790-5794 (2003).
34. New, M. I. Diagnosis and management of congenital adrenal hyperplasia. *Annu Rev Med* 49, 311-328 (1998).
35. Yamamoto, T. Latent adrenal insufficiency: concept, clues to detection, and diagnosis. *Endocr Pract* 24, 746-755 (2018).
36. Mitchell, I. C., et al. "Subclinical Cushing's syndrome" is not subclinical: improvement after adrenalectomy in 9 patients. *Surgery* 142, 900-905 (2007).
37. Lee, E. K. D. Y., & Choi, M. H. Technical and clinical aspects of cortisol as a biochemical marker of chronic stress. *BMB Rep* 48, 209 (2015).
38. Seger, C., & Salzmann, L. After another decade: LC–MS/MS became routine in clinical diagnostics. *Clin Biochem* 82, 2-11 (2020).
39. Jung, C., Greco, S., Nguyen, H. H., Ho, J. T., Lewis, J. G., Torpy, D. J., & Inder, W. J. Plasma, salivary and urinary cortisol levels following physiological and stress doses of hydrocortisone in normal volunteers. *BMC Endocr Disord* 14(1), 1-10.
40. Tudela, E., Muñoz, G., & Muñoz-Guerra, J. A. Matrix effect marker for multianalyte analysis by LC-MS/MS in biological samples. *J Chromatogr B* 901, 98–106 (2012).
41. Papanicolaou, D. A., et al. Nighttime salivary cortisol: a useful test for the diagnosis of Cushing's syndrome. *J Clin Endocrinol Metab* 87(10), 4515-4521 (2002).
42. Bacila, I., et al. Measurement of salivary adrenal-specific androgens as biomarkers of therapy control in 21-hydroxylase deficiency. *J Clin Endocrinol Metab* 104(12), 6417-6429 (2019).
43. Pasquali, R., et al. Cortisol and ACTH response to oral dexamethasone in obesity and effects of sex, body fat distribution, and dexamethasone concentrations: a dose-response study. *J Clin Endocrinol Metab* 87(1), 166-175 (2002).
44. Ospina, N. S., et al. ACTH stimulation tests for the diagnosis of adrenal insufficiency: systematic review and meta-analysis. *J Clin Endocrinol Metab* 101(2), 427-434 (2016).
45. Hannibal, K. E., & Bishop, M. D. Chronic stress, cortisol dysfunction, and pain: a psychoneuroendocrine rationale for stress management in pain rehabilitation. *Phys Ther* 94(12), 1816–1825 (2014).
46. Bakusic, J., et al. Study of temporal variability of salivary cortisol and cortisone by LC-MS/MS using a new atmospheric pressure ionization source. *Sci Rep* 9(1), 1–12 (2019).
47. Magda, B., et al. Charged derivatization and on-line solid phase extraction to measure extremely low cortisol and cortisone levels in human saliva with liquid chromatography–tandem mass spectrometry. *J Pharm Biomed Anal* 140, 223–231 (2017).
48. Antonelli, G., et al. Salivary cortisol and cortisone by LC–MS/MS: validation, reference intervals and diagnostic accuracy in Cushing's syndrome. *Clin Chim Acta* 451, 247–251 (2015).

49. Fustinoni, S., Polledri, E., & Mercadante, R. High-throughput determination of cortisol, cortisone, and melatonin in oral fluid by on-line turbulent flow liquid chromatography interfaced with liquid chromatography/tandem mass spectrometry. *Rapid Commun Mass Spectrom* 27(13), 1450–1460 (2013).
50. Niewoehner, C. B. 5. In *Endocrine Pathophysiology* (Second, pp. 85–105) (2004). Hayes Barton Press.
51. Stewart, P. M., Corrie, J. E. T., Shackleton, C. H. L., & Edwards, C. R. W. Syndrome of apparent mineralocorticoid excess. A defect in the cortisol-cortisone shuttle. *J Clin Invest* 82(1), 340–349 (1988).
52. Shida, A., et al. Cortisol levels after cold exposure are independent of adrenocorticotropic hormone stimulation. *PLoS One* 15(2), 1–20 (2020).
53. Depression. World Health Organization. 2021 [cited 2022Oct12]. Available from: https://www.who.int/news-room/fact-sheets/detail/depression
54. SAMHSA - Substance Abuse and Mental Health Services Administration. [cited 2022Oct12]. Available from: https://www.samhsa.gov/
55. Treatment. Depression and Bipolar Support Alliance. [cited 2022Oct12]. Available from: https://www.dbsalliance.org/wellness/treatment-options/therapy/
56. Winerman, L. By the numbers: Antidepressant use on the rise. American Psychological Association. [cited 2022Oct12]. Available from: https://www.apa.org/monitor/2017/11/numbers
57. Bogowicz, P., Curtis, H. J., Walker, A. J., Cowen, P., Geddes, J., & Goldacre, B. Trends and variation in antidepressant prescribing in English primary care: a retrospective longitudinal study. *BJGP Open* 5(4), BJGPO.2021.0020 (2021).
58. Luo, Y., Kataoka, Y., Ostinelli, E. G., Cipriani, A., & Furukawa, T. A. National Prescription Patterns of Antidepressants in the Treatment of Adults with Major Depression in the US Between 1996 and 2015: A Population Representative Survey Based Analysis. *Front Psychiatry* 11, 35 (2020).
59. Hillhouse, T. M., & Porter, J. H. A brief history of the development of antidepressant drugs: From monoamines to glutamate. *Exp Clin Psychopharmacol* 23(1), 1–21 (2015).
60. Ahmed, Ebtesam PD. Antidepressants in patients with advanced cancer: When they're warranted and how to choose therapy. Cancer Network. MJH Life Sciences; 2019 [cited 2022Oct12]. Available from: https://www.cancernetwork.com/view/antidepressants-patients-advanced-cancer-when-theyre-warranted-and-how-choose-therapy
61. Lovering, N. Blood tests for the best antidepressant: What is available? Psych Central. Psych Central; 2022 [cited 2022Oct12]. Available from: https://psychcentral.com/depression/blood-test-best-medication-for-depression
62. Arantes, A. C., da Cunha, K. F., Cardoso, M. S., Oliveira, K. D., & Costa, J. L. Development and validation of Quantitative Analytical Method for 50 drugs of antidepressants, benzodiazepines and opioids in oral fluid samples by liquid chromatography–tandem mass spectrometry. *Forensic Toxicology* 39(1), 179–97 (2020).
63. Koller, D., Zubiaur, P., Saiz-Rodríguez, M., Abad-Santos, F., & Wojnicz, A. Simultaneous determination of six antipsychotics, two of their metabolites and caffeine in human plasma by LC-MS/MS using a phospholipid-removal microelution-solid phase extraction method for sample preparation. *Talanta* 198, 159–68 (2019).
64. Mifsud Buhagiar, L., Sammut, C., Chircop, Y., Axisa, K., Sammut Bartolo, N., & Vella Szijj, J., et al. Practical liquid chromatography–tandem mass spectrometry method for the simultaneous quantification of amitriptyline, nortriptyline and their hydroxy metabolites in human serum. *Biomedical Chromatography* 33(12).
65. Wang, J., Huang, H., Yao, Q., Lu, Y., Zheng, Q., Cheng, Y., et al. Simple and accurate quantitative analysis of 16 antipsychotics and antidepressants in human plasma by ultrafast high-performance liquid chromatography/tandem mass spectrometry. *Ther Drug Monit* 37(5), 649–60 (2015).
66. Choong, E., Rudaz, S., Kottelat, A., Haldemann, S., Guillarme, D., & Veuthey, J.-L., et al. Quantification of 4 antidepressants and a metabolite by LC–MS for Therapeutic Drug Monitoring. *J Chromatogr B* 879(19), 1544–50 (2011).
67. Eureka Lab Division. Eureka Kit. 2022 [cited 2022Oct15]. Available from: https://www.eurekakit.com/en/
68. Baumann, P., Ulrich, S., Eckermann, G., Gerlach, M., Kuss, H. J., Laux, G., et al. The AGNP-TDM Expert Group Consensus Guidelines: focus on therapeutic monitoring of antidepressants. *Dialogues Clin Neurosci* 7(3), 231–47 (2005).
69. Mayo Clinic Laboratories. TEST ID: CITAL [Internet]. [cited 2022Oct12]. Available from: https://www.mayocliniclabs.com/test-catalog/overview/83730#Clinical-and-Interpretive
70. Test catalog - Mayo Clinic Laboratories. Test Definition: IMIPR Imipramine and Desipramine, Serum [Internet]. [cited 2022Oct12]. Available from: https://www.mayocliniclabs.com/test-catalog/
71. Suzanne Bentley MD. Imipramine level: Reference range, interpretation, collection and panels. Medscape; 2022 [cited 2022Oct12]. Available from: https://emedicine.medscape.com/article/2090130-overview

72. Rao, M., Hiemke, C., Grasmäder, K., & Baumann, P. Olanzapin: Pharmakologie, Pharmakokinetik und Therapeutisches Drug Monitoring. *Fortschr Neurol Psychiatr* 69(11), 510–7 (2004).
73. Viibryd (vilazodone) dosing, indications, interactions, adverse effects, and more. 2022 [cited 2022Oct15]. Available from: https://reference.medscape.com/drug/viibryd-vilazodone-999620
74. Fariha, R., Jabrah, M., Hill, C., Spooner, A., Deshpande, P., & Tripathi, A. Simultaneous detection of salivary cortisol and cortisone using an automated high-throughput sample preparation method for LC-MS/MS. *SLAS Technol* 27(4), 237–46 (2022).
75. Matuszewski, B. K., Constanzer, M. L., & Chavez-Eng, C. M. Strategies for the Assessment of Matrix Effect in Quantitative Bioanalytical Methods Based on HPLC−MS/MS. *Anal Chem* 75(13), 3019–30 (2003).
76. Marchei, E., Escuder, D., Pallas, C. R., Garcia-Algar, O., Gómez, A., & Friguls, B., et al. Simultaneous analysis of frequently used licit and illicit psychoactive drugs in breast milk by liquid chromatography tandem mass spectrometry. *J Pharm Biomed Anal* 55(2), 309–16 (2011).
77. Lin, E.-P., Chiu, T.-C., & Hsieh, M.-M. Dispersive liquid-liquid microextraction combined with acetonitrile stacking through capillary electrophoresis for the determination of three selective serotonin reuptake inhibitor drugs in body fluids. *J Sep Sci* 39(24), 4841–50 (2016).
78. Blanchard, J. Evaluation of the relative efficacy of various techniques for deproteinizing plasma samples prior to high-performance liquid chromatographic analysis. *J Chromatogr B* 226(2), 455–60 (1981).
79. Polson, C., Sarkar, P., Incledon, B., Raguvaran, V., & Grant, R. Optimization of protein precipitation based upon effectiveness of protein removal and ionization effect in liquid chromatography–tandem mass spectrometry. *J Chromatogr B* 785(2), 263–75 (2003).
80. Ohshima, H., & Kondo, T. Ph dependence of electrostatic interaction between ion-penetrable membranes. *Biophys Chem* 32(2-3), 161–6 (1988).
81. Iyer, H. V., & Przybycien, T. M. Protein precipitation: Effects of mixing on protein solubility. *AIChE J* 40(2), 349–60 (1994).
82. Bell, D. J., Hoare, M., & Dunnill, P. Chapters 1, 2, 3.1. In: Fiechter A, editor. Downstream processing. Berlin: Springer-Verlag; 1983. p. 2–25.
83. Azziz, R. Polycystic Ovary Syndrome. *Obstet Gynecol* **132**, 321–336 (2018).
84. Richardson, M. R. Current Perspectives in Polycystic Ovary Syndrome. *afp* **68**, 697–705 (2003).
85. Cooney, L. G. & Dokras, A. Beyond fertility: polycystic ovary syndrome and long-term health. *Fertility and Sterility* **110**, 794–809 (2018).
86. Ndefo, U. A., Eaton, A. & Green, M. R. Polycystic Ovary Syndrome. *P T* **38**, 336–355 (2013).
87. Chima, S. C. & Mamdoo, F. Ethical and legal dilemmas around termination of pregnancy for severe fetal anomalies: A review of two African neonates presenting with ventriculomegaly and holoprosencephaly. *Niger J Clin Pract* **18 Suppl**, S31-39 (2015).
88. Raiten, J. *et al.* Perioperative Point-of-Care Ultrasound and Transesophageal Echocardiography in Resource-Limited Settings—A Focus on Nepal and Bangladesh. *Journal of Cardiothoracic and Vascular Anesthesia* **34**, 2604–2610 (2020).
89. Lentscher, J. A. & Decherney, A. H. Clinical Presentation and Diagnosis of Polycystic Ovarian Syndrome. *Clinical Obstetrics and Gynecology* **64**, 3 (2021).
90. Hachey, L. M., Kroger-Jarvis, M., Pavlik-Maus, T. & Leach, R. Clinical Implications of Polycystic Ovary Syndrome in Adolescents. *Nursing for Women's Health* **24**, 115–126 (2020).
91. Liang, S.-J., Hsu, C.-S., Tzeng, C.-R., Chen, C.-H. & Hsu, M.-I. Clinical and biochemical presentation of polycystic ovary syndrome in women between the ages of 20 and 40. *Human Reproduction* **26**, 3443–3449 (2011).
92. Conlon, J. L., Malcolm, S. & Monaghan, M. Diagnosis and treatment of polycystic ovary syndrome in adolescents. *JAAPA* **34**, 15 (2021).
93. Wolf, W. M., Wattick, R. A., Kinkade, O. N. & Olfert, M. D. Geographical Prevalence of Polycystic Ovary Syndrome as Determined by Region and Race/Ethnicity. *Int J Environ Res Public Health* **15**, 2589 (2018).
94. Handelsman, D. J. *et al.* Direct measurement of pregnanediol 3-glucuronide (PDG) in dried urine spots by liquid chromatography-mass spectrometry to detect ovulation. *The Journal of Steroid Biochemistry and Molecular Biology* **211**, 105900 (2021).
95. Lei, B. U. W. & Prow, T. W. A review of microsampling techniques and their social impact. *Biomed Microdevices* **21**, 81 (2019).
96. Edelbroek, P. M., van der Heijden, J. & Stolk, L. M. L. Dried blood spot methods in therapeutic drug monitoring: methods, assays, and pitfalls. *Ther Drug Monit* **31**, 327–336 (2009).

97. Spooner, N., Lad, R. & Barfield, M. Dried Blood Spots as a Sample Collection Technique for the Determination of Pharmacokinetics in Clinical Studies: Considerations for the Validation of a Quantitative Bioanalytical Method. *Anal. Chem.* **81**, 1557–1563 (2009).
98. Barfield, M., Spooner, N., Lad, R., Parry, S. & Fowles, S. Application of dried blood spots combined with HPLC-MS/MS for the quantification of acetaminophen in toxicokinetic studies. *Journal of Chromatography B* **870**, 32–37 (2008).
99. Li, Y., Henion, J., Abbott, R. & Wang, P. The use of a membrane filtration device to form dried plasma spots for the quantitative determination of guanfacine in whole blood. *Rapid Commun Mass Spectrom* **26**, 1208–1212 (2012).
100. Wagner, M., Tonoli, D., Varesio, E. & Hopfgartner, G. The use of mass spectrometry to analyze dried blood spots. *Mass Spectrom Rev* **35**, 361–438 (2016).
101. Discenza, L., Obermeier, M. T., Westhouse, R., Olah, T. V. & D'Arienzo, C. J. A bioanalytical strategy utilizing dried blood spot sampling and LC-MS/MS in discovery toxicology studies. *Bioanalysis* **4**, 1057–1064 (2012).
102. Demirev, P. A. Dried blood spots: analysis and applications. *Anal Chem* **85**, 779–789 (2013).
103. Bowen, C. L., Hemberger, M. D., Kehler, J. R. & Evans, C. A. Utility of dried blood spot sampling and storage for increased stability of photosensitive compounds. *Bioanalysis* **2**, 1823–1828 (2010).
104. Fariha, R. *et al.* Simultaneous detection of salivary cortisol and cortisone using an automated high-throughput sample preparation method for LC-MS/MS. *SLAS Technology* **27**, 237–246 (2022). intro
105. D'Arienzo, C. J. *et al.* DBS sampling can be used to stabilize prodrugs in drug discovery rodent studies without the addition of esterase inhibitors. *Bioanalysis* **2**, 1415–1422 (2010).
106. Bowen, C. L., Volpatti, J., Cades, J., Licea-Perez, H. & Evans, C. A. Evaluation of glucuronide metabolite stability in dried blood spots. *Bioanalysis* **4**, 2823–2832 (2012).
107. Bowen, C. L. *et al.* Investigations into the environmental conditions experienced during ambient sample transport: impact to dried blood spot sample shipments. *Bioanalysis* **3**, 1625–1633 (2011).
108. Min, K. L., Ryu, J. Y. & Chang, M. J. Development and clinical applications of the dried blood spot method for therapeutic drug monitoring of anti-epileptic drugs. *Basic & Clinical Pharmacology & Toxicology* **125**, 215–236 (2019).
109. Blood Collection on Filter Paper for Newborn Screening Programs; Approved Standard (Paperback) | Joyride Bookshop. https://joyridebookshop.indielite.org/book/9781562388843.
110. Chace, D. H., Kalas, T. A. & Naylor, E. W. Use of Tandem Mass Spectrometry for Multianalyte Screening of Dried Blood Specimens from Newborns. *Clinical Chemistry* **49**, 1797–1817 (2003).
111. Cao, Z. *et al.* Simultaneous quantitation of four androgens and 17-hydroxyprogesterone in polycystic ovarian syndrome patients by LC-MS/MS. *J Clin Lab Anal* **34**, e23539 (2020).
112. Kahoun, D. *et al.* Development and validation of an LC-MS/MS method for determination of B vitamins and some its derivatives in whole blood. *PLOS ONE* **17**, e0271444 (2022).
113. Koal, T., Schmiederer, D., Pham-Tuan, H., Röhring, C. & Rauh, M. Standardized LC–MS/MS based steroid hormone profile-analysis. *The Journal of Steroid Biochemistry and Molecular Biology* **129**, 129–138 (2012).
114. Fanelli, F. *et al.* Serum steroid profiling by isotopic dilution-liquid chromatography–mass spectrometry: Comparison with current immunoassays and reference intervals in healthy adults. *Steroids* **76**, 244–253 (2011).
115. Wenkui Li & Francis L.S. Tse. Dried blood spot sampling in combination with LC-MS/MS for quantitative analysis of small molecules - Li - 2010 - Biomedical Chromatography - Wiley Online Library. https://analyticalsciencejournals.onlinelibrary.wiley.com/doi/10.1002/bmc.1367.
116. Shabir, I. *et al.* Morning plasma cortisol is low among obese women with polycystic ovary syndrome. *Gynecological Endocrinology* **29**, 1045–1047 (2013).
117. Langer, E. K. *et al.* Characterization of the elemental composition of newborn blood spots using sector-field inductively coupled plasma-mass spectrometry. *J Expo Sci Environ Epidemiol* **21**, 355–364 (2011).
118. Viswanathan, C. Perspectives on microsampling: DBS. *Bioanalysis* **4**, 1417–1419 (2012).
119. Evans, C. *et al.* Implementing Dried Blood Spot Sampling for Clinical Pharmacokinetic Determinations: Considerations from the IQ Consortium Microsampling Working Group. *AAPS J* **17**, 292–300 (2014).
120. Fanelli, F. *et al.* Androgen Profiling by Liquid Chromatography–Tandem Mass Spectrometry (LC-MS/MS) in Healthy Normal-Weight Ovulatory and Anovulatory Late Adolescent and Young Women. *The Journal of Clinical Endocrinology & Metabolism* **98**, 3058–3067 (2013).
121. Machado, M. C. *et al.* Rapid electrophoretic recovery of DNA from dried blood spots. *ELECTROPHORESIS* **40**, 1812–1819 (2019).
122. Keevil, B. Steroid Mass Spectrometry for the Diagnosis of PCOS. *Med Sci (Basel)* **7**, 78 (2019).

123. Grebe, S. K. & Singh, R. J. LC-MS/MS in the Clinical Laboratory – Where to From Here? *Clin Biochem Rev* **32**, 5–31 (2011).
124. Torres-Acosta, M. A., Lye, G. J. & Dikicioglu, D. Automated liquid-handling operations for robust, resilient, and efficient bio-based laboratory practices. *Biochemical Engineering Journal* **188**, 108713 (2022).
125. Fariha, R. *et al.* An in-depth analysis of four classes of antidepressants quantification from human serum using LC–MS/MS. *Sci Rep* **13**, 2115 (2023).
126. Sheehan, M. T. Polycystic Ovarian Syndrome: Diagnosis and Management. *Clin Med Res* **2**, 13–27 (2004).
127. Velija-Ašimi, Z. Evaluation of endocrine changes in women with the polycystic ovary syndrome during metformin treatment. *Bosn J Basic Med Sci* **13**, 180–185 (2013).
128. *Polycystic Ovary Syndrome: Current and Emerging Concepts*. (Springer, 2014). doi:10.1007/978-1-4614-8394-6.
129. Daghestani, M. H. Evaluation of biochemical, endocrine, and metabolic biomarkers for the early diagnosis of polycystic ovary syndrome among non-obese Saudi women. *Int J Gynaecol Obstet* **142**, 162–169 (2018).
130. Deng, Y. *et al.* Steroid hormone profiling in obese and nonobese women with polycystic ovary syndrome. *Sci Rep* **7**, 14156 (2017).
131. Xu, R. N. *et al.* Strategies for Developing Sensitive and Automated LC-MS/MS Assays of a Pharmaceutical Compound and Its Metabolite from Whole Blood Matrix. *Pharmaceutics* **2**, 159–170 (2010).
132. Dhayat, N. A. *et al.* Urinary steroid profiling in women hints at a diagnostic signature of the polycystic ovary syndrome: A pilot study considering neglected steroid metabolites. *PLoS One* **13**, e0203903 (2018).
133. Zhou, W. *et al.* Non-invasive urinary metabolomics reveals metabolic profiling of polycystic ovary syndrome and its subtypes. *Journal of Pharmaceutical and Biomedical Analysis* **185**, 113262 (2020).
134. Lee, K., Murphy, J. & Tripathi, A. Electro-DBS: A Simple Method to Rapidly Extract Genomic DNA from Dried Blood Spots. *Anal. Chem.* **94**, 13404–13412 (2022).
135. Mei, J. V., Alexander, J. R., Adam, B. W. & Hannon, W. H. Use of filter paper for the collection and analysis of human whole blood specimens. *J Nutr* **131**, 1631S–6S (2001).
136. Liu, G. *et al.* Evaluating and defining sample preparation procedures for DBS LC-MS/MS assays. *Bioanalysis* **2**, 1405–1414 (2010).
137. Li, Y., Henion, J., Abbott, R. & Wang, P. The use of a membrane filtration device to form dried plasma spots for the quantitative determination of guanfacine in whole blood. *Rapid Commun Mass Spectrom* **26**, 1208–1212 (2012).
138. Wuethrich, A. Green sample preparation in analytical separation sciences : electrophoretic concentration. (University Of Tasmania, 2016). doi:10.25959/23240495.v1.
139. Oren, I., Fleishman, S. J., Kessel, A. & Ben-Tal, N. Free Diffusion of Steroid Hormones Across Biomembranes: A Simplex Search with Implicit Solvent Model Calculations. *Biophysical Journal* **87**, 768–779 (2004).
140. Nakatsuji, H., Hayakawa, T. & Yonezawa, T. Molecules in an electric field. Model for molecular geometry. *J. Am. Chem. Soc.* **103**, 7426–7432 (1981).
141. The Engineering ToolBox (2010). *Relative Permittivity - the Dielectric Constant. [online] Available at: https://www.engineeringtoolbox.com/relative-permittivity-d_1660.html [December 8, 2023].*
142. Zhang, Z., Gao, Y., Chen, S. & Huang, J. Understanding Dynamics of Electrochemical Double Layers via a Modified Concentrated Solution Theory. *J. Electrochem. Soc.* **167**, 013519 (2019).
143. Ferreira Avelar, M. C., Nascentes, C. C. & Orlando, R. M. Electric field-assisted multiphase extraction to increase selectivity and sensitivity in liquid chromatography-mass spectrometry and paper spray mass spectrometry. *Talanta* **224**, 121887 (2021).
144. Nauruzbayeva, J. *et al.* Electrification at water–hydrophobe interfaces. *Nat Commun* **11**, 5285 (2020).
145. Voloshin, T. *et al.* Alternating electric fields (TTFields) in combination with paclitaxel are therapeutically effective against ovarian cancer cells in vitro and in vivo. *International Journal of Cancer* **139**, 2850 (2016).
146. Keefe, C. C. *et al.* Simultaneous Measurement of Thirteen Steroid Hormones in Women with Polycystic Ovary Syndrome and Control Women Using Liquid Chromatography-Tandem Mass Spectrometry. *PLoS One* **9**, e93805 (2014).
147. *Polycystic Ovary Syndrome: Current and Emerging Concepts*. (Springer, 2014). doi:10.1007/978-1-4614-8394-6.
148. Schofield, R. C., et al. "Sensitive Simultaneous Quantitation of Testosterone and Estradiol in Serum by LC–MS/MS without Derivatization and Comparison with the CDC HoSt Program." *J Chromatogr B* (2017). doi:10.1016/j.jchromb.2017.02.006.

149. Matsumoto, A. M., & Bremner, W. J. "Editorial: Serum Testosterone Assays – Accuracy Matters." *J Clin Endocrinol Metab* (2004). doi:10.1210/jc.2003-032175.
150. Kushnir, M. M., et al. "Liquid Chromatography-Tandem Mass Spectrometry Assay for Androstenedione, Dehydroepiandrosterone, and Testosterone with Pediatric and Adult Reference Intervals." *Clin Chem* (2010). doi:10.1373/clinchem.2010.143222.
151. Thienpont, L. M., et al. "State-of-the-Art of Serum Testosterone Measurement by Isotope Dilution-Liquid Chromatography-Tandem Mass Spectrometry." *Clin Chem* (2008). doi:10.1373/clinchem.2008.105841.
152. "Testing Your Testosterone: It's Tricky. Diagnosing and Confirming Low Testosterone Requires Thorough Lab Testing and Careful Interpretation of the Results." *Harvard Men's Health Watch* (2012).
153. Häkkinen, M. R., et al. "Analysis by LC–MS/MS of Endogenous Steroids from Human Serum, Plasma, Endometrium and Endometriotic Tissue." *J Pharm Biomed Anal* (2018). doi:10.1016/j.jpba.2018.01.034.
154. Sun, G., et al. "Quantitative Determination of Human Serum Testosterone via Isotope Dilution Ultra-Performance Liquid Chromatography Tandem Mass Spectrometry." *Mol Med Rep* (2020). doi:10.3892/mmr.2020.11235.
155. Endogenous Hormones and Breast Cancer Collaborative Group. "Endogenous sex hormones and breast cancer in postmenopausal women: reanalysis of nine prospective studies." *J Natl Cancer Inst* 94(8), 606-616 (2002).
156. Sofikerim, M., Eskicorapcı, S., Oruç, Ö., & Oezen, H. "Hormonal predictors of prostate cancer." *Urol Int* 79(1), 13-18 (2007).
157. Moal, V., et al. "Low serum testosterone assayed by liquid chromatography-tandem mass spectrometry. Comparison with five immunoassay techniques." *Clin Chim Acta* 386(1-2), 12-19 (2007).
158. Vesper, H. W., et al. "Interlaboratory comparison study of serum total Testosterone measurements performed by mass spectrometry methods." *Steroids* 74(6), 498-503 (2009).
159. Fariha, R., et al. "Simultaneous detection of salivary cortisol and cortisone using an automated high-throughput sample preparation method for LC-MS/MS." *SLAS Technol* 27(4), 237–46 (2022).
160. Opioid Use in the U.S. - Statistics & Facts. Accessed March 8, 2024. Available from: https://www.statista.com/topics/3197/opioid-use-in-the-us/#editorsPicks
161. National Institutes of Health HEAL Initiative. Available from: https://heal.nih.gov/
162. Sofuoglu, M., & Sewell, R. A. "Norepinephrine and stimulant addiction." *Addiction Biology* 14(2), 119-129 (2009). doi:10.1111/j.1369-1600.2008.00138.x
163. Lee, M. R., Rohn, M. C. H., Tanda, G., & Leggio, L. "Targeting the Oxytocin System to Treat Addictive Disorders: Rationale and Progress to Date." *CNS Drugs* 30(2), 109-123 (2016). doi:10.1007/s40263-016-0313-z
164. You, Z. D., Li, J. H., Song, C. Y., Wang, C. H., & Lu, C. L. "Chronic morphine treatment inhibits oxytocin synthesis in rats." *Neuroreport* 11(14), 3113-3116 (2000). doi:10.1097/00001756-200009280-00015
165. Carson, D. S. "Oxytocin Treatment for Amphetamine-Induced Social Impairments." *J Neurosci* 34(44), 14503-14505 (2014). doi:10.1523/JNEUROSCI.3509-14.2014
166. Sarnyai, Z., & Kovács, G. L. "Oxytocin in learning and addiction: From early discoveries to the present." *Pharmacology Biochemistry and Behavior* 119, 3-9 (2014). doi:10.1016/j.pbb.2013.11.019
167. Kosten, T., & George, T. "The Neurobiology of Opioid Dependence: Implications for Treatment." *SPP* 1(1), 13-20 (2002). doi:10.1151/spp021113
168. Stine, S. M., et al. "Yohimbine-induced withdrawal and anxiety symptoms in opioid-dependent patients." *Biological Psychiatry* 51(8), 642-651 (2002). doi:10.1016/S0006-3223(01)01292-6
169. Kamilar-Britt, P., & Bedi, G. "The prosocial effects of 3,4-methylenedioxymethamphetamine (MDMA): Controlled studies in humans and laboratory animals." *Neuroscience & Biobehavioral Reviews* 57, 433-446 (2015). doi:10.1016/j.neubiorev.2015.08.016
170. Swann, A. C., et al. "Norepinephrine and impulsivity: effects of acute yohimbine." *Psychopharmacology* 229(1), 83-94 (2013). doi:10.1007/s00213-013-3088-7
171. Keary, C. J., et al. "Toxicologic Testing for Opiates: Understanding False-Positive and False-Negative Test Results." *Prim Care Companion CNS Disord* (2012). doi:10.4088/PCC.12f01371
172. Hammer, R., et al. "Addiction: Current Criticism of the Brain Disease Paradigm." *AJOB Neurosci* 4(3), 27-32 (2013). doi:10.1080/21507740.2013.796328
173. Darke, S. "Self-report among injecting drug users: A review." *Drug and Alcohol Dependence* 51(3), 253-263 (1998). doi:10.1016/S0376-8716(98)00028-3
174. Marsch, L. A. "The efficacy of methadone maintenance interventions in reducing illicit opiate use, HIV risk behavior and criminality: a meta-analysis." *Addiction* 93(4), 515-532 (1998). doi:10.1046/j.1360-0443.1998.9345157.x

175. De Castro, A., et al. "Simultaneous Quantification of Methadone, Cocaine, Opiates, and Metabolites in Human Placenta by Liquid Chromatography-Mass Spectrometry." *J Anal Toxicol* 33(5), 243-252 (2009). doi:10.1093/jat/33.5.243
176. Qin, N., et al. "Determination of 37 fentanyl analogues and novel synthetic opioids in hair by UHPLC-MS/MS and its application to authentic cases." *Sci Rep* 10(1), 11569 (2020). doi:10.1038/s41598-020-68348-w
177. Nickerson, J. L., & Doucette, A. A. "Rapid and Quantitative Protein Precipitation for Proteome Analysis by Mass Spectrometry." *J Proteome Res* 19(5), 2035-2042 (2020). doi:10.1021/acs.jproteome.9b00867
178. Roy, S. D., & Flynn, G. L. "Solubility behavior of narcotis analgesics in aqueous media: solubilities and dissociation constants of morphine, fentanyl, and sufentanil." *Pharmaceutical Research* 05(9), 580-586 (1988). doi:10.1023/A:1015994030251
179. Cruickshank-Quinn, C., et al. "Multi-step Preparation Technique to Recover Multiple Metabolite Compound Classes for In-depth and Informative Metabolomic Analysis." *JoVE* (2014). doi:10.3791/51670
180. CDC. Data and Statistics About Opioid Use During Pregnancy. Centers for Disease Control and Prevention (2023), https://www.cdc.gov/pregnancy/opioids/data.html (accessed March 13, 2024).
181. Maternal and newborn health. World Health Organization (accessed March 13, 2024), https://www.who.int/europe/news-room/fact-sheets/item/maternal-and-newborn-health.
182. HCUPnet Data Tools – Healthcare Cost and Utilization Project (HCUPnet) (accessed March 13, 2024), https://datatools.ahrq.gov/hcupnet/.
183. CDC. Basics About Opioid Use During Pregnancy. Centers for Disease Control and Prevention (2022), https://www.cdc.gov/pregnancy/opioids/basics.html (accessed March 13, 2024).
184. Neonatal Abstinence Syndrome (NAS) (accessed March 13, 2024), https://www.marchofdimes.org/find-support/topics/planning-baby/neonatal-abstinence-syndrome-nas.
185. Anbalagan, S. & Mendez, M.D. Neonatal Abstinence Syndrome. StatPearls (2024), http://www.ncbi.nlm.nih.gov/books/NBK551498/ (accessed March 13, 2024).
186. Newborn Screening Tests (for Parents) (accessed March 13, 2024), https://kidshealth.org/en/parents/newborn-screening-tests.html.
187. Levels and trends in child mortality. UNICEF (2023), https://data.unicef.org/resources/levels-and-trends-in-child-mortality/ (accessed March 8, 2024).
188. Wilhelm, A.J., den Burger, J.C.G., & Swart, E.L. Therapeutic Drug Monitoring by Dried Blood Spot: Progress to Date and Future Directions. Clin Pharmacokinet. 53, 961-973 (2014). https://doi.org/10.1007/s40262-014-0177-7
189. Busardò, F.P., Carlier, J., Giorgetti, R., et al. Ultra-High-Performance Liquid Chromatography-Tandem Mass Spectrometry Assay for Quantifying Fentanyl and 22 Analogs and Metabolites in Whole Blood, Urine, and Hair. Front Chem. 7, (2019). https://doi.org/10.3389/fchem.2019.00184
190. Cruickshank-Quinn, C., Quinn, K.D., Powell, R., et al. Multi-step Preparation Technique to Recover Multiple Metabolite Compound Classes for In-depth and Informative Metabolomic Analysis. JoVE (89), 51670 (2014). https://doi.org/10.3791/51670
191. Chalabianloo, F., Fadnes, L.T., Høiseth, G., et al. Subjective symptoms and serum methadone concentrations: what should guide dose adjustments in methadone maintenance treatment? A naturalistic cohort study from Norway. Subst Abuse Treat Prev Policy. 16, 39 (2021). https://doi.org/10.1186/s13011-021-00367-w
192. Milone, M.C. Laboratory Testing for Prescription Opioids. J Med Toxicol. 8, 408-416 (2012). https://doi.org/10.1007/s13181-012-0274-7
193. Liao, H.C., Laha, T.J., Baird, G.S., Chan, K.K., & Hoofnagle, A.N. A Second-generation opioid LC-MS/MS assay improves laboratory workflow and capacity. Journal of Chromatography B. 1210, 123438 (2022). https://doi.org/10.1016/j.jchromb.2022.123438
194. Yasien, S., Ali, E., Javed, M., et al. Simultaneous Quantification of Opioids in Blood and Urine by Gas Chromatography-Mass Spectrometer with Modified Dispersive Solid-Phase Extraction Technique. Molecules. 27(19), 6761 (2022). https://doi.org/10.3390/molecules27196761
195. Agostini, M., Renzoni, C., Pierini, E., et al. Rapid, hydrolysis-free, dilute-and-shoot method for the determination of buprenorphine, norbuprenorphine and their glucuronides in urine samples using UHPLC-MS/MS. Journal of Pharmaceutical and Biomedical Analysis. 166, 236-243 (2019). https://doi.org/10.1016/j.jpba.2019.01.014
196. Mercieca, G., Odoardi, S., Mestria, S., Cassar, M., & Strano-Rossi, S. Application of ultrasound-assisted liquid–liquid microextraction coupled with gas chromatography and mass spectrometry for the rapid determination

of synthetic cannabinoids and metabolites in biological samples. J of Separation Science. 43(14), 2858-2868 (2020). https://doi.org/10.1002/jssc.202000181
197. Langman, L.J., Korman, E., Stauble, M.E., Boswell, M.V., Baumgartner, R.N., & Jortani, S.A. Therapeutic Monitoring of Opioids: A Sensitive LC–MS/MS Method for Quantitation of Several Opioids Including Hydrocodone and Its Metabolites. Ther Drug Monit. 35(3) (2013).
198. The American Cancer Society Medical and Editorial Content Team. Breast cancer statistics: How common is breast cancer? https://www.cancer.org/cancer/types/breast-cancer/about/how-common-is-breast-cancer.html (2023).
199. Madej-Czerwonka, B., Korga-Plewko, A., & Czerwonka, M. Modern breast cancer diagnostic methods. Curr. Issues Pharm. Med. Sci. 35, 1–5 (2022).
200. Imamura, Y., et al. Comparison of 2D- and 3D-culture models as drug-testing platforms in breast cancer. Oncol. Rep. 33, 1837–1843 (2015).
201. Bhadriraju, K., & Chen, C.S. Engineering cellular microenvironments to improve cell-based drug testing. Drug Discov. Today 7, 612–620 (2002).
202. Hutmacher, D.W., et al. Can tissue engineering concepts advance tumor biology research? Trends Biotechnol. 28, 125–133 (2010).
203. Mehta, G., et al. Opportunities and challenges for use of tumor spheroids as models to test drug delivery and efficacy. J. Controlled Release 164, 192–204 (2012).
204. Majumder, B., et al. Predicting clinical response to anticancer drugs using an ex vivo platform that captures tumour heterogeneity. Nat. Commun. 6, 6169 (2015).
205. Sośniak, J., & Opiela, J. 3D Cell Culture Technology – A New Insight Into in Vitro Research – A Review. Ann. Anim. Sci. 21, 1257–1273 (2021).
206. Badekila, A.K., Kini, S., & Jaiswal, A.K. Fabrication techniques of biomimetic scaffolds in three-dimensional cell culture: A review. J. Cell. Physiol. 236, 741–762 (2021).
207. Marchini, A., & Gelain, F. Synthetic scaffolds for 3D cell cultures and organoids: applications in regenerative medicine. Crit. Rev. Biotechnol. 42, 468–486 (2022).
208. Harris, A.R., Yuan, J.X., & Munson, J.M. Assessing multiparametric drug response in tissue engineered tumor microenvironment models. Methods 134–135, 20–31 (2018).
209. Hoarau-Véchot, J., Rafii, A., Touboul, C., & Pasquier, J. Halfway between 2D and Animal Models: Are 3D Cultures the Ideal Tool to Study Cancer-Microenvironment Interactions? Int. J. Mol. Sci. 19, 181 (2018).
210. Katt, M.E., Placone, A.L., Wong, A.D., Xu, Z.S., & Searson, P.C. In Vitro Tumor Models: Advantages, Disadvantages, Variables, and Selecting the Right Platform. Front. Bioeng. Biotechnol. 4, (2016).
211. Antoni, D., Burckel, H., Josset, E., & Noel, G. Three-Dimensional Cell Culture: A Breakthrough In Vivo. Int. J. Mol. Sci. 16, 5517–5527 (2015).
212. Dingle, Y.-T.L., et al. Three-Dimensional Neural Spheroid Culture: An In Vitro Model for Cortical Studies. Tissue Eng. Part C Methods 21, 1274–1283 (2015).
213. Frantz, C., Stewart, K.M., & Weaver, V.M. The extracellular matrix at a glance. J. Cell Sci. 123, 4195–4200 (2010).
214. Reichman, B.S., et al. Paclitaxel and recombinant human granulocyte colony-stimulating factor as initial chemotherapy for metastatic breast cancer. J. Clin. Oncol. 11, 1943–1951 (1993).
215. Lin, R.-Z., & Chang, H.-Y. Recent advances in three-dimensional multicellular spheroid culture for biomedical research. Biotechnol. J. 3, 1172–1184 (2008).
216. Monazzam, A., et al. Application of the multicellular tumour spheroid model to screen PET tracers for analysis of early response of chemotherapy in breast cancer. Breast Cancer Res. 9, R45 (2007).
217. Napolitano, A.P., et al. Scaffold-free three-dimensional cell culture utilizing micromolded nonadhesive hydrogels. BioTechniques 43, 494–500 (2007).
218. Napolitano, A.P., Chai, P., Dean, D.M., & Morgan, J.R. Dynamics of the Self-Assembly of Complex Cellular Aggregates on Micromolded Nonadhesive Hydrogels. Tissue Eng. 13, 2087–2094 (2007).
219. An, R., Turek, J., Matei, D.E., & Nolte, D. Live tissue viability and chemosensitivity assays using digital holographic motility contrast imaging. Appl. Opt. 52, A300 (2013).
220. Barisam, M., Saidi, M., Kashaninejad, N., & Nguyen, N.-T. Prediction of Necrotic Core and Hypoxic Zone of Multicellular Spheroids in a Microbioreactor with a U-Shaped Barrier. Micromachines 9, 94 (2018).
221. LaPlaca, M.C., Cullen, D.K., McLoughlin, J.J., & Cargill, R.S. High rate shear strain of three-dimensional neural cell cultures: a new in vitro traumatic brain injury model. J. Biomech. 38, 1093–1105 (2005).
222. Bandu, R., et al. Liquid chromatography/mass spectrometry-based plasma metabolic profiling study of escitalopram in subjects with major depressive disorder. J. Mass Spectrom. 53, 385–399 (2018).

223. Seger, C., & Salzmann, L. After another decade: LC–MS/MS became routine in clinical diagnostics. Clin. Biochem. 82, 2–11 (2020).
224. Khalilpour, A., Kilic, T., Khalilpour, S., Álvarez, M.M., & Yazdi, I.K. Proteomic-based biomarker discovery for development of next generation diagnostics. Appl. Microbiol. Biotechnol. 101, 475–491 (2017).
225. Kapałczyńska, M., et al. 2D and 3D cell cultures – a comparison of different types of cancer cell cultures. Arch. Med. Sci. (2016). https://doi.org/10.5114/aoms.2016.63743.
226. Duval, K., et al. Modeling Physiological Events in 2D vs. 3D Cell Culture. Physiology 32, 266–277 (2017).
227. Fontoura, J.C., et al. Comparison of 2D and 3D cell culture models for cell growth, gene expression and drug resistance. Mater. Sci. Eng. C 107, 110264 (2020).
228. Breslin, S., & O'Driscoll, L. The relevance of using 3D cell cultures, in addition to 2D monolayer cultures, when evaluating breast cancer drug sensitivity and resistance. Oncotarget 7, 45745–45756 (2016).
229. Souza, A.G., et al. Comparative Assay of 2D and 3D Cell Culture Models: Proliferation, Gene Expression and Anticancer Drug Response. Curr. Pharm. Des. 24, 1689–1694 (2018).
230. Shyam, R., Reddy, L.V.K., & Palaniappan, A. Fabrication and Characterization Techniques of In Vitro 3D Tissue Models. Int. J. Mol. Sci. 24, 1912 (2023).
231. Nicolaou, K.C., et al. Paclitaxel as an anticancer agent: isolation, activity, synthesis and stability. Open Med. 6, 527–536 (2011).
232. Richheimer, S.L., Tinnermeier, D.M., & Timmons, D.W. High-performance liquid chromatographic assay of taxol. Anal. Chem. 64, 2323–2326 (1992).
233. Berthod, A., & Carda-Broch, S. Determination of liquid–liquid partition coefficients by separation methods. J. Chromatogr. A 1037, 3–14 (2004).
234. Singla, A.K., Garg, A., & Aggarwal, D. Paclitaxel and its formulations. Int. J. Pharm. 235, 179–192 (2002).
235. Wei, Z., You, J.B., Zeng, H., & Zhang, X. Interfacial Partitioning Enhances Microextraction by Multicomponent Nanodroplets. J. Phys. Chem. C 126, 1326–1336 (2022).
236. Surapaneni, M.S., Das, S.K., & Das, N.G. Designing Paclitaxel Drug Delivery Systems Aimed at Improved Patient Outcomes: Current Status and Challenges. ISRN Pharmacol. 2012, 1–15 (2012).
237. Nicolaou, K.C., Riemer, C., Kerr, M.A., Rideout, D.R., & Wrasidlo, W.W. Design, synthesis and biological activity of protaxols. Nature 364, 464–466 (1993).
238. Rodriguez, J., Elola, M.D., Martí, J., & Laria, D. Surface Behavior of Aprotic Mixtures: Dimethyl Sulfoxide/Acetonitrile. J. Phys. Chem. C 121, 14618–14627 (2017).
239. Vantangoli, M.M., Madnick, S.J., Huse, S.M., Weston, P., & Boekelheide, K. MCF-7 human breast cancer cells form differentiated microtissues in scaffold-free hydrogels. PLOS ONE 10(8) (2015).